Qualitative and Asymptotic Theory of Detonations

Luiz Faria

Qualitative and Asymptotic Theory of Detonations

Thesis by

Luiz Maltez Faria

In Partial Fulfillment of the Requirements

For the Degree of

Doctor of Philosophy

King Abdullah University of Science and Technology, Thuwal,

Kingdom of Saudi Arabia

November, 2014

The thesis of Luiz Maltez Faria is approved by the examination committee

Committee Chairperson: Dr. Aslan Kasimov

Committee Member: Dr. Rodolfo Rosales

Committee Member: Dr. David Ketcheson

Committee Member: Dr. Ravi Samtaney

Committee Member: Dr. David Keyes

External Examiner: Dr. Kevin Zumbrun

ABSTRACT

Qualitative and Asymptotic Theory of Detonations

Luiz Maltez Faria

Shock waves in reactive media possess very rich dynamics: from formation of cells in multiple dimensions to oscillating shock fronts in one-dimension. Because of the extreme complexity of the equations of combustion theory, most of the current understanding of unstable detonation waves relies on extensive numerical simulations of the reactive compressible Euler/Navier-Stokes equations. Attempts at a simplified theory have been made in the past, most of which are very successful in describing steady detonation waves. In this work we focus on obtaining simplified theories capable of capturing not only the steady, but also the unsteady behavior of detonation waves.

The first part of this thesis is focused on qualitative theories of detonation, where *ad hoc* models are proposed and analyzed. We show that equations as simple as a forced Burgers equation can capture most of the complex phenomena observed in detonations. In the second part of this thesis we focus on rational theories, and derive a weakly nonlinear model of multi-dimensional detonations. We also show, by analysis and numerical simulations, that the asymptotic equations provide good quantitative predictions.

ACKNOWLEDGEMENTS

First, I would like to thank my advisor, Prof. Aslan R. Kasimov, for his continuous guidance. Much of what I know today was learned either in his classroom or his office, where I was always welcomed. Working with him over the past years has been a real pleasure, and his enthusiasm kept me always motivated. Furthermore, I appreciate the freedom I was given to do my research at my own pace, pursuing my own ideas.

I would also like to thank Prof. Rodolfo R. Rosales, who has been both a collaborator and an examiner of my work throughout my Ph.D. His critical comments and insightful suggestions have been of great help, particularly regarding weakly nonlinear theories.

I am grateful to KAUST for providing a stimulating environment where research could flourish, and to all my former teachers and classmates. I am particularly grateful to my friend Abdullatiff Haji Ali, for always stimulating discussions and tremendous help with coding, specially at the early stages of my Ph.D.

Finally, I would like to thank my wife and my son, for their infinite patience and understanding of an often absent-minded husband and father. Without their support this work would not exist.

To my mother

TABLE OF CONTENTS

LIST OF ABBREVIATIONS

CJ	Chapman-Jouguet
DSD	Detonation Shock Dynamics
LLE	Largest Lyapunov Exponent
ODE	Ordinary Differential Equation
PDE	Partial Differential Equation
RH	Rankine-Hugoniot
TVD	Total Variation Dimishing
UTSD	Unsteady Small Disturbance Transonic
WENO	Weighted Essentially Non-Oscillatory
ZND	Zel'dovich-von Neumann-Döring

LIST OF FIGURES

LIST OF TABLES

Chapter 1

Introduction

The purpose of this thesis is to study shock waves in reactive media by introducing and analyzing simple models which reproduce, at both the qualitative and quantitative levels, the dynamical features of solutions of the reactive Euler/Navier-Stokes equations. As we shall demonstrate, the mechanism responsible for complex dynamics in detonation waves can be in fact rather simple.

We begin by reviewing in this Introduction some of the basic aspects of detonation theory. We explain in Section 1.1 what is a detonation, and how to mathematically describe it. We then review in Section 1.2 the Chapman-Jouguet (CJ) and the Zel'dovich-von Neumann-Döring (ZND) theories of detonation waves, which provide a starting point for much of the analytical understanding of detonations. In Section 1.3 we explain the limitations of the ZND theory, and discuss the rich dynamical behavior observed in both experiments and numerical simulations of the reactive Euler equations. We then conclude the introductory part by presenting in Section 1.4 and Section 1.5 a survey of the existing simplified models in detonation theory. The goal of this Introduction is to (1) set the common background needed, and (2) motivate the work performed in the subsequent chapters, where it is shown that detonations are amenable to theories much simpler than the complex equations of combustion

theory.

The main body of this thesis is structured so that, to a large extent, each chapter can be read independently. This requires some small repetition of content, but we hope that the advantages in readability will outweigh the disadvantages. The chapters have been further grouped into two main parts, depending on whether they take a *qualitative* approach to modeling through toy models (Part I), or a *quantitative* approach through rational asymptotic theories (Part II).

In the first part, we propose and analyze toy models capable of capturing the complex dynamics observed in detonation waves. Since these are not derived from first physical principles, they can only provide qualitative information. Their value, however, lies in the contrast between their simplicity and the rich dynamics they predict. We start by showing in Chapter 2 that a very simple forced Burgers equations, when constructed properly, contains all of the essential features of one-dimensional detonations, including pulsating and chaotic solutions. We then explore some natural extensions of the 1D qualitative theory in order to incorporate more complex effects. In Chapter 3, we focus on the effect of losses on the structure and stability of detonations. We show that, much like in the reactive Euler equations, the inclusion of algebraic losses complicates the analysis due to the presence of an embedded sonic point. We then conclude the qualitative part by extending, in Chapter 4, the one-dimensional theory to two dimensions. We show that both the linear stability and the nonlinear dynamics of the two-dimensional extension are in good qualitative agreement with the reactive Euler equations.

In the second part, we develop a multi-dimensional weakly nonlinear theory of detonation waves, where a systematic and asymptotic reduction is performed starting from the reactive compressible Navier-Stokes equations. In Chapter 5, we present the asymptotic derivation, together with a detailed study of the asymptotic model

proposed. We show that the reduced asymptotic equations, although much simpler than the compressible reactive Navier-Stokes equations, contain the essential features of one- and multi-dimensional detonation waves. Furthermore, since the asymptotic theory is *quantitative*, we compare its predictions with solutions of the full system of equations they are intended to approximate, and find a good quantitative agreement. Finally, we derive in Chapter 6 other interesting asymptotic models which incorporate more complex effects such as heat dissipation, viscous forces, and species diffusion.

The main contributions of this thesis can be summarized as follows:

- We propose and analyze in Chapter 2 the simplest partial differential equation (PDE) capable of reproducing the complex dynamics of 1D detonation waves, including chaotic solutions.

- By extending the analog to account for the effect of losses in Chapter 3, we discover a new integration algorithm which is able to circumvent the usual difficulty associated with the presence of a sonic singularity in the steady state profile.

- In Chapter 4, we introduce the first two-dimensional analog of detonation waves. Furthermore, we show that such a simple toy model contains complex multi-dimensional structures.

- We derive in Chapter 5 a new weakly nonlinear model for detonation waves, starting from the compressible reactive Navier-Stokes equations. We then show that the asymptotic theory retains the essential ingredients required to model unstable multi-dimensional detonations.

- In Chapter 6, we derive other asymptotic models which can be used to study, rationally, the effect of algebraic loss terms in detonations, as well as the effect

of heat/species diffusion. They provide a much simpler basis from which one may try to understand the role played by different dissipative processes.

We now begin with a short introduction to detonation theory. For a more in-depth discussion, the reader is encouraged to look at the classic book of Fickett and Davis [2].

1.1 Detonations and reactive Euler equations

The phenomenon of detonation was discovered in the late nineteenth century as a supersonic combustion wave that propagates around a thousand times faster than an ordinary flame. The precise nature of detonation was elucidated in the works of Mikhelson [3], Chapman [4], and Jouguet [5] (CJ theory) at the turn of the twentieth century and of Zel'dovich [6], von Neumann [7], and Döring [8] in the 1940's (ZND theory). It was established that a *detonation* is a shock wave that propagates in a reactive medium where exothermic chemical reactions are ignited as a result of the heating by the shock compression. The energy released in these reactions, in turn, feeds back to the shock in the form of compression waves and thus sustains the shock motion. The dynamics of such shock–reaction coupling is highly nonlinear due to the sensitivity of the chemical reactions to temperature, making the problem significantly more challenging than shock dynamics in inert media.

From a mathematical point of view, detonations are often modeled by the compressible reactive Navier-Stokes/Euler equations [9], depending on whether or not diffusive effects are taken into account. For simplicity of exposition, we present here the modeling equations when no dissipative effects are considered (a more general treatment will be considered later in Chapter 5). The governing equations, expressing the laws of conservation of mass, momentum, and energy, and the chemical heat

release, are thus given by:

$$\begin{aligned}
\frac{\mathrm{D}\rho}{\mathrm{D}t} + \rho\nabla\cdot\mathbf{u} &= 0, && (1.1)\\
\rho\frac{\mathrm{D}\mathbf{u}}{\mathrm{D}t} &= -\nabla p, && (1.2)\\
\rho\frac{\mathrm{D}e}{\mathrm{D}t} &= -p\nabla\cdot\mathbf{u}, && (1.3)\\
\frac{\mathrm{D}\Lambda_i}{\mathrm{D}t} &= W_i, && (1.4)
\end{aligned}$$

where $\frac{D}{Dt}(\cdot) = \frac{\partial}{\partial t}(\cdot) + \mathbf{u}\cdot\nabla(\cdot)$ is the material (Lagrangian) derivative, and W_i is the reaction rate of the $i-th$ species. Here, ρ is the density, $v = 1/\rho$ is the specific volume, $\boldsymbol{u}$ is the velocity vector, p is the pressure, e is the total internal energy, and Λ_i is the available mass fraction of the $i-th$ product. In order to close the system, we need to prescribe an equation of state, $e = e(p, \rho, \Lambda_1, \ldots, \Lambda_m)$, some thermodynamic relation, $p = p(\rho, T)$, and the reaction rates, $W_i(p, \rho, \Lambda_1, \ldots, \Lambda_m)$, for each reaction variable, Λ_i.

We note here that in most practical applications, only approximate expressions for the equations of state and for the reaction rates are available, which brings added complexity to the problem of modeling detonations. Although there is interest in detailed chemistry and complex equations of state [10], this thesis will focus primarily on simple equations of state and chemical kinetics. In fact, in order to keep the theory tractable, we assume when needed that the system is an ideal mixture of polytropic gases, all having the same heat capacity, and that the chemical kinetics can be well approximated by a single irreversible Arrhenius-type reaction. Even with these simplifying assumptions, we shall see that detonations still contain very complex dynamics.

In the next section, we describe briefly the CJ and ZND theories, which form the basis for much of our analytical understanding of detonation waves.

1.2 CJ and ZND theories

The first theoretical description of detonations goes back to the works of Mikhelson [3], Chapman [4], and Jouguet [5]. It assumes that a detonation is a shock wave moving into a reactive mixture, but with all of the chemical energy being released instantaneously at the shock, so reactions happen over an infinitesimally thin region. Detonations in the CJ theory are not classical gas dynamic shocks, in the sense that the Rankine-Hugoniot conditions have to be modified to account for the fact that energy actually increases across the shock due to chemical reactions. The CJ description is illustrated schematically in Figure 1.1.

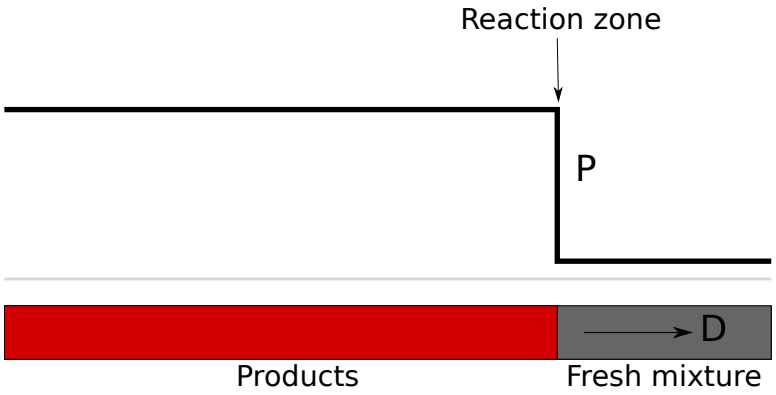

Figure 1.1: CJ description of a detonation wave. The wave moves from left to right with speed D. The reaction zone is assumed infinitely thin, with all energy being released inside the shock.

Although successful in predicting the detonation velocity, by assuming an infinitely thin reaction zone, the CJ theory was incapable of describing the region of heat release. Furthermore, the CJ theory relied on the crucial assumption that the velocity of the burnt state is sonic relative to the detonation shock, but it did not provide any justification as to why that should be the case. A better theoretical description of detonations, and the one we shall explain in more detail, was developed forty years later through the independent works of Zeldovich (1940), von Neumann (1942), and Döring (1943).

In the ZND theory, a detonation consists of a classical gas-dynamic shock, followed closely by chemical reactions that the shock itself triggers. It allows for a finite-width reaction zone to exist, although still treating the lead shock as a discontinuity. Notice that this is consistent with typical sizes of both structures: while the lead shock in a detonation tends to be on the order of a few mean free paths, reaction zones tend to be on the order of a few hundreds or thousands [2]. A schematic description of the ZND wave is shown in Figure 1.2. Contrasting the ZND description, Figure 1.2, with the CJ description, Figure 1.1, we see that the main difference is the presence of a finite-width reaction zone.

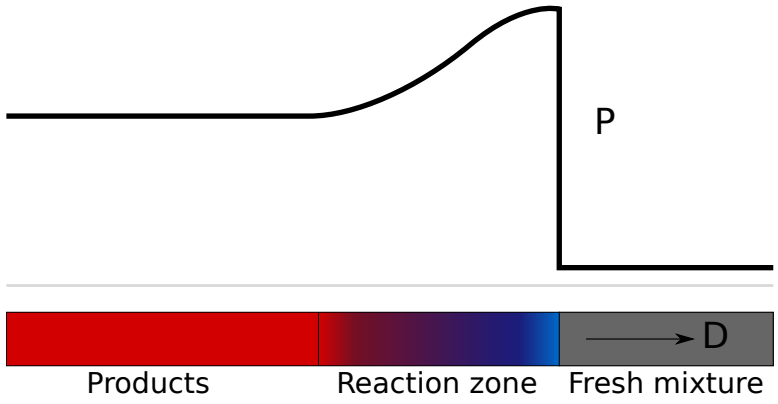

Figure 1.2: Schematics of the ZND description of a detonation wave. The whole profile moves from left to right, without changing its shape, with constant speed D.

The mathematics of the ZND theory is straightforward. It consists of a search for special types of traveling wave solutions to the reactive Euler equations given by a shock wave moving into an unreacted and quiescent mixture. In the ZND theory, thus, detonations are solutions of (1.1-1.4) which depend only on $\eta = x - Dt$, where D is the detonation speed (this far, an unknown of the problem). Inserting this ansatz, the reactive Euler equations, (1.1-1.4), reduce to the following system of ordinary

differential equations (ODEs):

$$(U-D)\,\rho_\eta + \rho\,(U)_\eta = 0, \tag{1.5}$$

$$\rho(U-D)u_\eta + p_\eta = 0, \tag{1.6}$$

$$\rho\,(U-D)\,e_\eta + pU_\eta = 0, \tag{1.7}$$

$$(U-D)\,\Lambda_{i\eta} = W_i(p,\rho,\Lambda_1,\ldots,\Lambda_m), \tag{1.8}$$

where U denotes the x component of velocity. Letting $\bar{U} = U - D$, algebraic manipulations of (1.5-1.8) yield:

$$(\bar{U}\rho)_\xi = 0, \tag{1.9}$$

$$(\bar{U}^2\rho + p)_\xi = 0, \tag{1.10}$$

$$(e + \frac{p}{\rho} + \frac{\bar{U}^2}{2})_\xi = 0, \tag{1.11}$$

$$\bar{U}\Lambda_{i\xi} = W_i. \tag{1.12}$$

Equations (1.9-1.11) are valid everywhere in the flow except at the shock, where the Rankine-Hugoniot (RH) conditions are required, and represent quantities which are conserved in a frame moving with speed D. In order to proceed any further with the calculation, we need to prescribe an equation of state, $e = e(p,\rho,\Lambda_1,\ldots,\Lambda_m)$, a thermodynamic relation, $p(\rho,T)$, and the reaction rates, $W_i(p,\rho,\Lambda_1,...,\Lambda_m)$. We consider here the case of an ideal polytropic gas with a single step irreversible reaction,

$A \to B$, and take

$$pv = RT, \tag{1.13}$$

$$W = \begin{cases} K(1-\Lambda)\exp\left(-E/RT\right) & \text{for } T \geq T_i, \\ 0 & \text{for } T < T_i, \end{cases} \tag{1.14}$$

$$e(p, v, \lambda) = pv/\left(\gamma - 1\right) - Q\Lambda. \tag{1.15}$$

Here R and γ have their usual meaning in the context of gas dynamics: $\gamma = c_p/c_v$ is the ratio of specific heats, and R is the universal gas constant divided by the molecular weight. The other parameters, not present in inert flows, are: E (activation energy), which measures how sensitive the chemical reactions are to temperature fluctuations; Q (energy of heat release) describes how much chemical energy is contained in the mixture; T_i (activation temperature) provides a threshold for temperature below which no chemical reactions take place; K (pre-exponential factor) measures the average collision frequency between molecules.

Denoting the values in the ambient state ahead of the wave by $\rho = \rho_a,\ U = 0,\ p = p_a$, and integrating (1.9-1.11) from a point ahead of the shock to an arbitrary point behind it, we obtain

$$\bar{U}\rho = -D\rho_a, \tag{1.16}$$

$$\bar{u}^2\rho + p = D^2\rho_a + p_a, \tag{1.17}$$

$$e + pv + \frac{\bar{U}^2}{2} = e_a + p_a v_a + \frac{D^2}{2}, \tag{1.18}$$

$$\Lambda_\xi = \frac{W(p, \rho, \Lambda)}{\bar{U}}. \tag{1.19}$$

Substituting $\bar{U} = -D\rho_a/\rho$ into (1.17) yields

$$p - p_a = -(\rho_a D)^2 (v - v_a). \tag{1.20}$$

Further eliminating $\bar{U}$ and D from (1.18) gives

$$e(p, v, \Lambda) - e(p_a, v_a, 0) + \frac{1}{2}(p + p_a)(v - v_a) = 0. \tag{1.21}$$

Equation (1.20) is known as the Rayleigh-Mikhelson line, and (1.21) is referred to as the Hugoniot curve (which is parametrized by Λ). Clearly then, for any $0 \leq \Lambda \leq 1$, the conservation laws imply that the states p, v must lie at the intersection between (1.20) and (1.21). In order to better understand what states belong to this intersection, it is useful to plot the Rayleigh-Mikhelson line and the Hugoniot curve in the $p - v$ plane. Equation (1.20) gives a straight line of slope proportional to D^2. The exact form of $e(p, v; \Lambda)$ is more complicated, but its basic shape can be seen in Figure 1.3, where we plot the Hugoniot curves for $\Lambda = 0$ and $\Lambda = 1$ (black), and the straight lines represent two Rayleigh-Mikhelson lines for different values of the wave speed D (red and blue).

The problem of connecting the pre-shock state (state (1) in Figure 1.3) to a fully-burnt post-reaction state, $\Lambda = 1$, can be split into three possibilities, depending on the value of D:

1. For D greater than some critical number, D_{CJ}, (red curve in Figure 1.3), there are two possible values at the end of the reaction zone, represented by the numbers (5) and (6) in Figure 1.3, where $\Lambda = 1$. These are known as strong and weak detonations, respectively.

2. For $D < D_{CJ}$, there is no way to connect the pre-shock state, $\Lambda = 0$, to the

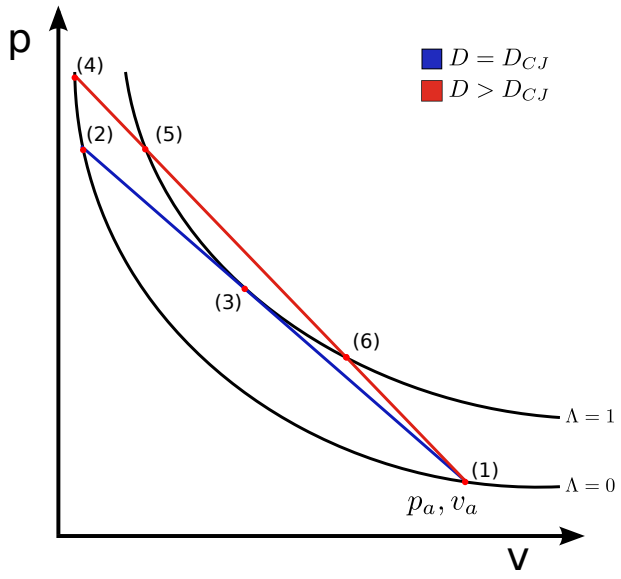

Figure 1.3: ZND wave diagram. The black curves represent the Hugoniot curves for $\Lambda = 0$ and $\Lambda = 1$, and the colored straight lines are the Rayleigh-Mikhelson lines for the Chapman-Jouguet and overdriven cases.

post-reaction state, $\Lambda = 1$. Thus there are no such solutions with $D < D_{CJ}$.

3. For $D = D_{CJ}$ (blue curve in Figure 1.3), there is a unique way to connect pre-shock state to the state at the end of the reaction zone by means of an inert shock followed by a smooth curve. This unique velocity, D_{CJ}, is known as the Chapman-Jouguet velocity, and has a special place in detonation theory.

The ratio D/D_{CJ} is typically referred to as the degree of overdrive. Notice that $D = D_{CJ}$ is the smallest velocity at which we can have a traveling wave solution, and it can be shown that for $D = D_{CJ}$, the velocity of the burnt products becomes sonic relative to the lead shock, explaining the original CJ hypothesis. This is the velocity at which a self-sustained detonation wave propagates. For $D > D_{CJ}$, one of the two solutions (the weak detonation) can be easily dismissed (if the heat release is monotonic) because in order to connect the post-shock state (number (4) in Figure 1.3) to the final point of the weak detonation (number (6) in Figure 1.3), an entropy-violating shock is needed. Therefore, only strong detonations are Lax-admissible in

the context of the inviscid theory.

Having chosen $D \geq D_{CJ}$, we can compute the spatial dependence of the profile by solving the ODE for Λ given by (1.19) (with D fixed, we can write u, p, ρ as functions of Λ, such that we obtain an ODE). This will give the full profile of a one-dimensional traveling wave with a shock discontinuity moving into an unperturbed region. When needed, we shall refer to this special type of solutions as a *ZND wave*. Although we have assumed an equation of state given by (1.15) and a reaction rate given by (1.14), the ZND theory applies to more general cases. In fact, the essential requirements for the ZND theory to be applicable are:

1. The wave is one-dimensional and steady.

2. The lead shock is a jump discontinuity (inviscid description).

3. The detonation is moving into an ambient state where no chemical reactions are taking place.

To illustrate the ZND theory with a concrete example, we choose (in appropriate dimensionless units) $E = 20,\ Q = 25,\ \gamma = 1.2$, and plot in Figure 1.4 the profiles for T, ρ, and p for a CJ detonation, where we have solved

$$\Lambda_\xi = \frac{W(p(\Lambda), \rho(\Lambda), \Lambda)}{U(\Lambda) - D}$$

subject to the boundary condition that $\Lambda(0) = 0$. As we can see, the computed traveling wave profile agrees well with the schematic of Figure 1.2.

The calculation above demonstrates that, under suitable assumptions, the reactive Euler equations admit a special type of traveling wave solutions (ZND wave), where a shock moves into an unperturbed state. It says nothing regarding the stability of

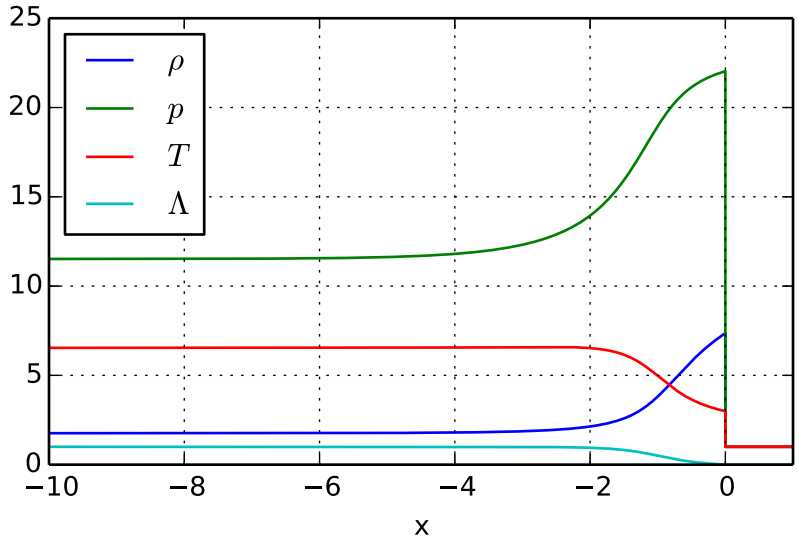

Figure 1.4: Steady-state ZND profiles for the Arrhenius rate.

such waves, or the possibility of other (multidimensional and/or non-steady) solutions. These are important questions which we address in the next section.

1.3 Detonation dynamics

The ZND theory explains rather well a detonation wave as a traveling wave achieved by a balance between the nonlinearity and the energy release in chemical reactions. The applicability of the ZND theory, however, depends crucially on the stability of a planar, steady detonation. If the traveling wave profile were unstable to transverse modes, then the one-dimensionality assumption would break down. But even if the wave remains one-dimensional, it is possible for longitudinal modes to become unstable, violating the steadiness assumption.

The first experimental observations suggesting that detonation fronts might not be stable were given as early as 1927 [11], well before the development of the ZND theory, with the observation of the spin phenomenon. With better experimental techniques it was later realized that, in fact, most gaseous detonations tend to be

unstable in practice, with complex multi-dimensional patterns forming [12, 13]. Since the ZND theory assumes a steady, one-dimensional traveling wave, the experimental observation of instability (and its rather generic nature) immediately put into question the usefulness of the ZND description of detonations. Interestingly, although multi-dimensional and highly unsteady, detonations were observed to travel at speeds very close to the CJ prediction. Some further theoretical understanding was needed.

Partial reconciliation between theory and experiments came 20 years later, in the pioneering works of Erpenbeck [14, 15], by a linear stability analysis. Erpenbeck showed that, for large enough values of the activation energy (E) and/or heat release (Q), the ZND solutions are linearly unstable. The analysis of Erpenbeck therefore explained why the ZND waves are rarely observed in experiments. From then on much improved numerical calculations of linear stability have been performed [16, 17, 18, 19, 20], all demonstrating the rich linear spectrum present in the reactive Euler equations. Linear stability analysis, however, has a limited power as it is a linear theory. It is capable of predicting for which parameters the ZND wave is unstable to infinitesimal perturbations, and even typical growth rates and spatial scales related to unstable wave numbers, but it provides no description beyond the onset of instabilities, when nonlinearities become important.

What happens after the onset of instabilities was first answered, in the context of the reactive Euler equations, by the numerical simulations of Fickett and Wood [21]. It was shown that, when unstable, the solutions tend to a limit cycle which oscillates around the ZND wave. Thus, even when unstable, ZND solutions provide some rough approximation of the true nonlinear dynamics. With the improvement of computers and numerical algorithms, detailed numerical studies of the reactive Euler equations have further shown that, as the activation energy is increased, solutions appear to go from stable to unstable through a supercritical Hopf bifurcation. From that point

on, further increase in the activation energy yields a sequence of period-doubling bifurcations leading to chaos [22, 23]. Recently, tools from dynamical systems have also been applied to the one-dimensional detonation dynamics to characterize the type of chaos observed [24].

Although linear stability provides some helpful insights into the complex dynamics, and numerical simulations can illustrate what happens after the onset of instabilities, understanding the underlying mechanisms responsible for the rich dynamics requires simpler models. Here, we do not insist on asymptotic approaches, since much can be learned even from qualitative theories, as long as they capture the essential elements of detonations.

Since this thesis is concerned with simplified models of detonations, we present in the next subsection a brief review of the literature on the subject. We focus first on the qualitative theories (Section 1.4), and then discuss the asymptotic approaches (Section 1.5), examining their main advantages and drawbacks.

1.4 Review of qualitative models

All of the models reviewed in this section belong to the category of *toy models*, also called *analogs*. They are not derived, and therefore need no justification. Being a qualitative approach, there is some controversy on whether or not such *ad hoc* approach has any value. We of course believe that it does, but a discussion of analogs, and where they may triumph over rational theories, seems appropriate.

Given Fickett's great exposition on the "nature of analogs" in his 1979 paper [25], we refrain from attempting to motivate it ourselves, and cite instead his original words:

> "An analog is a *qualitative* representation of the original. (There may

> of course be the added bonus that the original reduces to the analog in some special or limiting case, but this is by no means necessary.) The analog is constructed or designed, not derived. The design involves a trade off: one tries to maximize simplicity while minimizing the loss of important properties of the original. Simplicity is the analog's strong point. Specifically: (i) exact solutions are easier to find and more likely to exist, (ii) the tedium of routine mathematical manipulations is greatly reduced, and (iii) the essential ideas are less likely to be obscured by extraneous detail—in the full system one may fail to see the forest for the trees."

By taking a qualitative approach, one is free to experiment with the equations at will, without the need to rationally justify the steps taken. The usefulness of the analog will depend on how much of the original phenomena it can capture, versus how simple it is.

The first simplified model of detonations was proposed by Fickett in 1979 [25]. His goal was to use a reduced system which would still capture the coupling between the flow and the chemistry. Motivated by Burgers equation and in analogy with gas dynamics, Fickett modified Burgers equation by introducing an extra variable capable of changing the density. He then added an extra equation, corresponding to a reaction rate, to close the system. In its simplest form, the analog can be written as

$$u_t + (\frac{u^2}{2} + q\lambda)_x = 0, \tag{1.22}$$

$$\lambda_t = \omega(u, \lambda), \tag{1.23}$$

where $\omega(\lambda, u)$ is the reaction rate, and q is a constant. The original analog represents an irreversible chemical reaction where the chemicals change as $A \rightarrow B$ with λ :

$0 \to 1$, but other possibilities have been studied as well [26]. Similar to the ignition-temperature kinetics, the reaction is assumed to be triggered by a shock front which is moving into an unperturbed state.

Fickett's model contains all of the ZND theory discussed in Section 1.2, and much can be learned from studying it. In fact, Fickett himself went on later and wrote a book on this analog [27], in which he explains most of the main features and challenges of detonation problems through the simple model.

We have thus far deferred the discussion of the specific form of $\omega(u, \lambda)$, without which the analog is incomplete. As we shall see throughout this thesis, most of the complexity of detonations lies precisely in this choice, which determines how the chemical reactions are affected by the flow. Going back to Fickett's original work, he considered:

$$\omega = k\left(1-\lambda\right)^{1/2},$$

where k is a constant, for which all of the ZND theory becomes explicitly computable, and therefore simpler. The main drawback, however, is that Fickett's model as presented in [25] contains only stable traveling waves, and therefore cannot be used to study the complex stability properties of detonations.[1]

Another analog closely related to Fickett's was introduced independently by Majda in 1981 [29]. Majda's analog is given by

$$\left(u+q\lambda\right)_t + \left(\frac{u^2}{2}\right)_x = \beta u_{xx}, \tag{1.24}$$

$$\lambda_t = \left(1-\lambda\right)\phi\left(u\right), \tag{1.25}$$

[1] Fickett did some preliminary calculations regarding stability, and it appears he was aware of instabilities in his model, provided a more complex form of the reaction rate is assumed [27]. He did not demonstrate what happens after instability however. He also investigated the stability of a square wave in the context of his analog, showing that pathological instabilies do occur in the limit of infinitely fast reaction rate and finite induction zone [28].

where β, q are constants representing a viscosity-like effect and the energy of heat release, respectively. Majda analyzed his model in great detail, showing existence of traveling wave solutions.

The most important contribution of Majda's work is that, in a rigorous way, the effect of viscosity is considered. He showed that, even in the presence of some viscosity, a theory analogous to the ZND theory exists for viscous detonations, with strong, weak, and CJ cases. The stability of these solutions, however, was not investigated by Majda.

The main criticism of the Majda model is that it has never been shown, numerically or analytically, that the combustion waves present in (1.24) and (1.25) can become unstable. In fact, most of the current belief is towards stability, with many works suggesting that Majda's analog [17, 30] is always stable (for some forms of $\phi(u)$ in (1.25), of course).

The two previously mentioned analogs, Fickett's and Majda's, were thus lacking one of the main features of real detonations: instabilities. It was believed, in fact, that such a simple theory could not capture all of detonation dynamics. This was proven wrong in the recent work of Radulescu and Tang [31], where it was shown that a modification of (1.22) can reproduce all the instabilities and chaotic dynamics observed in the reactive Euler equations. Their modification, which is motivated by chain-branching kinetics, is given by

$$u_t + \left(\frac{u^2}{2} + Q\lambda_r\right)_x = 0, \tag{1.26}$$

$$(\lambda_i)_t = -K_i H(\lambda_i) \exp\left[\alpha\left(u/2D_{CJ}\right) - 1\right], \tag{1.27}$$

$$(\lambda_r)_t = K_r\left(1 - H\left(\lambda_i\right)\right)\left(1 - \lambda_r\right)^{\nu}. \tag{1.28}$$

The rationale behind the above equations is that the exothermic chemical reactions,

measured by λ_r, are preceded by an induction zone, controlled by λ_i, where energy is not released. The size of this induction zone depends exponentially on the main variable, u. We avoid giving a detailed explanation of all other parameters, $K_i,\ K_r,\ \alpha,\ \nu$, which can be found in the original work [31].

The authors showed, by numerical simulations, that for certain choices of parameters, the detonation waves of (1.26-1.28) bifurcate from stable to unstable, and that further destabilization leads to a period doubling cascade, and possibly chaos. This was an interesting discovery, as it suggested that the underlying dynamics may be in fact captured by Burgers-like systems.

The main weakness of the Radulescu-Tang analog, one could argue, is that some simplicity has been lost. The equations are still amenable to analysis, but the number of parameters and the need for more complicated chemistry deviates from the main strength of an analog: simplicity. Also, since the reactive Euler equations admit pulsating—and even chaotic— solutions with a single step Arrhenius kinetics, the extra complexity in reaction rate seems unnecessary. We reiterate, however, that [31] was the first time that the complex dynamics of detonations (including chaos) was reduced to a much simpler system.

1.5 Review of asymptotic theories

While the previous section surveyed some existing analogs in detonation theory, we focus in this section on asymptotic theories. Asymptotic theories are *quantitative* in nature and, any predictions they make must also appear in the more general system in the appropriate limit. The converse, however, is not generally true, and important features of the general model may not be present in the asymptotic equations.

The art of asymptotic modeling consists of knowing which effects are important

and which are negligible for a given phenomenon, and then finding the correct limit in which only the important terms are retained. We present below a brief review of five asymptotic models in detonation theory. Since our focus is on weakly nonlinear theories, closer attention is payed to the weakly nonlinear theory of Rosales and Majda [32].

Shortly after Majda introduced his simplified combustion model, Rosales, in a joint work with Majda, showed that a weakly nonlinear asymptotic theory can yield a very similar set of equations [32]. The Rosales-Majda model is derived in arbitrary dimensions, but for simplicity we shall present here the one-dimensional formulation of the model, with a wave moving into a constant unperturbed state. The equations then take the form

$$u_t + \left(\frac{u^2}{2} + \frac{q}{2}\lambda\right)_x = \beta u_{xx}, \tag{1.29}$$

$$\lambda_x = -k\left(1-\lambda\right)\exp\left(\theta u\right), \tag{1.30}$$

where we have focused on the reaction rate obtained by a single-step Arrhenius kinetics. Here, β represents the effect of viscous terms, k is the pre-exponential factor, q is the energy of heat release, and θ is the rescaled activation energy.

It is not very hard to see that the traveling wave solutions of (1.29-1.30) are exactly analogous to the traveling wave solutions of the Majda analog, and therefore the theory developed in [29] directly applies to the Rosales-Majda model. This means (1.29-1.30) admit traveling wave solutions similar to ZND waves, and contain strong, weak, and CJ detonations.

Since (1.29-1.30) is derived from the reactive Navier-Stokes equations, which admit unstable detonations, one may expect the same to be present in the asymptotic theory. It appears, however, that this is not the case (at least for simple Arrhenius kinetics),

and that detonation waves (weak and strong) of (1.29-1.30) are always stable [33, 34].

In order to better understand how unstable waves, a feature present in the general formulation using the reactive Navier-Stokes equations with Arrhenius kinetics, faded from the asymptotic equations, it is helpful to look into the nature of instabilities in detonations, the asymptotic behavior of the neutral stability boundary, and the scaling assumed in the derivation of the Rosales-Majda theory.

Postponing the more technical details to Chapter 5, let us briefly mention here the main assumptions of the Rosales-Majda model. First, it is a weakly-nonlinear theory, and therefore waves must have small amplitude. This requires Q, the heat release parameter, to be small (in an appropriate dimensionless formulation). Then, for the chemistry to be affected by such a weak flow, one must choose E, the activation energy, to be large. Letting ϵ be the small parameter in their derivation, related to the amplitude of the wave, the Rosales-Majda theory assumes $Q = O(\epsilon^2),\ E = O(1/\epsilon)$. That this scaling is expected to produce only stable waves can be understood by looking at the neutral stability curve in the $Q - E$ plane.

In the limit of large E, the neutral stability curve appears to follow a scaling $Q \sim 1/E$, at least in some asymptotic approach [35], with detonations being unstable if $Q \gtrsim 1/E$ [36]. Then, since the Rosales-Majda theory assumes $Q \sim 1/E^2 \ll 1/E$, we see that the asymptotic approximation is valid in a limit where the general equations themselves possess only stable detonations. Modifying the assumptions of the asymptotic theory, however, is not as straightforward as one may hope. Simply changing $Q = O(\epsilon)$ or $E = O(1/\epsilon^2)$ in the original formulation of the Rosales-Majda theory produces equations which are either not weakly nonlinear (and therefore not amenable to the simplifications of weakly nonlinear theories), or that have infinitely fast reaction rates. Later in Chapter 5, we will explain how to overcome these difficulties.

Another interesting asymptotic simplification is given by the detonation shock

dynamics (DSD) theory. Its main goal is to extend the ZND theory in order to account for curvature effects and unsteadiness of the wave [37, 38]. It assumes small shock curvature, $\kappa \ll 1$, and slow time evolution, $\partial_t \ll 1$. It also relies on the fact that a sonic point exists some distance away from the shock, and therefore that the shock evolution is completely determined by the flow between the shock and the sonic locus.

Depending on the relative sizes of κ and ∂_t, different results are obtained. In the simplest form, if one assumes that $\partial_t \ll \kappa$, then curvature effects dominate, and the final result of DSD theory is a relation of the form

$$F(D, \kappa) = 0,$$

which determines how fast the shock moves (D) at a given curvature (κ). If one assumes, instead, that the unsteadiness of the wave has an effect comparable to curvature, then the relation becomes

$$F(\dot{D}, D, \kappa) = 0,$$

where $\dot{D}$ denotes the shock acceleration.

Many extensions of DSD theory have been carried out [39, 40, 41], and by retaining higher order terms one obtains relations which are more complex, e.g., $F\left(\ddot{D}, \dot{D}, D, \kappa\right) = 0$, but the basic ideas remain unchanged.

DSD theory is a very practical theory since it provides a shock evolution equation that reduces the spatial dimension of the problem by 1, and does not assume that the shock is weak. The main disadvantage of DSD theory is that the functional relations between D and its derivatives, and curvature, tend to be very complicated.

Nonetheless, if carried to high enough order, these theories have been demonstrated to reproduce both unstable pulsating detonations and some form of cellular patterns [39].

The third theory we shall mention is the Bourlioux-Majda-Roytburd model [42, 43], which is a modulation theory for the eigenfunction of weakly unstable detonation waves. It is obtained by expanding the dependent variables, near the stability boundary, in a series of the form

$$\mathbf{q} = \mathbf{q}_0(x) + \epsilon A\left(\epsilon^2 t\right)\mathbf{e}\left(x\right)\exp\left(i\Im\left(\sigma\right)t\right) + c.c + O(\epsilon^2),$$

where $\mathbf{q}_0$ is the steady-state (ZND) solution, and $\sigma, \mathbf{e}$ are the eigenvalue and eigenvector corresponding to $\mathbf{q}_0$. It is assumed that the parameters (overdrive, heat release, activation energy) are chosen so that the ZND wave is unstable, but close enough to the neutral stability boundary. In this case, there is only one unstable eigenvalue, σ, with $\Re\left(\sigma\right) \gtrapprox 0$. The main finding is that the amplitude function A, in one dimension, solves a Landau-Stuart equation. The original one-dimensional work has been extended to multiple dimensions by the same authors [44], and it was shown that similar theories can be developed provided the instabilities are mainly triggered by a single unstable mode. There is, however, no evidence that the asymptotic model reproduces not only instabilities, but also period doubling, chaos, and multi-dimensional cellular patterns similar to those in full reactive Euler equations.

The main difficulty with this asymptotic theory is that the eigenvalues and eigenfunctions of a detonation wave (i.e., the linearized spectrum) need to be known in order to perform the asymptotic expansions, and finding these is generally quite challenging.

The fourth model we cover, derived by Clavin and He [45], exploits the fact that,

provided a strong overdrive is present, a quasi-isobaric approximation is appropriate for detonation waves. Overdriven detonations are usually associated with piston-driven detonations, where the detonation propagates at speeds which are higher than the CJ velocity. When the degree of overdrive is high, the detonations resemble more and more an inert shock, with chemical reactions playing only a secondary role. If the limit is chosen appropriately, however, it is possible to have a highly overdriven detonation which is still unstable. In the Clavin-He theory, a limit of high overdrive and ratio of specific heats close to unity is considered. In order to avoid singularities which arise in that model when employing simple Arrhenius kinetics, the authors considered a more complex reaction rate. With their proposed reaction rate, a parameter measuring the induction zone sensitivity to temperature fluctuations is then assumed large, which allows for small perturbations to affect the strongly overdriven flow.

The final result of the model is an integral equation which relates the shock temperature, T_s, to its history,

$$1 + bT_s(t) = \int_0^\infty W\left(T_s(t-\tau), \tau\right) d\tau,$$

where b is a constant and W is a known function. The authors showed that, provided the temperature sensitivity is high enough (in their new reaction rate function), the solutions of their model contain unstable waves. In subsequent work, the authors showed what appears to be cellular structures in a multidimensional form of their model [46]. It remains unclear, however, how quantitatively close their predictions are to the full reactive Euler equations regarding the nonlinear dynamics.

The last theory we review, developed by Clavin and Williams [47] is based on a weakly nonlinear approximation of a detonation wave in the limit of small overdrive,

small heat release, large activation energy, and $\gamma \to 1$. By looking at perturbation of the ZND profile, the authors derive a forced Burgers equation, together with an equation for the reaction rate function. Although the final result is similar to that of Rosales and Majda, the derivation of Clavin-Williams appears to be different. In particular, they assume an inviscid and one-dimensional wave, and look at the non-linear evolution of perturbations to the ZND profile. Rosales and Majda, on the other hand, derive their theory in multi-dimensions with dissipative effects retained. The main novelty of the Clavin-Williams theory is that by applying the extra assumption that $\gamma - 1$ is small, the asymptotic form of the reaction rate is modified. Finally, they show that in some limits their reduced system contains instabilities.

As we shall see later, our multi-dimensional weakly nonlinear theory, when restricted to the one-dimensional inviscid case, contains the Clavin-Williams model, and therefore we postpone further details to Chapter 5.

Both the asymptotic models and the analogs that we covered in the last two sections have much increased our understanding of detonations. Some have shed light on the steady state structures, others on nonlinear dynamics; some emphasized the physical mechanisms, others the complex mathematics. Despite their differences, all models discussed share the same goal: to obtain a simpler description of detonation waves.

Part I

Qualitative theory of unsteady detonations

Chapter 2

Reactive Burgers equation

Here, we analyze properties of an equation that we propose to model the dynamics of unstable one-dimensional detonation waves. The equation is

$$u_t + \frac{1}{2}\left(u^2 - uu\left(0_-, t\right)\right)_x = f\left(x, u\left(0_-, t\right)\right), \quad x \leq 0, \quad t > 0.$$

It describes a detonation shock at $x = 0$ with the reaction zone in $x < 0$. We investigate the nature of the steady-state solutions of this nonlocal hyperbolic balance law, the linear stability of these solutions, and the nonlinear dynamics. We establish the existence of instability followed by a cascade of period-doubling bifurcations leading to chaos.

2.1 Introduction

We begin this thesis by studying possibly the simplest manifestation of instabilities in detonation waves: pulsating detonations. As we discussed in Section 1.3, a steady planar detonation wave is rarely observed in experiments. Complex time-dependent and multi-dimensional structures tend to develop [48, 2]. Numerical simulations of the equations of reactive gas dynamics are able to reproduce at a qualitative level

the complex structures observed in experiments (see, e.g., [49, 44, 50]). Obtaining physical insights into the basic mechanisms of the instability is greatly facilitated by simplified modeling and remains challenging.

In one dimension, the instabilities of the reactive shock wave manifest themselves in the form of a "galloping detonation" [2], wherein the shock speed oscillates around its steady value. It has been shown through extensive numerical experiments that as the activation energy, E, a parameter in the equations measuring the temperature sensitivity of the chemical reactions, is varied, the shock speed transitions from a constant to an oscillatory function. Further increase of E leads to a period-doubling bifurcation cascade, which ultimately results in the shock moving at a chaotic speed [22, 23]. The precise mechanism for such instabilities is still not completely understood.

In this chapter, we show that a very simple model, which consists of a single nonlocal partial differential equation (PDE), is capable of reproducing the complexity observed in one-dimensional simulations of reactive Euler equations. The model possesses traveling wave solutions precisely analogous to those of the ZND theory (i.e. Section 1.2), with both the Chapman-Jouguet (i.e., self-sustained) and the overdriven solutions present. Furthermore, stability analysis and unsteady simulations of the model demonstrate the complexity seen in galloping detonations, in particular, their chaotic dynamics. These findings suggest that a theory much simpler than the full reactive Euler equations may be capable of describing the rich shock dynamics observed in detonation waves.

Simplified models have been used in the past to study detonations. Both rational asymptotic theories and *ad hoc* models have been introduced previously to gain insight into the dynamics of detonation. The reader can find extensive references in the recent review articles and books [51, 48, 52], or in Section 1.4 and Section 1.5. The most

relevant to this chapter is the theory of weakly nonlinear detonations [32], which we shall use in order to motivate the toy model introduced. Before [32], Fickett [25] and Majda [29] independently introduced *ad hoc* analog models, which were based on the idea of extending Burgers equation by an additional equation modeling chemical reactions. The effect of chemical reactions in these analogs appears as a modification of the flux function to include the chemical energy term. The analog models received much attention in the past [25, 28, 27, 31, 53] and continue to attract interest from a mathematical point of view [17]. These simplified models possess a theory analogous to ZND theory, with its Chapman-Jouguet, strong, and weak detonation solutions. The weakly nonlinear model [32] is a result of an asymptotic reduction of the reactive Navier-Stokes equations. It applies in any number of spatial dimensions, reducing in one dimension to equations very similar to those of the analogs and therefore also containing the theory of ZND waves. The analog models have previously been thought to perform poorly in describing galloping one-dimensional instabilities and the transition to chaos. However, the recent work of Radulescu and Tang [31] demonstrates that a modified version of Fickett's analog, to include a two-stage chemical reaction with an inert induction zone and a following reaction zone, reproduces much of the complexity of detonations in reactive Euler equations. We suggest that even a much simpler scalar equation can capture many of the known phenomena of pulsating detonation waves.

The remainder of this chapter is structured as follows. In Section 2.2, we introduce the model and discuss its connection with the weakly nonlinear model. Next, we develop a general theory for the proposed equation and compute the possible ZND solutions. In Section 2.3, we derive a dispersion relation for the linear stability, and prove certain important properties about the distribution of the eigenvalues. Finally, in Section 2.4, we focus on a specific example, for which we perform an extensive

numerical study. With the example, we calculate the linear stability spectrum, the onset of instabilities, and the long-time nonlinear dynamics of solutions. Using tools from dynamical system theory, we show that the solution goes through a sequence of period doubling bifurcations to chaos, much like in the reactive Euler equations.

2.2 The model

Our model construction is based on two basic ideas: weakly nonlinear approximation [32] and non-locality of the chemical energy release rate [25]. The precise nature of this non-locality is explained below. The weakly nonlinear theory of detonation in one dimension, in the inviscid limit, results in the following simplified system[32]:

$$u_t + \left(\frac{u^2}{2} + \frac{q}{2}\lambda\right)_\eta = 0, \tag{2.1}$$

$$\lambda_\eta = \omega\left(\lambda, u\right), \tag{2.2}$$

where t and η are time and space variables, respectively; λ is the mass fraction of reaction products, going from 0 ahead of the shock to 1 in the fully burnt mixture; u can be thought of as, for example, temperature; $\omega(\lambda, u)$ is the asymptotic reduction of the original reaction rate; and q is a constant representing the chemical heat release. Note that (2.2) propagates waves instantaneously since the time derivative is missing in the equation. Nevertheless, (2.1–2.2) constitutes a hyperbolic system.

In [32], (2.1–2.2) are derived under the assumption of weak heat release and high activation energy. This is consistent with a weakly nonlinear theory in which (in appropriate dimensionless units), the waves have amplitude $O(\epsilon)$ and the heat release has size $O(\epsilon^2)$, while the activation energy is $O(1/\epsilon)$, where $0 < \epsilon \ll 1$.

Consider a shock moving into an unreacted ($\lambda = 0$), unperturbed ($u = 0$) region.

At the shock, we apply the Rankine-Hugoniot conditions to (2.1) to obtain

$$-D\left[u\right]+\frac{1}{2}\left[u^{2}\right]+\frac{q}{2}\left[\lambda\right]=0, \tag{2.3}$$

where D is the shock speed and the brackets denote the jump across the shock in the enclosed variables. Using $[\lambda]=0$ and that $u=0$ ahead of the shock, it follows from (2.3) that $D=\dot{\eta}_s=u_s/2$, where $\eta_s(t)$ is the shock position and $u_s=u\left(\eta_s^-,t\right)$ denotes the post-shock value of u. A change of variables to the shock-attached frame, given by $x=\eta-\eta_s(t)$, yields

$$u_t+\left(\frac{u^2}{2}+\frac{q}{2}\lambda-Du\right)_x=0, \tag{2.4}$$

$$\lambda_x=\omega\left(\lambda,u\right), \tag{2.5}$$

for $x\leq 0$ and $u=0,\ \lambda=0$ for $x>0$.

Now we make the important assumption that $\omega(\lambda,u)=\omega(\lambda,u_s)$. This simplifying assumption is the reason why we call the model nonlocal, because the change of λ at any given point x at time t is determined not by $u\left(x,t\right)$ at that point, but by u at the shock, $x=0$. This means that any change of $u_s\left(t\right)$ propagates instantaneously over the whole domain, $x<0$. Note that such assumption is sometimes used in modeling detonation in condensed explosives. The idea behind it is that the energy release is primarily controlled by how hard the explosive is hit by the shock [27].[1]

As a consequence of the assumed form of ω, equation (2.5) can now be formally integrated over x to yield $\lambda=F(x,u_s)$. Upon differentiation of the latter with respect to x and substitution into (2.4) (letting $qF_x/2=f$), we obtain one non-local equation

[1]Much later in Chapter 5, after a new weakly nonlinear theory of detonations is derived, we will be able to motivate this assumption through asymptotic ideas. Recall, however, that toy models require no such justifications, and therefore the work performed in this chapter remains valuable even in the absence of an asymptotic justification.

on the half-line, $x \leq 0$, given by

$$u_t + \frac{1}{2}\left(u^2 - uu_s\right)_x = f\left(x, u_s\right). \tag{2.6}$$

Conversely, it can be shown that for any positive function, f, a function $\omega(\lambda, u_s)$ can be found such that (2.6) is equivalent to the system given by (2.4-2.5).

The shock, which is now located at $x = 0$ at any t, must satisfy the Lax conditions, that is, $c(0^-, t) > 0 > c(0^+, t)$, where $c = u - u_s/2$ denotes the characteristic speed in (2.6). It follows that $D\left(t\right) = u_s/2 = c\left(0^-, t\right) > 0$.

Initial data for (2.6) are given as $u\left(x, 0\right) = g\left(x\right)$ for $x < 0$, where $g\left(x\right)$ is a suitable function and $u\left(x, 0\right) = 0$ for $x > 0$ is assumed implicitly. An important feature of (2.6) is that the boundary value of the unknown, u_s, is contained within the equation. This is one of the key reasons for the observed complexity of the shock dynamics. While the boundary information from the shock at $x = 0$ is propagated instantaneously throughout the solution domain at $x < 0$, there is a finite-speed influence propagating from the reaction zone toward the shock along the characteristics of (2.6).

In characteristic form, (2.6) can be written as

$$\frac{du}{d\tau} = f\left(x, u_s\right), \tag{2.7}$$

$$\frac{dx}{d\tau} = u - \frac{u_s}{2}, \tag{2.8}$$

where the characteristic speed is $c = u - u_s/2$. Therefore, (2.6) incorporates, within a single scalar equation, the nonlinear interaction of two waves. One is the usual Burgers wave propagating toward the shock at a finite speed, c. The other is of an unusual type, as it represents an instantaneous effect by the state u_s at the shock, $x = 0$, on the whole solution region $x < 0$. Physically, this second wave corresponds

to the particle paths carrying the reaction variable. In the weakly nonlinear limit, these paths have, effectively, an infinite velocity.

2.3 Steady solutions and their stability

In this section, we explore some general properties of the proposed model. Keeping in mind the connection with detonation theory, we restrict our attention to $f(x, u_s)$ such that $\int_{-\infty}^{0} f(x, u_s)\, dx = q/2 = const$. This condition means that the amount of energy released by reactions is finite and fixed. We consider only exothermic reactions; hence, $f(x, u_s) \geq 0$. Although these assumptions facilitate some of the computations, they are not required for most of the results presented here, and more general forms of the forcing can be considered without adding much more complexity to the analysis.

2.3.1 Rankine-Hugoniot and Lax Entropy Conditions

At the shock, located originally at $\xi = 0$, we apply the Rankine-Hugoniot conditions,

$$-\dot{s}\,[u] + \frac{1}{2}\left[u^2\right] - \frac{1}{2}u^-\,[u] = 0, \tag{2.9}$$

where $[z] = z^+ - z^-$ denotes the jump in z across the shock and $\dot{s}$ is the shock speed. From 2.9, we immediately find that $\dot{s} = 0$, that is the shock is stationary at any $t > 0$. This is of course a simple consequence of moving to the shock-attached frame, which led to the modified flux of the particular form. In the laboratory frame, the shock moves with the speed equal to $D = u\,(0, t)\,/2$. So in reality, we are solving a free-boundary problem, albeit posed in an unusual form.

Finally, we require the shock to be a Lax shock, meaning that $c(0^-) > 0 > c(0^+)$, where c denotes the speed of the characteristic in (2.6). This implies $u(0, t) > 0$ for

all t, and thus in the laboratory frame of reference the shock never changes direction. Given initial data $g(x) > 0$ and forcing function $f > 0$ we are guaranteed to have a Lax shock for all time. Thus the shock is always located at zero, and it is always a Lax admissible shock.

2.3.2 Steady-state solutions

Let $u_0(x)$ denote a steady-state smooth solution of (2.6). It is a solution of

$$\left(u_0 - \frac{u_{0s}}{2}\right) u_0' = f(x, u_{0s}), \tag{2.10}$$

where " $'$ " denotes the derivative with respect to x and $u_{0s} = u_0(0)$ is the steady-state value of u at $x = 0$, which is to be found together with $u_0(x)$. Integration of (2.10) from 0 to x yields a quadratic equation for u_0,

$$u_0^2 - u_0 u_{0s} = 2\int_0^x f(y, u_{0s})\, dy,$$

where the integration constant vanishes in view of the boundary condition at $x = 0$. The solution profile is thus given by

$$u_0(x) = \frac{u_{0s}}{2} + \sqrt{\frac{u_{0s}^2}{4} + 2\int_0^x f(y, u_{0s})\, dy}. \tag{2.11}$$

The plus sign is chosen here to satisfy the boundary condition at $x = 0$. We note that for $u_0(x)$ in (2.11) to be real, f must be constrained so that at any x, the expression under the square root is non-negative. Effectively, this is the requirement of overall exothermicity of the source term.

The choice of u_{0s} depends on the behavior of the solution at $x \to -\infty$. For the

square root in equation (2.11) to be real at $x = -\infty$, we require that

$$u_{0s} = \zeta \left(2\sqrt{2\int_{-\infty}^{0} f\left(y, u_{0s}\right) dy} \right) \tag{2.12}$$

with some $\zeta \geq 1$. The effect of ζ, which is the analog of the overdrive factor in detonation theory, on the shape and the stability of the traveling wave can be readily appreciated in the non-dimensional formulation given in Section 2.4. The case with $\zeta = 1$ whereby

$$u_{0s} = 2\sqrt{2\int_{-\infty}^{0} f\left(y, u_{0s}\right) dy}, \tag{2.13}$$

is an important special case commonly referred to as the Chapman-Jouguet solution, because the characteristic speed at $x = -\infty$ is $c_0\left(-\infty\right) = u_0\left(-\infty\right) - u_{0s}/2 = 0$. Therefore, the characteristics point toward the shock everywhere at $x < 0$ becoming vertical at $x = -\infty$. Cases where $\zeta > 1$ are related to piston-driven detonations wherein the state at $x = -\infty$ remains subsonic, i.e., $c > 0$. In the context of the Euler detonations, they are known to be more stable than Chapman-Jouguet waves [16, 20].

2.3.3 Spectral stability of the steady-state solution

Consider the linear stability of the steady-state solution obtained in the previous subsection. For simplicity, we limit the analysis to the CJ case, but the overdriven solution can be similarly analyzed, as is done later in Chapter 4. Let $u\left(x,t\right) = u_0\left(x\right) + \epsilon u_1\left(x,t\right) + O\left(\epsilon^2\right)$ with $\epsilon \to 0$ and linearize (2.6). We find that

$$u_{1t} + \left(u_0 - \frac{u_{0s}}{2}\right) u_{1x} + u_0' u_1 = \left(\frac{\partial f}{\partial u_s}\left(x, u_{0s}\right) + \frac{u_0'}{2}\right) u_1\left(0,t\right). \tag{2.14}$$

The steady-state characteristic speed is

$$c_0 = u_0 - \frac{u_{0s}}{2} = \sqrt{2\int_{-\infty}^{x} f\left(y, u_{0s}\right) dy}, \tag{2.15}$$

and the coefficient on the right-hand side of the linearized equation above is

$$b_0 \equiv \frac{\partial f}{\partial u_s}\left(x, u_{0s}\right) + \frac{u_0'}{2} = \frac{\partial f}{\partial u_s}\left(x, u_{0s}\right) + \frac{f\left(x, u_{0s}\right)}{2c_0\left(x\right)} = \frac{\partial f}{\partial u_s}\left(x, u_{0s}\right) + \frac{1}{2}c_0(x)'. \tag{2.16}$$

Both c_0 and b_0 are functions of x.

Thus, the linear stability problem requires that the following linear non-local PDE with variable coefficients,

$$u_{1t} + c_0 u_{1x} + c_0' u_1 = b_0 u_1\left(0, t\right), \tag{2.17}$$

be solved subject to appropriate initial data, $u_1\left(x, 0\right)$. If spatially bounded (in some norm, to be defined below) solutions of (2.17) grow in time, then instability is obtained. At this point, we can proceed with either the Laplace transform in time (as in [14]) or normal modes (as in [16]). We choose the latter and substitute the normal modes,

$$u_1 = \exp\left(\sigma t\right) v\left(x\right), \tag{2.18}$$

into (2.17), to obtain

$$c_0 v' + c_0' v + \sigma v = b_0\left(x\right) v\left(0\right).$$

This equation can be integrated directly to yield

$$\exp\left(\sigma \int_0^x \frac{dy}{c_0\left(y\right)}\right) c_0\left(x\right) v\left(x\right) - c_0\left(0\right) v\left(0\right) = v\left(0\right) \int_0^x b_0\left(\xi\right) \exp\left(\sigma \int_0^\xi \frac{dy}{c_0\left(y\right)}\right) d\xi.$$

Denoting $p = \int_x^0 dy/c_0\,(y) \geq 0$, we obtain the final solution for the amplitude of the normal mode

$$v\,(x) = v\,(0)\,p'\,(x)\,e^{\sigma p(x)}\left[\int_x^0 b_0\,(\xi)\,e^{-\sigma p(\xi)}d\xi - c_0\,(0)\right]. \tag{2.19}$$

The existence of an unstable eigenvalue with $\Re(\sigma) > 0$ and bounded $v(x)$ is equivalent to normal-mode instability. On physical grounds, we require that f be integrable in x at any given t (i.e., the L^1 norm of f is bounded). This requirement follows from the implicit assumption that f is in fact the $x-$derivative of some reaction progress variable, λ, varying between 0 and 1. We impose the same constraint on u, hence $v \in L^1\,(\mathbb{R}^-)$.

Note that $|e^{\sigma p(x)}/c_0(x)| \to \infty$ as $x \to -\infty$ for $\Re\,(\sigma) > 0$, therefore, the factor in front of the brackets in (2.19) tends to infinity as $x \to -\infty$. To prevent this growth, the term in the brackets must vanish as $x \to -\infty$. In fact, this condition is also sufficient for instability.

Theorem 1. *Provided that* $\|b_0(\xi)\|_{L_1} < \infty$*, the existence of a* σ *with* $\Re(\sigma) > 0$ *such that*

$$\int_{-\infty}^0 b_0\,(z)\,e^{-\sigma p(z)}dz - c_0\,(0) = 0, \tag{2.20}$$

is both necessary and sufficient for the existence of unstable normal modes.

Proof. If condition (2.20) is not satisfied, then $|v(x)| \nrightarrow 0$ as $x \to -\infty$. Now, suppose that (2.20) is satisfied. Then, $v(x)$ takes the form

$$v\,(x) = \frac{v\,(0)}{c_0(x)}e^{\sigma p(x)}\left[\int_x^0 b_0\,(\xi)\,e^{-\sigma p(\xi)}d\xi - \int_{-\infty}^0 b_0\,(\xi)\,e^{-\sigma p(\xi)}d\xi\right]. \tag{2.21}$$

$$= \frac{v\,(0)}{c_0\,(x)}\int_{-\infty}^x b_0\,(\xi)\,e^{-\sigma(p(\xi)-p(x))}d\xi. \tag{2.22}$$

We now show that $\|v(x)\|_{L^1} < \infty$. From (2.22), it follows by changing the integration limits that

$$\begin{aligned}
\|v\|_{L^1} &= \int_{-\infty}^{0} \left| \frac{v(0)}{c_0(x)} \int_{-\infty}^{x} b_0(\xi)\, e^{-\sigma(p(\xi)-p(x))} d\xi \right| dx, \\
&\leq |v(0)| \int_{-\infty}^{0} \int_{-\infty}^{x} \frac{1}{|c_0(x)|} \left| b_0(\xi)\, e^{-\sigma(p(\xi)-p(x))} d\xi \right| dx, \\
&\leq |v(0)| \int_{-\infty}^{0} \int_{-\infty}^{x} \frac{1}{|c_0(x)|} \left| b_0(\xi)\, e^{-\sigma(p(\xi)-p(x))} \right| d\xi\, dx, \\
&\leq |v(0)| \int_{-\infty}^{0} \int_{\xi}^{0} \frac{1}{|c_0(x)|} |b_0(\xi)|\, e^{-\Re(\sigma)(p(\xi)-p(x))} dx\, d\xi.
\end{aligned}$$

We change the integration variable in the inner integral from x to $z = p(\xi) - p(x)$, so that $dx = -dz/p'(x) = c_0(x)\, dz$. Then,

$$\|v\|_{L^1} \leq |v(0)| \int_{-\infty}^{0} \int_{0}^{p(\xi)-p(0)} |b_0(\xi)|\, e^{-\Re(\sigma)z} dz\, d\xi, \tag{2.23}$$

$$\leq |v(0)| \frac{1}{\Re(\sigma)} \int_{-\infty}^{0} |b_0(\xi)| \left(1 - e^{-\Re(\sigma)(p(\xi)-p(0))}\right) d\xi, \tag{2.24}$$

$$\leq \frac{|v(0)|}{\Re(\sigma)} \|b_0\|_{L^1}, \tag{2.25}$$

which proves that the unstable perturbations are bounded in the L^1 norm provided that $b_0 \in L^1(\mathbb{R}^-)$. Thus, (2.20) is necessary and sufficient for the existence of unstable normal modes. □

It is interesting that the dispersion relation (2.20) closely resembles that of [54, 55], where the detonation dynamics is analyzed in the asymptotic limit of strong overdrive. In this limit, the entire flow downstream of the lead shock has a small Mach number relative to the shock, hence the post-shock pressure remains nearly constant. For this reason, such approximation is called quasi-isobaric. However, the underlying assumptions in the present model and those in the quasi-isobaric theory are quite

different. For example, in [54, 55], the authors assume that the detonation overdrive (i.e., the detonation speed normalized by the Chapman-Jouguet speed) is large and that the ratio of specific heats is close to unity. The weak nonlinearity in [32], on the other hand, comes from the small heat release assumption.

Another important result is that, under appropriate assumptions on f, the unstable modes have a bounded growth rate. This result shows that the so-called "pathological" instability, inherent to square-wave models of detonation in the Euler equations [56, 57], does not occur in our model for smooth steady-state solutions. However, in Subsection 2.4.2.2 we show that this pathological instability occurs in the square-wave limit of our model, when f is replaced by a delta function.

Theorem 2. *Given that* $\|b_0 c_0\|_{L_\infty} = M < \infty$*, there exist no eigenvalues with* $\sigma_r > M/c_0\,(0)$.

Proof. Notice that

$$\left|\int_{-\infty}^{0} b_0(x)e^{-\sigma p(x)}dx\right| \;\leq\; \int_{-\infty}^{0}\left|b_0(x)e^{-\sigma p(x)}\right|dx = \int_{-\infty}^{0}\left|b_0(x)e^{-\sigma_r p(x)}\right|dx.$$

Let $z = p(x)$ and note that this function is invertible since p is monotonic. Substitution into the previous integral yields

$$\begin{aligned}\int_{-\infty}^{0}|b_0(x)e^{-\sigma_r p(x)}|dx &= \int_{0}^{\infty}|b_0(p^{-1}(z))c_0(p^{-1}(z))|e^{-\sigma_r z}dx \\ &\leq \max_{-\infty\leq x\leq 0}|b_0c_0|\int_0^\infty e^{-\sigma_r z}dx = \frac{1}{\sigma_r}\max_{-\infty\leq x\leq 0}|b_0c_0|,\end{aligned}$$

and thus for $\sigma_r > \left(\max_{\infty\leq x\leq 0}|b_0c_0|\right)/c_0(0)$, we obtain

$$\left|\int_{-\infty}^{0} b_0(x)e^{-\sigma p(x)}dx\right| \leq \frac{1}{\sigma_r}\max_{\infty\leq x\leq 0}|b_0c_0| < c_0(0).$$

This contradicts the dispersion relation stated in Theorem 1, where we required

$$\int_{-\infty}^{0} b_0(x)e^{-\sigma p(x)}dx = c_0(0),$$

and therefore there can be no eigenvalue with $\sigma_r > \left(\max_{\infty \leq x \leq 0} |b_0 c_0|\right)/c_0(0)$. □

If $f(x, u_{0s})$ is integrable and bounded and $\frac{\partial f}{\partial u_s}(x, u_{0s})$ is bounded, then it can be shown that $b_0 c_0 \in L^\infty$. These constraints are sufficient to eliminate the pathological instabilities in which arbitrarily large growth rates are present.

Theorem 3. *If $\|b_0 c_0\|_{L^\infty} = M < \infty$, there exists a bounded interval I large enough that all eigenvalues with $\sigma_r > 0$ have imaginary part $|\sigma_i| < I$.*

Proof. By application of the Riemann-Lebesgue lemma, we find after changing the integration variable to $z = p(x)$,

$$\begin{aligned}\int_{-\infty}^{0} b_0(x)e^{-\sigma p(x)}dx &= \int_{0}^{\infty} b_0(x)c_0(x)e^{-\sigma z}dz \\ &= \int_{0}^{\infty} \left(b_0(x)c_0(x)e^{-\sigma_r z}\right) e^{i\sigma_i z}dz \to 0 \text{ as } \sigma_i \to \infty\end{aligned}$$

provided that $b_0(p^{-1}(z))c_0(p^{-1}(z))e^{-\sigma_r z} \in L^1$. If $\sigma_r > 0$ and $b_0 c_0$ is bounded, then it follows that indeed $b_0(p^{-1}(z))c_0(p^{-1}(z))e^{-\sigma_r z} \in L^1$. Therefore, the integral above vanishes as $\sigma_i \to \infty$, which cannot happen because the integral should equal to $c_0(0) = u_{0s}/2 > 0$. Notice that, unlike Theorem 2, the bound on the imaginary part of the root is not quantitative. Better estimates of the integral above are needed to obtain a computable bound. □

Theorem 4. *$\sigma = 0$ is never an eigenvalue.*

Proof. Notice that the condition $\int_{-\infty}^{0} b_0(\xi)\, e^{-\sigma p(\xi)} d\xi - c_0(0) = 0$ is still necessary for the eigenfunctions to remain bounded, even when $\sigma = 0$, since in that case the

eigenfunctions are given by

$$v\left(x\right)=v\left(0\right)p'\left(x\right)\left[\int_{x}^{0}b_{0}\left(\xi\right)d\xi-c_{0}\left(0\right)\right],$$

and therefore $\int_{-\infty}^{0}b_{0}\left(\xi\right)d\xi-c_{0}\left(0\right)=0$ is still required in order for $v(x)\rightarrow 0$ as $x\rightarrow-\infty$. Substituting for b_0, we have

$$\begin{aligned}\int_{-\infty}^{0}\left[\frac{\partial f}{\partial u_{s}}\left(\xi,u_{0s}\right)+\frac{1}{2}c_{0}(\xi)'\right]d\xi-c_{0}\left(0\right) &= 0,\\ \int_{-\infty}^{0}\frac{\partial f}{\partial u_{s}}\left(\xi,u_{0s}\right)d\xi &= c_{0}(0)/2.\end{aligned}$$

Since we assume that f integrates to a constant (independent of u_{0s}), then

$$\int_{-\infty}^{0}\frac{\partial f}{\partial u_{s}}\left(\xi,u_{0s}\right)d\xi = \frac{d}{du_{s}}\int_{-\infty}^{0}f\left(\xi,u_{0s}\right)d\xi=0.$$

But $c_0(0)=u_{0s}/2>0$, and therefore no such eigenvalue can exist. Thus, at the onset of instability, the eigenvalues must have non-zero frequency. □

Because $\sigma=0$ is never an eigenvalue, when the behavior of the system as a function of parameters is explored, the transition from a stable steady state to instability usually involves a Hopf bifurcation. In our numerical calculations we find that this bifurcation is a supercritical Hopf bifurcation, similar to what happens in detonations [58], so that a stable time periodic solution takes over from the steady state.

2.4 An example

In the previous section, we presented necessary and sufficient conditions for the normal-mode instability of a traveling wave profile. We now focus on a specific choice

of $f(x, u_s)$ and illustrate with it the general results on the linear instability. We also examine, by means of numerical simulations, what happens once the traveling-wave solution becomes unstable as a bifurcation parameter is varied. The example mimics, on a qualitative level, a situation wherein the chemical reaction has an induction zone that delays the beginning of an energetic exothermic reaction. The idea is to have a function that peaks at some distance away from the shock, with this distance depending on the shock strength. A simple choice for such a function is

$$f = \frac{q}{2}\frac{1}{\sqrt{4\pi\beta}}\exp\left[-\frac{\left(x - x_i\left(u_s\right)\right)^2}{4\beta}\right]. \tag{2.26}$$

Here, x_i is the point where f peaks and that point depends on the current state at the shock, $u_s = u\left(0, t\right)$. The parameter β determines the width of the reaction zone. As $\beta \to 0$, f tends to $\frac{q}{2}\delta\left(x - x_i\right)$ where δ is the Dirac delta function; this limit yields what is called a square-wave profile, wherein f kicks in only at $x = x_i$. We choose x_i as

$$x_i\left(t\right) = -k\left(\frac{u_{0s}}{u_s\left(t\right)}\right)^{\alpha}, \tag{2.27}$$

which depends on the shock strength, u_s, the steady-state shock strength, u_{0s}, and the parameters $k > 0$ and $\alpha \geq 0$. Remembering the connection with the weakly nonlinear model, where $f = q\lambda_x/2$, we require that

$$\int_{-\infty}^{0} f(x, u_s)\ dx = \frac{q}{2}, \tag{2.28}$$

and thus renormalize f as follows:

$$f \to \frac{q}{2}\frac{f}{\int_{-\infty}^{0} f dx} = \frac{q}{\left(1 + \mathrm{Erf}\left[\frac{k\left(\frac{u_s}{u_{0s}}\right)^{-\alpha}}{2\sqrt{\beta}}\right]\right)\sqrt{4\pi\beta}}\exp\left[-\frac{\left(x + k\left(\frac{u_{0s}}{u_s}\right)^{\alpha}\right)^2}{4\beta}\right].$$

Next, the variables are rescaled as follows: $u = u_{0s}\tilde{u}, \quad x = k\tilde{x}, \quad t = k\tilde{t}/u_{0s}$, and $\beta = k^2\tilde{\beta}$. Using $u_{0s} = 2\zeta\sqrt{q}$, that follows from (2.12) and (2.28), equation (2.6) takes the following dimensionless form

$$\tilde{u}_{\tilde{t}} + \left(\frac{\tilde{u}^2}{2} - \frac{\tilde{u}\tilde{u}\left(0,\tilde{t}\right)}{2}\right)_{\tilde{x}} = \tilde{f}(\tilde{x},\tilde{u}_s), \tag{2.29}$$

where

$$\tilde{f}(\tilde{x},\tilde{u}_s) = \frac{1}{4\zeta^2\left(1+\mathrm{Erf}\left[\frac{\tilde{u}(0,\tilde{t})-\alpha}{2\sqrt{\tilde{\beta}}}\right]\right)}\frac{1}{\sqrt{4\pi\tilde{\beta}}}\exp\left[-\frac{\left(\tilde{x}+\left(\tilde{u}\left(0,\tilde{t}\right)\right)^{-\alpha}\right)^2}{4\tilde{\beta}}\right]. \tag{2.30}$$

This equation contains only three parameters, α, which is a measure of the shock-state sensitivity of the source function (analogous to the activation energy in Euler detonations), $\tilde{\beta} = \beta/k^2$, which is the width of $\tilde{f}$ (analogous to the ratio of the reaction-zone length, $\sqrt{\beta}$, and the induction-zone length, k), and ζ, which is the overdrive factor. The role of the latter is now easily appreciated: it scales the forcing term by ζ^{-2} such that the overdrive reduces the magnitude of the forcing and hence has a stabilizing effect.

Our focus below is on the Chapman-Jouguet case, $\zeta = 1$, which leaves only α and β as the parameters of the model. We shall examine overdriven cases in Chapter 4. Although the expression for the forcing is a little bit cumbersome, its shape is simply that of a Gaussian shifted to the left of $x = 0$ by $\tilde{u}(0,\tilde{t})^{-\alpha}$ and renormalized to integrate to a constant on $(-\infty, 0)$. A few examples of $\tilde{f}$ are shown in Figure 2.1 for different values of u_s and fixed α, β. The main qualitative feature of $\tilde{f}$ is that it has a maximum at some distance from $x = 0$ and that the maximum is close to the shock when u_s is large and far from the shock when u_s is small. These features mimic the behavior of the reaction rate in the Euler equations as a function of the

lead-shock speed.

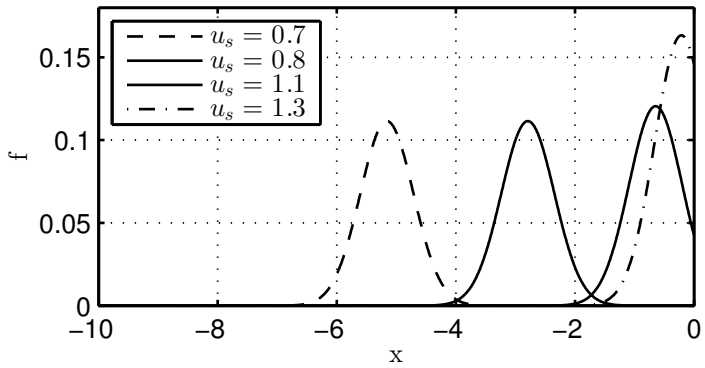

Figure 2.1: The forcing function, f, at various u_s.

From now on, we drop the tilde notation, but it should be understood that all the variables below are dimensionless.

2.4.1 Steady-state solutions

The steady state Chapman-Jouguet solutions can be computed as shown in Subsection 2.3.2. Figure 2.2 shows how β affects the traveling wave profile. The picture suggests a square wave in the limit $\beta \to 0$.

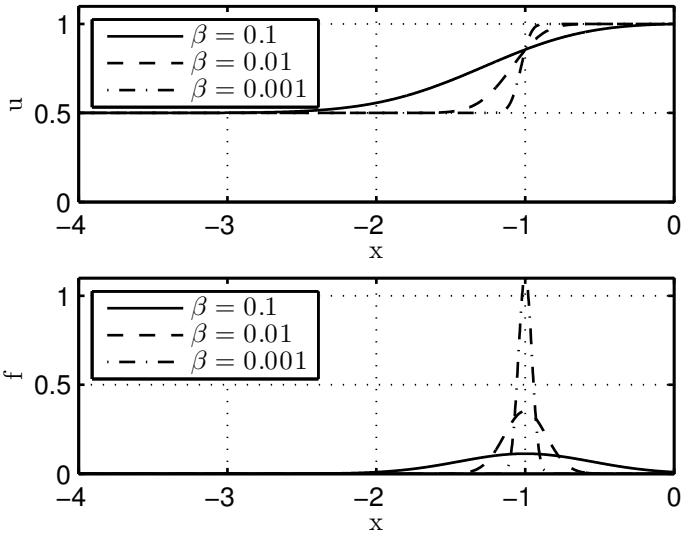

Figure 2.2: Steady-state solution profiles and the forcing function as β is varied.

It is important to remember that α plays no role in the steady state profiles since $u_{0s} = 1$ in dimensionless form. In some sense, α represents the sensitivity to changes in the steady profile. Next, we study the linear stability of these traveling wave profiles in the $\alpha - \beta$ parameter space.

2.4.2 Linear stability analysis

2.4.2.1 The dispersion relation

By Theorem 1, spectral instability is equivalent to (2.20) provided $\|b_0\|_{L^1} < \infty$. A straightforward computation shows that

$$\|b_0\|_{L^1} = \int_{-\infty}^{0} \left| \frac{\partial f}{\partial u_s}(x, u_{0s}) + \frac{f(x, u_{0s})}{2c_0(x)} \right| dx < \infty,$$

and therefore spectral stability of (2.29) is equivalent to

$$\int_{-\infty}^{0} b_0(\xi)\, e^{-\sigma p(\xi)} d\xi = c_0(0),$$

where b_0, c_0, and p are defined as in Subsection 2.3.3. Although we have reduced the spectral stability of our problem to finding complex roots of a single equation, the equation is (although analytic in σ) numerically difficult. For a given α and β, an equation with three levels of nested integration must be solved,

$$\int_{-\infty}^{0} \left(\frac{\partial f(\xi, u_{0s})}{\partial u_s} + \frac{\partial}{\partial \xi} \sqrt{\frac{1}{2} \int_{-\infty}^{\xi} f(y, u_{0s})\, dy} \right) \exp\left[-\sigma \int_{\xi}^{0} \frac{dx}{\sqrt{2 \int_{-\infty}^{x} f(y, u_{0s})\, dy}} \right] d\xi = \frac{u_{0s}}{2}, \tag{2.31}$$

where $\sigma = \sigma_r + i\sigma_i$ and f is given by (2.30). Interestingly, the original formulation of the linear stability problem by Erpenbeck [14] requires the same three levels of numerical integration (the steady-state solution, then the solution of the adjoint homogeneous problem, and then the evaluation of the dispersion relation). Due to the highly oscillatory nature of the exponential term in (2.31), in general, these integrals require nearly machine-precision evaluation of the functions in the integrands in order to obtain the eigenvalues with only a few significant digits of accuracy. Except for the limiting case of $\beta = 0$, we find the roots numerically using Matlab's *fsolve* function, which uses a version of Newton's method, and then we use Cauchy's argument principle to verify that we have found all the roots in a given region of the complex plane. When $\beta = 0$, we compute the roots analytically, and they serve as initial guesses in the numerical continuation root-finding procedure when β is small.

2.4.2.2 The square-wave limit

When $\beta \to 0$, we obtain the square-wave solution. In this limit, it can be shown that

$$\frac{\partial}{\partial u_s} f(x, u_{0s}) = -\alpha \frac{\partial}{\partial x} f(x, u_{0s}) + O\left(\frac{1}{\sqrt{\beta}} e^{-\frac{1}{4\beta}}\right) f(x, u_{0s}).$$

Even though $f(x, u_{0s})$ tends to a delta function when $\beta \to 0$, this function is integrated in the dispersion relation and, therefore, the contribution of the second term above to the dispersion relation is exponentially small in the limit due to the

$O\left(\frac{1}{\sqrt{\beta}}e^{-\frac{1}{4\beta}}\right)$ factor. In the limit, the dispersion relation (2.20) becomes

$$\begin{aligned}\int_{-\infty}^{0} b_0(x)\ e^{-\sigma p(x)}dx &= \int_{-\infty}^{0}\left(\frac{\partial f}{\partial u_s}(x,u_{0s})+\frac{1}{2}\frac{\partial}{\partial x}(c_0(x))\right)e^{-\sigma p(x)}\ dx\\ &= \int_{-\infty}^{0}\left(-\alpha\frac{\partial f}{\partial x}(x,u_{0s})\right)e^{-\sigma p(x)}dx\\ &+ \int_{-\infty}^{0}\left(\frac{1}{2}\frac{\partial}{\partial x}(c_0(x))\right)e^{-\sigma p(x)}\ dx+O\left(\frac{1}{\sqrt{\beta}}e^{-\frac{1}{4\beta}}\right).\end{aligned}$$

Integrating by parts and ignoring the small $O\left(\frac{1}{\sqrt{\beta}}e^{-\frac{1}{4\beta}}\right)$ term, we find that

$$\begin{aligned}-\alpha\int_{-\infty}^{0}\frac{\partial f}{\partial x}(x,u_{0s})\,e^{-\sigma p(x)}dx+\frac{1}{2}\int_{-\infty}^{0}\frac{\partial}{\partial x}(c_0(x))\,e^{-\sigma p(x)}dx &= c_0(0),\\ -\alpha\left[f(0,u_{0s})-\sigma\int_{-\infty}^{0}\frac{f(x,u_{0s})}{c_0(x)}e^{-\sigma p(x)}dx\right]+\frac{1}{2}\int_{-\infty}^{0}\frac{\partial}{\partial x}(c_0(x))\,e^{-\sigma p(x)}dx &= c_0(0),\\ -\alpha f(0,u_{0s})+\left(\alpha\sigma+\frac{1}{2}\right)\int_{-\infty}^{0}\frac{\partial}{\partial x}(c_0(x))\,e^{-\sigma p(x)}dx &= c_0(0),\\ -\alpha f(0,u_{0s})+\left(\alpha\sigma+\frac{1}{2}\right)\left[c_0(0)-\sigma\int_{-\infty}^{0}e^{-\sigma p(x)}dx\right] &= c_0(0),\\ -\alpha f(0,u_{0s})+\alpha\sigma c_0(0)-\left(\alpha\sigma^2+\frac{\sigma}{2}\right)\int_{-\infty}^{0}e^{-\sigma p(x)}dx &= \frac{c_0(0)}{2},\\ -\alpha f(0,u_{0s})+\alpha\sigma c_0(0)-\left(\alpha\sigma^2+\frac{\sigma}{2}\right)\int_{0}^{\infty}c_0(x)e^{-\sigma z}dz &= \frac{c_0(0)}{2}.\end{aligned}$$

Noticing that in the limit $\beta\to 0$,

$$c_0(x)\to\begin{cases}\frac{1}{2} & x\geq -1\\ 0 & x<-1\end{cases},\qquad p(x)=\int_x^0\frac{dy}{c_0(y)}\to\begin{cases}\infty & x<-1\\ -2x & x\geq -1\end{cases},$$

we obtain

$$\lim_{\beta\to 0}\left[-\alpha f(0,u_{0s})+\alpha\sigma c_0(0)-\left(\alpha\sigma^2+\frac{\sigma}{2}\right)\int_0^\infty c_0\left(p^{-1}(z)\right)e^{-\sigma z}dz-\frac{c_0(0)}{2}+o(1)\right]=$$
$$\frac{\alpha\sigma}{2}-\left(\frac{\alpha\sigma^2}{2}+\frac{\sigma}{4}\right)\int_0^2 e^{-\sigma x}dx-\frac{1}{4}=$$
$$\left(\frac{\alpha\sigma}{2}+\frac{1}{4}\right)e^{-2\sigma}-\frac{1}{2}=0.$$

Therefore, the dispersion relation in the square-wave limit takes a very simple form of a transcendental equation,

$$e^{2\sigma}=\alpha\sigma+\frac{1}{2}. \tag{2.32}$$

This dispersion relation has exactly the same form as that of Fickett's analog [28], which in his case, arose from his differential-difference equation for shock perturbation. Therefore, it predicts the same pathological instability as in the classical square-wave detonations. Pathological instability implies that the linear stability problem for the square wave is ill-posed in the sense of Hadamard. For completeness, we exhibit below the solutions to this equation, since they are used as initial guesses in our algorithm to compute the solutions when β is small, but not zero. Let $\sigma=\sigma_r+i\sigma_i$ and separate the real and imaginary parts of (2.32),

$$e^{2\sigma_r}\cos(2\sigma_i)=\alpha\sigma_r+\frac{1}{2},\qquad e^{2\sigma_r}\sin(2\sigma_i)=\alpha\sigma_i.$$

If σ_r is to be large, the first equation requires $\cos(2\sigma_i)$ to be small, i.e., σ_i should be close to $\pi/4+n\pi/2$, $n=0,1,2,....$ We let

$$\sigma_i=\frac{\pi}{4}+\frac{n\pi}{2}+\varepsilon, \tag{2.33}$$

where ε is a small correction. From the second equation above, we find $\sin(2\sigma_i) \approx 1$ and therefore $\sigma_r \approx \frac{1}{2}\ln(\alpha\sigma_i)$. For this σ_r to be large, we need n to be large, in which case

$$\sigma_r \approx \frac{1}{2}\ln(n). \tag{2.34}$$

Thus, the square-wave dispersion relation admits arbitrarily large growth rates that occur at simultaneously large frequencies. It is interesting that the growth rate increases with frequency logarithmically. Similar growth happens in the square-wave model of detonations in the reactive Euler equations (see, e.g., [56, 57]). However, in the latter, the dispersion relation involves several exponential functions due to the presence of multiple time scales associated with different families of waves propagating from the shock into the reaction zone. Waves of different families of characteristics propagate at different speeds resulting in several different time intervals for the signals to propagate from the shock to the "fire" and back. Since in the limit of large frequencies one of the exponentials dominates, the dispersion relation becomes essentially the same as in our model. In the numerical calculations of detonation instability in the Euler equations with finite-rate chemistry, but high activation energies [18], a similarly slow growth can be seen. However, we do not know if the growth is logarithmic in frequency.

Remark 5. Theorem 2 is not contradicted here since $\|b_0 c_0\| \notin L^\infty$ in the limit, because now $f \notin L^\infty$.

2.4.2.3 The unstable spectrum for $\beta > 0$

The pathological instability of the model as $\beta \to 0$ was shown to be caused by an infinite number of unstable eigenvalues, with the real part arbitrarily large. From Theorem 2, we know that if $\|b_0 c_0\|_{L^\infty} = M < \infty$, then there can be no unstable

eigenvalues with $\sigma_r > M/c_0(0)$. A quick computation shows that if $\alpha < \infty$ and $\beta > 0$, then the real part of the unstable spectrum of (2.29) is bounded from above.

Next, we fix $\alpha = 4.05$ and numerically investigate the effect of β on the eigenvalues. Using as initial guess the eigenvalues found from the square-wave dispersion relation, (2.32), we use Matlab's numerical root finder, *fsolve,* to locate the eigenvalues for successively larger values of β [2]. Figure 2.3a shows the results, reaffirming that for any value of $\beta > 0$, there is only a finite number of unstable eigenvalues. Furthermore, it suggests that the magnitude of β is closely related to the frequencies of the unstable eigenvalues. This can be understood as follows: as the shock is perturbed, it creates waves that propagate into the reaction zone. If β is large enough, the reaction zone is smooth and there is little resonance between the shock and the peak of the reaction in the reaction zone. However, as β is decreased, the sharp peak in the reaction zone reflects waves back to the shock and this resonance causes the instability. If β is small but positive, then high enough frequencies do not "see" the sharp peak in the reaction rate and are not reflected back to the shock. A similar mechanism is at work in Euler detonations as well. For example, in [59], as the length of the main heat-release layer is decreased relative to that of the induction zone, the detonation is found to become more unstable.

We also look at the effect of α on the distribution of the eigenvalues. In Fig. 2.3b, we show the spectrum for fixed $\beta = 0.001$ and varying α. This figure suggests that the eigenvalues are merely shifted when α is decreased. Interestingly, the imaginary part of the dominant eigenvalue, i.e. the one with the largest real part, is always the same as we change α and keep β fixed. This observation was tested for different values of

[2] The roots of the dispersion relation when $\beta = 0$ are close to the roots when $\beta \gtrapprox 0$ for eigenvalues which are not very oscillatory (σ_i not too large). However, the highly oscillatory roots are stable when $\beta \gtrapprox 0$, but unstable when $\beta = 0$, and therefore we expect the initial guesses coming from the $\beta = 0$ case to be far off in those cases.

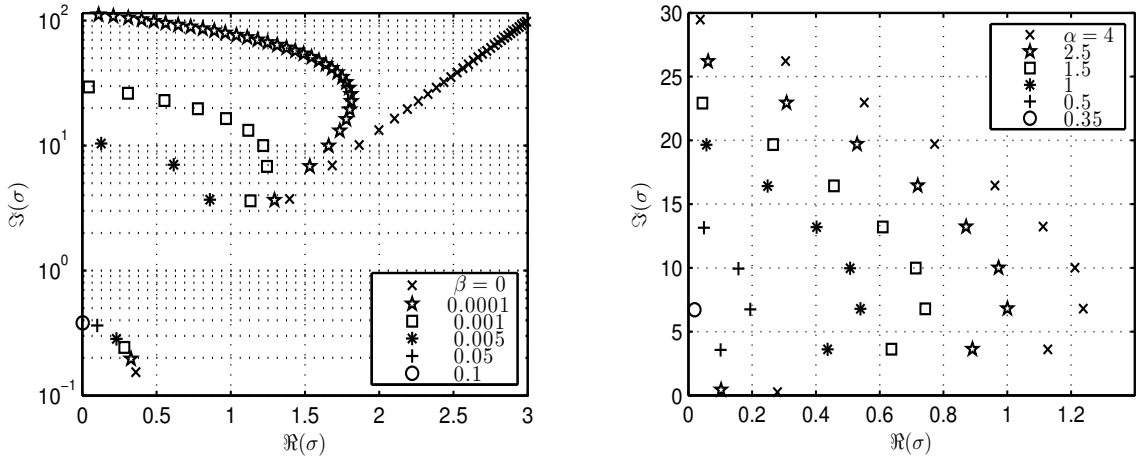

(a) The spectrum for $\alpha = 4.05$ with β varied. (b) The spectrum for $\beta = 0.001$ with α varied.

Figure 2.3: The linear spectrum.

β. As β decreases, the frequency of the most unstable mode is seen to increase.

To ensure that no roots of the dispersion relation have been lost in the numerical computations, we apply the argument principle to (2.20). Since

$$F(\sigma) = \int_{-\infty}^{0} b_0(\xi)\, e^{-\sigma p(\xi)} d\xi - c_0(0)$$

has no poles in the region $\sigma_r \geq 0$ (which follows from $\|b_0\|_{L_1} < \infty$), the argument principle guarantees that the number of zeros, N, of $F(\sigma)$ in a closed contour C (counting multiplicity) is given by

$$N = \frac{1}{2\pi i} \int_C \frac{F'(z)}{F(z)} dz. \tag{2.35}$$

This can be related to the winding number of a curve by the substitution $w = F(z)$, which yields $N = \frac{1}{2\pi i} \int_{F(C)} dw/w$. We show in Figure 2.4 two Nyquist plots of the dispersion relation, corresponding to parameters with 2 and 20 unstable eigenvalues. The predictions agree with the number of roots found using the root solver.

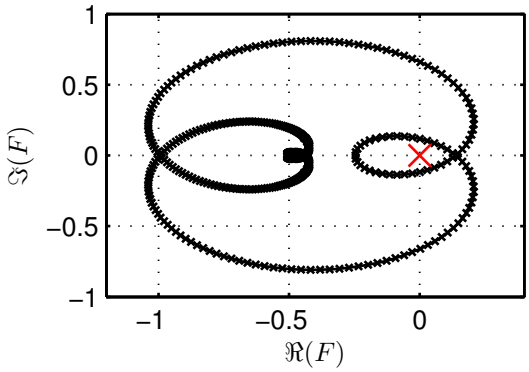

(a) $\alpha = 4.05$, $\beta = 0.05$. Weakly unstable case with two eigenvalues, one shown in Fig. 2.3 and the other its complex conjugate.

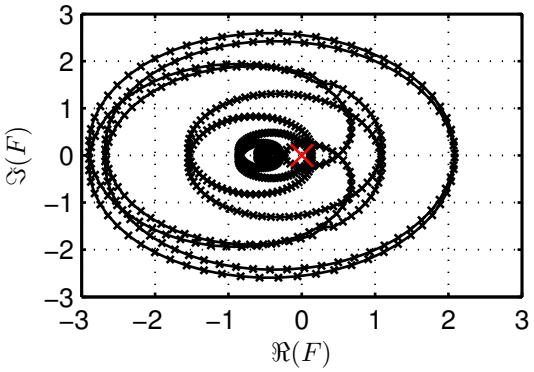

(b) $\alpha = 4.05$, $\beta = 0.005$. Highly unstable case with twenty eigenvalues, ten shown in Fig. 2.3 and their complex conjugates.

Figure 2.4: Values of $w = F(z)$ along a large semi-circle in the right-half plane of the z-plane (radius 10 for 2.4a and 100 for 2.4b), plotted in the F-plane. The total number of loops around the origin in the F-plane gives the winding number, which is equal to the number of unstable eigenvalues.

2.4.2.4 The neutral curves

We follow the first five unstable eigenvalues (ordered according to their imaginary part) and show their neutral curves in Figure 2.5. We see that for large values of β, the lowest frequency eigenvalue is the one that first becomes unstable, but for very small values of β, the stability of the traveling wave is controlled by the higher frequency perturbations. Moreover, the smaller the β, the higher the frequency of the most unstable mode, consistent with our earlier calculation of the square-wave-limit pathology. The whole unstable region is given by the union of the unstable regions for each eigenvalue and is generally located at large-enough α for any given β or small-enough β for any given α.

2.4.3 Numerical simulations

The previous subsection was concerned with the linear stability of traveling wave solutions of (2.29). We were able to compute the spectrum of unstable modes and

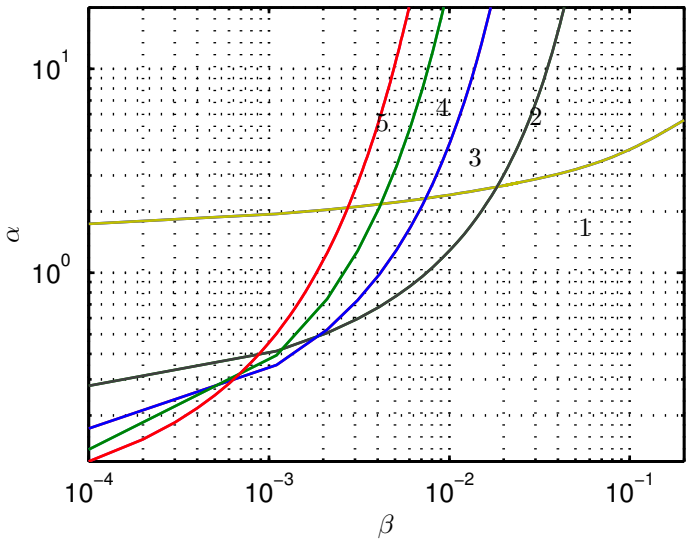

Figure 2.5: The neutral curves for the first five eigenvalues. The numbers next to each curve correspond to the index of the eigenvalue. Below the envelope of the curves we have spectral stability.

obtain the neutral curves in the $\alpha - \beta$ parameter space. In this subsection, we investigate the behavior of solutions in the nonlinear regime by numerically solving the PDE using the algorithm described in Appendix A. All the simulations start with a steady-state solution, and instabilities (when present) are triggered by the numerical discretization error alone. The goal of this section is to demonstrate that, as in detonation waves in the reactive Euler equations, the shock-dynamics goes through a Hopf bifurcation followed by a period doubling cascade, when the sensitivity parameter, α, is varied, suggesting a possible chaotic regime for large-enough α.

2.4.3.1 Linear growth and comparison with stability analysis

We first compare the results obtained from the linear stability analysis with the numerical results from the simulation. We perform a least-squares fit on the deviation from the steady-state value of the form $\sum_{k=1}^{n} c_k e^{\sigma_{r_k} t} \cos(\sigma_{i_k} t + \delta_k)$, where n is the number of unstable eigenvalues found in the linear stability analysis. For instance,

when $\beta = 0.1$ and $\alpha = 4.05$, we expect from Fig. 2.3 one unstable mode to appear, and thus, at least for a small time interval, we expect the solution to behave like $e^{\sigma_k t}$, up to translation and scaling. The results obtained from the comparison are presented in Table 2.1. We restrict ourselves to fitting up to two eigenvalues (8 parameters), and fit up to a time when the perturbation is of the order 10^{-7}. The original perturbation is of the order 10^{-15}.

β	σ from theory	σ from numerics
0.10	$0.00309 + 0.38144i$	$0.00311 + 0.38152i$
0.01	$0.20092 + 0.30431i$	$0.20581 + 0.29964i$
	$0.61295 + 3.78512i$	$0.61298 + 3.78507i$

Table 2.1: Comparison of eigenvalues from stability analysis and from numerics at $\alpha = 4.05$.

The first case of $\beta = 0.1$ in Table 2.1 is near the neutral curve, and both the growth and frequency of the perturbation are well captured by the linear stability predictions. Simulations show that for this "slightly unstable" regime, the predicted frequency is valid well into the nonlinear regime, an observation often made in detonation simulations as well. In the second case, when $\beta = 0.01$, we see a larger discrepancy between the linear theory and the numerical simulations, especially when capturing the effect of the least unstable mode. This is to be expected, since the effects of all unstable modes except for the most unstable one quickly become negligible as the dominant mode starts to grow. This second case is far from the neutral curve and much more unstable, with the growth rate two orders of magnitude larger than in the first case. Very fast growth of the perturbations is likely to result in nonlinear effects starting to play an important role early.

2.4.3.2 Limit cycles and period-doubling bifurcations

We now study the long-time asymptotic behavior of solutions that start from a small perturbation (given by the discretization error) of the initial steady-state solution. The shock value of the solution, $u_s(t)$, is analyzed. For all the simulations that follow, we fix $\beta = 0.1$ and vary α. When α slightly exceeds the critical value $\alpha_c \approx 4.02$, predicted by the linear analysis as the neutral boundary, the numerical solutions show that the steady-state solution is unstable with the long-time evolution leading to a limit cycle.

For a range of α between α_c and $\alpha_1 \approx 4.72$, the long time dynamics is that of a simple limit cycle (Figure 2.6a). Subsequent increase of α leads to a period doubling bifurcation. When α is between α_1 and $\alpha_2 \approx 4.91$, we observe the limit cycle shown in Figure 2.6c. This period doubling process continues until eventually, at $\alpha = \alpha_\infty \approx 4.97$, the solution (apparently) becomes chaotic. Figure 2.6e illustrates the behavior of $u_s\,(t)$ for very large values of t (around $20,000$), when all the transients are likely to have vanished. The respective power spectra, computed using a large time window, $10,000 < t < 22,000$, are also shown. In the periodic case, the power spectrum is clearly marked by peaks in the natural frequency and its harmonics, as seen in Figure 2.6b and Figure 2.6d. In Figure 2.6f, although there is a dominant frequency in the signal, many other frequencies are present, indicating possible aperiodicity or chaos. Further analysis of the computational results is required to establish whether the solution is indeed chaotic, which is done in the subsequent sections.

Although we focus on $u_s(t)$, the behavior presented in Figure 2.6 is not unique to the shock value. That said, we must pick an "interesting" point, meaning a point close enough to the shock, if we want to capture the rich dynamics. After the Hopf bifurcation occurs, $u\,(x,t)$ is periodic in time and as the bifurcation parameter (α

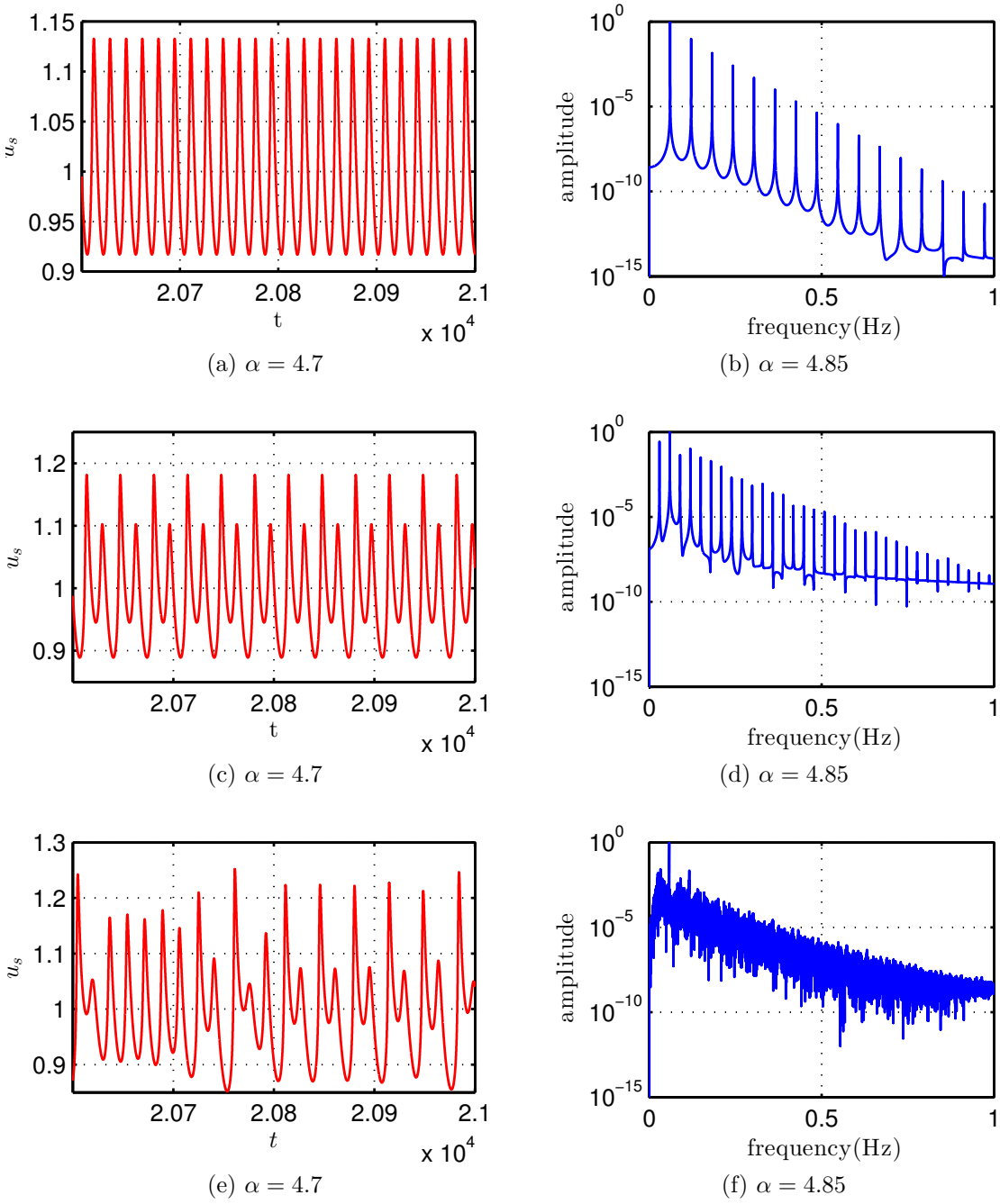

(a) $\alpha = 4.7$ (b) $\alpha = 4.85$

(c) $\alpha = 4.7$ (d) $\alpha = 4.85$

(e) $\alpha = 4.7$ (f) $\alpha = 4.85$

Figure 2.6: Left column – $u_s(t)$ for β=0.1 and different values of α. Right column – corresponding power spectra.

in this case) is increased further, $u(x,t)$ appears to become chaotic. This is illustrated in Figure 2.7, where the color represents $u(x,t)$ and the white lines are the characteristics.

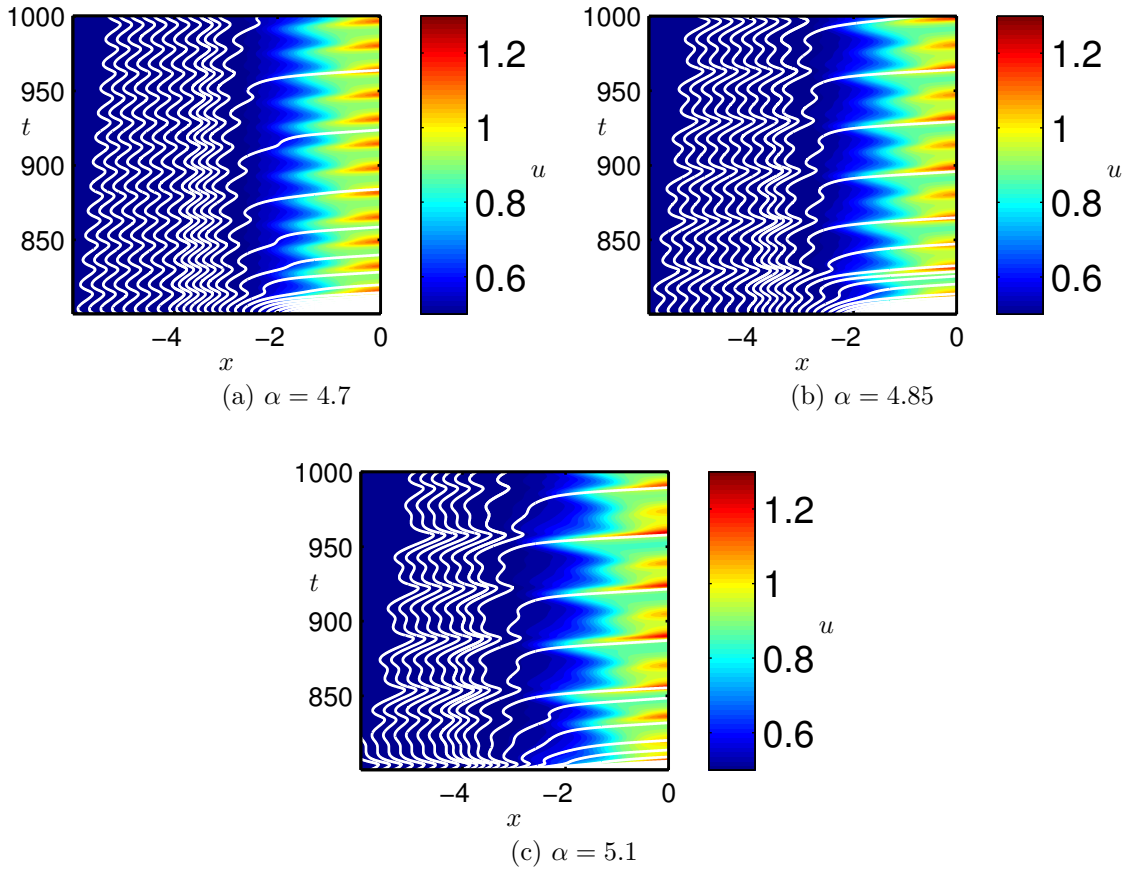

(a) $\alpha = 4.7$

(b) $\alpha = 4.85$

(c) $\alpha = 5.1$

Figure 2.7: Characteristic fields (white curves) at various α, at periods 1, 2, and chaotic. The color shows the magnitude of u.

The bifurcation process is best illustrated by means of a bifurcation diagram, where the local maxima of the shock value, $u_s(t)$, are plotted at different values of the bifurcation parameter α (Figure 2.8).

The bifurcation points, presented in Table 2.2, are used to compute the Feigenbaum number, which appears to approach the well-known constant $\delta \approx 4.669$.

n	1	2	3	4	5
α_n	4.02	4.7202	4.9100	4.95565	4.96553
F_n	$\cdots$	$\cdots$	3.69	4.16	4.62

Table 2.2: Bifurcation points.

The bifurcation diagram in Figure 2.8 and the power spectra in Figure 2.6 all sug-

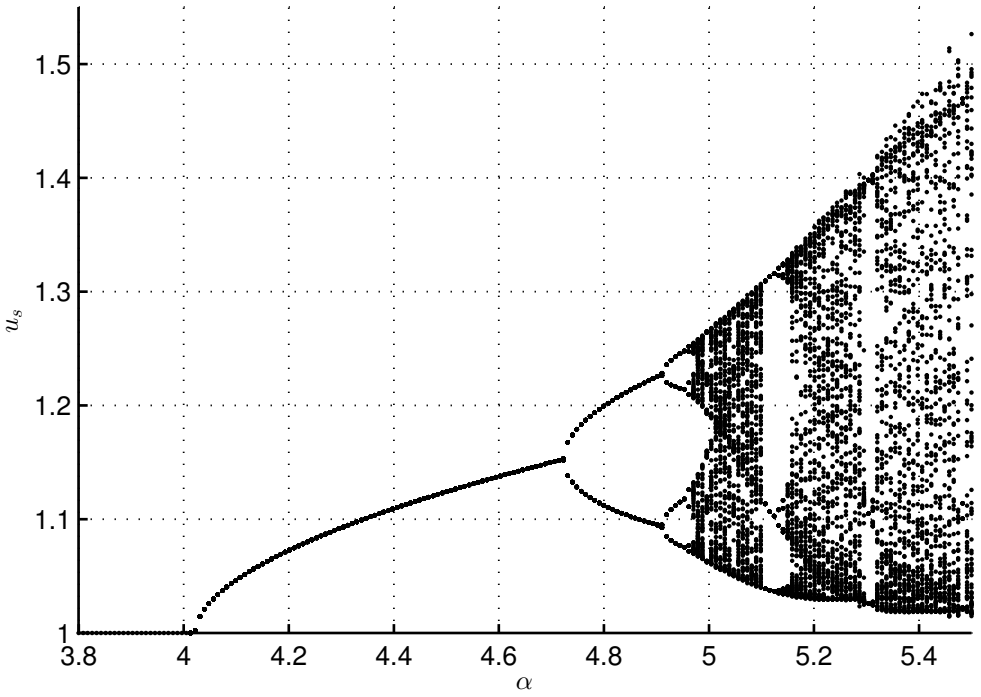

Figure 2.8: The bifurcation diagram showing the local maximum, $u_s^{\max}$ for $\beta = 0.1$ and varying α

gest (although they do not prove) that the chaos in the system is real. In Subsection 2.4.4, we analyze the apparently chaotic series of $u_s(t)$ at very large t, i.e., on the attractor.

An interesting feature of the example presented above is that, as in the reactive Euler equations (e.g., [60]), inner shocks can form inside the smooth region, $x < 0$. These shocks subsequently overtake the leading shock, rendering its dynamics non-smooth. The inner-shock formation is simply due to the wave breaking and it depends on the initial data as well as the parameters in f. For example, as the parameter α, which controls the shock-state sensitivity, is increased, the characteristics are seen to converge toward each other at large t, until, at a critical value of α, the characteristics collide into an inner shock. This shock then overtakes the leading shock at $x = 0$ as shown in Figure 2.9. A point to emphasize is that the characterization of chaos when

such non-smooth dynamics is present is not easy, in particular due to difficulties of computing the solution with high accuracy. Our analysis of chaos is therefore limited to moderate values of α, when we know that the internal shock does not form, yet a chaotic signal is observed.

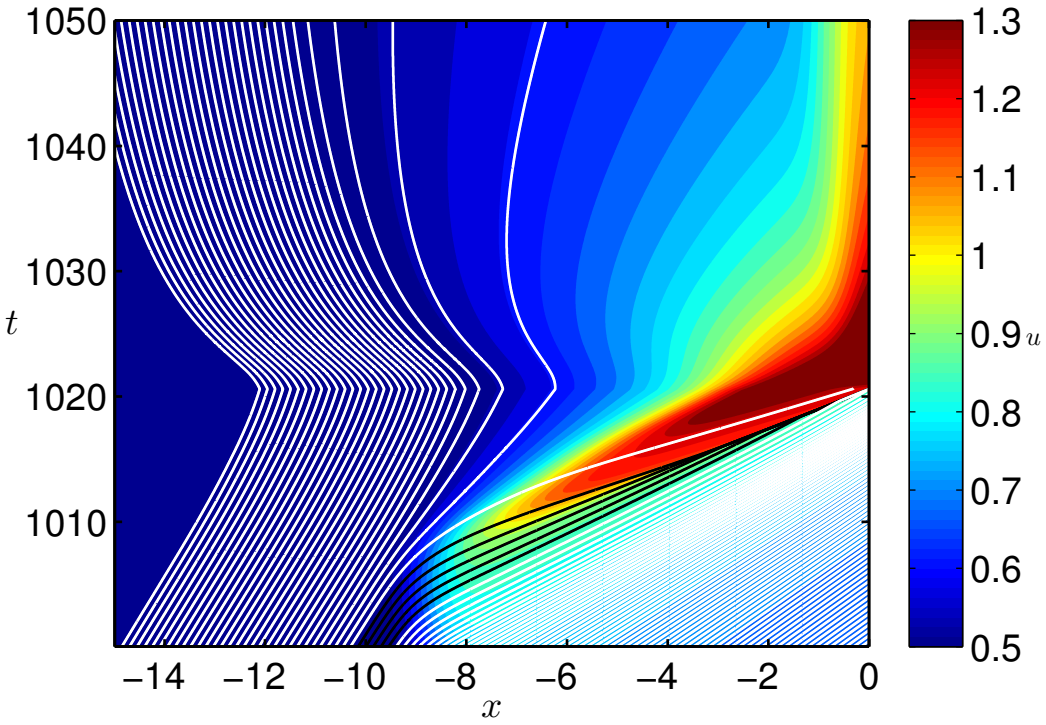

Figure 2.9: Formation of an internal shock wave. The vertical axis is t and the horizontal axis is x. The color shows the magnitude of u. White curves are the forward characteristics.

2.4.4 Time series analysis

In this section, we use tools of dynamical systems to understand the shock signal. The shock signal represents a one-dimensional measurement of the infinite dimensional phase space where the solutions live. Relying on Takens theorem [61], we embed the signal in higher dimensions by choosing a delay, τ, and an embedding dimension, m. We then use this embedded m-dimensional signal to compute quantities of interest,

such as the correlation dimension and the largest Lyapunov exponent. The numerical calculations are performed using the open source software OPENTSTOOL [62].

2.4.4.1 Delay reconstruction of the attractor

We embed the signal $u_s^n = u_s(t_n)$ in m-dimensions by creating the points

$$\begin{aligned} p_1 &= (u_s^1, u_s^{1+\tau}, \cdots, u_s^{1+(m-1)\tau}), \\ p_2 &= (u_s^2, u_s^{2+\tau}, \cdots, u_s^{2+(m-1)\tau}), \\ &\vdots \quad \vdots \quad \vdots \\ p_N &= (u_s^N, u_s^{N+\tau}, \cdots, u_s^{N+(m-1)\tau}), \end{aligned}$$

where N is limited by the number of available values of u_s. The m-dimensional points $(p_1, \cdots, p_N)$ then live in an attractor of dimension at most m. It was shown by Takens that provided $m > 2d + 1$, where d is the dimension of the attractor where u_s lives, there exists a diffeomorphism between the reconstructed attractor and the "actual" attractor (in the limit of the infinite amount of noise-free data). This immediately allows us to use the reconstructed attractor to compute quantities such as the correlation dimension and the Lyapunov spectrum.

Notice that although in theory any choice of τ will allow such reconstruction, in practice the situation is quite delicate. The finite amount of noise-polluted data makes the choice of τ a non-trivial issue, still subject of much current research. Since no fail-proof method appears to exist, we choose τ as the first minimum of the mutual information function of u_s. The reasons for such a choice can be found in [63]. In the next subsection, we explore how the reconstructed attractor, its dimension, and the largest Lyapunov exponent change as we vary the sensitivity parameter, α. We choose $\alpha = 4.7, 4.85, 4.96, 4.97, 5, 5.1$ and see how these quantities change as the dynamic goes

from periodic to chaotic.

2.4.4.2 Largest Lyapunov exponent (LLE)

A chaotic system is characterized by at least one positive Lyapunov exponent. This means that information must be lost in the system as time progresses. Predictability is thus highly limited. Because the largest Lyapunov exponent (LLE) determines the dominant rate at which information is lost, we are primarily interested in the LLE. The magnitude of the LLE gives an indication of how quickly nearby trajectories in the phase space diverge as time progresses. The inverse of the LLE is an estimate of the relevant time scale for this divergence. Thus, the larger the LLE, the more chaotic the dynamics are. In particular, Table 2.3 shows how sensitive this exponent is to small changes in the parameter α near the onset of chaos, where α is the "activation energy" parameter, measuring the sensitivity of the reaction to the shock strength. Several methods are available to compute the LLE, and we choose to use the one presented in [64]. The algorithm used here is discussed in Appendix B.

The sequence of period doubling bifurcations observed in Figure 2.8 and Table 2.2 suggests that the sequence first saturates at $\alpha_c \approx 4.97$. After this critical value, the solution seems to become aperiodic, as indicated by its power spectrum. We compute the LLE for values of α slightly below and slightly above α_c in order to illustrate the drastic change in the magnitude of LLE. The values of LLE are presented in Table 2.3, where the error estimates are merely educated guesses of a confidence interval obtained from running the algorithm for different embedding dimensions (from dimension 3 to 10). It is particularly difficult to obtain quantitative error estimates because the sources of error are unknown and the algorithm requires some subjective choice of a "range" (see Appendix B).

A study of the dependence of the LLE on the embedding dimension is presented

α	4.85	4.96	4.97	5	5.1
LLE	0	0	$0.004 \pm 2 \cdot 10^{-4}$	$0.018 \pm 3 \cdot 10^{-5}$	$0.032 \pm 8 \cdot 10^{-4}$
D_C	$1 \pm 3 \cdot 10^{-4}$	$1 \pm 2 \cdot 10^{-2}$	$1.67 \pm 7 \cdot 10^{-2}$	$1.87 \pm 3 \cdot 10^{-2}$	$1.91 \pm 2 \cdot 10^{-2}$

Table 2.3: The largest Lyapunov exponent and correlation dimension for different values of α, the bifurcation parameter.

in the Chapter B. Although precise error estimates are not available, there is still some value in the predictions made; namely, a clear difference is observed between $\alpha = 4.96$ and $\alpha = 4.97$, which corresponds to the apparent saturation point of the bifurcation diagram presented in Figure 2.8.

2.4.4.3 Correlation dimension estimate

While the Lyapunov exponent measures the rate at which information is lost in a dynamical system, the correlation dimension gives an upper bound on the number of degrees of freedom a system has. This is an important concept to distinguish deterministic chaos from stochastic chaos. For simple attractors, the correlation dimension is an integer, but for strange or chaotic attractors the dimension is fractal. We compute the correlation dimension of our time series using the algorithm presented in [65] (see Appendix C for details of the algorithm). The results for different values of α are shown in Table 2.3. The magnitude of D_C is seen to be about 1.9 in the chaotic regime. The implication is that the dynamics of the system is nearly two-dimensional, i.e., a two-dimensional phase space is, in principle, sufficient to describe the observed dynamics (locally). Of course, this gives no hint at what that description should be, but the importance of D_C is in providing an estimate of the degrees of freedom involved.

2.5 Conclusions

A simple model equation consisting of an inviscid Burgers equation forced with a term that depends on the current shock speed was analyzed by calculating its steady-state solutions, the linear stability properties of these solutions, and the nonlinear, time-dependent evolution that starts with the steady state as an initial condition. It was found that the theory and numerical results for the model equation parallel those of the reactive Euler equations of one-dimensional gas dynamics, which have been extensively used to describe detonation waves.

The steady-state theory of the model is analogous to that of the ZND theory of detonation, describing both self-sustained and overdriven solutions. The normal-mode linear stability theory of the model is qualitatively similar to the detonation stability theory, reproducing comparably complex spectral behavior. The nonlinear dynamics, computed with a high-accuracy numerical solver, exhibit the Hopf bifurcation from a stable solution to a limit cycle, together with a subsequent cascade of period-doubling bifurcations, resulting eventually in what is, very likely, chaos. All of these features have their counterparts in the solutions of the reactive Euler equations. The qualitative agreement between the two systems, so drastically different in their complexity, hints at the possibility that a theory for the observed complex dynamics of one-dimensional detonations may in fact be rather simple.

Chapter 3

Detonations with losses: a toy model approach

We consider in this chapter a simplified model for the dynamics of one-dimensional detonations with generic losses, extending the work presented in Chapter 2. It consists of a single partial differential equation that reproduces, at a qualitative level, the essential properties of unsteady detonation waves with losses. In particular, we investigate the effects of shock curvature and friction on the detonation dynamics. To calculate steady-state solutions, a novel approach to solving the detonation eigenvalue problem is introduced that avoids the well-known numerical difficulties associated with the presence of a sonic point. By using unsteady numerical simulations of the simplified model, we also explore the nonlinear stability of steady-state or quasi-steady solutions.

3.1 Introduction

A gaseous detonation is a phenomenon exhibiting rich dynamical features. One-dimensional planar detonations propagate with a velocity that can be steady, periodic, or chaotic [23]. In multiple dimensions, the detonation front includes complex struc-

tures resulting in cellular patterns formed by triple-point trajectories [2, 48]. Quasi-steady curved detonations, characteristic of condensed explosives, possess multiple-valued solutions at a given curvature [51]. The same multiplicity of solutions exists in one-dimensional detonations in the presence of heat and momentum losses [66, 67, 68]. This range of complex dynamical properties of detonations poses a challenge in terms of theoretical understanding of conditions in which they arise and of features they exhibit. The linear stability theory for idealized systems, asymptotic theories of weakly curved detonation, and other asymptotic models have significantly advanced our understanding of the detonation phenomenon (see recent reviews in [51]). However, many problems still require further theoretical study, including the mechanism of detonation cell formation, the nature of critical conditions of detonation propagation in systems with losses, the linear and nonlinear instability in systems described by complex reactions and equations of state, and others.

Elucidation of key physical mechanisms of the complex phenomena of detonation dynamics is greatly facilitated by simplified models, including those of *ad hoc* nature [25]. Such models can highlight in the clearest possible way the processes responsible for a particular qualitative trait in the observed dynamics. A wide range of dynamical properties of one-dimensional detonations, including chaotic solutions, is reproduced in [31] with a simple extension of Fickett's analog [25] to model the chemical reaction with a well-defined induction zone followed by a heat-release zone. In Chapter 2, it was shown that a model consisting of just a single scalar equation is also capable of qualitatively capturing the dynamics of one-dimensional detonations in the reactive Euler equations, including instability and chaos. The most important implication of these simplified models is that the true nature of the complex dynamics of detonations appears to be governed by a simple mechanism, thus providing a strong indication that a rational reduction of the reactive Euler equations that retains the same essential

physical ingredients as the simple models may be feasible.

3.2 A model with generic losses

We recall the model studied in Chapter 2, given by the following equation:

$$\frac{\partial u}{\partial t} + \frac{\partial}{\partial x}\left(\frac{u^2}{2} - \frac{u u_s}{2}\right) = f\left(x, u_s\right), \tag{3.1}$$

where $x \leq 0$ is the reaction zone behind the shock propagating from left to right. Equation (3.1) is written in a shock-attached frame; the shock location is hence at $x = 0$ at all times, t. The unknown, $u\left(x, t\right)$, plays the role of, e.g., pressure, while u_s is the solution u evaluated at the shock, and it is related to the shock speed through shock conditions. The forcing function, f, is chosen to mimic the behavior of the reaction rate in the reactive Euler equations. In particular, it is taken to have a maximum at some distance away from the shock, $x_f = x_f\left(u_s\right)$, with function x_f chosen to depend sensitively on the shock state, u_s. The following choice,

$$f = \frac{a}{\sqrt{4\pi\beta}} \exp\left[-\frac{\left(x + u_s^{-\alpha}\right)^2}{4\beta}\right], \tag{3.2}$$

where $a = \left[4\left(1 + \operatorname{erf}\left(u_s^{-\alpha}/2\sqrt{\beta}\right)\right)\right]^{-1}$, is used in numerical calculations below. In this form, the model is dimensionless with u scaled so that $u_s = 1$ in the steady state (see Section 2.4). Parameters α and β are analogous to the activation energy in the reactive Euler equations with Arrhenius kinetics and to the ratio of the reaction-zone length to the induction-zone length, respectively. Note that the total chemical energy released corresponds to $\int_{-\infty}^{0} f(x, u_s(t))dx$, which is constant for the forcing term (3.2) regardless of the value of $u_s(t)$. This follows from $f \sim \lambda_x$, as discussed in Section 2.2. Thus, the total energy released is always the same even in the presence of instabilities.

Our focus in this section is to explore the effect of generic losses on the solutions of (3.1). For this purpose, we modify the forcing to add a damping term,

$$\frac{\partial u}{\partial t} + \frac{\partial}{\partial x}\left(\frac{1}{2}u^2 - Du\right) = f\left(x, D\right) - g(x, u, \varphi). \tag{3.3}$$

Here, $D = u_s/2$ is the detonation speed, which is obtained using the Rankine-Hugoniot conditions with the state upstream of the shock taken to be $u = 0$, φ is a parameter of the problem, which may be time dependent, and g is a function that represents the loss[69]. Friction losses are modeled by taking $g = c_f u|u|$, with the friction coefficient c_f, while the effects of curvature are modeled by taking $g = \kappa u^2/\left(1 + \kappa x\right)$, where κ is the shock curvature, generally dependent on time.

3.2.1 Steady and quasi-steady solutions

If φ is a constant, then we can search for steady-state solutions of (3.3). If φ is time-dependent, but slowly varying in time, then we search for quasi-steady solutions of (3.3). In both cases, the problem requires solving the following ODE:

$$\left(u - D\right)u' = f\left(x, D\right) - g(x, u, \varphi) \tag{3.4}$$

on $x \in [a, 0]$ with $u(0) = 2D$ as the shock condition. Here and below, primes denote the x derivative, d/dx. The left end of the integration region depends on the context. The main problem is to determine the detonation speed, D, such that the corresponding solution, $u\left(x, t\right)$, of (3.4) is a smooth function of x. This is a nonlinear eigenvalue problem for D because such smooth solutions do not necessarily exist for every D at a given φ. For physically interesting choices of f and g, there usually exists a sonic point where $u = D$, which is a singular point of (3.4). For smoothness of u, it is

necessary that the right-hand side of (3.4) vanishes at the sonic point. These conditions constitute the generalized Chapman-Jouguet conditions of detonation theory and serve to determine the eigenvalue relation, $H(D, \varphi) = 0$, that yields D for a given φ. Typically, $D(\varphi)$ is a multiple-valued function having a turning-point shape.

The nonlinear ODE (3.4) cannot, in general, be solved analytically. Therefore, a numerical integration method is required. In one such method, for a trial value of D, (3.4) is integrated from $x = 0$ toward $x = a$. The correct value of D has to correspond to $u - D = 0$ and $f - g = 0$ at $x = x_*$. These conditions are not satisfied in most cases, and, therefore, equation (3.4) is very stiff as $u \to D$, making the numerical integration prohibitively expensive and/or inaccurate. As an alternative to this method, the sonic locus, $x_*(D, \varphi)$, is found first for a trial value of D. Then, the solution of (3.4) is found analytically in the neighborhood of x_* in order to get out of the sonic point by a small step to $x_* + \Delta x$, with a subsequent numerical integration from $x_* + \Delta x$ toward the shock. For the correct value of D, the Rankine-Hugoniot conditions at $x = 0$ must be satisfied. This algorithm is more robust numerically. However, its drawback is that it requires the knowledge of the sonic state and the ability to solve the equation (or the system of equations, in general) in the neighborhood of the sonic locus analytically. Even though, in our case, it is straightforward to do so, in more complicated problems, this approach is not feasible (see [66] for example). Below we propose a different algorithm that is much simpler, more robust, and easier to generalize.

3.2.2 Transonic integration algorithm

Here, we describe an algorithm for numerical integration of the system of ODE for the transonic structure of traveling-wave solutions of reactive Euler equations in one

spatial dimension. Because the algorithm works for a general one-dimensional system of hyperbolic balance laws, we begin with such a system. Then, we illustrate the method through both the toy model, (3.4), and the reactive Euler equations.

Consider a system of hyperbolic balance laws,

$$\boldsymbol{q}_t + \mathbf{F}(\boldsymbol{q})_x = \mathbf{s}\left(\mathbf{q}\right), \tag{3.5}$$

where $\mathbf{q}$ is the vector of unknowns, $\mathbf{F}$ is the flux vector, and $\mathbf{s}$ is a source term. We look for traveling wave solutions $\boldsymbol{q} = \boldsymbol{q}(x - Dt) = \boldsymbol{q}(\eta)$, consisting of a shock followed by a smooth flow downstream. The state upstream of the shock, $\eta > 0$, is assumed to be uniform and steady, $\boldsymbol{q} = \boldsymbol{q}_a = constant$. Then, $\mathbf{q}$ solves

$$\left(\mathbf{F}(\boldsymbol{q}) - D\boldsymbol{q}\right)_\eta = \mathbf{s} \tag{3.6}$$

in smooth parts of the flow, where $\eta = 0$ is the shock position and $\eta < 0$ is the downstream region. At $\eta = 0$, the following shock conditions are satisfied:

$$-D\left[\mathbf{q}\right] + \left[\mathbf{F}\right] = 0, \tag{3.7}$$

with $[Z] = Z^+ - Z^-$ denoting the jump in the quantity Z across the shock. Given a state ahead and the shock speed, the solution of (3.7) can be written as $\boldsymbol{q}(0^-) = \boldsymbol{q}_{RH}(D, \boldsymbol{q}_a)$. The shock speed, D, is an unknown of the problem and must be found together with the profiles of $\mathbf{q}$ at $\eta < 0$.

A well-known difficulty in solving (3.6) arises when one of the eigenvalues of the matrix $\partial\mathbf{F}/\partial\boldsymbol{q} - D\mathbf{I}$ vanishes at some point $\eta_* < 0$ (a sonic point), thus producing a singular system of ODE, $\left(\partial\mathbf{F}/\partial\boldsymbol{q} - D\mathbf{I}\right)\mathbf{u}_\eta = \mathbf{s}$ [70]. This feature is an essential ingredient of any self-sustained shock wave and is thus relevant in many applications

where such traveling shock-wave solutions arise (e.g., traffic flow problems [71], hydraulic jumps [72]). Should there be a vanishing eigenvalue, a regularity condition is called upon where, for boundedness of $\boldsymbol{q}_\eta$, it is required that

$$\mathbf{l}_* \cdot \mathbf{s}_* = 0 \quad \text{when} \quad \lambda_* = 0, \tag{3.8}$$

where λ_* is the special eigenvalue of $\partial\mathbf{F}/\partial\boldsymbol{q} - D\mathbf{I}$ that vanishes at η_* and $\mathbf{l}_*$ is the corresponding left eigenvector. Condition (3.8) serves as a closure condition that identifies admissible shock speeds, D.

Because analytic integration of (3.6) is rarely possible, a numerical procedure is required. When a vanishing eigenvalue exists somewhere in the flow, we need a numerical algorithm to determine the values of D for which (3.8) is satisfied. Importantly, the location of the critical point is unknown *a priori*. A simple approach to solving this problem is to make a guess for D and integrate from $\eta = 0$ up to the singular point, and then check whether or not $\mathbf{l}_* \cdot \mathbf{s}_* = 0$ is satisfied. This is a numerically ill-conditioned procedure since the system becomes stiffer as one approaches the singular point, the latter generally having a saddle-point nature.

Our integration procedure avoids the numerical problems associated with the presence of a sonic point. The key idea is based on the use of a new dependent variable given by

$$\boldsymbol{z} = \mathbf{G}(\boldsymbol{q}; D) = \mathbf{F}(\boldsymbol{q}) - D\boldsymbol{q}. \tag{3.9}$$

The governing system of ODEs written in terms of $\mathbf{z}$ becomes

$$\boldsymbol{z}_\eta = \mathbf{s}(\boldsymbol{q}), \tag{3.10}$$

and it needs to be solved subject to the shock conditions, $\boldsymbol{z}(0) = \mathbf{F}(\boldsymbol{q}_0) - D\boldsymbol{q}_0$, with

$\mathbf{q}_0$ denoting the post-shock state. In order for this change of variables to be successful, it must be invertible so that $\boldsymbol{q} = \mathbf{G}^{-1}(\boldsymbol{z}, D)$. The inversion is guaranteed to be well defined as long as the Jacobian, $\partial\mathbf{G}/\partial\mathbf{q} = \partial\mathbf{F}/\partial\mathbf{q} - D\mathbf{I}$, is not singular, which is the case away from sonic points. It is important to note that, in general, the inversion results in multiple solution branches. In order to choose the correct branch, we need to ensure that $\mathbf{G}^{-1}\left(\boldsymbol{z}(0)\right) = \boldsymbol{q}_0$.

The main advantage of the new variable is that (3.10) is not stiff even as one approaches the singular point and thus the problem of finding the values of D such that (3.8) is satisfied becomes regular. The analytical inversion of $\mathbf{G}$ may not in general be possible as it depends on the specific form of the equation of state. Nevertheless, the general procedure remains valid and, once the sonic points are found, the inversion can be done numerically. The method outlined here is applicable to a wide range of problems, as we illustrate below (see also [66] for a recent application of the method).

In the specific case of the toy model considered in this chapter, where we are interested in solving (3.4), we introduce $z = (u - D)^2$ as a new variable instead of u. Then, (3.4) becomes

$$z' = 2\left(f\left(x, D\right) - g(x, u, \varphi)\right), \tag{3.11}$$

which has a regular right-hand side. Notice that the inverse of the transformation from u to z is *double-valued*, $u = D \pm \sqrt{z}$. At the shock, $u(0) = 2D > D$, and, therefore, between the shock and the sonic point, we have $u = D + \sqrt{z}$. Hence

$$z' = 2\left(f\left(x, D\right) - g(x, D + \sqrt{z}, \varphi)\right). \tag{3.12}$$

Downstream of the sonic point, the square root changes its branch. Therefore, $u = D - \sqrt{z}$. The sonic condition in the new variable is very simple: $z' = 0$ at $z = 0$. These conditions are clearly independent of the specific form of the right-hand side

of (3.4). The equations are no longer stiff as one approaches the sonic point. If the solution beyond the sonic point is required, then $z' = 2\left(f\left(x, D\right) - g(x, D - \sqrt{z}, \varphi)\right)$ must be solved at $x < x_*$.

Another simple example arises in the analysis of the radially symmetric reactive Euler equations. The problem of finding a quasi-steady solution of a curved expanding detonation leads to the following ODE for the flow velocity (e.g., [38]):

$$\frac{du}{d\lambda} = \frac{\Phi}{u^2 - c^2}\frac{u}{\omega}, \tag{3.13}$$

where $\omega = k\left(1-\lambda\right)\exp(-\gamma\vartheta/c^2)$ is the reaction rate, ϑ is the activation energy, $\Phi = \left(\gamma - 1\right)q\omega - \kappa c^2\left(u + D\right)$ is the thermicity, κ is the shock curvature, q is the heat release, and $c^2 = \gamma p_0 + \left(\gamma - 1\right)\left[\left(D^2 - u^2\right)/2 + q\lambda\right]$ is the sound speed squared. The integration domain is $0 \leq \lambda \leq 1$ with $u(0) = u_s(D)$ given by the Rankine-Hugoniot condition. The sonic singularity occurs here at $u = c$ and hence we introduce $z = \left(u - c\right)^2$ to obtain

$$\frac{dz}{d\lambda} = 2\left(u - c\right)\left(1 - \frac{\partial c}{\partial u}\right)\frac{du}{d\lambda} = 2\left(1 - \frac{\partial c}{\partial u}\right)\frac{\Phi u}{\omega}, \tag{3.14}$$

which is regular at the sonic point. After the correct branch of the inversion is identified, the generalized Chapman-Jouguet condition at the sonic point in terms of the new variables is that $dz/d\lambda = 0$ at the sonic point, $\lambda = \lambda^*$, where $z(\lambda^*) = 0$. This provides a much simpler and faster way of solving the generalized Chapman-Jouguet condition and allows for integration from the shock toward the sonic point without any difficulty.

Finally, we mention that since linear stability analysis consist of analyzing perturbations to the steady-state, an efficient and robust way of numerically calculating

the steady profiles is crucial to a successful linear stability algorithm.

3.2.3 On linear stability analysis of detonations with losses

Once the steady or quasi-steady solutions are obtained, the question of their linear stability arises. The problem without losses was analyzed extensively in Chapter 2, where it was shown that the analysis parallels that of the reactive Euler equations.

We begin with the stability of steady-state solutions. Let $u_0(x)$ be the solution of

$$\frac{d}{dx}\left(\frac{1}{2}u_0^2 - D_0 u_0\right) = f\left(x, D_0\right) - g(x, u_0, \varphi), \tag{3.15}$$

where φ is a constant and D_0 is such that the generalized Chapman-Jouguet condition is satisfied. Consider then a perturbation of this solution of the form $D = D_0 + \epsilon\sigma\exp(\sigma t)$ and $u = u_0(x) + \epsilon u_1(x)\exp(\sigma t)$, where σ is the growth rate to be found. Inserting these expansions into (3.3) yields

$$\sigma u_1 + \left(u_0 u_1 - D_0 u_1 - \sigma u_0\right)' = \sigma\frac{\partial f}{\partial D}\left(x, D_0\right) - u_1\frac{\partial g}{\partial u}(x, u_0, \varphi), \tag{3.16}$$

which can be solved exactly to give the eigenfunction,

$$u_1\left(x\right) = \frac{\sigma}{c_0(x)}e^{p(x,\sigma)}\left[\int_0^x\left(\frac{\partial f}{\partial D}\left(x, D_0\right) + u_0'\right)e^{-p(\xi,\sigma)}d\xi + 2D_0\right],$$

where $c_0 = u_0 - D_0$ and

$$p(x,\sigma) = \int_x^0\left[\sigma + \frac{\partial g}{\partial u}(\xi, u_0(\xi), \varphi)\right]\frac{d\xi}{c_0(\xi)}$$

are functions of f and g, which are known in terms the steady-state solution, $u_0\left(x\right)$. Noticing that $c_0 \to 0$ at the sonic point, x_*, boundedness of the eigenfunctions requires

the following dispersion relation to hold:

$$\int_{x_*}^{0} \left(\frac{\partial f}{\partial D} (\xi, D_0) + u_0' \right) e^{-p(\xi,\sigma)} d\xi - 2D_0 = 0, \tag{3.17}$$

This is of the same form as in the ideal case with the only change due to g appearing in the expression for p. Hence, the stability analysis of the equation with losses is similar to the ideal case analyzed earlier in (2).

For quasi-steady problems, the stability analysis is a bit subtler. Consider

$$\frac{\partial u}{\partial t} + \frac{\partial}{\partial x} \left(\frac{1}{2} u^2 - Du \right) = f(x, D) - g(x, u, \varphi), \tag{3.18}$$

where φ is a slowly varying function of time. Then, the steady-state solution for u does not exist in general. We then consider solutions that are slowly evolving in time by using a slow time variable, $\tau = \delta t$, $0 < \delta \ll 1$, such that $\varphi = \varphi(\tau)$. Then,

$$\delta \frac{\partial u}{\partial \tau} + \frac{\partial}{\partial x} \left(\frac{1}{2} u^2 - Du \right) = f(x, D) - g(x, u, \varphi(\tau)). \tag{3.19}$$

Let $u_\delta(x, \tau)$ be the exact solution of (3.19) with $D = D_\delta(\tau)$ as the speed. Then, the spectral stability of this solution requires looking at the evolution of $D = D_\delta(\tau) + \epsilon\sigma \exp(\sigma t)$ and $u = u_\delta(x, \tau) + \epsilon u_{\delta 1}(x, \tau) \exp(\sigma t)$. It is important to observe that these expansions express $O(1)$ time-scale variations around the slow, $O(1/\delta)$, time-scale leading solution. Putting these expressions into (3.19), we obtain, to first order,

$$\delta \frac{\partial u_{\delta 1}}{\partial \tau} + \sigma u_{\delta 1} + \frac{\partial}{\partial x} (u_\delta u_{\delta 1} - D_\delta u_{\delta 1} - \sigma u_\delta) \quad = \tag{3.20}$$

$$\sigma \frac{\partial f}{\partial D} (x, D_\delta) - u_{\delta 1} \frac{\partial g}{\partial u} (x, u_\delta, \varphi). \tag{3.21}$$

Next, we perform an asymptotic expansion in δ: $u_\delta = u_0 + O(\delta)$, $u_{\delta 1} = u_1 + O(\delta)$,

$D_\delta = D_0 + O(\delta)$. Then, to leading order, the quasi-steady solution satisfies

$$\frac{d}{dx}\left(\frac{1}{2}u_0^2 - D_0 u_0\right) = f\left(x, D_0\right) - g(x, u_0, \varphi), \tag{3.22}$$

which, together with the shock and sonic conditions, gives the eigenvalue problem for D_0. The linear stability equation is, to leading order in δ, given by the same equation as (3.16) and hence the dispersion relation is also given by (3.17). Notice here that the implicit assumption $\partial u_0/\partial\tau = O(1)$ is required for the validity of the asymptotic expansion in δ. This is seen to break down at a turning point of the $D_0 - \varphi$ curve if such a point exists.

3.3 Numerical results

In this section, we investigate numerically two types of losses, frictional and those due to shock curvature. For detonation with frictional losses, we consider

$$\frac{\partial u}{\partial t} + \frac{\partial}{\partial x}\left(\frac{1}{2}u^2 - Du\right) = f\left(x, D\right) - c_f u|u|, \tag{3.23}$$

where $x \in (-\infty, 0]$ and c_f is a constant friction coefficient[1]. The goal of the following calculations is to determine the role of c_f in the existence and structure of the steady-state solutions of (3.23). Using the algorithm described in Subsection 3.2.2, we compute the dependence of the wave velocity on the friction coefficient. Figure 3.1 shows $u_s = 2D$ as a function of c_f, where we can see the characteristic turning-point behavior with two solutions coexisting at $c_f < c_{fc}$ for some critical c_{fc}, and steady-state solutions no longer existing if $c_f > c_{fc}$.

[1] In the last chapter of this thesis, Chapter 6, we show that the choice $g = c_f u|u|$ can be motivated by an asymptotic analysis of the reactive Euler equations with friction losses.

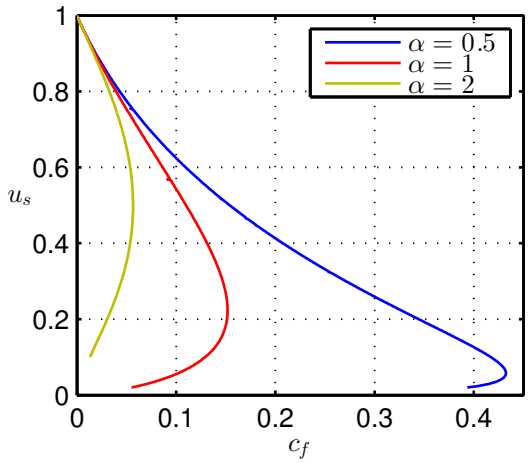

Figure 3.1: The $u_s - c_f$ relation for the steady-state solution of (3.23) for detonation with friction.

Of particular interest is the question of stability of these steady-state solutions. It is generally believed, using physical arguments, that the lower branch of the steady-state u_s-c_f curve is always unstable while the top branch can be stable or unstable, although to our knowledge no stability analysis of detonations with losses has ever been performed. In order to explore the nature of these instabilities, we solve (3.23) numerically using a second-order finite volume method with a min-mod limiter [73]. We begin with a perturbation around the steady-state solutions at different locations of the u_s-c_f curve, both on the top and bottom branches. We choose α and β such that the corresponding ideal solution (i.e. $c_f = 0$) is stable.

We find that as we increase c_f along the top branch, there is a critical value above which the detonation becomes unstable, indicating that the losses have a destabilizing effect. The black curve in Figure 3.2a shows the computed solutions at $c_f = 0.1$, corresponding to a stable state on the upper branch, and the black curve in Figure 3.2b shows the computed solution at $c_f = 0.125$, corresponding to an unstable state on the upper branch. Note that the instability of the steady-state solutions on the top branch is associated with a transition to a limit cycle, likely arising through a Hopf

bifurcation when c_f exceeds a critical value. These oscillations take place around the steady-state solution.

As we solve the problem starting on the bottom branch, we find that the steady-state solution on the branch is indeed unstable, but, unlike the solutions on the top branch, there is no oscillation around the bottom branch. The solution tends in fact toward the top branch with time, indicating that the bottom branch is generally a repelling equilibrium while the top branch is attracting. The dynamics of this instability is quite different from that on the top branch. It involves a generation of internal shock waves in the reaction zone that overtake the lead shock and, eventually, after multiple such overtaking, the solution settles on the top branch. The discontinuous behavior of the red curves in Figure 3.2 occurs precisely when an internal shock wave catches up with the lead shock. At that moment, there is a rapid increase of u_s. The general trend of the solution appears to be physically reasonable, reflecting the strong instability of the lower branch of the D-c_f curve and the attracting character of the upper branch. Very likely, the bottom branch contains a linear spectrum which is dominated by non-oscillatory eigenvalues. It is interesting that very similar behavior was observed in experiments on initiation of spherical detonation in hydrocarbon-air mixtures [74].

Next, we look at spherically expanding detonation solutions. The shock-frame version of (3.1) for a diverging detonation is given by

$$\frac{\partial u}{\partial t}+\frac{1}{2}\frac{\partial}{\partial x}\left(u^2-uu_s\right)=f\left(x,u_s\right)-\frac{u^2}{x+r_s}, \tag{3.24}$$

where $r_s\left(t\right)$ denotes the shock radius such that $dr_s/dt=D=u_s/2$. When $\partial u/\partial t$ is

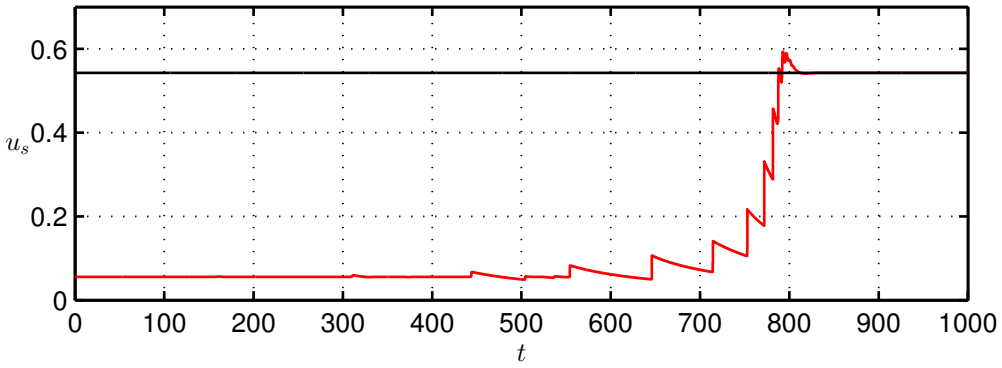

(a) At $c_f = 0.1$, the top branch is stable. The integration is carried out starting both from the top branch (black curve) and the bottom branch (red curve).

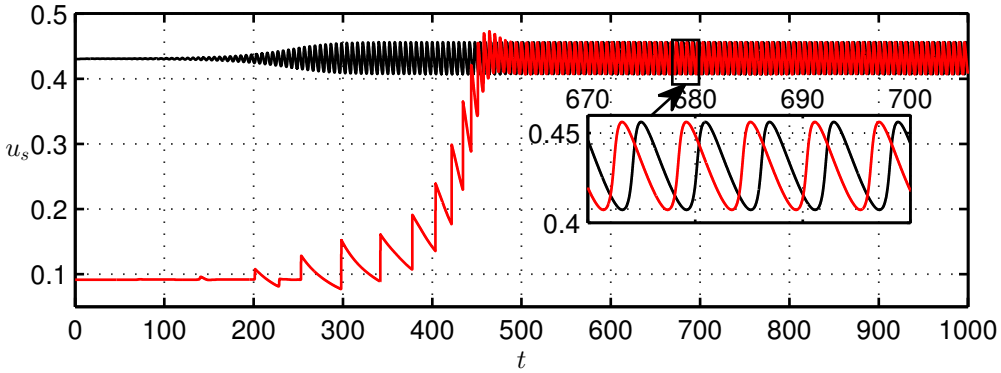

(b) At $c_f = 0.125$, the top branch is unstable. The integration is carried out starting both from the top branch (black curve) and the bottom branch (red curve). The pulsating instability is due purely to the presence of friction.

Figure 3.2: Time evolution of solutions for detonation with friction starting with the middle curve of Fig. 3.1 at $\alpha = 1$ and two different values of c_f.

dropped (quasi-steady solution), (3.24) can be written as

$$\frac{du_0}{dx} = \frac{f(x, u_s) - \kappa u_0^2/(1 + \kappa x)}{u_0 - u_s/2}, \tag{3.25}$$

where $\kappa = 1/r_s$ is the mean curvature of the shock. This equation must be solved subject to $u_0(0) = u_s$ and to some appropriate condition at $x = -r_s$, i.e., at $r = 0$.

Equation (3.25) is solved using the algorithm described earlier. In Figure 3.3a, we show the computed dependence of u_s on κ for various values of α at $\beta = 0.1$. The usual turning-point behavior is seen with the critical curvature decreasing as

α increases. This is similar to that in the Euler detonations wherein the activation energy leads to the same effects [37, 40]. One important difference is that, in Figure 3.3a, there are only two branches, the lower branch tending to $u_s = 0$ and $\kappa = 0$, while in the Euler equations, there are in general three branches, the lower branch tending to $D = c_a$, the ambient sound speed, and $\kappa \to \infty$. In Figure 3.3b, we also show the solution profiles that correspond to the $u_s - \kappa$ curves in Figure 3.3a at a particular value of $\kappa = 0.1$, but at two different values of u_s, one on the upper branch and one on the lower. A notable feature of these profiles is the existence of an internal maximum of u, which does not exist in the planar solution at the same parameters.

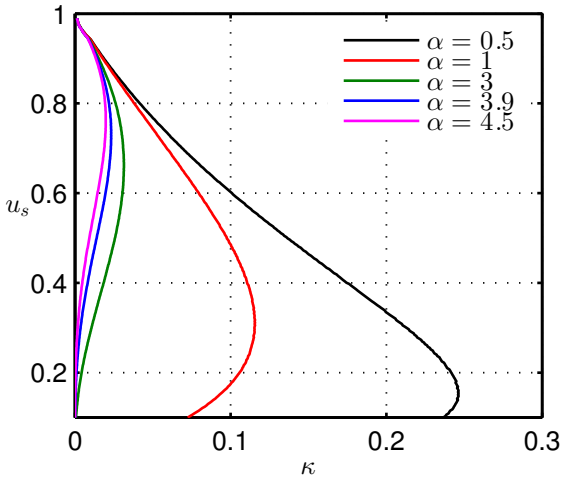

(a) Quasi-steady $u_s - \kappa$ curves at $\beta = 0.1$ fixed and variable α.

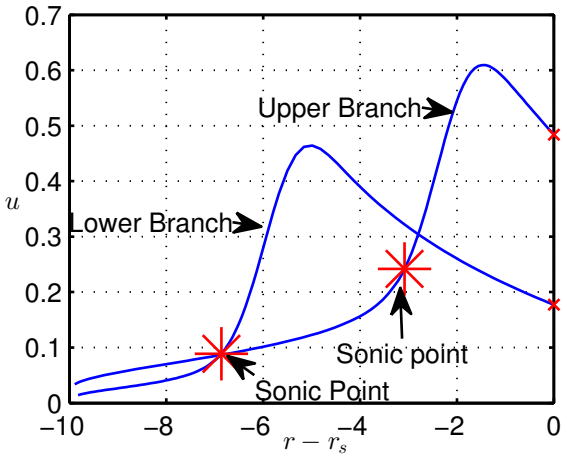

(b) The quasi-steady solution profiles $u_0(x)$ on the top and the bottom branches of the $u_s - \kappa$ curve in (a) at $\alpha = 1$ and $\kappa = 0.1$.

Figure 3.3: Quasi-steady solutions.

In order to understand better the role of the curvature term in (3.24), we solve the equation simulating the direct initiation of gaseous detonation. In the laboratory

frame of reference, (3.24) takes the form

$$\frac{\partial u}{\partial t}+\frac{\partial}{\partial r}\left(\frac{u^2}{2}\right)=-\frac{u^2}{r}+\begin{cases} f\left(r-r_s,u\left(r_s,t\right)\right), & r<r_s, \\ 0, & r>r_s. \end{cases} \tag{3.26}$$

We solve this equation using a fifth-order WENO algorithm discussed in Appendix A, and the initial conditions corresponding to a localized source of the type $u\left(r,0\right)=u_i$ at $0<r<r_i$ and $u\left(r,0\right)=0$ at $r>r_i$. Here, r_i is the radius of the initial hot spot and u_i is its "temperature". The point-blast initiation is simulated keeping r_i fixed at some small value and varying u_i, a measure of the source energy per unit volume.

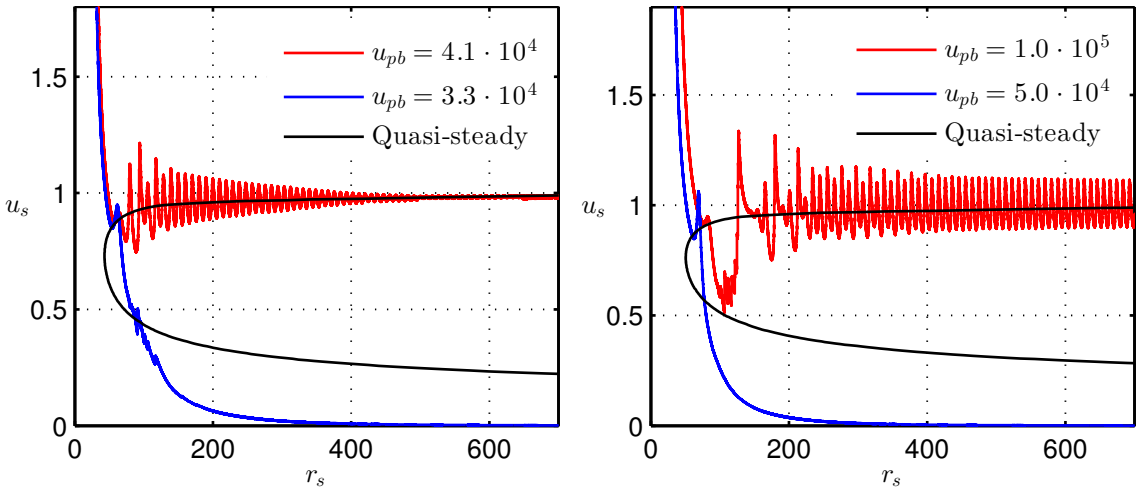

(a) Stable solutions at $\alpha=3.9$ (b) Unstable solutions at $\alpha=4.5$

Figure 3.4: Initiation and failure for stable and unstable solutions. In both figures, $\beta=0.1$, the length of the computational domain is $L=10^3$, and the number of grid points used is $N=10^4$.

Our findings are displayed in Figure 3.4. We select two sets of parameters for α and β such that one corresponds to a stable planar solution and the other to an unstable planar solution. For each case, we vary u_i to see if the detonation initiates or fails. Exactly as in the Euler detonations [75], we observe that above a certain critical value, u_{ic}, there is an initiation; below, there is failure. Moreover, the curvature in our

model also plays a destabilizing role. As one can see in Figure 3.4a, the detonation that is stable in the planar case oscillates in the presence of significant curvature. The oscillations are large in magnitude and irregular at first, around $r_s = 100$ to about $r_s = 150$, before settling down to regular decaying oscillations. A similar trend is seen in the unstable case, shown in Figure 3.4b, where the range of the irregular oscillations extends from about $r_s = 120$ to $r_s = 400$ before settling down to regular periodic oscillations. When the curvature is significantly diminished (i.e. $r_s \gg 1$), the detonation dynamics is essentially that of a planar wave. Hence, all the phenomena observed in [76, 77] carry over to the present study. However, the destabilizing effect of curvature, clearly seen in Figure 3.4, requires further analysis in order to reveal the underlying mechanisms. An additional factor that contributes to the instability of the solutions is β. For planar solutions, we have shown in [76] that smaller β lead to more unstable solutions, and we expect the same effect to be preserved in the curved detonations as well.

3.4 Conclusions

A reactive Burgers equation with nonlocal forcing and appropriate damping is shown to capture, at a qualitative level, the dynamics of detonations with friction and of radially diverging detonations. Using a new integration algorithm, we have found that for curved detonations and for non-ideal detonations, steady/quasi-steady solutions exist, which have a characteristic turning-point shape in the plane of the shock speed versus curvature or a friction coefficient. Unsteady numerical simulations of our model equation reproduce the dynamics of the point-blast initiation, capturing the initiation/failure phenomenon. The curvature or the presence of friction are found to play a destabilizing role in the dynamics of non-ideal detonation. The present

calculations together with our earlier study of the planar model demonstrate that the reactive Burgers equation is capable of reproducing, qualitatively, most of the dynamical properties of one-dimensional detonations, whether ideal or with losses.

Chapter 4

Qualitative theory in two dimensions

In this chapter, we propose and analyze a two-dimensional analog for unstable detonation waves. The simplified model extends the scalar forced Burgers equation, presented in Chapter 2, and is shown to capture some of the multi-dimensional nature of detonations waves. The linear stability spectrum is analyzed by means of Laplace transform, and it is observed that nonzero transverse wave numbers typically posses the maximum growth rate, therefore dominating the stability criterion. By numerical simulations, we also show that solutions of the model tend, in the long time limit, to form multi-dimensional patterns.

4.1 Introduction

The fact that very simple mathematical models, such as the logistic map, can produce extremely rich solutions was a surprising and counterintuitive discovery in mathematics [78]. It suggested that complex behavior need not always be described by complicated equations. The hope with such simple models is that they can shed some light into the fundamental mechanism responsible for complexity, while neglecting details

which only obscure the relevant underlying dynamics. In this chapter, we introduce a simple system of partial differential equations capable of reproducing some of the dynamics of two-dimensional detonations.

Detonations are a type of combustion process in which strong pressure waves ignite, and are sustained by, chemical reactions. Unlike ordinary flames, detonations tend to propagate at extremely high velocities (several thousand meters per second), and convert energy at a very fast rate. Even in the simplest, idealized case, the equations of combustion theory pose a formidable challenge from a theoretical point of view, since they couple a compressible flow description (Euler/Navier-Stokes equations) to chemical kinetics. In fact, the main difficulty of reactive flows lies precisely in this two-way coupling: the wave initiates chemical reactions, and the reactions sustain the wave, with either ceasing to exist without the other. To make matters even more complicated, detonations tend to be multi-dimensional and unsteady. It is not surprising thus that theories simpler than the reactive Euler/Navier-Stokes equations are highly desirable.

The first attempt at a reduced qualitative description of detonations goes back to the works of Fickett [25, 27], who introduced a toy model as a vehicle to better understand (and explain) the intricacies of detonation theory. Others have similarly taken a qualitative approach. Majda, for example, focused on the effect of viscosity on the combustion waves, and showed through a simplified model that a theory analogous to the ZND theory exists for viscous detonations [29]. Radulescu and Tang have recently demonstrated that simplified models can capture not only the steady states, but also much of the unsteady dynamics of one-dimensional detonations [31]. Along the same lines, we have shown that even a scalar forced Burgers equations contains all the ingredients necessary to reproduce the complexity of one-dimensional detonations, including a rich linear spectrum and chaotic solutions. All of these works, however, are

limited to a one-dimensional description, and therefore cannot capture the important effects played by transverse waves. In this chapter, we present a multi-dimensional analog of detonations, and show through stability analysis and numerical simulations that even multi-dimensional effects are amenable to much simpler treatments than in the full system of reactive Euler equations. Our model appears to be the first to treat multi-dimensional effects in detonations by means of analogs.

This chapter is organized as follows. In Section 4.2, we propose the two-dimensional toy model, and provide some motivation based on the theory of weakly curved hyperbolic waves. We then present in Section 4.3 the traveling wave solutions, together with a formulation of the linear stability problem by means of the Laplace transform. Finally, we illustrate in Section 4.4 the linear stability theory and nonlinear dynamics by studying a concrete example. We demonstrate that: (1) transverse waves are typically more unstable than purely longitudinal perturbations, and (2) when unstable, the traveling wave solutions tend to form multi-dimensional patterns of variable complexity, depending on the distance from the neutral stability boundary.

4.2 The two-dimensional analog

We take as a starting point the one-dimensional toy model introduced in Chapter 2, i.e.,

$$u_t + \frac{1}{2}\left(u^2\right)_x = f\left(x - x_s, u_s\right), \tag{4.1}$$

where x_s denotes the x position and u_s denotes the state immediately after the detonation shock. In order to extend (4.1) to two dimensions we need, as a minimum, another variable (v) describing the transverse velocity, and a relation between u and v. Since this is a qualitative theory, we are free to extend it as we like, but some ways make more physical sense than others. Here, we consider an extension motivated by

the asymptotic form of weakly curved hyperbolic waves, where the dependence on the transverse direction is typically linear, and reinforces the fact that weakly nonlinear quasi-planar waves generate no vorticity to leading order. We thus propose the following two-dimensional toy model as an extension of (4.1):

$$u_t + \frac{1}{2}\left(u^2\right)_x + v_y = f(x - x_s, u_s), \tag{4.2}$$

$$v_x - u_y = 0. \tag{4.3}$$

Notice that, since (4.2-4.3) is not derived by a rational approximation of a physical system, the main justification for the form of the proposed model comes *a posteriori* by investigating its properties. We shall show later in Chapter 5 (see also [79]), however, that (4.2-4.3) are related to a weakly nonlinear multi-dimensional asymptotic theory, which although harder to analyze, can be obtained by a systematic reduction of the reactive Euler equations.

For the purpose of the calculations that follow, it is convenient to rewrite (4.2-4.3) in a shock-attached frame. In general the shock surface is represented by the zero of a level-set function, say $\psi(x, y, t)$. We let $\psi = x - s(y, t)$, where $s(y, t)$ is assumed to be a single valued function giving the x position of the shock, and therefore the shock location is given by $x = s(y, t)$. This parametrization contains the assumption that the shock does not curve too much. Then, introducing a shock-attached variable, $\xi = x - s(y, t)$, (4.2-4.3) becomes

$$u_t + (u - s_t)u_\xi + v_y - s_y v_\xi = f(\xi, u_s), \tag{4.4}$$

$$u_y - s_y u_\xi - v_\xi = 0. \tag{4.5}$$

The quantities s_t and s_y are related to the state at the shock by the jump conditions,

which are given by

$$s_t [u] - \frac{1}{2} \left[u^2\right] + s_y [v] = 0, \tag{4.6}$$

$$s_y [u] + [v] = 0, \tag{4.7}$$

where $[\cdot]$ represents, as before, the jump of a given quantity across the shock. Equations (4.2-4.3), together with the jump conditions (4.6-4.7), are the main focus of this chapter.

4.3 Traveling wave solutions and stability analysis

We investigate the one-dimensional traveling wave solutions of (4.2-4.3), together with their stability properties. Notice that, since in the one-dimensional case, the proposed system reduces to (4.1), which was studied in Chapter 2, the traveling wave solutions are identical. For completeness, we repeat the discussion here with minimal details. The reader is encouraged to review Section 2.3 for details.

4.3.1 Traveling wave solutions

Since we are interested in the stability properties of ZND waves, we start by computing the one-dimensional traveling wave solutions of (4.2-4.3). Assuming that the state ahead of the shock is given by $u = 0,\ v = 0$, we obtain from (4.2-4.3) that

$$u_0(\xi) = \frac{u_{0s}}{2} + \sqrt{\frac{u_{0s}^2}{4} - 2\int_x^0 f\left(z, u_{0s}\right) dz}, \tag{4.8}$$

$$v_0(\xi) = 0, \tag{4.9}$$

where $u_{0s}/2 = D$ represents, by the jump conditions, the steady shock velocity. For the proposed solution to remain real, we require

$$u_{0s} = \zeta \left(2\sqrt{2 \int_{-\infty}^{0} f\left(y, u_{0s}\right) dy} \right), \tag{4.10}$$

with $\zeta \geq 1$. If $\zeta = 1$ (CJ case), then it can be shown that the characteristics at the end of the reaction zone (when $f = 0$) are sonic relative to the lead shock. When $\zeta > 1$, detonations move faster than the CJ wave. These latter cases are usually interpreted as overdriven detonations, where a piston at the end of the reaction zone accelerates the flow so that no sonic point exists. Overdriven detonations are not self-sustained, and characteristics from $-\infty$ can catch up with the lead shock and affect its dynamics. In fact the larger the overdrive, the closer a detonation shock looks to an inert piston-induced shock, and therefore in the limit of large overdrive detonations are expected to be stable.

4.3.2 Linear stability

We consider in this subsection the multi-dimensional linear stability of solutions given by (4.8-4.9). We begin by expanding $u = u_0(\xi) + \epsilon u_1(\xi, y, t) + O(\epsilon^2)$, $v = \epsilon v_1(\xi, y, t) + O(\epsilon^2)$, $s = Dt + \epsilon s_1(y, t) + O(\epsilon^2)$, where u_0, v_0 are the steady profiles, and $D = u_{0s}/2$ is the steady shock speed. Inserting these expressions into (4.4-4.5) and letting $\epsilon \to 0$, we obtain

$$u_{1t} + \left(u_0 - \frac{u_{0s}}{2}\right) u_{1\xi} + u_0' u_1 + v_{1y} = \left(\frac{\partial f}{\partial u_s}\left(x, u_{0s}\right) + \frac{u_0'}{2}\right) u_1\left(0, t\right), \tag{4.11}$$

$$u_{1y} - u_{0\xi} s_{1y} - v_{1\xi} = 0. \tag{4.12}$$

Similarly, the linearized shock conditions are given by

$$s_{1t} = \frac{u_{1s}}{2}, \tag{4.13}$$

$$s_{1y} = -\frac{v_{1s}}{u_{0s}}. \tag{4.14}$$

As done in Subsection 2.3.3, it is convenient to introduce

$$c_0 = u_0 - u_{0s}/2, \qquad b_0 = \frac{\partial f}{\partial u_s}(x, u_{0s}) + \frac{u_0'}{2},$$

so that we can write (4.11-4.12) as

$$u_{1t} + c_0 u_{1\xi} + u_0' u_1 + v_{1y} = b_0 u_{1s}, \tag{4.15}$$

$$u_{1y} - v_{1\xi} = -u_{0\xi} v_{1s}/u_{0s}, \tag{4.16}$$

where c_0, b_0, u_{0s} are functions of the steady-state profile (assumed to be known), and $u_{1s} = u_1(\xi = 0^-, y, t),\ v_{1s} = v_1(\xi = 0^-, y, t)$ denote the perturbed quantities evaluated immediately after the shock. Whether or not solutions of (4.15-4.16), that grow in time, exist is precisely the linear stability question we answer below.

We diverge somewhat from the analysis performed in Subsection 2.3.3, and solve the linearized system by means of the Laplace transform. This will prove helpful in connecting the shooting method of Lee and Stewart, employed in [16], to the Laplace transform method of Erpenbeck. Below we follow closely [14].

Because (4.15-4.16) has constant coefficients in y, it is first convenient to Fourier

transform in the transverse direction:

$$\hat{u}_t + c_0\hat{u}_\xi + u_0'\hat{u} + i\ell\hat{v} = b_0\hat{u}_s, \tag{4.17}$$

$$i\ell\hat{u} - \hat{v}_\xi = -\frac{u_0'\hat{v}_s}{u_{0s}}, \tag{4.18}$$

where

$$\hat{u}(\xi,\ell,t) = \int_{-\infty}^{\infty} e^{-i\ell y}u_1(\xi,y,t)dy, \qquad \hat{u}_s(\ell,t) = \hat{u}(0,\ell,t), \tag{4.19}$$

$$\hat{v}(\xi,\ell,t) = \int_{-\infty}^{\infty} e^{-i\ell y}v_1(\xi,y,t)dy, \qquad \hat{v}_s(\ell,t) = \hat{v}(0,\ell,t). \tag{4.20}$$

The parameter ℓ represents the transverse wave number. Then, after Laplace transforming (4.17-4.18) in t, we obtain

$$\sigma U - \hat{u}(\xi,k,0) + c_0U' + u_0'U + i\ell V = b_0U_s, \tag{4.21}$$

$$ikU - V' = -\frac{u_0'V_s}{u_{0s}}, \tag{4.22}$$

where

$$U(\xi,\ell,\sigma) = \int_0^{\infty} e^{-\sigma t}\hat{u}(\xi,\ell,t)dt, \qquad U_s(\ell,\sigma) = \int_0^{\infty} e^{-\sigma t}\hat{u}_s(\ell,t)dt, \tag{4.23}$$

$$V(\xi,\ell,\sigma) = \int_0^{\infty} e^{-\sigma t}\hat{v}(\xi,\ell,t)dt, \qquad V_s(\ell,\sigma) = \int_0^{\infty} e^{-\sigma t}\hat{v}_s(\ell,t)dt. \tag{4.24}$$

Rewriting (4.21-4.22) in matrix form, we have

$$\mathbf{A}\cdot\frac{d}{d\xi}\mathbf{W} = \mathbf{B}\cdot\mathbf{W} + \tilde{\mathbf{F}}(\xi;\sigma,k), \tag{4.25}$$

with

$$\mathbf{W} = \begin{bmatrix} U \\ V \end{bmatrix}, \quad \mathbf{A} = \begin{bmatrix} c_0 & 0 \\ 0 & 1 \end{bmatrix}, \quad \mathbf{B} = \begin{bmatrix} -\sigma - u_0' & -i\ell \\ i\ell & 0 \end{bmatrix}, \quad \tilde{\mathbf{F}} = \begin{bmatrix} \hat{u}(\xi, \ell, 0) + b_0 U_s \\ u_0' V_s / u_{0s} \end{bmatrix}.$$

Two cases arise now, which are very different in terms of the analytic complexity. The first is the overdriven case, where $\zeta > 1$ in (4.10). The assumption $\zeta > 1$ implies that $c_0 > 0 \; \forall \; x$, and therefore, no sonic point exists in the steady state. Thus, $\mathbf{A}$ is invertible everywhere, and we can recast the Laplace-transformed ODE as

$$\frac{d}{d\xi}\mathbf{W} = \mathbf{C} \cdot \mathbf{W} + \mathbf{F}(\xi; \sigma, k), \tag{4.26}$$

where

$$\mathbf{C} = \mathbf{A}^{-1}\mathbf{B} = \begin{bmatrix} \left(-\sigma - u_0'\right)/c_0 & -i\ell/c_0 \\ i\ell & 0 \end{bmatrix}, \quad \mathbf{F} = \begin{bmatrix} \left(\hat{u}(\xi, \ell, 0) + b_0 U_s\right)/c_0 \\ u_0' V_s / u_{0s} \end{bmatrix}.$$

Notice that due to the overdrive assumption, $\mathbf{C}$ is a bounded matrix. The second case, which is considerably harder, is the Chapman-Jouguet case, wherein $c_0(\xi) \to 0$ as $\xi \to -\infty$. Then, $\mathbf{A}$ is no longer invertible at the sonic point, and a necessary condition for $\frac{d}{d\xi}\mathbf{W}$ to remain bounded as $\xi \to -\infty$ is that the right hand side of (4.25) be orthogonal to the left eigenvector corresponding to the vanishing eigenvalue of $\mathbf{A}$, i.e.,

$$\begin{aligned} \lim_{\xi \to -\infty} \mathbf{l}_i \cdot \mathbf{A}\frac{d}{d\xi}\mathbf{W} &= \lim_{\xi \to -\infty} \lambda_i \mathbf{l}_i \cdot \frac{d}{d\xi}\mathbf{W} \\ &= \lim_{\xi \to -\infty} \mathbf{l}_i \cdot \left(\mathbf{B} \cdot \mathbf{W} + \tilde{\mathbf{F}}(\xi; \sigma, k)\right) \\ &= 0, \end{aligned}$$

where λ_i is the vanishing eigenvalue and $\mathbf{l}_i$ the corresponding eigenvector. It is easy to check that, given the form of $\mathbf{A}$, $\mathbf{B}$, and $\mathbf{F}$, this implies

$$(\sigma + u_0'(\xi))\, U + i\ell V \to 0 \qquad \text{as} \qquad \xi \to -\infty. \tag{4.27}$$

Equation (4.27) is called the radiation, or boundedness condition. For the remainder of this chapter, we focus on overdriven detonations, and therefore avoid the main difficulties related to the vanishing of c_0.

It is well known that we can write the general solution of (4.26) in terms of the the boundary data at $\xi = 0$ and the fundamental matrix of the homogeneous problem [80]:

$$\mathbf{W}(\xi;\sigma,\ell) = \mathbf{H}(x;\sigma,\ell)\cdot\left[\mathbf{H}^{-1}(0;\sigma,\ell)\cdot\mathbf{W}(0;\sigma,\ell) + \int_0^x \mathbf{H}^{-1}(z;\sigma,\ell)\cdot\mathbf{F}(z;\sigma,\ell)dz\right], \tag{4.28}$$

where

$$H = \begin{bmatrix} \mathbf{h}_1 & \mathbf{h}_2 \\ \downarrow & \downarrow \end{bmatrix}, \tag{4.29}$$

and $\mathbf{h}_1, \mathbf{h}_2$ solve the homogeneous problem

$$\frac{d}{d\xi}\mathbf{G} = \mathbf{C}\cdot\mathbf{G}. \tag{4.30}$$

Denote $\delta = \lim_{\xi\to-\infty} c_0(\xi) > 0$, by the overdrive assumption. Notice that

$$\mathbf{C}_{-\infty} = \lim_{\xi\to-\infty}\mathbf{C}(\xi) = \begin{bmatrix} -\sigma/\delta & -i\ell/\delta \\ i\ell & 0 \end{bmatrix} \tag{4.31}$$

is a constant matrix, and $\int_{-\infty}^0 |\mathbf{C}(x) - \mathbf{C}_{-\infty}|dx < \infty$. Therefore, in the limit as

$\xi \to -\infty$, the general solution of the homogeneous problem is asymptotic to the solution of the constant coefficient problem [80],

$$\frac{d}{d\xi}\mathbf{G} = \mathbf{C}_{-\infty} \cdot \mathbf{G}. \tag{4.32}$$

This means

$$\mathbf{h}_1 \sim e^{\lambda_1 \xi}\mathbf{q}_1,\ \mathbf{h}_2 \sim e^{\lambda_2 \xi}\mathbf{q}_2,$$

where

$$\lambda_1 = \frac{-\sigma - \sqrt{4\delta\ell^2 + \sigma^2}}{2\delta},\ \lambda_2 = \frac{-\sigma + \sqrt{4\delta\ell^2 + \sigma^2}}{2\delta},$$

and $\mathbf{q}_1, \mathbf{q}_2$ are the respective eigenvalues/eigenvectors of $\mathbf{C}_{-\infty}$. When $\Re(\sigma) > 0$, we have $\Re(\lambda_1) < 0$, and thus $\mathbf{h}_1$ grows exponentially towards $\xi = -\infty$.

If we represent the inverse of $\mathbf{H}$ as

$$\mathbf{H}^{-1} = \begin{bmatrix} \boldsymbol{\theta}_1 & \to \\ \\ \boldsymbol{\theta}_2 & \to \end{bmatrix}, \tag{4.33}$$

then it can be shown that $\boldsymbol{\theta}_i(\xi) \sim e^{-\lambda_i}\boldsymbol{\pi}_i$, where $\boldsymbol{\pi}_i$ are constant vectors. With this notation, we can represent the general solutions of (4.26) by

$$\mathbf{W}(\xi) = \left(\boldsymbol{\theta}_1(0) \cdot \mathbf{W}(0) + \int_0^\xi \boldsymbol{\theta}_1(z) \cdot \mathbf{F}(s)ds\right)\mathbf{h}_1 + \left(\boldsymbol{\theta}_2(0) \cdot \mathbf{W}(0) + \int_0^\xi \boldsymbol{\theta}_2(z) \cdot \mathbf{F}(s)ds\right)\mathbf{h}_2. \tag{4.34}$$

Notice now that since $\mathbf{h}_1 \sim e^{\lambda_1 \xi}\mathbf{q}_1$, and $\Re(\lambda_1) < 0$, boundedness of $\mathbf{W}(\xi)$ as $\xi \to -\infty$ requires a very particular choice of $\boldsymbol{\theta}_1(0) \cdot \mathbf{W}(0)$ to eliminate the exponentially growing part of the solution. This choice is precisely

$$\boldsymbol{\theta}_1(0) \cdot \mathbf{W}(0) = \lim_{x \to -\infty} \int_x^0 \boldsymbol{\theta}_1(z) \cdot \mathbf{F}(z)dz. \tag{4.35}$$

That this choice is also sufficient to guarantee bounded solutions is less obvious, but a proof can be found in [14]. Inserting back the definition for $\mathbf{F}$, we get

$$\boldsymbol{\theta}_1(0)\cdot\mathbf{W}(0)=\int_{-\infty}^{0}\boldsymbol{\theta}_1\cdot\begin{bmatrix}\left(\hat{u}(\xi,\ell,0)+b_0U_s\right)/c_0\\ u_0'V_s/u_{0s}\end{bmatrix}dz. \tag{4.36}$$

Finally, using the linearized jump condition (4.13-4.14), we can relate U_s to V_s by

$$\sigma V_s=-i\ell u_{0s}\left(U_s/2+\hat{s}(\ell,0)\right). \tag{4.37}$$

Inserting (4.37) into (4.36), and solving for U_s, we obtain

$$U(0) \;=\; \frac{\boldsymbol{\theta}_1(0)\cdot\begin{bmatrix}0\\ i\ell u_{0s}\hat{s}(k,0)\end{bmatrix}+\sigma\int_{-\infty}^{0}\boldsymbol{\theta}_1\cdot\begin{bmatrix}\hat{u}(\xi,k,0)/c_0\\ i\ell u_0'\hat{s}(k,0)\end{bmatrix}}{\boldsymbol{\theta}_1(0)\cdot\begin{bmatrix}\sigma\\ -\frac{i\ell u_{0s}}{2}\end{bmatrix}-\int_{-\infty}^{0}\boldsymbol{\theta}_1\cdot\begin{bmatrix}\sigma b_0/c_0\\ \frac{i\ell}{2}u_0'\end{bmatrix}dz}. \tag{4.38}$$

Since the numerator depends only on the initial perturbation and on the steady state solution, and since $\boldsymbol{\theta}_1$ exponentially decays as $\xi\to-\infty$, it is easy to see that the numerator is regular. The poles therefore correspond to the roots of the denominator, i.e.,

$$\boldsymbol{\theta}_1(0)\cdot\begin{bmatrix}\sigma\\ -\frac{i\ell}{2}\end{bmatrix}=\int_{-\infty}^{0}\boldsymbol{\theta}_1\cdot\begin{bmatrix}\sigma b_0/c_0\\ \frac{i\ell}{2}u_0'\end{bmatrix}dz. \tag{4.39}$$

The function $\boldsymbol{\theta}_1$ can be computed by solving the adjoint homogeneous problem

$$\begin{aligned} \frac{d}{d\xi}\boldsymbol{\theta} &= -\mathbf{A}(\xi;\sigma,\ell)^T \cdot \boldsymbol{\theta}, \\ &= \begin{bmatrix} (\sigma + u_0')/c_0 & -i\ell \\ i\ell/c_0 & 0 \end{bmatrix} \boldsymbol{\theta}, \end{aligned} \tag{4.40}$$

subject to the boundedness condition that $\boldsymbol{\theta}$ be bounded at $-\infty$, which means it is parallel to the eigenvector associated with the positive eigenvalue.

In the case where $\ell = 0$, the adjoint homogeneous problem (4.40) simplifies to the scalar equation

$$\frac{d}{d\xi}\theta = (\sigma + u_0')/c_0\theta, \tag{4.41}$$

which has solutions

$$\theta = \frac{\theta(0)\exp(-\sigma p(x))c_0(x)}{c_0(0)}. \tag{4.42}$$

Inserting (4.42) back in (4.39) yields

$$c_0(0) = \int_{-\infty}^{0} b_0(z)e^{-\sigma p(z)}dz, \tag{4.43}$$

which is the same dispersion relation obtained in Subsection 2.3.3 by means of normal modes. Therefore we can see that, in the context of the simple toy model presented here, both Laplace transform and normal modes yield the same stability criterion.

In general, however, (4.40) cannot be solved analytically, and an approximate numerical scheme is needed to obtain the eigenvalues. The eigenvalues are thus given

by the roots of

$$R(\sigma,k)=\boldsymbol{\theta}_1(0)\cdot\begin{bmatrix}\sigma\\ -\frac{i\ell}{2}\end{bmatrix}-\int_{-\infty}^{0}\boldsymbol{\theta}_1\cdot\begin{bmatrix}\sigma b_0/c_0\\ \frac{i\ell u_{0s}}{2}u_0'\end{bmatrix}dz, \tag{4.44}$$

where $\boldsymbol{\theta}_1$ solves (4.40) and is parallel to the decaying solution at $\xi=-\infty$,

$$\boldsymbol{\theta}_1(-\infty)=a\begin{bmatrix}\frac{\sigma+\sqrt{4\ell^2\delta+\sigma^2}}{2}\\ i\ell\end{bmatrix}, \tag{4.45}$$

for some constant a.

4.4 An example

In this section, we study the properties of (4.2-4.3) for our (by now favorite) choice of f,

$$f=\frac{q}{\left(1+\mathrm{Erf}\left[\frac{k\left(\frac{u_s}{u_{0s}}\right)^{-\alpha}}{2\sqrt{\beta}}\right]\right)\sqrt{4\pi\beta}}\exp\left[-\frac{\left(x+k\left(\frac{u_{0s}}{u_s}\right)^{\alpha}\right)^2}{4\beta}\right].$$

It is convenient to rescale the variables as: $u=u_{0s}\tilde{u}$, $v=u_{0s}^{3/2}\tilde{v}$, $x=k\tilde{x}$, $y=k\tilde{y}/\sqrt{u_{0s}}$, $t=k\tilde{t}/u_{0s}$, so as to obtain

$$\tilde{u}_{\tilde{t}}+\frac{1}{2}\left(\tilde{u}^2\right)_{\tilde{x}}+\tilde{v}_{\tilde{y}} = \tilde{f}(\tilde{x}-\tilde{x}_s,\tilde{u}_s), \tag{4.46}$$

$$\tilde{v}_{\tilde{x}}-\tilde{u}_{\tilde{y}} = 0. \tag{4.47}$$

where $\tilde{f}$ is defined as,

$$\tilde{f}(\tilde{x}-\tilde{x}_s,\tilde{u_s}) = \frac{1}{4\zeta^2\left(1+\mathrm{Erf}\left[\frac{\tilde{u}(0,\tilde{t})^{-\alpha}}{2\sqrt{\tilde{\beta}}}\right]\right)}\frac{1}{\sqrt{4\pi\tilde{\beta}}}\exp\left[-\frac{\left(\tilde{x}-\tilde{x}_s+\left(\tilde{u}\left(0,\tilde{t}\right)\right)^{-\alpha}\right)^2}{4\tilde{\beta}}\right]. \tag{4.48}$$

The same three parameters, α, $\tilde{\beta}$ and ζ, as found in Chapter 2 are again obtained. They represent, respectively, the sensitivity of the reaction rate to variations on the shock, the ratio of the lengths of the reaction zone to the induction zone, and the degree of overdrive.

The role of the ζ now becomes clear: it scales the amplitude of the source term, with the effect of chemical reactions going to zero as $\zeta \to \infty$. We show in Figure 4.1 the effect of the overdrive factor on the steady detonation profile. For large enough overdrive, the wave is almost constant, being sustained primarily by the imposed left boundary condition. From here on we drop the tilde notation, and all variables are assumed to be dimensionless.

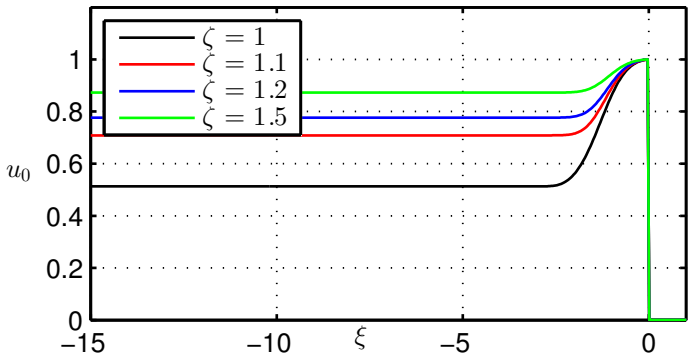

Figure 4.1: Steady-state solution profiles for (4.2-4.3) as the overdrive is varied while keeping all other parameters fixed.

We focus next on the role played by multi-dimensional effects on (1) the linear stability properties and (2) the full nonlinear dynamics. Our goal is to show that multi-dimensional instabilities typically dominate one-dimensional instabilities, and

that complex multi-dimensional structures tend to form when solving (4.46-4.47) numerically. We start with the linear stability analysis.

4.4.1 Multidimensional linear stability analysis

We obtain the linear spectrum of (4.46-4.47) by means of Laplace transform. As shown in Subsection 4.3.2, the poles of the Laplace transform (corresponding to instabilities should they lie on the right-half of the complex plane) are given by the zeros of

$$R(\sigma,\ell) = \boldsymbol{\theta}_1(0)\cdot\begin{bmatrix}\sigma\\ \frac{i\ell}{2}\end{bmatrix} - \int_{-\infty}^{0}\boldsymbol{\theta}_1\cdot\begin{bmatrix}\sigma b_0/c_0\\ \frac{i\ell u_{0s}}{2}u_0'\end{bmatrix}dz. \tag{4.49}$$

The main difficulty with numerically solving the dispersion relation is that, in general, the bounded solutions of the adjoint homogeneous problem (θ_1 in the current notation) cannot be found analytically. Therefore, each single evaluation of $R(\sigma,\ell)$ requires solving a system of linear ODEs (4.40) in order to obtain $\boldsymbol{\theta}_1$, evaluating the integral $\int_{-\infty}^{0}\boldsymbol{\theta}_1\cdot\begin{bmatrix}\sigma b_0/c_0\\ \frac{i\ell u_{0s}}{2}u_0'\end{bmatrix}dz$, and then computing the difference $\boldsymbol{\theta}_1(0)\cdot\begin{bmatrix}\sigma\\ \frac{i\ell}{2}\end{bmatrix} - \int_{-\infty}^{0}\boldsymbol{\theta}_1\cdot\begin{bmatrix}\sigma b_0/c_0\\ \frac{i\ell u_{0s}}{2}u_0'\end{bmatrix}dz$. This can be quite costly, especially when performing a parametric study for varying α and β.

We investigate first the effect of the overdrive on the stability of the wave. As discussed before, based on the simple physical argument that overdriven detonations are "closer" to inert shocks, we expect the overdrive to have a stabilizing effect. This is confirmed in Figure 4.2, where we plot the growth rate, σ_r, as a function of the transverse wave number, ℓ, for $\beta = 0.1,\ \alpha = 4.05$, and increasing overdrive $\zeta = 1.05, 1.1, 1.2$. We see that the overdrive factor indeed has a stabilizing effect. We also observe that certain transverse waves are more unstable than purely longitudinal

disturbances ($\ell = 0$), and therefore we expect multi-dimensional effects to play a role even when the traveling wave is stable to one-dimensional perturbations.

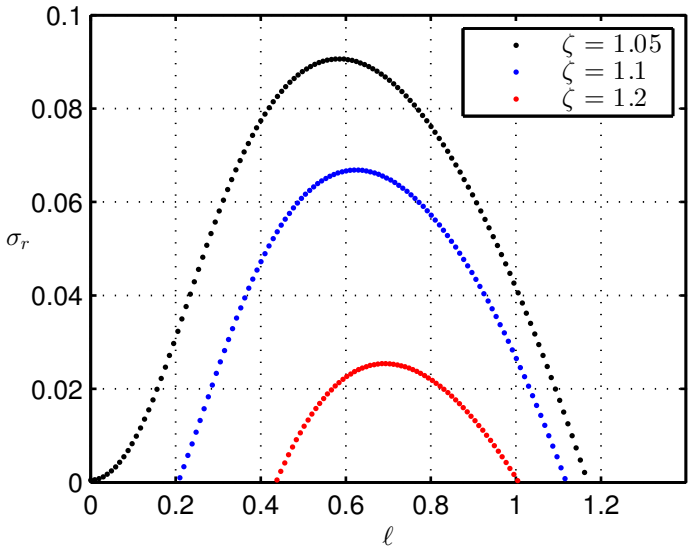

Figure 4.2: Dispersion relation for $\beta = 0.1$, $\alpha = 4.05$, and varying degree of overdrive.

We also study the effect of α on the stability of the traveling waves. Since α measures the sensitivity of the forcing to changes in the steady traveling wave speed, we expect larger values of α to correspond to more unstable waves. In particular, we expect the growth rate of the perturbations, σ_r, to increase with α. This is precisely what is observed in Figure 4.3, where we plot the effect of α on the multi-dimensional stability of the wave. We notice that α seems to have very little effect on the most unstable transverse mode, and for the parameters plotted in Figure 4.3, we can observe that the most unstable wave is given by $\ell \approx 0.6$, regardless of the value of α. This is consistent with the one-dimensional picture, where we observed that α had very little effect on the imaginary part of the eigenvalues (see Figure 2.3b in Chapter 2).

The linear stability results presented in this section suggest that two-dimensional effects play an important role in the ZND waves. In the next section we investigate, by means of numerical simulations, what happens after the onset of instabilities.

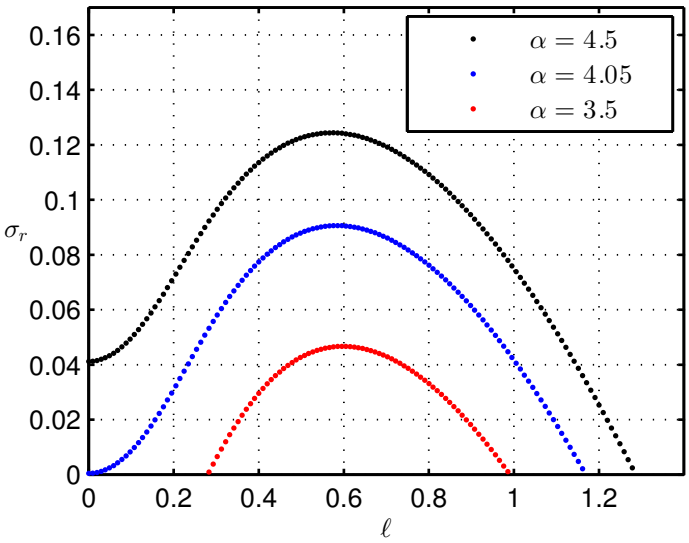

Figure 4.3: Dispersion relation for $\beta = 0.1$, $f = 1.05$, and varying α .

4.4.2 Numerical simulations

In this section, we investigate, by means of numerical simulations what happens in the large-time limit to ZND solutions which are unstable. The numerical simulation of (4.2-4.3) pose an interesting problem. On the one hand, this is a nonlinear hyperbolic system, and shocks can form from smooth initial data. On the other hand, it has characteristic surfaces which are orthogonal to time. This means that evolution in the given time coordinate is a nonlocal operation. It is expected that problems could arise if we attempt some explicit numerical scheme since it is impossible to satisfy a typical CFL condition. Even if $f \equiv 0$, in which case the equations reduce to

$$u_t + \left(u^2\right)_x + v_y = 0, \tag{4.50}$$

$$v_x - u_y = 0, \tag{4.51}$$

the numerical algorithm is not straightforward (see [81, 82] or Subsection 5.5.2.1).

The algorithm employed to solve (4.2-4.3), which uses a semi-implicit time dis-

cretization, is discussed in Chapter 5, where a detailed numerical study of asymptotic equations much similar to (4.2-4.3) is performed. We show in this section that the two-dimensional toy model exhibits many of the interesting features of real multi-dimensional detonations.

All numerical simulations are initialized with the traveling ZND solution found in Subsection 4.3.1. The equations are solved in an inertial frame of reference moving with constant speed $D = 1/2$, which is (after the non-dimensionalization performed in Section 4.4) the speed of the ZND wave. The top and bottom boundary conditions are that of a wall. We employ an inflow boundary condition on the right, and an outflow on the left. Using a shock-fitting algorithm, as was done in the one-dimensional case, is not easy, and therefore we adopt the more standard shock capturing approach. In fact, solving for multi-dimensional detonation waves in a shock-attached frame is still subject of current research.

First, we check that when linear stability results predict a stable traveling wave, as is the case for α small enough, the numerical solver is able to correctly capture the ZND structure and the wave speed, even when a small amplitude perturbation is imposed on the exact ZND profile. In Figure 4.4, we show the evolution of the ZND wave subjected to small perturbation.

The parameters are chosen so that the stability analysis predicts a linearly stable wave. The imposed perturbation is given by $\delta = \sum_{n=1}^{20} 10^{-4} \sin(n\pi y/L_y)$, where L_y is the y length of the domain. In Figure 4.4a and Figure 4.4b we show the profiles for u and v at $t = 0$, and in Figure 4.4c and Figure 4.4d we plot them again at $t = 2000$. We see that the amplitude of the perturbation in v has decayed from 10^{-3} to 10^{-9} over a time interval of 2000 units. We can also see that in the inertial frame moving with speed $D = 1/2$, the lead shock remains at $x = 0$, which means the correct speed is captured by the numerical algorithm.

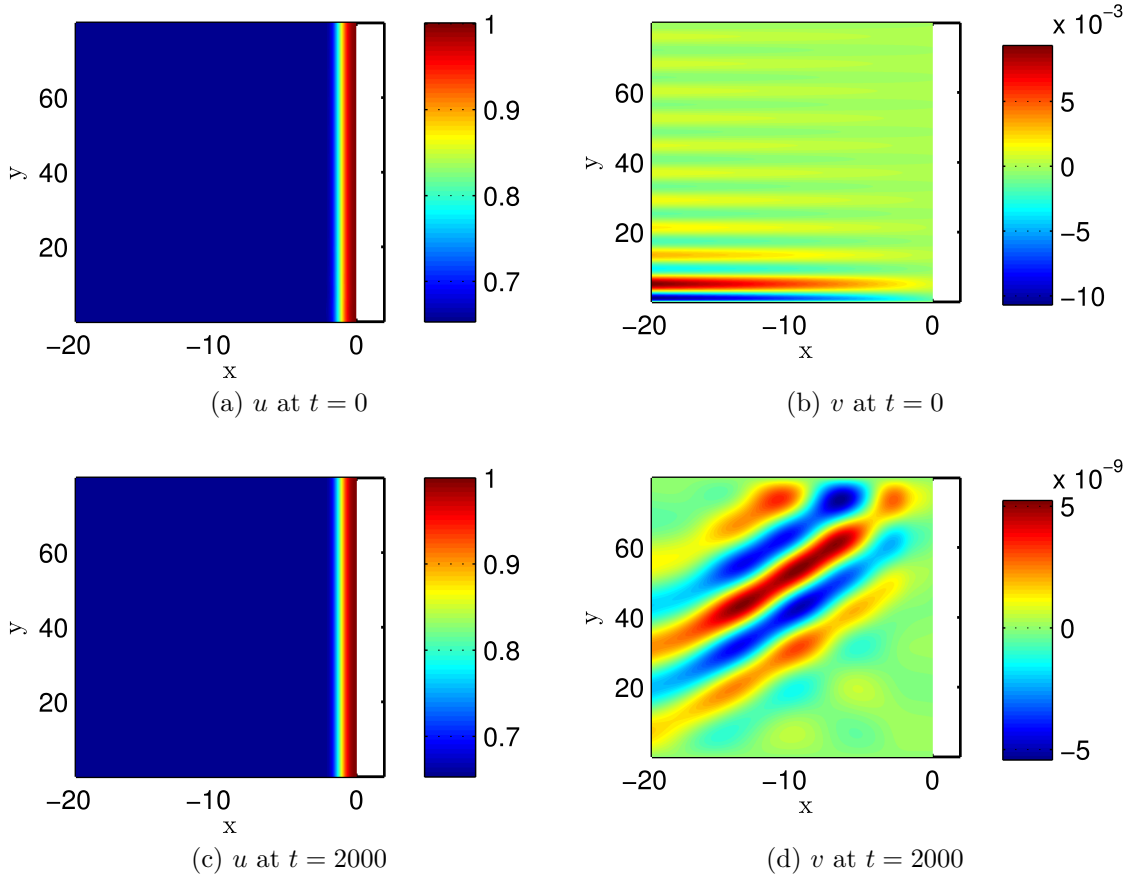

(a) u at $t = 0$

(b) v at $t = 0$

(c) u at $t = 2000$

(d) v at $t = 2000$

Figure 4.4: Stable ZND wave for $\zeta = 1.05,\ \alpha = 2,\ \beta = 0.1$.

It is more interesting to see what happens when the parameters are chosen so that eigenvalues with positive real part are present. If the ZND wave is only weakly unstable (meaning the parameters are close to the neutral stability boundary), very regular multi-dimensional patterns are observed (see Figure 4.5), which at a qualitative level match rather well with cellular patterns observed in gaseous detonations in dilute mixtures [48, 2, 9]. We see the appearance of certain regions where the induction zone, measured by the distance between the shock and the peak of f, is significantly reduced, and in these regions the energy is released shortly after the lead shock (Figure 4.5b). The transverse waves, however, appear to be smooth.

We investigate next the effect of the overdrive parameter, ζ, on the nonlinear

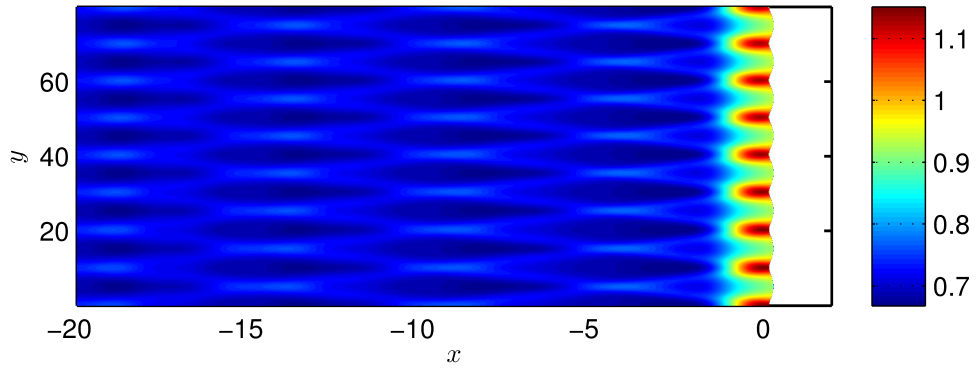

(a) u at time $t = 1000$

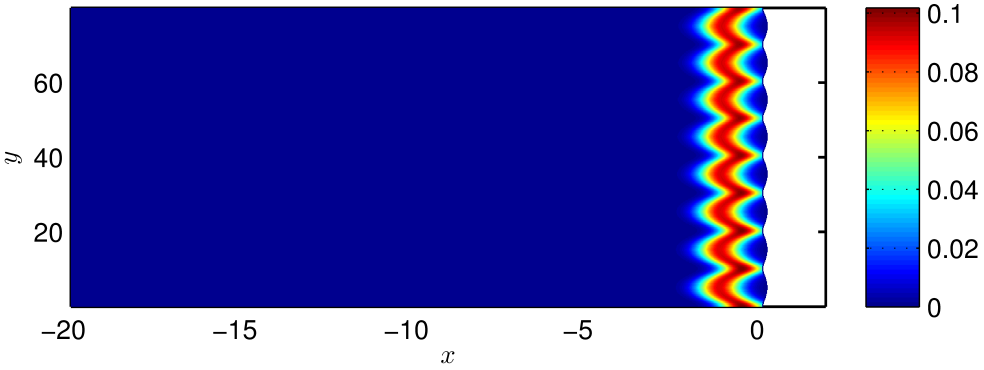

(b) f at time $t = 1000$

Figure 4.5: Large time dynamics for $\beta = 0.1$, $\alpha = 4.05$, $\zeta = 1.1$. This corresponds to a weakly unstable regime, with regular structures forming, and small transverse velocities.

dynamics of the wave. In Figure 4.6, we show the large time dynamics for varying degree of overdrive. We notice first that waves which are near the Chapman-Jouguet case are more unstable, with stronger transverse variations. Furthermore, it appears that for smaller overdrive the cellular patterns become larger. Both of these findings are consistent with the linear stability prediction, shown in Figure 4.2, where it can be seen that (1) smaller ζ corresponds to larger growth rates, and (2) the wavelength of the most unstable eigenvalue increases with decreasing degree of overdrive.

Finally, in Figure 4.7 we experiment with the effect of α on the stability and structure of the detonation wave. We see that, as in the one-dimensional case, larger

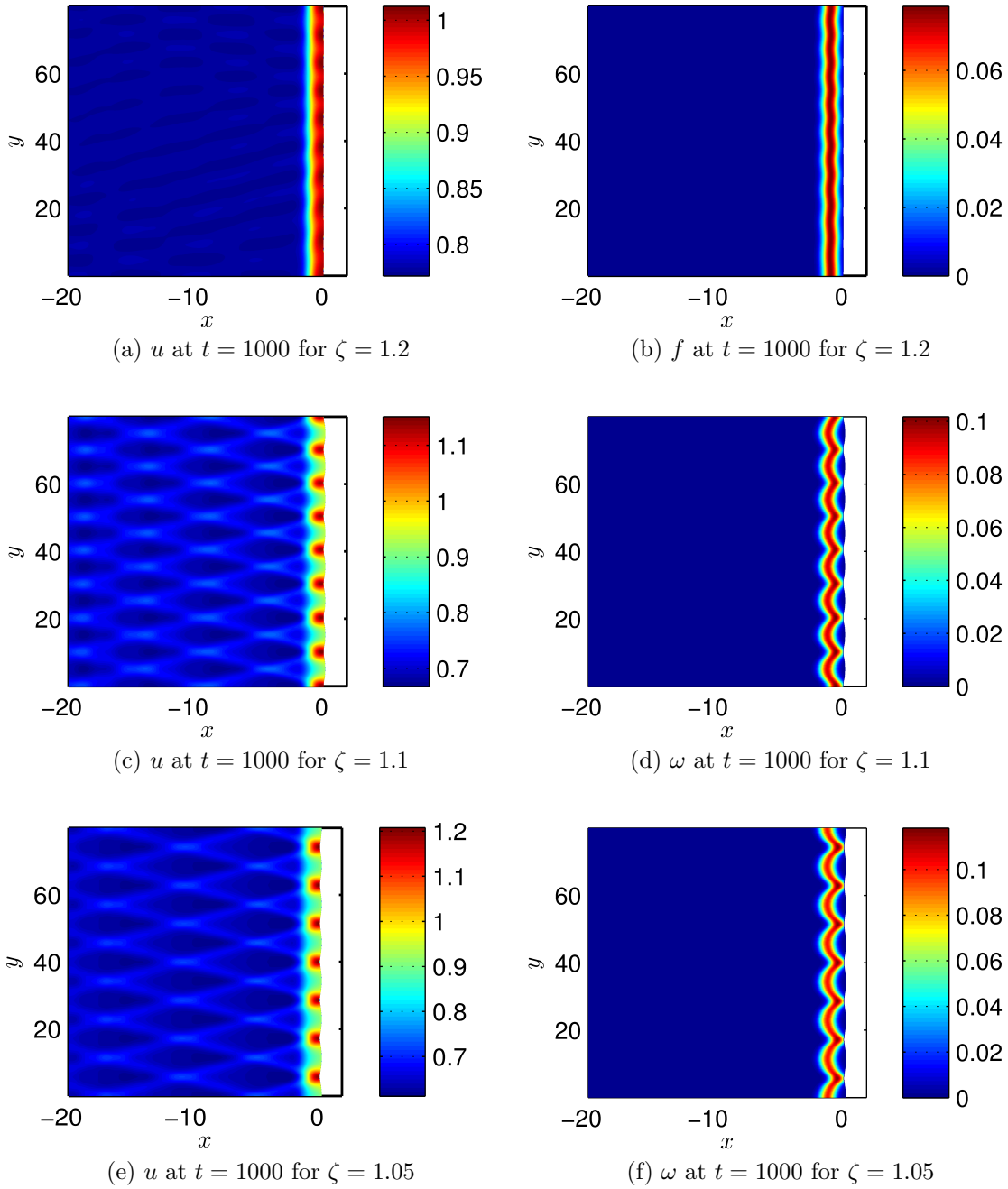

(a) u at $t = 1000$ for $\zeta = 1.2$

(b) f at $t = 1000$ for $\zeta = 1.2$

(c) u at $t = 1000$ for $\zeta = 1.1$

(d) ω at $t = 1000$ for $\zeta = 1.1$

(e) u at $t = 1000$ for $\zeta = 1.05$

(f) ω at $t = 1000$ for $\zeta = 1.05$

Figure 4.6: The parameters are $\alpha = 4.05$, $\beta = 0.1$.

values of α (recall that α measures the shock state sensitivity of the reaction rate) can be associated with more complex dynamics. In particular, we observe that by increasing α to a large-enough value, the patterns which form become more complex, up to the point where no regular cellular patterns can be identified (Figure 4.7e).

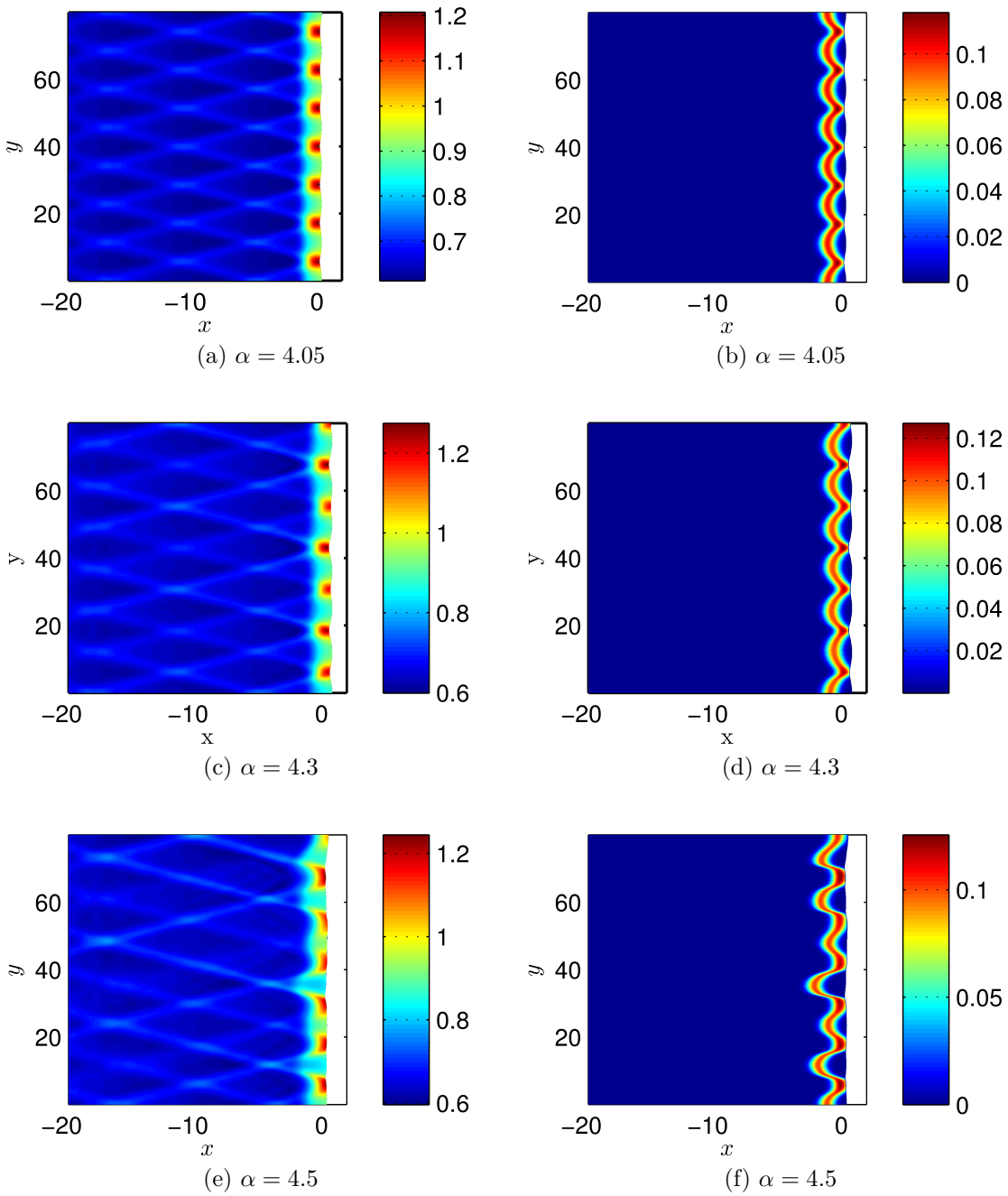

(a) $\alpha = 4.05$ (b) $\alpha = 4.05$

(c) $\alpha = 4.3$ (d) $\alpha = 4.3$

(e) $\alpha = 4.5$ (f) $\alpha = 4.5$

Figure 4.7: Large time behavior. The parameters are $f = 1.05$, $\beta = 0.1$.

Unlike the one dimensional case studied in Chapter 2, quantitatively characterizing two-dimensional dynamics is far more challenging. It does seem, however, that the solutions go through some sort of bifurcation, where the transverse waves go from having one maximum (Figure 4.7a), to two maxima (Figure 4.7c), to apparently

many (Figure 4.7e). Further study of this model will be presented elsewhere [83].

4.5 Conclusions

We have presented a two-dimensional extension of the model proposed in Chapter 2. The extension is shown to capture the multi-dimensional characteristics of detonations, where transverse waves play an important role.

The multi-dimensional linear stability properties of the traveling wave solutions were analyzed by means of Laplace transform. It was shown that the dispersion relation consists of an integral equation, much like the explicit formula derived in Chapter 2. Evaluation of the dispersion relation is a computationally intensive procedure, where solutions of the homogeneous adjoint problem have to be found for each evaluation of the dispersion relation.

It was shown that, akin to detonations in the reactive Euler equations, the overdrive factor has a stabilizing effect on the traveling wave, with highly overdriven detonations being more stable than their CJ counterparts.

Finally, we show by numerical simulations that solutions of (4.2-4.3) contain multi-dimensional structures of varying complexity. In particular, we observed that very regular cells tend to form when the parameters are near the stability boundary, and that the further we get from the stability boundary, the more irregular the patterns become.

The fact that the simple system studied in this chapter can capture the main features of detonation waves provides some hope that a multi-dimensional asymptotic theory of comparable simplicity exists. The development of asymptotic theories is the focus of the remainder of this thesis. But even in the presence of asymptotic theories, toy models retain their interest due to their elegance and richness.

Part II

Asymptotic theory of detonations

Chapter 5

Theory of weakly nonlinear self-sustained detonations

We propose in this chapter a theory of weakly nonlinear multi-dimensional self-sustained detonations based on asymptotic analysis of the reactive compressible Navier-Stokes equations. We show that these equations can be reduced to a model consisting of a forced, unsteady, small disturbance, transonic equation and a rate equation for the heat release. In one spatial dimension, the model simplifies to a forced Burgers equation. Through analysis, numerical calculations and comparison with the reactive Euler equations, the model is demonstrated to capture such essential dynamical characteristics of detonations as the steady-state structure, the linear stability spectrum, the period-doubling sequence of bifurcations and chaos in one-dimensional detonations, and cellular structures in multi-dimensional detonations.

5.1 Introduction

While the previous chapters aimed at a qualitative understanding of detonation through simplified analogs, this chapter is concerned with developing a rational asymptotic theory. As we shall see, the toy models studied in Chapter 2-4 are very

close in nature to weakly nonlinear theories of hyperbolic waves. In fact, the main difficulty is in how to account for the chemical reactions in a way that is both tractable and nontrivial. Even at the qualitative level, weakly nonlinear reactive and non-reactive shocks behave in a very different way.

In ZND theory, a detonation is assumed to be one-dimensional and in a steady-state in a Galilean frame moving with the wave. The theory is successful in explaining the fundamental nature of a detonation as a coupled shock-reaction zone system. However, in experiments with gaseous detonations, it was observed as early as 1926 that detonations tend to be unsteady and multi-dimensional with rather complex structures and dynamics [84, 48, 2]. To explain these dynamics, theoretical efforts focused on analysis of the stability of ZND solutions began in the 1960's in the works of Zaidel, Pukhnachev, Schelkin and, most comprehensively, Erpenbeck (see [2] for an early literature review). The theory of linear stability of gaseous detonations was found to be rather involved especially with regard to specific numerical computations for real gaseous mixtures. Much later, Lee and Stewart [16] revisited the stability problem and solved it for an idealized system by employing a relatively straightforward normal-mode approach. Solving the linear stability problem for real complex gaseous mixtures or for systems with losses remains an open problem.

Linear stability theory is successful in predicting, for idealized systems, why and how ZND detonations are unstable to linear perturbations. It is able to predict the neutral stability boundary and the most unstable modes and thus the characteristic length scales of various multi-dimensional structures seen in experiments. However, the predictive power of linear stability theory is limited by its very nature as a linear theory. Gaseous detonations are known to be highly nonlinear and unsteady. The lead shock of such a detonation wave propagates with strong oscillations in its velocity and with a highly non-uniform flow behind the shock that involves additional

shocks propagating transversely to the lead shock with triple points forming at their intersection. The triple points in complex detonation waves propagating in tubes with walls covered with soot leave fish-scale traces called detonation cells [84, 48, 2], and these detonations are termed cellular.

Theoretical prediction of the origin and structure of cellular detonations remains an outstanding and challenging open problem. However, some progress has been achieved with use of the tools of asymptotic analysis that allow for insight into the nature of the problem under various limiting conditions (see Section 1.5). For example, large activation energy [18], small heat-release [85, 47, 52], slow time evolution and small shock curvature [39, 38], weak nonlinearity [79, 32], strong overdrive [52] and other limiting assumptions lead to relatively simple asymptotic models. These asymptotic theories in general describe idealized systems and are thus also limited in their predictive power. Nevertheless, they provide important information about the mechanisms involved in the existence of particular qualitative traits in the real phenomenon.

Two fundamental structural and dynamical properties of gaseous detonations are first that they propagate in a galloping regime in narrow tubes, as characterized by large amplitude pulsations in an essentially one-dimensional wave, and second that the structure of detonation fronts in large channels/tubes or open environments is cellular. From a theoretical point of view, the basic problem is to describe and explain, at least at a qualitative level, the origin and dynamics of these galloping and cellular detonations. Importantly, such detonations have been reproduced and extensively studied in numerical simulations of the reactive Navier-Stokes/Euler equations with simplified descriptions of the chemical reactions and equations of state [9]. Thus, from a modeling standpoint, the use of these equations is frequently appropriate. Some features of pulsating and cellular detonations have been reproduced theoretically in

[86, 52]. However, the following questions remain: (1) Can an asymptotic theory predict the observed period-doubling sequence of bifurcations in one-dimensional detonations and the self-sustained cellular structures in two-dimensional detonations? (2) How quantitatively close are the asymptotic predictions to the numerical results from the reactive Navier-Stokes/Euler equations?

Our aim here is to develop a theory that captures the linear and nonlinear dynamics of self-sustained detonations, especially with regard to the bifurcation sequence seen in numerical simulations of one-dimensional detonations and the cellular structures found in two-dimensional detonations. Our theory is asymptotic and relies on a number of approximations, namely small heat release, large activation energy, slow time evolution, weak curvature and the Newtonian limit ($0 < \gamma - 1 \ll 1$, where γ is the ratio of specific heats). We build on the theory developed in [79, 32] by employing, as an additional approximation, the Newtonian limit (also used in [47] in one spatial dimension for Euler equations) for two-dimensional detonations with retained dissipative effects. The resulting system is a coupled set of three nonlinear partial differential equations. When the dissipative terms are neglected, it is a hyperbolic system for which we compute the traveling wave solutions analogous to ZND waves, their multi-dimensional linear stability properties and full nonlinear dynamics. We provide a quantitative comparison with the results from the reactive Euler equations for all three asymptotic predictions: the steady-state solutions, the linear stability spectrum and the cellular structure. The analysis of the reduced system with retained viscous dissipation is a very interesting problem, but it is postponed for future work.

As we show in Section 5.3, the two-dimensional reactive Navier-Stokes equations reduce to a forced version of the unsteady, small disturbance, transonic (UTSD)

equations given by

$$u_\tau + uu_x + v_y = -\frac{1}{2}\lambda_x + \mu u_{xx}, \tag{5.1}$$

$$v_x = u_y, \tag{5.2}$$

$$\lambda_x = -k(1-\lambda)\exp\left(\theta\left(\sqrt{q}u + q\lambda\right)\right), \tag{5.3}$$

where u, v and λ represent leading-order corrections to the x velocity, y velocity and reaction progress variable. The right-hand side of (5.3) is the leading-order contribution of the reaction rate assumed for simplicity to follow a single step Arrhenius kinetics. The parameters μ, k, θ and q are the rescaled viscosity, pre-exponential factor, activation energy and heat release, respectively. We find that this reduced asymptotic model captures, at both the qualitative and quantitative levels, not only the ZND structure, but also the linear stability spectrum, the pulsating nonlinear dynamics of one-dimensional detonations and the cellular dynamics of two-dimensional detonations.

We also mention the attempts at understanding the nonlinear dynamics of detonations via the use of qualitative models (see Section 1.4) such as those introduced by Fickett [25] and Majda [29]. The idea behind these models is to produce simplified systems that, although not derived from first principles, are capable of reproducing the observed complexity of the solutions of reactive Euler equations while considerably simplifying the analysis. The qualitative models of Fickett and Majda are closely related to the weakly nonlinear theory of detonations developed in [32]. Although these models and the asymptotic theory of Rosales and Majda have enjoyed some success in explaining certain features of different types of traveling wave solutions of reactive Euler/Navier-Stokes equations (i.e., weak and strong detonations), they were shown to lack the necessary complexity needed to reproduce the dynamical properties of

real detonations with the rate functions used in prior work [17]. However, simple *ad hoc* modifications of these models can reproduce much of the complexity of one-dimensional detonations as we have shown in Chapter 2-4 (see also [31, 77, 69, 76]). In the present chapter, we show how to produce an asymptotic theory that overcomes the limitations mentioned above.

The remainder of this chapter is organized as follows. In Section 5.2, we state the main governing equations together with the modeling assumptions regarding the medium and the chemical reactions. In Section 5.3, we develop an asymptotic approximation of the governing equations and obtain the weakly nonlinear reduced system. We then investigate in Section 5.4 the possible traveling wave solutions of the asymptotic equations and their linear stability properties. Both the traveling wave solutions and stability spectrum of the asymptotic model are compared with their corresponding results in the reactive Euler system. For the case with no dissipative effects, predictions of the asymptotic model are calculated numerically in Section 5.5, and a quantitative comparison with the predictions of the reactive Euler equations is presented as well. Finally, in Section 5.6, we discuss the results as well as point out some remaining open problems.

5.2 The main governing equations of reactive flow

We assume that the medium is described by the following system of equations expressing, respectively, the laws of conservation of mass, momentum and energy, and

the chemical heat release:

$$\begin{aligned}
\frac{\mathrm{D}\rho}{\mathrm{D}t} + \rho\nabla\cdot\mathbf{u} &= 0, && (5.4)\\
\rho\frac{\mathrm{D}\mathbf{u}}{\mathrm{D}t} &= \mathrm{div}\left(\mathbf{T}\right), && (5.5)\\
\rho\frac{\mathrm{D}e}{\mathrm{D}t} &= \mathbf{T}:\mathbf{D} - \mathrm{div}\left(\mathbf{q}_e\right), && (5.6)\\
\rho\frac{\mathrm{D}\Lambda}{\mathrm{D}t} &= \rho\tilde{W} - \mathrm{div}(\mathbf{q}_\Lambda). && (5.7)
\end{aligned}$$

Here, $\mathrm{D}/\mathrm{D}t = \partial/\partial t + \mathbf{u}\cdot\nabla$ is the material derivative, $\mathrm{v} = 1/\rho$ is the specific volume, ρ is the density, $\mathbf{u}$ is the velocity, $\mathbf{T}$ is the Cauchy stress tensor, $\mathbf{D} = \left(\nabla\mathbf{u} + \nabla\mathbf{u}^T\right)/2$ is the deformation tensor, $\mathbf{T}:\mathbf{D} = \sum_{i,j} T_{ij}D_{ij}$ denotes double contraction of tensors, $e = e_i - \tilde{Q}\Lambda$ is the total internal energy per unit mass, $\tilde{Q}$ is the heat release per unit mass, $\mathbf{q}_e$ and $\mathbf{q}_\Lambda$ represent the flux of energy and species, respectively, $\tilde{W}(\Lambda, T)$ is the rate of reaction and Λ is the reaction-progress variable that changes from $\Lambda = 0$ in the fresh mixture to $\Lambda = 1$ in the fully burnt products.

We make the following standard modeling assumptions (e.g., [87]):

1. The fluid is Newtonian, with the Stokes assumption on the bulk viscosity, so that $\mathbf{T} = -\left(p + \frac{2}{3}\mu\mathrm{div}\left(\mathbf{u}\right)\right)\mathbf{I} + 2\tilde{\mu}\mathbf{D}$, where $\tilde{\mu}$ is the dynamic viscosity, p is the pressure and $\mathbf{I}$ is the identity tensor.

2. The species flux is given by Fick's law, $\mathbf{q}_\Lambda$ = -$\rho\tilde{d}\nabla\Lambda$, with $\tilde{d}$ denoting the diffusion coefficient.

3. The energy flux has contributions from both the heat conduction (given by Fourier's law) and the species diffusion, so that $\mathbf{q}_e = -\tilde{\kappa}\nabla T + \tilde{Q}\rho\tilde{d}\nabla\Lambda$, where $\tilde{\kappa}$ is the heat diffusion coefficient.

4. The medium is a perfect gas described by the ideal-gas equation of state, $p = \rho RT$, with the internal energy given by $e_i = p\mathrm{v}/\left(\gamma - 1\right)$, where R is the universal

gas constant divided by the molecular weight and γ is the ratio of specific heats, assumed to be constant. These are simplifying modeling assumptions by which the molecular weight and the ratio of specific heats are assumed constant throughout the reaction. In real multicomponent mixtures, these change during the reaction (for details, see [87]).

5. For simplicity, we take the rate of reaction to be $\tilde{W} = \tilde{k}(1-\Lambda)\exp(-\tilde{E}/RT)$, with the added ignition temperature assumption that $\tilde{W} = 0$ for $T < T_i$ for some temperature, T_i. Here, $\tilde{k}$ is the rate constant and $\tilde{E}$ is the activation energy. More general rate functions can be considered, in principle, as long as appropriate sensitivity to temperature is preserved.

With these assumptions, we can then rewrite (5.4-5.7) as

$$\begin{aligned}
\frac{\mathrm{D}\rho}{\mathrm{D}t} + \rho\nabla\cdot\mathbf{u} &= 0, && (5.8)\\
\rho\frac{\mathrm{D}\mathbf{u}}{\mathrm{D}t} &= \nabla\cdot\left(-\left(p+\frac{2}{3}\tilde{\mu}\mathrm{div}\,(\mathbf{u})\right)\mathbf{I} + 2\tilde{\mu}\mathbf{D}\right), && (5.9)\\
\rho\frac{\mathrm{D}e}{\mathrm{D}t} &= -p\nabla\cdot\mathbf{u} - \frac{2}{3}\tilde{\mu}\left(\nabla\cdot\mathbf{u}\right)^2 + \tilde{\mu}\left(\nabla\mathbf{u} : \nabla\mathbf{u}\right) + \tilde{\mu}\left(\nabla\mathbf{u} : \nabla\mathbf{u}^T\right)\\
&+ \nabla\cdot\left(\tilde{\kappa}\nabla T - \tilde{Q}\rho\tilde{d}\nabla\Lambda\right), && (5.10)\\
\rho\frac{\mathrm{D}\Lambda}{\mathrm{D}t} &= \rho\tilde{W} + \nabla\cdot(\rho\tilde{d}\nabla\Lambda). && (5.11)
\end{aligned}$$

For the analysis that follows, it is convenient to use $e = e_i - \tilde{Q}\lambda = RT/(\gamma-1) - \tilde{Q}\Lambda$ to express the energy equation as

$$\begin{aligned}
\rho\frac{\mathrm{D}T}{\mathrm{D}t} - \frac{\gamma-1}{R\gamma}\frac{\mathrm{D}p}{\mathrm{D}t} &= \frac{\gamma-1}{R\gamma}\Bigg(\tilde{Q}\rho\tilde{W} - \frac{2}{3}\tilde{\mu}\left(\nabla\cdot\mathbf{u}\right)^2 + \tilde{\mu}\left(\nabla\mathbf{u} : \nabla\mathbf{u}\right) && (5.12)\\
&+ \tilde{\mu}\left(\nabla\mathbf{u} : \nabla\mathbf{u}^T\right) + \nabla\cdot(d\nabla T)\Bigg). && (5.13)
\end{aligned}$$

We shall focus on the two-dimensional case for simplicity. Consider a localized

wave moving into an equilibrium, quiescent state and let ρ_a, p_a, T_a and $u_a = \sqrt{p_a/\rho_a}$ denote, respectively, the density, pressure, temperature and Newtonian sound speed in the fresh mixture ahead of the wave. We rescale the dependent variables with respect to this reference state. The independent variables are rescaled as follows:

$$x = \frac{X - D_0 t}{x_0}, \quad y = \frac{Y}{y_0}, \quad \tau = \frac{t}{t_0}, \tag{5.14}$$

where X and Y are the original spatial variables and D_0 is a typical wave speed, which is to be determined in the process of deriving the asymptotic model by requiring non-triviality of the leading-order corrections. The length scales, x_0, y_0 and the time scale, t_0, are chosen to reflect the appropriate physics of weakly nonlinear waves. We assume that $\epsilon = x_0/(u_a t_0)$ is small, which means that the spatial scale of interest in the x-direction, which is related to the size of the reaction zone, is small compared with the typical distance covered by acoustic waves in time t_0. For the transverse dimension, we assume the scaling $y_0 = x_0/\sqrt{\epsilon}$. This follows from the fact that, along a weakly curved front, a distance ϵ in the normal direction corresponds to a distance $O(\sqrt{\epsilon})$ in the transverse direction.

Several dimensionless groups appear upon rescaling of the governing equations. We define the Reynolds, Prandtl and Lewis numbers, respectively, as follows:

$$\mathrm{Re} = \frac{\rho_a u_a x_0}{\tilde{\mu}}, \quad \mathrm{Pr} = \frac{c_p \mu}{\tilde{\kappa}}, \quad \mathrm{Le} = \frac{\tilde{\kappa}}{\rho_a c_p \tilde{d}}, \tag{5.15}$$

where $c_p = \gamma R/(\gamma - 1)$. Writing $\mathbf{u} = (U, V)^T$, it is convenient to introduce the differential operator:

$$L = \partial_\tau + \frac{1}{\epsilon}(U - D_0)\partial_x + \frac{1}{\sqrt{\epsilon}} V \partial_y. \tag{5.16}$$

Introducing the dimensionless parameters,

$$Q = \frac{\tilde{Q}}{RT_a}, \quad E = \frac{\tilde{E}}{RT_a}, \quad K = t_0 \tilde{k} \exp\left(-E\right), \tag{5.17}$$

the non-dimensional governing equations become (see Appendix D for details):

$$\begin{aligned}
L[\rho] + \rho\left(\frac{1}{\epsilon}U_x + \frac{1}{\sqrt{\epsilon}}V_y\right) &= 0, && (5.18)\\
\rho L[U] + \frac{1}{\epsilon}p_x &= \frac{1}{3\epsilon\mathrm{Re}}\left(U_{xx} + \sqrt{\epsilon}V_{xy}\right) + \frac{1}{\epsilon\mathrm{Re}}\left(U_{xx} + \epsilon U_{yy}\right), && (5.19)\\
\rho L[V] + \frac{1}{\sqrt{\epsilon}}p_y &= \frac{1}{3\epsilon\mathrm{Re}}\left(\sqrt{\epsilon}U_{xy} + \epsilon V_{yy}\right) + \frac{1}{\epsilon\mathrm{Re}}\left(V_{xx} + \epsilon V_{yy}\right), && (5.20)\\
\rho L[T] - \frac{(\gamma-1)}{\gamma}L[p] &= \frac{\gamma-1}{\gamma}\Bigg(Q\rho W - \frac{2}{3\epsilon\mathrm{Re}}\left(U_x + \sqrt{\epsilon}V_y\right)^2\\
&+ \frac{1}{\epsilon\mathrm{Re}}\left(U_x^2 + \epsilon U_y^2 + V_x^2 + \epsilon V_y^2\right)\Bigg)\\
&+ \frac{\gamma-1}{\gamma}\frac{1}{\epsilon\mathrm{Re}}\left(U_x^2 + \sqrt{\epsilon}U_y V_x + \sqrt{\epsilon}V_x U_y + \epsilon V_y^2\right)\\
&+ \frac{1}{\epsilon\mathrm{RePr}}\left(T_{xx} + \epsilon T_{yy}\right), && (5.21)\\
\rho L[\Lambda] &= \rho W + \frac{1}{\epsilon\mathrm{RePrLe}}\left(\left(\rho\Lambda_x\right)_x + \epsilon\left(\rho\Lambda_y\right)_y\right), && (5.22)
\end{aligned}$$

where W is defined as

$$W = K(1-\Lambda)\exp\left[E\left(1 - \frac{1}{T}\right)\right]. \tag{5.23}$$

5.3 Weakly nonlinear approximation of detonations

We develop an asymptotic simplification of the above general formulation by considering a weakly nonlinear detonation wave, for which we assume that the heat release

is small, the activation energy is large and the Newtonian limit, $0 < \gamma - 1 \ll 1$, holds. To be precise, we start from (5.18-5.22) and make the following assumptions:

1. $K = k/\epsilon$, $k = O(1)$. This assumption is chosen to ensure that the reaction rate affects the leading order expansion of Λ. Since $K = t_0\tilde{k}$, this assumption implies that the characteristic time scale, t_0, of weakly nonlinear detonations is large compared to the collision time, $1/\tilde{k}$, i.e., $\epsilon t_0 \sim (1/\tilde{k})$.

2. $(\gamma - 1)\, Q/\gamma = \epsilon^2 q$, $q = O\,(1)$. This assumption implies that the heat release does not play a role at the linear level. It does not mean that the chemistry is unimportant, but that the heat release must have the appropriate size to balance the nonlinear effects. The extra factor of $(\gamma - 1)\,/\gamma$ in front of Q arises naturally in the governing equations (see (5.21)) and is retained in the definition of q. With the further assumption below of small $\gamma - 1$, this implies that Q is $O\,(\epsilon)$.

3. $E = \theta/\epsilon^2$, $\theta = O\,(1)$. This ensures that small temperature deviations – which are $O\,(\epsilon^2)$ for weak shocks in the Newtonian limit – have an $O\,(1)$ influence on the reaction rate.

4. $\gamma - 1 = \gamma_1\epsilon$, $\gamma_1 = O\,(1)$. This assumption is needed to balance the temperature fluctuations with both the acoustics and chemistry at the same order. Without this assumption, the leading order corrections for density, velocity and temperature all behave the same way, as in a weakly nonlinear inert shock [88, 89]. As we show later, having a temperature profile that is different from density/velocity profiles is crucial, as it allows the model derived here to incorporate the dynamical instabilities of detonation waves.

5. Le and Pr are $O\,(1)$, while Re is $O(1/\epsilon)$. Other scalings that highlight different

transport effects are of course possible, but they are not considered in this chapter.

To understand some of the intuition behind the asymptotic ordering above, recall the following well-known fact for weak shocks [90]. If the shock strength is measured by the relative jump in pressure across the shock, $\Delta p = (p_s - p_a)/p_a$ (subscripts s and a denoting post- and pre-shock states, respectively), then the shock Mach number is $\mathrm{M} = 1 + [(\gamma+1)/(4\gamma)]\,\Delta p + O\left((\Delta p)^2\right)$ and the shock temperature is $T_s/T_a = 1 + [(\gamma-1)/\gamma]\,\Delta p + O\left((\Delta p)^2\right)$. Therefore, for weak shocks, with $\mathrm{M} - 1 = O(\epsilon)$, in the Newtonian limit, $\gamma - 1 = O(\epsilon)$, the leading-order temperature correction is $O(\epsilon^2)$. That is, all variables have an $O(\epsilon)$ jump across the shock, but the temperature jump is smaller, only $O(\epsilon^2)$. In the chosen asymptotic approximation, we therefore expect similar temperature behavior in the reaction zone as well, at least with inviscid detonations.

Now, we assume the following expansions in the reaction zone:

$$\rho = 1 + \rho_1\epsilon + \rho_2\epsilon^{3/2} + \rho_3\epsilon^2 + o(\epsilon^2), \tag{5.24}$$

$$T = 1 + T_1\epsilon + T_2\epsilon^{3/2} + T_3\epsilon^2 + o(\epsilon^2), \tag{5.25}$$

$$p = 1 + p_1\epsilon + p_2\epsilon^{3/2} + p_3\epsilon^2 + o(\epsilon^2), \tag{5.26}$$

$$\boldsymbol{u} = \mathbf{u}_1\epsilon + \mathbf{u}_2\epsilon^{3/2} + \mathbf{u}_3\epsilon^2 + o(\epsilon^2), \tag{5.27}$$

$$\Lambda = \lambda + o(\epsilon). \tag{5.28}$$

The fractional powers appear here because we aim at capturing weak curvature effects in the detonation front. These effects induce a flow velocity transverse to the front, which is $O(\sqrt{\epsilon})$ smaller than the longitudinal velocity. Expansions of this type are standard for waves incorporating the weak-curvature effect (e.g., [91]).

Expanding $p = \rho T$, we find that $p_1 = \rho_1 + T_1$, $p_2 = \rho_2 + T_2$ and $p_3 = \rho_3 + T_3 + \rho_1 T_1$. Using these relations to eliminate pressure perturbations, inserting (5.24-5.28) into (5.18-5.22) yields (see Appendix E for details)

$$\begin{aligned}
&(-D_0\rho_{1x} + U_{1x}) + \sqrt{\epsilon}\,(-D_0\rho_{2x} + U_{2x} + V_{1y}) + \\
&\quad \epsilon\,(\rho_{1\tau} - D_0\rho_{3x} + U_1\rho_{1x} + U_{3x} + \rho_1 U_{1x} + V_{2y}) &&= o(\epsilon), && (5.29)\\
&(-D_0 U_{1x} + T_{1x} + \rho_{1x}) + \sqrt{\epsilon}\,(-D_0 U_{2x} + T_{2x} + \rho_{2x}) + \\
&\epsilon\,(U_{1\tau} - D_0 U_{3x} + U_1 U_{1x} + T_1\rho_{1x} + T_{3x} + \rho_{3x} - \rho_1\rho_{1x}) &&= \frac{4}{3}\frac{1}{\mathrm{Re}}\,(U_1)_{xx} + o(\epsilon), && (5.30)\\
&(-D_0 V_{1x}) + \sqrt{\epsilon}\,(-D_0 V_{2x} + T_{1y} + \rho_{1y}) + \\
&\quad \epsilon\,(V_{1\tau} - D_0 V_{3x} + U_1 V_{1x} + T_{2y} + \rho_{2y}) &&= \frac{1}{\mathrm{Re}}\,(V_1)_{xx} + o(\epsilon), && (5.31)\\
&(-D_0 T_{1x}) + \sqrt{\epsilon}\,(-D_0 T_{2x}) + \\
&\epsilon\left(T_{1\tau} - D_0 T_{3x} + U_1 T_{1x} + \frac{\gamma_1}{\gamma} D_0\,(\rho_{1x} + T_{1x})\right) &&= \epsilon q\omega + o(\epsilon), && (5.32)\\
&\qquad -D_0\lambda_x &&= \omega + o(1). && (5.33)
\end{aligned}$$

Because of the weak heat release assumption, we need to expand only the reaction progress variable and the reaction rate to the leading order. As we shall see later, the leading-order corrections to temperature are of order ϵ^2, i.e., $T_1 = T_2 = 0$, and therefore the leading-order reaction rate is given by

$$\omega = k(1-\lambda)\exp(\theta T_3)\,. \tag{5.34}$$

Balancing $O(1)$ terms, we find that

$$\begin{bmatrix} -D_0 & 1 & 0 & 0 \\ 1 & -D_0 & 0 & 1 \\ 0 & 0 & -1 & 0 \\ 0 & 0 & 0 & -1 \end{bmatrix} \begin{bmatrix} \rho \\ U \\ V \\ T \end{bmatrix}_{1x} = \begin{bmatrix} 0 \\ 0 \\ 0 \\ 0 \end{bmatrix}. \tag{5.35}$$

This homogeneous system has non-trivial solutions if and only if the coefficient matrix (denoted by $\mathbf{A}$ from now on) is singular. Therefore, we must have $D_0 = \pm 1$. We focus on a right-going wave for which $D_0 = 1$.

After substituting $D_0 = 1$, we integrate the first equation in (5.35) to obtain $U_1 = u(x, y, \tau) + \bar{U}(y, \tau)$, $\rho_1 = u(x, y, \tau) + \bar{\rho}\,(y, \tau)$ for some, so far arbitrary, functions $\bar{U}\,(y, t)$ and $\bar{\rho}\,(y, t)$. In order for our asymptotic expansions to hold as we approach the upstream state, which is assumed to be quiescent and uniform at all times, we require $\rho_1 = U_1 \equiv 0$ as $x \to \infty$ (upstream of the wave). As a consequence, it follows that $\bar{U}(y, t) = \bar{\rho}\,(y, t) \equiv 0$. Had we considered the case where the wave moves into a non-uniform background, the functions $\bar{\rho}$ and $\bar{U}$ would provide the freedom needed to match the asymptotic expansion in the wave zone to the flow ahead (see, e.g., [32]). A similar reasoning can be used to deduce from the third and fourth equation in (5.35) that $T_1 = V_1 \equiv 0$.

At $O(\epsilon^{1/2})$, we obtain

$$\begin{bmatrix} -1 & 1 & 0 & 0 \\ 1 & -1 & 0 & 1 \\ 0 & 0 & -1 & 0 \\ 0 & 0 & 0 & -1 \end{bmatrix} \begin{bmatrix} \rho \\ U \\ V \\ T \end{bmatrix}_{2x} = \begin{bmatrix} 0 \\ 0 \\ -u_y \\ 0 \end{bmatrix}, \tag{5.36}$$

with the same matrix of coefficients, $\mathbf{A}$, as before. Since $\mathbf{A}$ is singular, this system has solutions if and only if the right-hand side is orthogonal to $\mathbf{l}_0 = [1\,1\,0\,1]$, which spans the left null-space of $\mathbf{A}$. Clearly, this condition is always satisfied here. Note that from the third and fourth equation in 5.36, we obtain that $V_{2x} = u_y$ and $T_2 = 0$, i.e., letting

$$v = V_2 \tag{5.37}$$

such that

$$v_x = u_y. \tag{5.38}$$

Finally, at $O(\epsilon)$, we obtain

$$\begin{bmatrix} -1 & 1 & 0 & 0 \\ 1 & -1 & 0 & 1 \\ 0 & 0 & -1 & 0 \\ 0 & 0 & 0 & -1 \end{bmatrix} \begin{bmatrix} \rho \\ U \\ V \\ T \end{bmatrix}_{3x} = \begin{bmatrix} -u_\tau - 2uu_x - v_y \\ -u_\tau + \frac{4}{3}\frac{1}{\epsilon \mathrm{Re}} u_{xx} \\ -\rho_{2y} \\ q\omega - \frac{\gamma_1}{\gamma} u_x \end{bmatrix}. \tag{5.39}$$

Notice that since $\mathrm{Re} = O(1/\epsilon)$, all terms in (5.39) are $O(1)$. The solvability condition for this system is that the right-hand side be orthogonal to $\mathbf{l}_0 = [1\,1\,0\,1]$, which yields:

$$2u_\tau + 2uu_x + v_y = q\omega - \frac{\gamma_1}{\gamma} u_x + \frac{4}{3}\frac{1}{\epsilon \mathrm{Re}} u_{xx}. \tag{5.40}$$

This equation together with

$$v_x = u_y, \tag{5.41}$$

$$\lambda_x = -\omega, \tag{5.42}$$

forms a closed system of equations. The temperature dependence in the leading order rate function, (5.34), can be eliminated by integrating the last equation in (5.39),

$$T_3 = \frac{\gamma_1}{\gamma} u + q\lambda, \tag{5.43}$$

giving

$$\omega = k(1-\lambda) \exp\left(\theta\left(\frac{\gamma_1}{\gamma} u + q\lambda\right)\right). \tag{5.44}$$

Therefore, we obtain

$$\begin{aligned} 2u_\tau + 2uu_x + \frac{\gamma_1}{\gamma} u_x + v_y &= -q\lambda_x + \frac{4}{3}\frac{1}{\epsilon \mathrm{Re}} u_{xx}, & (5.45)\\ v_x &= u_y, & (5.46)\\ \lambda_x &= -k(1-\lambda) \exp\left(\theta\left(\frac{\gamma_1}{\gamma} u + q\lambda\right)\right). & (5.47) \end{aligned}$$

As can be seen from (5.39), species and heat diffusion play no role in the asymptotic equations up to $O(\epsilon)$. Had we considered different asymptotic orderings for the Lewis and Prandtl numbers, these effects would introduce diffusive terms in the energy and the reaction-rate equations. This complicates the analysis, and therefore we consider no such effects in this chapter, and hence the only effective diffusion in the asymptotic model comes from the viscous dissipation. The effect of heat diffusion is explored later in Chapter 6.

It is convenient to further rescale the variables as:

$$x \mapsto x - \gamma_1/(2\gamma)\,\tau,\ y \mapsto 2^{-1/2} q^{-1/4} y,\ \tau \mapsto q^{-1/2}\tau,\ u \mapsto q^{1/2} u,\ v \mapsto 2^{1/2} q^{3/4} v, \tag{5.48}$$

where the scale for u is chosen so that the traveling wave solution found later in Section 5.4.1 has speed 1. We also choose $\epsilon = (\gamma - 1)/\gamma$, which means that $\gamma_1 = \gamma$.

Other choices of ϵ are possible as long as ϵ and $\gamma - 1$ are of the same asymptotic order when $\epsilon \to 0$. These choices, although equivalent in the limit $\epsilon \to 0$, will have some effect on the quantitative numerical predictions for finite ϵ. With this rescaling and the choice of ϵ, we obtain our final asymptotic system of equations of weakly nonlinear detonation:

$$u_\tau + uu_x + v_y = -\frac{1}{2}\lambda_x + \mu u_{xx}, \tag{5.49}$$

$$v_x = u_y, \tag{5.50}$$

$$\lambda_x = -k(1-\lambda)\exp\left[\theta\left(\sqrt{q}u + q\lambda\right)\right], \tag{5.51}$$

where $\mu = 2/\left(3\sqrt{q}\epsilon \mathrm{Re}\right)$ is the dimensionless viscosity coefficient.

In the inviscid case, (5.49-5.51) must be supplemented by the appropriate jump conditions across shocks. If the shock locus is defined by $\phi(x, y, \tau) = x - s(y, \tau) = 0$ and $[z]$ denotes the jump of z across the shock, the Rankine-Hugoniot conditions are:

$$s_\tau [u] - \frac{1}{2}\left[u^2\right] + s_y [v] = 0, \tag{5.52}$$

$$s_y [u] + [v] = 0, \tag{5.53}$$

$$[\lambda] = 0. \tag{5.54}$$

These equations follow from the conservation form of (5.49-5.51).

Implicit in the definition (5.23) of the rate of reaction, W, lies the ignition temperature assumption, such that $W \equiv 0$ for $T < T_i/T_a$. Thus, the leading order reaction rate, ω, given by (5.34) also satisfies $\omega \equiv 0$ for $T_3 < \left(T_i/T_a - 1\right)/\epsilon^2$ or, equivalently, for $u + q\lambda < \left(T_i/T_a - 1\right)/\epsilon^2$. In order to prevent reactions from occurring in the ambient state, a reasonable constraint on the ignition temperature is that it be larger than the ambient temperature, T_a. Furthermore, for the ZND solution to exist, it is

necessary that the ignition temperature, T_i, be smaller than the temperature at the von Neumann state of the ZND solution. In the weakly nonlinear regime considered in this paper, we must therefore have $0 < T_i - T_a = O(\epsilon^2)$. This should be viewed as a modeling assumption about the chemical kinetics. Notice that in the inviscid case, the ignition temperature, if taken to be $T_i \gtrapprox T_a$, has no effect on the ZND profiles and their stability properties. Simply, it states that the reactions occur only after the shock and therefore, $\omega = 0$ ahead of the wave. When considering viscous effects, however, the traveling wave profiles and their dynamical evolution will depend on the ignition temperature and T_i should therefore be considered as another parameter that affects the properties of the solutions.

For the convenience of the reader, in Table 5.1, we collect the relations between various dimensionless and dimensional quantities.

Dimensional	Dimensionless	Physical meaning
$\tilde{Q}$	$Q = \tilde{Q}/RT_a = \epsilon q$	Heat release
$\tilde{E}$	$E = \tilde{E}/RT_a = \theta/\epsilon^2$	Activation energy
$\tilde{k}$	$K = t_0\tilde{k}\exp(-E) = k/\epsilon$	Reaction pre-factor
t	$\tau = t/t_0 = \epsilon t u_a/x_0$	Time
X	$x = (X - D_0 t)/x_0 - \tau$	Longitudinal direction
Y	$y = \left(\sqrt{2\epsilon}q^{1/4}/x_0\right)Y$	Transverse direction
$\tilde{\mu}$	$\mu = 2/\left(3\sqrt{q}\epsilon\mathrm{Re}\right)$	Viscous dissipation

Table 5.1: Summary of scaling relationships.

The relationships between the asymptotic variables u, v and λ and the physical (dimensionless, rescaled with the upstream state) quantities, ρ, U, V, T and Λ are

given by

$$\rho = 1 + \epsilon\sqrt{q}u + O(\epsilon^{3/2}), \tag{5.55}$$

$$U = \epsilon\sqrt{q}u + O(\epsilon^{3/2}), \tag{5.56}$$

$$V = \epsilon^{3/2}\sqrt{2}q^{3/4}v + O(\epsilon^2), \tag{5.57}$$

$$T = 1 + \epsilon^2\left(\sqrt{q}u + q\lambda\right) + O(\epsilon^{5/2}), \tag{5.58}$$

$$\Lambda = \lambda + O(\epsilon). \tag{5.59}$$

For the remainder of the paper, we focus exclusively on the inviscid case such that the asymptotic equations take the form

$$u_\tau + uu_x + v_y = -\frac{1}{2}\lambda_x, \tag{5.60}$$

$$v_x = u_y, \tag{5.61}$$

$$\lambda_x = -k(1-\lambda)\exp\left[\theta\left(\sqrt{q}u + q\lambda\right)\right]. \tag{5.62}$$

An important connection is now made with the qualitative work performed in Part I, where it was assumed that the reaction rate depends on the shock state only, i.e., $\omega\left(\lambda, u\right) \approx \omega\left(\lambda, u_s\right)$. The discussion that follows is rather informal, and intended only to motivate the non locality assumption so frequently employed in Part I. The important observation is that, for $q \gg 1$, $\theta q = O(1)$, the main contribution of u in (5.62) will come from region where $\lambda \ll 1$. In particular, given the rescaling we performed in (5.48), the ZND solutions are always $O(1)$, even for large q (see Section 5.4). Therefore for u to contribute to the reaction rate we need $q\lambda \approx \sqrt{q}u$, which happens for $\lambda = O(1/\sqrt{q})$. This means the reaction rate is affected by u only when $\lambda \approx 0$, and since $\lambda = 0$ ahead of the shock, we know that λ is near zero only close to the shock, where u is well approximated by u_s (assuming u_x is bounded). Thus, a

reasonable ansatz for a uniformly valid (for $\lambda \in [0,1]$) asymptotic approximation for the reaction rate, in the limit of large q and small θ, is given by

$$\begin{aligned}\omega &= k\,(1-\lambda)\exp\left(\theta\left(\sqrt{q}u + q\lambda\right)\right)\\ &\approx k\,(1-\lambda)\exp\left(\theta\left(\sqrt{q}u_s + q\lambda\right)\right)\end{aligned}$$

It is important to note that $u \not\approx u_s$ everywhere, and thus a simple Taylor series does not justify the approximation. The key factor is that u always appears through the combination $T_3 = \sqrt{q}u + q\lambda$, and therefore when $u \not\approx u_s$ the $q\lambda$ terms dominates.

We note here that without the chemical reaction, (5.60-5.62) reduce to

$$u_\tau + \left(\frac{u^2}{2}\right)_x + v_y = 0, \tag{5.63}$$

$$v_x = u_y, \tag{5.64}$$

which are canonical equations appearing in the analysis of various physical phenomena modeled by weakly-nonlinear quasi-planar hyperbolic waves. In terms of the velocity potential, ϕ, such that $\nabla\phi = (u, v)$, these equations can be rewritten as

$$\phi_{x\tau} + \left(\frac{\phi_x}{2}\right)_x^2 + \phi_{yy} = 0, \tag{5.65}$$

which is the well-known UTSD equation [92]. In nonlinear acoustics, this equation is also known as the Zabolotskaya-Khokhlov equation [93].

In the following sections, we investigate the steady-state solutions of (5.60-5.62), their spectral stability and nonlinear dynamics, and demonstrate that the asymptotic theory contains the essential features of not only the steady-state one-dimensional, but also the unsteady and multi-dimensional traveling waves of the reactive Euler

equations.

5.4 Traveling wave solutions and their linear stability

In this section, we analyze the traveling wave solutions of the asymptotic equations and their spectral stability, showing that the asymptotic solutions are analogous to their ZND counterparts. We start by presenting the one-dimensional traveling wave solutions in Section 5.4.1, which are the basis for the one- and multi-dimensional stability analyses presented in Section 5.4.2.

5.4.1 Traveling wave solutions of the asymptotic model

Seeking the one-dimensional traveling wave solutions of the inviscid asymptotic model (5.60-5.62) of the form $\bar{u} = \bar{u}(x - \bar{D}\tau)$, we obtain

$$\bar{u} = \bar{D} + \sqrt{\bar{D}^2 - \bar{\lambda}}, \tag{5.66}$$

where $\bar{D}$ is the speed of the wave and the bar denotes the steady state. It is easily seen that, for the solution to remain real at the end of the reaction zone, we must choose $\bar{D} \geq 1$. The precise choice of the value is related to the degree of overdrive of the wave. Even though the overdriven detonations can be included in the analysis, we focus on the important case of a self sustained detonation in which the steady state has a sonic point at the end of the reaction zone. Then, $\bar{D} = 1$ and

$$\bar{u} = 1 + \sqrt{1 - \bar{\lambda}}, \tag{5.67}$$

where $\bar{\lambda}$ solves

$$\bar{\lambda}_\xi = -k\left(1-\bar{\lambda}\right)\exp\left(\theta\left(\sqrt{q}\bar{u}+q\bar{\lambda}\right)\right) \tag{5.68}$$

with $\xi = x-\tau$ and boundary condition $\bar{\lambda}(0)=0$ (this is analogous to the ZND theory, see [2]). This solution is used in the analysis that follows.

The steady-state structure of the asymptotic model contains substantial information about the underlying modeling assumptions. A crucial *qualitative* feature of the structure is that, because of the behavior of the leading order correction to temperature, $T_3 = u + q\lambda$, it is possible to have a maximum of the reaction-rate function, (5.68), inside the reaction zone, as we show in Fig. 5.1. The presence of the internal

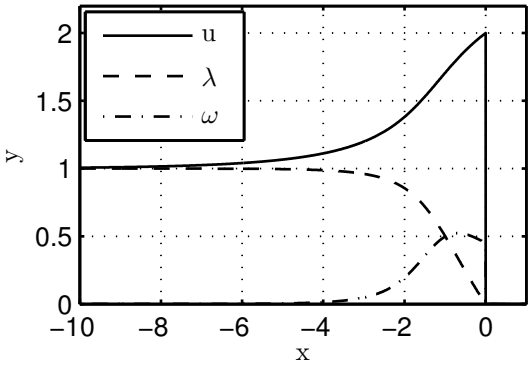

Figure 5.1: Steady-state profiles and the rate function of the asymptotic solution for $q = 1.7$ and $\theta = 1.7$.

maximum in the reaction rate appears to be an important factor responsible for the observed unsteady dynamics of real detonations, consistent with our previous work on a closely related model equation [77, 76]. In fact, we have verified that even the qualitative models of Fickett,

$$u_t + \left(\frac{u^2}{2}+q\lambda\right)_x = 0, \qquad \lambda_t = \omega(\lambda,u), \tag{5.69}$$

and Majda (in the inviscid limit),

$$(u + q\lambda)_t + \left(\frac{u^2}{2}\right)_x = 0, \qquad \lambda_t = \omega(\lambda, u), \tag{5.70}$$

are capable of capturing the one-dimensional instabilities of detonation waves if the reaction rate is taken as (5.44). We recall that, in these models, the reaction rate usually takes the form

$$\omega = (1 - \lambda)\,\varphi(u)\,, \tag{5.71}$$

where the ignition function, $\varphi(u)$, is

$$\varphi = \begin{cases} \varphi_0(u)\,, & u > u_i \\ 0, & u < u_i \end{cases}, \tag{5.72}$$

and u_i is the "ignition-temperature" parameter (see, e.g., [17, 29]). The new rate function, given by (5.44), reflects the crucially important feature of the heat-release in unstable detonations, which exhibits a maximum inside the reaction zone. Thus, both Fickett's and Majda's models possess the necessary complexity needed to capture the qualitative dynamics of one-dimensional unstable detonations provided that the reaction-rate function is chosen appropriately.

The steady-state solution also provides a first *quantitative* test of the accuracy of the asymptotic approximation. In Figure 5.2, we show a comparison between the ZND solutions of the reactive Euler equations and their asymptotic counterparts as predicted by the present theory. We see that the asymptotic approximation performs rather well when the heat release is small and the activation energy is large, i.e., when $Q \sim \epsilon$ and $E \sim 1/\epsilon^2$. For example, for the realistic value of $\gamma = 1.2$ ($\epsilon = 1/6$), the relative error is only a small percentage (Figure 5.2c). As expected, for the smaller

value of $\gamma = 1.1$ ($\epsilon = 1/11$), the agreement is seen to improve (Figure 5.2b and Figure 5.2d), with the maximum relative error approximately two percent of the flow velocity. As expected, the approximation worsens as the values of $\gamma - 1$ and Q increase or the value of E decreases.

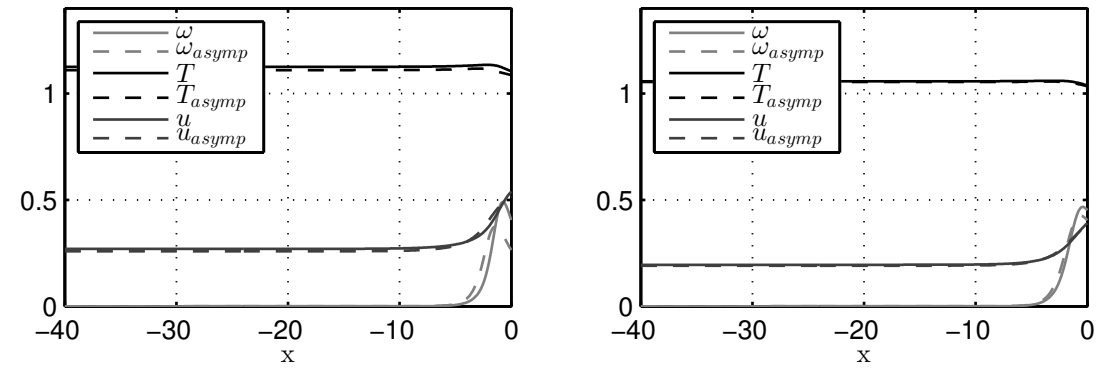

(a) Profiles for $\gamma = 1.2,\ Q = 0.4,\ E = 50;\ \epsilon = 1/6$.(b) Profiles for $\gamma = 1.1,\ Q = 0.4,\ E = 50;\ \epsilon = 1/11$.

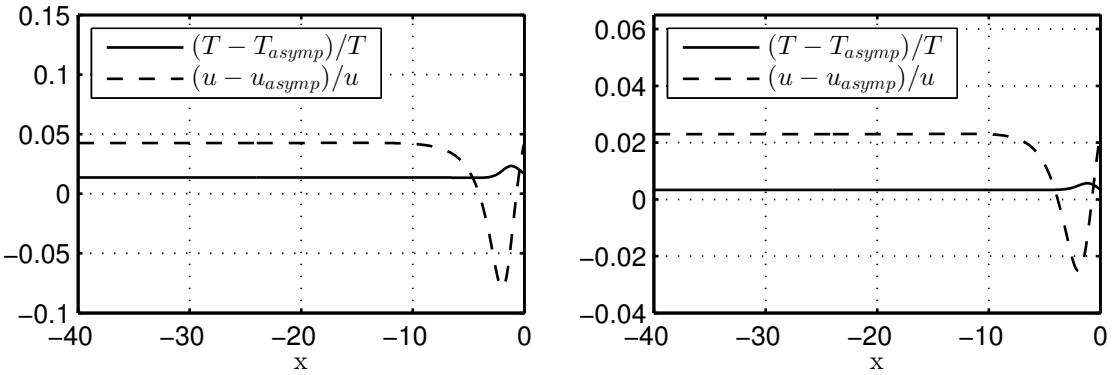

(c) Error for $\gamma = 1.2,\ Q = 0.4,\ E = 50;\ \epsilon = 1/6$. (d) Error for $\gamma = 1.1,\ Q = 0.4,\ E = 50;\ \epsilon = 1/11$.

Figure 5.2: Comparison between the exact and asymptotic steady-state ZND profiles. The asymptotic solutions are calculated using (5.55-5.59).

5.4.2 Linear stability theory for the asymptotic model

With the steady-state solutions in reasonable agreement with the reactive Euler equations, we next investigate their stability properties. It is well known that the reactive Euler equations for the ideal-gas equation of state and simple-depletion Arrhenius

kinetics predict that the steady-state detonations are unstable when the activation energy is large enough at a fixed heat release [15, 20, 16]. In this section, we analyze the linear stability of the traveling wave solutions obtained in the previous section to see if the asymptotic theory agrees with the Euler equations in this regard as well. We show that, indeed, the steady-state detonation waves become unstable if either the heat release or the activation energy crosses a certain threshold. We also demonstrate that multi-dimensional effects play a nontrivial role in the onset of instabilities.

To proceed with the analysis, let $\bar{u}$ and $\bar{\lambda}$ be the steady-state solution obtained in Section 5.4.1. Rewriting (5.60-5.62) in a shock-attached frame, $\chi = x - s(y,\tau)$, where $s(y,\tau)$ is the shock position, we obtain

$$\begin{aligned} u_\tau + (u - s_\tau)\, u_\chi + \frac{1}{2}\lambda_\chi + v_y - s_y v_\chi &= 0, && (5.73)\\ u_y - s_y u_\chi - v_\chi &= 0, && (5.74)\\ \lambda_\chi &= -k\,(1-\lambda)\exp\left(\theta\left(\sqrt{q}u + q\lambda\right)\right). && (5.75) \end{aligned}$$

Next, we expand the solution in normal modes,

$$\begin{aligned} u &= \bar{u}(\chi) + \delta u_1(\chi)\exp\left(\sigma\tau + ily\right) + O\left(\delta^2\right), && (5.76)\\ v &= \delta v_1(\chi)\exp(\sigma\tau + ily) + O(\delta^2), && (5.77)\\ \lambda &= \bar{\lambda}(\chi) + \delta\lambda_1(\chi)\exp\left(\sigma\tau + ily\right) + O\left(\delta^2\right), && (5.78)\\ s &= \bar{D}\tau + \delta\exp\left(\sigma\tau + ily\right), && (5.79) \end{aligned}$$

and let $\delta \to 0$. The linearized equations are then

$$\left(\bar{u} - \bar{D}\right) u_1' = -(\sigma + \bar{u}')u_1 + \sigma\bar{u}' - ilv_1 - \frac{1}{2}\left(g(\chi)u_1 + h(\chi)\lambda_1\right), \tag{5.80}$$

$$v_1' = ilu_1 - il\bar{u}', \tag{5.81}$$

$$\lambda_1' = g(\chi)u_1 + h(\chi)\lambda_1, \tag{5.82}$$

where the prime denotes a differentiation with respect to χ and

$$g(\chi) = -\frac{\partial\omega}{\partial u}\left(\bar{u}, \bar{\lambda}\right) = -k\theta\sqrt{q}\left(1 - \bar{\lambda}\right)\exp\left[\theta\left(\sqrt{q}\bar{u} + q\bar{\lambda}\right)\right], \tag{5.83}$$

$$h(\chi) = -\frac{\partial\omega}{\partial\lambda}\left(\bar{u}, \bar{\lambda}\right) = -k\left[\theta q\left(1 - \bar{\lambda}\right) - 1\right]\exp\left[\theta\left(\sqrt{q}\bar{u} + q\bar{\lambda}\right)\right]. \tag{5.84}$$

The boundary conditions for (5.80-5.82) are obtained from linearizing (5.52-5.54):

$$u_1(0) = 2\sigma; \qquad v_1(0) = -2il; \qquad \lambda_1(0) = 0. \tag{5.85}$$

Noticing that for self sustained detonation, $\bar{u} - \bar{D} \to 0$ as $\chi \to -\infty$, we require that the right-hand side of (5.80) vanish in the limit as well, i.e.,

$$H(\sigma, l) = -(\sigma + \bar{u}')u_1 + \sigma\bar{u}' - ilv_1 - \frac{1}{2}\left(g(\chi)u_1 + h(\chi)\lambda_1\right) \to 0 \quad \text{as } \chi \to -\infty.$$

Because $\bar{u'} \to 0,\ g(\chi) \to 0$ as $\chi \to -\infty$, this solvability condition (alternatively called the "boundedness" or the "radiation" condition [16]) simplifies to

$$-\sigma u_1 - ilv_1 - \frac{1}{2}h\left(-\infty\right)\lambda_1 \to 0 \quad \text{as } \chi \to -\infty. \tag{5.86}$$

To eliminate the numerical inconvenience of $\sigma = 0,\ l = 0$ always being an eigenvalue – a consequence of the translation invariance of the traveling wave – we rescale u_1

and λ_1 by σ and v_1 by il. The stability problem is then posed as follows:

Solve

$$\left(\bar{u} - \bar{D}\right) u_1' = -(\sigma + \bar{u}')u_1 + \bar{u}' + \frac{l^2}{\sigma} v_1 - \frac{1}{2}\left(g(\chi)u_1 + h(\chi)\lambda_1\right), \tag{5.87}$$

$$v_1' = \sigma u_1 - \bar{u}', \tag{5.88}$$

$$\lambda_1' = g(\chi)u_1 + h(\chi)\lambda_1, \tag{5.89}$$

subject to $u_1(0) = 2,\ v_1(0) = -1$ and $\lambda_1(0) = 0$ at the shock and the boundedness condition (5.86) at negative infinity.

The preceding eigenvalue problem is solved numerically using the shooting method of [16]. We solve the problem for different values of θ, q and l, which are the only remaining parameters. Consistent with the behavior of the stability spectrum of detonation waves in reactive Euler equations [16], we find that unstable modes do exist either for large enough q or for large enough θ. We also find that the transverse modes, where $l \neq 0$, tend to be more unstable than purely longitudinal disturbances [20].

First, we consider the purely one-dimensional problem, i.e., with $l = 0$. In Fig. 5.3, we show the contour plot of the absolute value of the stability function,

$$|H(\sigma, 0)| = \left| -(\sigma + \bar{u}')u_1 + \sigma\bar{u}' - \frac{1}{2}\left(g(\chi)u_1 + h(\chi)\lambda_1\right) \right|, \tag{5.90}$$

as a function of real and imaginary parts of σ. The valleys in the plot of $|H(\sigma, 0)|$, which correspond to the darker regions in Figure 5.3, provide an initial guess for the location of eigenvalues. A root solver is then used wherein the complex function, $H(\sigma, 0)$, is set to zero in order to accurately locate the eigenvalues. An increasing number of unstable eigenvalues is seen as the neutral boundary is crossed by increasing

the heat release, q, for a given value of the activation energy, θ. The qualitative behavior of the spectrum is in agreement with that known for the Euler detonations [16]. Furthermore, Figure 5.3a and Figure 5.3d show the migration of the oscillatory complex conjugates, with $\sigma_i \neq 0$, into non-oscillatory unstable modes that are also observed in the Euler equations [18]. Finally, in Figure 5.3e and Figure 5.3f, we see that far into the unstable regime, many eigenvalues are found, indicating a complexity of the linear spectrum.

We also obtain the neutral stability curves for the first two unstable eigenvalues in the asymptotic model, as shown in Figure 5.4a. It is seen that the lowest frequency mode 1 is more unstable than mode 2 for a wide range of q and θ. Substantially away from the neutral boundary, the non-oscillatory root may become dominant, as is seen in the example shown in Figure 5.3c and Figure 5.3d.

In Figure 5.4b, we plot the neutral curve for the lowest frequency eigenvalue, indicated by the solid line in Figure 5.4a, in the plane of the heat release, Q, and the activation energy, E. The result is compared with the neutral curve computed directly from the reactive Euler equations [16] and a reasonably close agreement between the two is seen. We observe that, as expected, the agreement improves with smaller Q and larger E. Finally, since the asymptotic model allows for easy calculations of the high activation energy/small heat release limit, we extend the prediction of the neutral boundary to rather high values of $E \approx 250$ and note that the asymptotic curve follows the scaling $Q \sim 1/E$ very well.

If $l \neq 0$, then there is the possibility that transverse waves will trigger the instabilities. This occurs in the Euler equations, where it is found that multi-dimensional instability prevails over purely longitudinal instability. Again, using the shooting method, we solve (5.87-5.89) numerically for various values of l. Solving for the roots

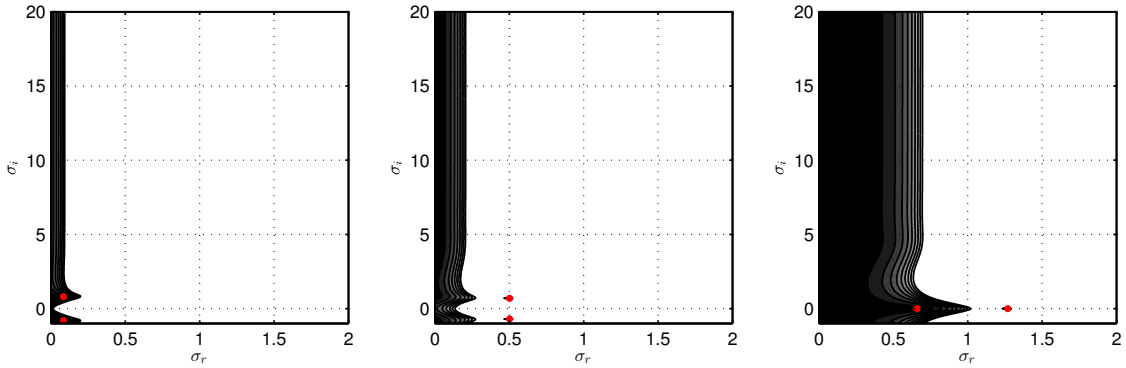

(a) $q = 1.8$ (b) $q = 2.2$ (c) $q = 2.6$

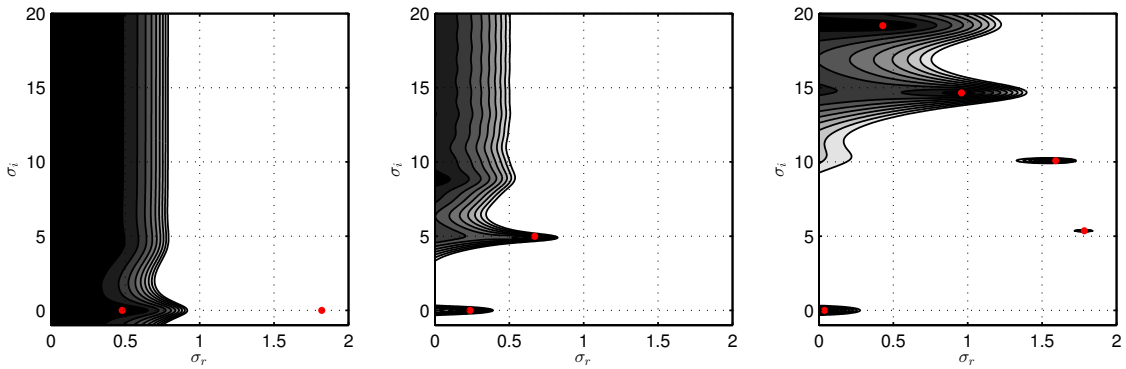

(d) $q = 2.75$ (e) $q = 3.5$ (f) $q = 4.5$

Figure 5.3: Contour plots of the spectral function (5.90) for $\theta = 1.8$ and increasing q. Note that the real part of the non-oscillatory root increases with q. The red dots in the figures represent the eigenvalues. In (e) and (c), the dominant non-oscillatory root is not shown.

of the radiation function,

$$H(\sigma, l) = -(\sigma + \bar{u}')u_1 + \sigma\bar{u}' - ilv_1 - \frac{1}{2}\left(g(\chi)u_1 + h(\chi)\lambda_1\right), \tag{5.91}$$

at $\chi = -\infty$, we obtain the two-dimensional stability spectrum. We first fix $q = 1.7$ and vary $\theta = 1.65, 1.60, 1.55$. In Figure 5.5, we show the real and imaginary parts of the unstable modes for relatively small values of l. It is seen that the model predicts purely two-dimensional instabilities for a certain range of the transverse wave numbers, and that increasing the activation-energy parameter, θ, has a destabilizing

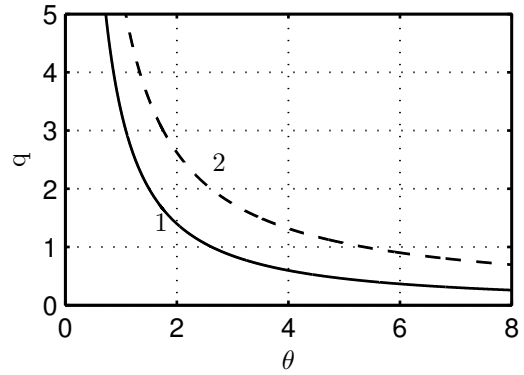

(a) Neutral stability boundaries for the first two low-frequency modes in the asymptotic model. The modes are unstable to the right of the curves.

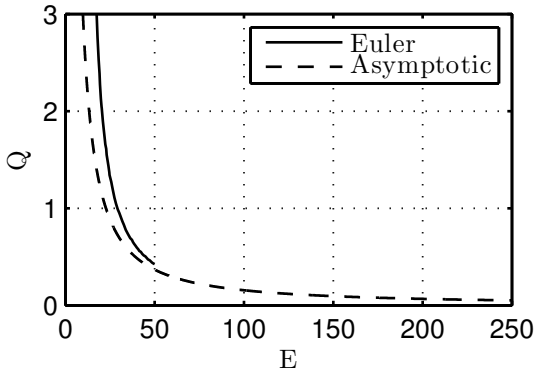

(b) Comparison of the asymptotic and the exact [16] neutral stability boundaries for $\gamma = 1.2$, in the heat release, Q, versus activation energy, E, plane.

Figure 5.4: Neutral stability curves.

effect on the steady-state solutions.

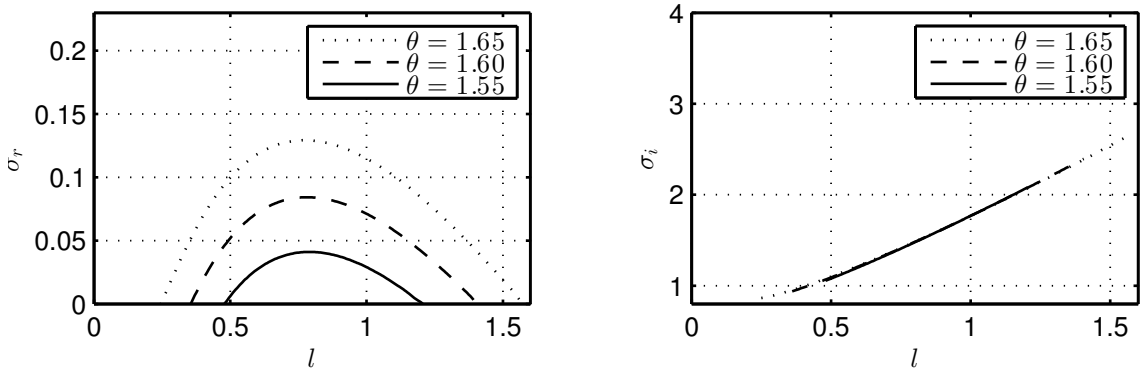

Figure 5.5: Growth rate and frequency for the most unstable mode versus the wavenumber, l, for several values of the activation energy, θ.

We also perform a quantitative comparison between the two-dimensional stability of the asymptotic model and the known stability diagram for the Euler equations. We choose the values of $\gamma = 1.2$, $Q = 0.4$ and $E = 50$. Then, after performing the appropriate conversion between dimensionless variables, we compare the asymptotic results with those obtained in [1] (see Figure 5.6). We observe a fair agreement. There are, however, some differences. We see that for the parameters chosen in Figure 5.6, the asymptotic model predicts one-dimensional instabilities, while the reactive

Euler equations do not. Also, we observe that the disagreement between the imaginary parts of the eigenvalues increases with increasing wavenumber. This should be expected because short transverse wavelengths cannot be represented accurately in the weak curvature limit assumed for this model. In the next section, we investigate the long-time nonlinear dynamics of the asymptotic solutions in regimes corresponding to linearly unstable steady-state one-dimensional solutions. The calculations are performed in both one and two spatial dimensions.

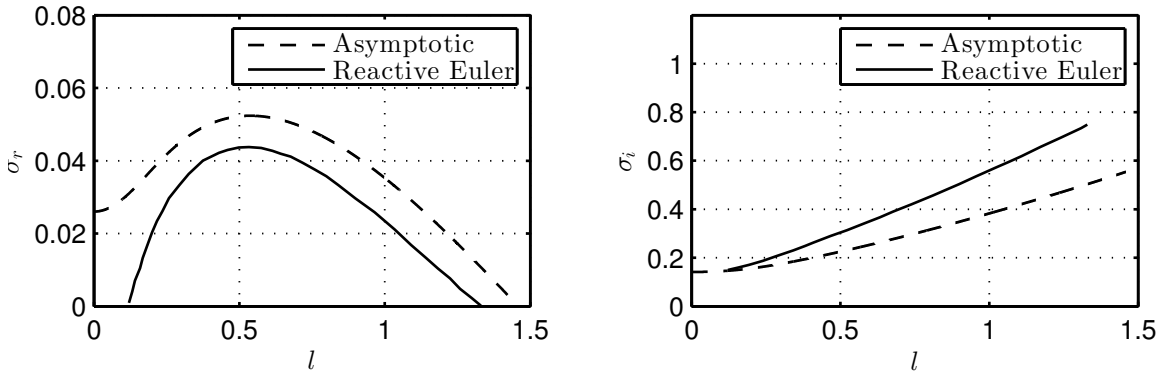

Figure 5.6: Comparisons of the growth rate and frequency for the most unstable mode versus the wave number, for $Q = 0.4$ and $E = 50$. The dashed curve corresponds to the model in this paper. The solid line corresponds to the reactive Euler equations as computed in [1].

5.5 Nonlinear dynamics of the asymptotic model

In the previous section, we showed that the asymptotic model exhibits the same linear stability behavior as the reactive Euler equations. The question of what happens after the onset of instabilities can be investigated through numerical simulations of the model equations. We show below that the traveling wave solutions of the asymptotic model reproduce, in both one and two spatial dimensions, the complexity observed in solutions of the reactive Euler equations.

5.5.1 Galloping detonations

We focus here on the ability of the asymptotic model to predict the complex nonlinear dynamics of pulsating (galloping) detonations. We perform a detailed numerical investigation of the large time asymptotic behavior of oscillatory solutions of the model. In the one-dimensional inviscid case, the system given by (5.49-5.51) reduces to

$$u_\tau + uu_x = -\frac{1}{2}\lambda_x, \tag{5.92}$$

$$\lambda_x = -k(1-\lambda)\exp(\theta(\sqrt{q}u + q\lambda)). \tag{5.93}$$

This system resembles the one derived in [32] with one crucial difference – as a consequence of the $\gamma - 1 = O(\epsilon)$ assumption, the reaction rate function in (5.93) has a more complicated λ-dependence, which is in fact at the heart of the complexity of the solutions obtained here. System (5.92-5.93) is also the same as in [47], where the $\gamma - 1 = O(\epsilon)$ assumption is used.

We solve (5.92-5.93) numerically in a shock-attached frame [60], using a second-order finite volume scheme with a second-order Total Variation Diminishing (TVD) Runge-Kutta temporal discretization [73]. Because no differentiation across the shock is performed, true second-order convergence is obtained for the cases tested, which include the convergence to various stable steady-state ZND solutions. We further verified the numerical algorithm by performing a cross-validation between the linear stability solver and the numerical solver. That is, we made sure that for several values of q, the linear stability prediction of the neutral boundary agrees with the neutral stability boundary of the numerical scheme for the nonlinear model. For example, when $q = 1.7$, the linear stability curve in Figure 5.4a indicates that $\theta_c = 1.710$ is the neutral value of the activation energy, i.e., the ZND wave is unstable for $\theta > \theta_c$

and stable for $\theta < \theta_c$. Numerical simulations of (5.92-5.93) with θ slightly above and slightly below θ_c confirm this prediction, as shown in Figure 5.7, where the shock state, u_s, is plotted as a function of time.

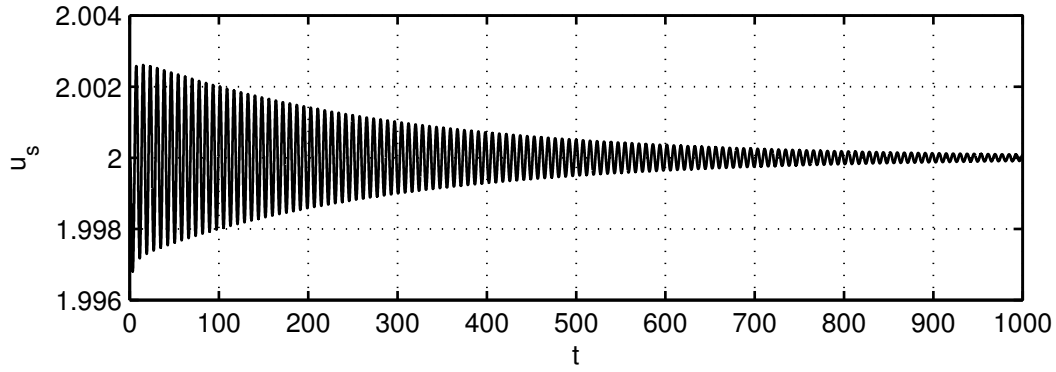

(a) Stability of the ZND solution at $\theta = 1.705 < \theta_c,\ q = 1.7$.

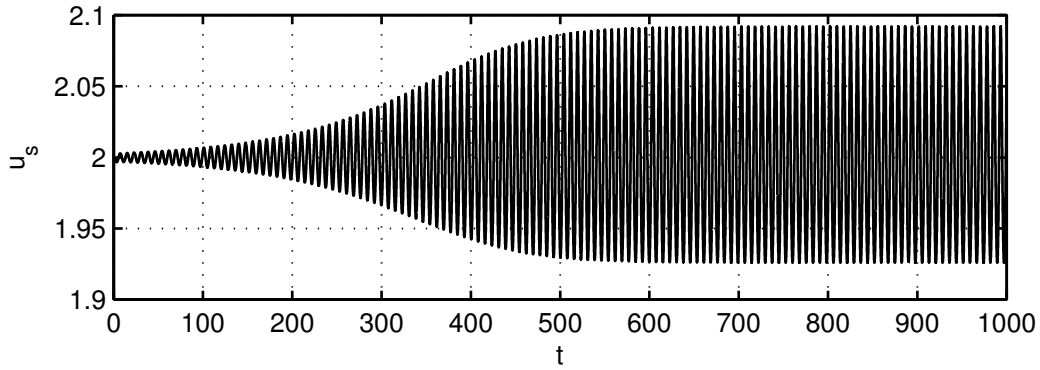

(b) Instability of the ZND solution and the limit-cycle attractor at $\theta = 1.715 > \theta_c,\ q = 1.7$. Notice that the amplitude of the limit cycle scales roughly as the square root of the distance to the bifurcation point, as in a super-critical Hopf bifurcation.

Figure 5.7: Nonlinear dynamics of (5.92-5.93) near the neutral boundary, $\theta_c = 1.710$, as predicted by the linear stability theory for $q = 1.7$.

We also compute solutions of (5.92-5.93) further away from the neutral boundary in order to check if the model captures a sequence of bifurcations leading to chaos as occurs in the reactive Euler equations [22, 23]. Such a sequence of bifurcations is indeed present in the model. Long time simulations show that the solutions tend to either a fixed point, a limit cycle or (what appears to be) a chaotic attractor. We run the simulations at $q = 5$ and plot the post-shock state, u_s (by the Rankine-Hugoniot

conditions, $u_s = 2D$, where D is the shock speed), as a function of time for several different types of solution, as shown in Figure 5.8. Beyond the stability boundary, the shock velocity becomes oscillatory. Near the neutral boundary, the oscillations have a small amplitude and are periodic (Figure 5.8a), but the structure of each period becomes more complex as we move away from the neutral boundary by increasing the activation energy (Figure 5.8b and Figure 5.8c). Eventually, a value of θ is reached at which no obvious period is evident as seen in Figure 5.8d.

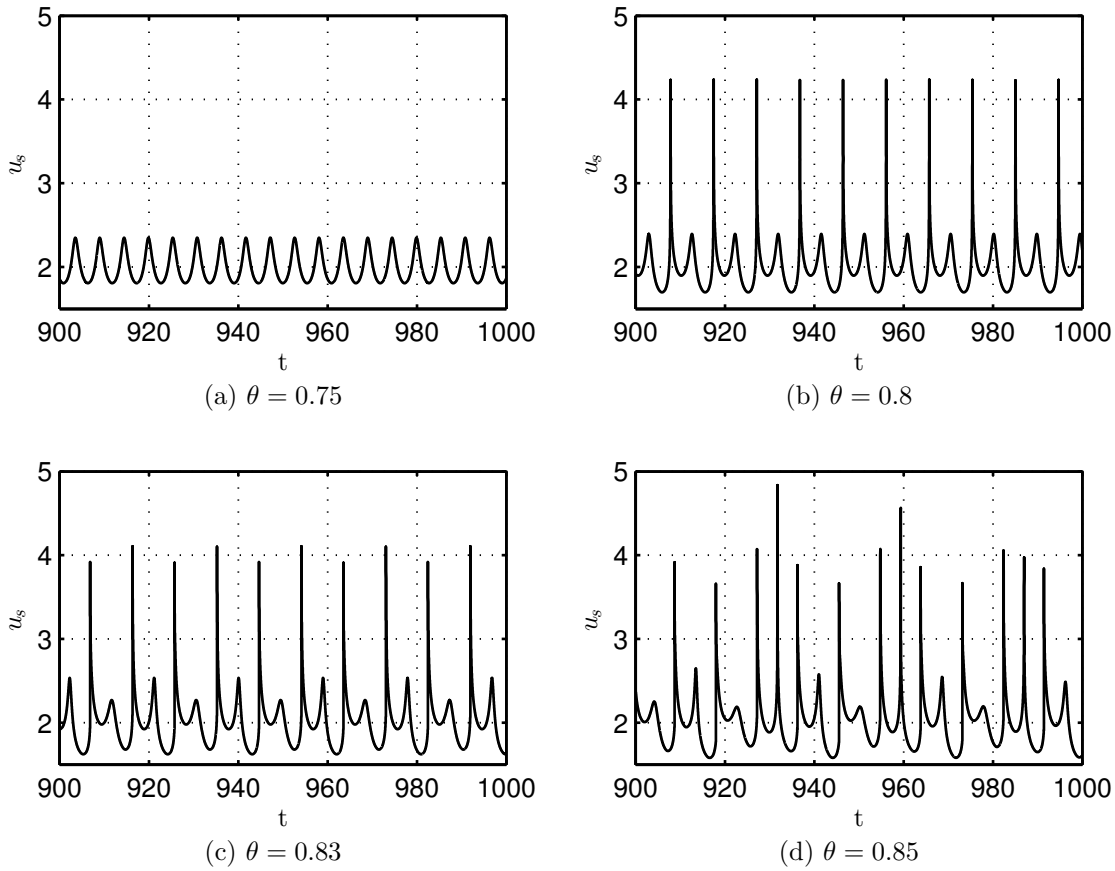

(a) $\theta = 0.75$ (b) $\theta = 0.8$

(c) $\theta = 0.83$ (d) $\theta = 0.85$

Figure 5.8: The shock state as a function of time for increasing values of θ and fixed $q = 5$ showing pulsations of different complexity.

The behavior described in the previous paragraph can be understood in terms of a period doubling sequence of bifurcations where the period becomes longer and more complex with each bifurcation. In order to construct a bifurcation diagram

illustrating this process, we proceed as follows: for each value of θ, we follow the evolution of the solution until it settles on the attractor. Then, we extract the set of local minima for $u_s(\tau)$ – a finite set for any periodic solution. The values of these minima are then plotted versus the bifurcation parameter, θ. The result is shown in Figure 5.10, which is reminiscent of the standard Feigenbaum period doubling cascade leading to chaos [94].

It is important to note that the further we move into the unstable region, the harder it is to numerically capture the wave dynamics with good accuracy. That is, in the highly unstable regime ($\theta \gtrapprox 0.85$ in Figure 5.10), the quantitative details of the bifurcation diagram are sensitively dependent on the grid resolution. In a truly chaotic regime, such sensitivity is intrinsic and reflects the nature of the system. However, another reason, which is at play even before the apparently chaotic regime sets on, is that the wave dynamics can involve spatial scales that undergo large changes (by orders of magnitude) during the wave evolution. This is a direct consequence of the Arrhenius exponential dependence of the reaction rate, which can trigger large variations in the reaction rate from moderate changes in the temperature when the activation energy is large. This issue of stiffness associated with high-activation energy detonations in unstable regimes is discussed next in more detail.

In theoretical and numerical studies of detonation, a widely used spatial scale is taken to be the half-reaction length, $x_{1/2}$, defined as the distance from the shock where half of the energy is released in the ZND solution. The space is then non-dimensionalized, as done in this work, so that the half-reaction happens over a unit length. The numerical resolution is thus measured as a number of points per this unit of length. Although appropriate for stable or weakly unstable detonations, the ZND half-reaction length and therefore the resolution measured on this scale become less meaningful when considering unstable detonations at high activation energies. The

reason is that the energy release can become extremely localized during the dynamical evolution of pulsating waves and therefore the actual number of grid points used to capture the heat release region can significantly decrease.

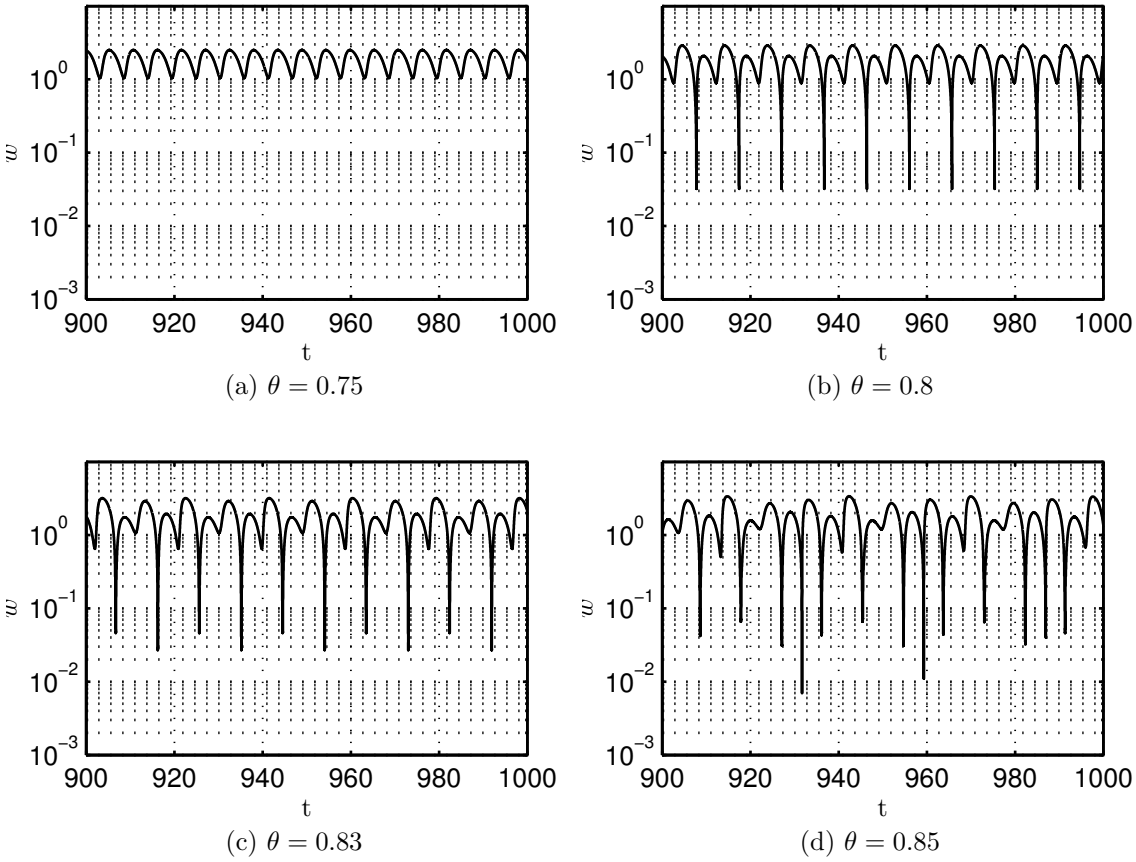

(a) $\theta = 0.75$ (b) $\theta = 0.8$

(c) $\theta = 0.83$ (d) $\theta = 0.85$

Figure 5.9: The width of the reaction zone as a function of time. The simulations were performed in a domain of length $L = 30$ and with $N = 30,000$ grid points ($dx = 10^{-3}$).

In order to provide a more quantitative measure of the variations of relevant spatial scales during the time evolution of a pulsating detonation, we introduce the width of the reaction zone as the smallest value, w_m, such that there exists an interval, $\mathcal{I}$, of length w_m, where m percent of the energy is released. For nice enough rate functions, $w_{1/2}$ of the ZND solution is roughly equivalent to the half-reaction length, $x_{1/2}$. Notice, however, that for chemical reactions with large induction zones and/or

localized heat release, the values of $w_{1/2}$ and $x_{1/2}$ are significantly different, with $w_{1/2}$ becoming a more relevant spatial scale. In the calculations below, we use $m = 0.95$ such that $w_{0.95}$ represents, at a given time, the smallest width containing 95% of the heat release.

In Figure 5.9, we show $w_{0.95}$ as a function of time during the detonation evolution. We fix the numerical resolution at 1000 points per half-reaction length ($dx = 0.001$), which may be considered an overkill for a steady ZND wave. We then compute $w_{0.95}$ as a function of time at different activation energies. As can be seen in Figure 5.9a, in the weakly unstable regime, the width of the heat-release zone changes by a factor of about two during the time evolution of the wave; the heat release region is still well resolved. Further into the unstable regime (Figure 5.9b and Figure 5.9c), we see that the relevant size of the reaction zone can shrink by more than an order of magnitude and, thus, even with 1000 points per half-reaction length, there are times when only about 30 points are used to resolve the heat-release region. If we increase the activation energy even further, stepping into the apparently chaotic regime, we observe very short windows of time when only about 10 points are being used per heat-release zone.

Because of the difficulties outlined above, without resorting to adaptive mesh refinement, $500 - 1000$ points per half-reaction length are needed to obtain a bifurcation diagram with features that are essentially grid independent away from the chaotic regimes (see Figure 5.10). While recognizing that such sensitivity to initial conditions or discretization errors is natural for chaotic dynamics, caution is clearly required when interpreting the results of numerical simulations of unstable detonations with high activation energies.

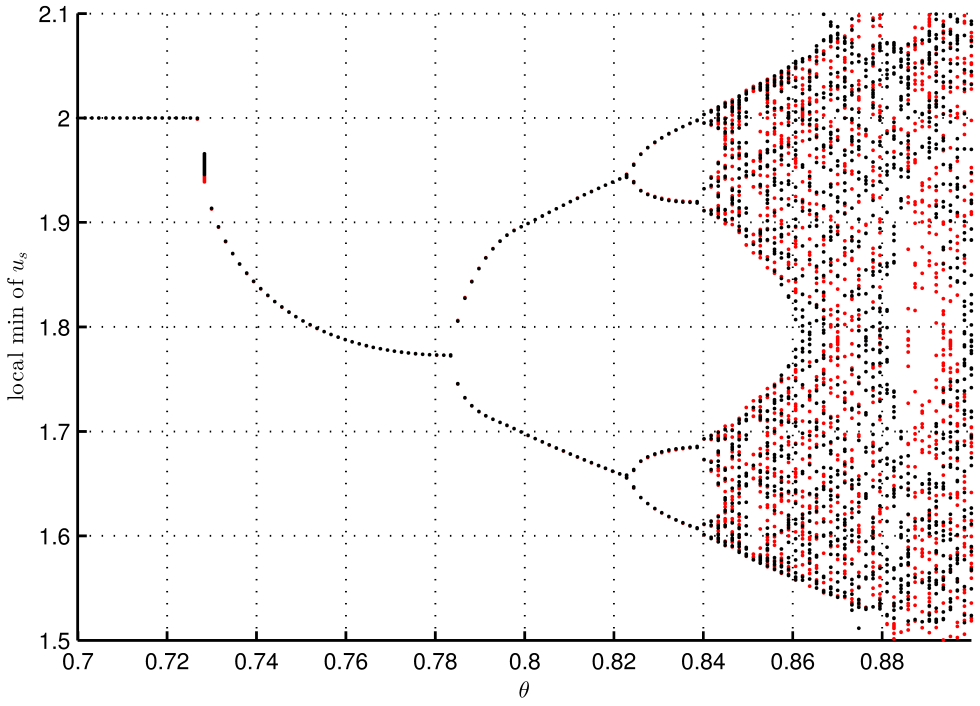

Figure 5.10: The bifurcation diagram at $q = 5$ showing the local minima of the attractor solution's shock value, $u_s(\tau) = u(0, \tau)$, as a function of the dimensionless activation energy, θ. The simulations were carried out at two different resolutions: $N = 15,000$ (red) and $N = 30,000$ (black) grid points on the computational domain of length $L = 30$. We see that away from the chaotic regimes, the predictions are nearly identical.

5.5.2 Cellular detonation

Multi-dimensional instability is very important in gaseous detonations and results in cellular structures involving triple-point interactions on the detonation lead shock [9, 48, 2]. It is therefore crucial to check if the asymptotic model, (5.49-5.51), can reproduce the dynamics of not only one-dimensional, but also multi-dimensional detonations. As we have seen in Subsection 5.4.2, multi-dimensional instabilities can be dominant in the asymptotic model, with the dispersion relation showing a maximum growth rate for some nonzero transverse wave number l (see Figure 5.5). In this section, we calculate the long-term dynamics of detonation waves when two-dimensional

effects are present. In particular, we show that the asymptotic model retains the essential complexity required to reproduce multi-dimensional cellular patterns. Solving (5.60-5.62) numerically turns out to be a non-trivial task and requires special care. In the following subsection, we present a discussion of the algorithm employed in this work.

5.5.2.1 Numerical algorithm for the two-dimensional asymptotic system

In order to appreciate the subtlety associated with (5.60-5.62), we note that the equations comprise a nonlinear hyperbolic system with one of its characteristic planes orthogonal to time. This means that:

- The initial data are given on a characteristic surface, the $x - y$ plane. The absence of a time derivative in (5.50-5.51) requires the initial conditions to satisfy $v_x = u_y$, $\lambda_x = \omega(\lambda, u)$.
- Evolving in τ is a nonlocal procedure and, in the presence of a shock, care has to be taken to avoid spurious numerical oscillations.

Many existing numerical methods for solving (5.63-5.64) are based on a formal rewriting of the system as a single equation,

$$u_{xt} + \left(\frac{u^2}{2}\right)_{xx} + u_{yy} = 0, \tag{5.94}$$

by cross-differentiation and substitution. Two concerns arise with this approach. First, the validity of such a transformation is not obvious when u and v are discontinuous functions. Second, in the presence of chemical reactions, differentiation of (5.60) with respect to x produces a delta forcing at the ignition-temperature locus due to the discontinuous nature of the reaction rate. Thus, the techniques based on

solving (5.94) are inadequate for our purposes.

Another common technique is to solve for the potential, ϕ, that satisfies

$$\phi_{x\tau} + \left(\frac{\phi_x}{2}\right)_x^2 + \phi_{yy} = 0. \tag{5.95}$$

Again, when chemical reactions are present, complications arise because the reaction rate now becomes an exponential function of ϕ_x and the discretization errors in ϕ_x therefore exponentially amplify, requiring very high-order methods for good accuracy.

The method we employ here is based on a direct semi-implicit discretization of (5.49-5.50) following some of the ideas found in [81]. In this method, all terms except for v_y are treated explicitly. By choosing second-order spatial and temporal discretization, we obtain an algorithm that is formally second order in time and space (see Appendix G for a self-convergence test). The general procedure is outlined here to explain our reasoning for the choice of the algorithm.

Assuming that the solution at time $\tau = \tau^n$ is known, we evolve it to $\tau = \tau^{n+1}$ as follows:

1. First, we employ a semi-implicit time discretization, where the v_y term is treated implicitly. The motivation for this comes from the fact that some waves propagate infinitely fast in the $x - y$ plane. In the simple case of a forward Euler time discretization, we obtain

$$\begin{aligned} \frac{u^{n+1} - u^n}{\Delta\tau} + (F^n(u))_x + v_y^{n+1} &= \lambda_x^n, & (5.96)\\ v_x^{n+1} &= u_y^{n+1}, & (5.97)\\ \lambda_x^{n+1} &= \omega\left(\lambda^{n+1}, u^{n+1}\right), & (5.98) \end{aligned}$$

where $F(u) = u^2/2$. A more quantitative reason for treating v_y implicitly

can be seen from the von Neumann stability analysis of the linearized system without chemical reactions, wherein a fully explicit scheme can be unstable (see Appendix F for details).

2. We approximate the explicit terms λ_x^n and F_x^n using a shock-capturing scheme, e.g., finite volume method [73].

3. Using (5.97), we write a forward difference representation of $v_{i,j}^{n+1}$ in terms of $u_{i,j}^{n+1}$ and $u_{i',j}^{n+1}$ for $i' > i$. For instance, a first-order forward difference scheme can be used, i.e.,

$$v_{i,j}^{n+1} = v_{i+1,j}^{n+1} - \Delta x \left(u_{i,j}^{n+1}\right)_y, \tag{5.99}$$

where the y derivative approximation is postponed until the next step. The use of the forward difference here is a consequence of up-winding the infinitely fast waves propagating from right to left.

4. Approximate the y derivatives, e.g., by centered differences, to obtain the fully discrete scheme:

$$\begin{aligned} u_{i,j}^{n+1} &= u_{i,j}^n + \Delta\tau \Bigg[-\frac{1}{2}\left(\lambda_x\right)_{i,j}^n - \left(F_x\right)_{i,j}^n \\ &- \frac{1}{2\Delta y}\left(v_{i,j+1}^{n+1} - 2v_{i,j}^{n+1} + v_{i,j-1}^{n+1}\right)\Bigg], \qquad (5.100) \\ v_{i,j}^{n+1} &= v_{i+1}^{n+1} - \frac{\Delta x}{2\Delta y}\left(u_{i,j+1}^{n+1} - u_{i,j}^{n+1} + u_{i,j-1}^{n+1}\right). \qquad (5.101) \end{aligned}$$

5. In order to solve (5.100-5.101), sweep from right to left, assuming the right boundary values of u and v are known at all times, in the following way:

   (a) For some fixed i, insert (5.101) into (5.100) and solve the linear system for the vector $u_{i,j}^{n+1}$.

(b) With $u_{i,j}^{n+1}$ find $v_{i,j}^{n+1}$ using (5.101).

(c) Repeat (a),(b) with $i = i - 1$ until the left boundary is reached.

6. Finally, compute λ^{n+1} by solving (5.98) with a boundary condition on the right of the domain, which is given by

$$\lambda_x^{n+1}(x_{right}, y) = 0. \tag{5.102}$$

Notice that (5.98) is actually an initial value problem for λ^{n+1} for fixed y wherein $-x$ is a time-like direction. It can be solved with any initial value solver (e.g., a Runge-Kutta method) if desired.

It may seem counterintuitive at first that the simplified model requires a semi-implicit method while the reactive Euler equations can be solved explicitly. The reason is that the asymptotic approximation is performed in a limit where the reactive Euler equations themselves would have to be treated implicitly. In order to understand this, we look at the three waves present in the Euler equations. Since the weak heat release approximation implies that the detonation velocity is nearly acoustic, and an acoustic wave induces no flow behind it, we see that the speed of the forward acoustic characteristic, given by $u+c-D$ in a frame moving with the wave, is actually an $O(\epsilon)$ quantity ($D \approx c$ and $u \approx \epsilon$). The entropy and backward acoustic characteristics, on the other hand, have $O(1)$ speeds. In the asymptotic model, a slow time, τ, is chosen so that the dynamics happen on $O(1)$ time scales and therefore some characteristics have speeds of $O(1/\epsilon)$ in the slow time variable. When an explicit method is used to solve the Euler equations in this limit, a typical CFL condition would require a time step, $\Delta\tau \sim \epsilon\Delta x$, and as $\epsilon \to 0$, it becomes clear that the time step restriction becomes unattainable and an implicit method is needed.

The infinite characteristic velocity arises because the x, y plane is a characteristic surface for the equations. A simple rotation in space-time "resolves", to some extent, this issue such that in the "rotated" space-time the system behaves as a standard system of conservation laws. The trade-off for recovering a classical hyperbolic system with finite wave speeds is that one must now consider a grid with moving boundaries. This idea can be exploited to produce fully explicit schemes as shown in [82] for the case without reactions.

5.5.2.2 Two-dimensional cellular detonations

Using the algorithm described in the previous section, we solve (5.60-5.62) in a frame moving with constant speed, $D_0 = 1$. All simulations are initialized with the one-dimensional ZND solutions obtained in Subsection 5.4.1. We then investigate, in the context of the asymptotic equations: (1) the effect of the width of the channel on nonlinear stability properties of the traveling wave solutions; (2) the effect of the periodic boundary conditions; and (3) the effect of increasing heat release on the wave dynamics.

In Figure 5.11, we show the profile of u at $\tau \approx 500$ for varying widths of the domain, L_y, in the y direction. The y boundaries are modeled as rigid walls, appropriate for a detonation in a two-dimensional channel (i.e., a channel with negligible depth). The parameters are fixed at $q = 1.7$ and $\theta = 1.65$, for which the linear stability calculation shows that the ZND wave is unstable only to two-dimensional perturbations. In a channel of width $L_y = 2$, the ZND wave remains stable, as seen in Figure 5.11a, as the spacing is too narrow for the two-dimensional instability to develop. Increasing the width of the channel, however, allows for a number of transverse modes to be excited[1], leading to the formation of a multi-dimensional cellular

[1]Recall that for a channel with finite width, L_y, the allowed transverse wave numbers, l, are given

pattern as shown in Figure 5.11c and Figure 5.11d. The cell size appears to remain around 10 in all Figure 5.11(b-d).

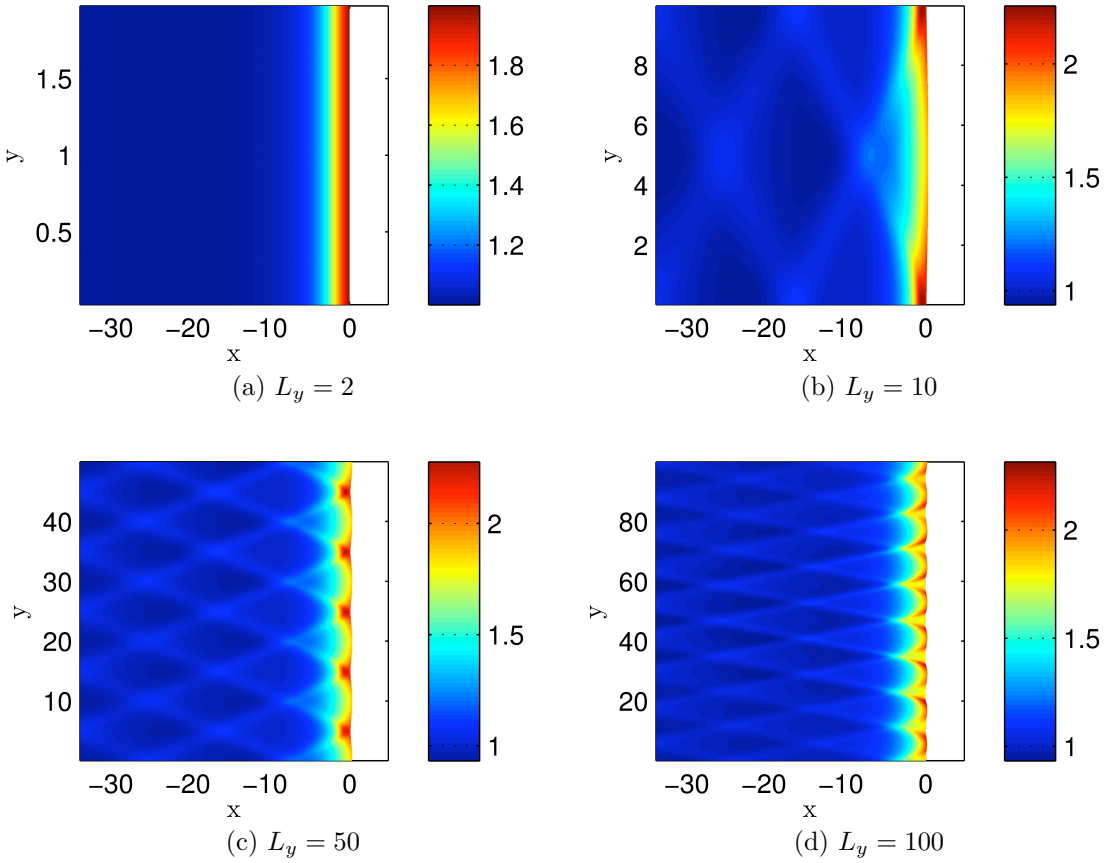

(a) $L_y = 2$ (b) $L_y = 10$

(c) $L_y = 50$ (d) $L_y = 100$

Figure 5.11: Dynamics of the asymptotic model in channels of different widths. The plots show the asymptotic variable u. The parameters are $q = 1.7$, $\theta = 1.65$, as in Fig. 5.5. The white region corresponds to the ambient state ahead of the wave, with $u = 0$.

When we replace the solid wall boundary conditions with periodic conditions, we observe a two-dimensional version of a spinning detonation. There is only one family of transverse shock waves that all propagate in the same direction. Such a wave can be imagined to form in a narrow gap between two concentric cylindrical tubes, as in a rotating detonation engine [84]. A snapshot of the solution field, u, is shown in

by $l = \pi n/L_y$, where $n \in \mathbb{Z}$. Therefore, only a discrete set of modes can be excited, and larger L_y typically allows for more unstable modes to appear.

Figure 5.12, where relatively strong transversely propagating shocks can be seen.

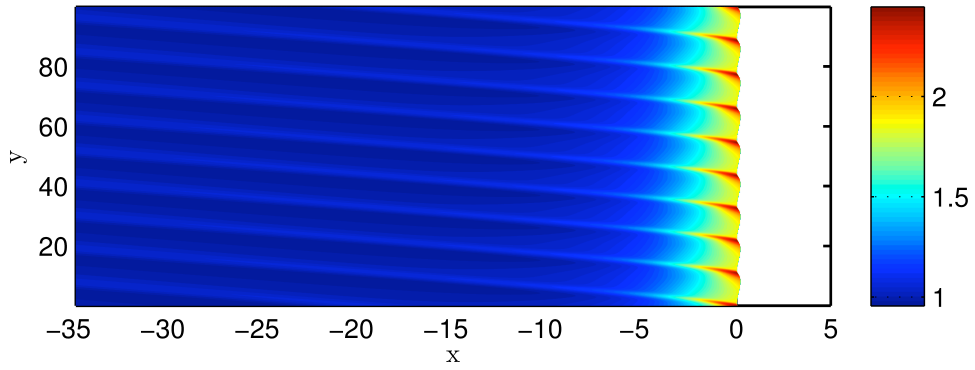

Figure 5.12: Detonation in a channel of width $L = 100$ with periodic boundary conditions. Parameters are $q = 1.7$ and $\theta = 1.65$.

In Figure 5.13, we show the effect of the heat release on the solution structure. We fix $\theta = 1.7$ and increase the value of q from 1.7 to 2.5. Consistent with the behavior of detonations in the reactive Euler equations, regular cells are observed at small q, as in Figure 5.13a and Figure 5.13b, but with increasing q, the structure of the detonation front becomes more complex with the formation of irregular cells as in Figure 5.13d.

All of the previous results show that, at least at a qualitative level, the asymptotic model captures many important characteristics of multi-dimensional detonations. Next, we investigate how *quantitatively* close the predictions are to the solutions of the reactive Euler equations. The numerical simulations of the reactive Euler equations were carried out using PyCLAW [95], which provides, among other things, a Python wrapper for the classic routines in CLAWPACK. The software requires the user to provide a Riemann solver. We use a Roe-linearized Riemann solver with a Harten-Hyman entropy fix [73]. The classic package of PyCLAW employs a second-order finite volume algorithm with a fractional step method for the time evolution [73]. For the numerical simulations, the reactive Euler equations were non-dimensionalized in the conventional form by the ambient state with velocities scaled by $u_a = \sqrt{p_a/\rho_a}$, spatial variables scaled by the half-reaction length, $x_{1/2}$, and time

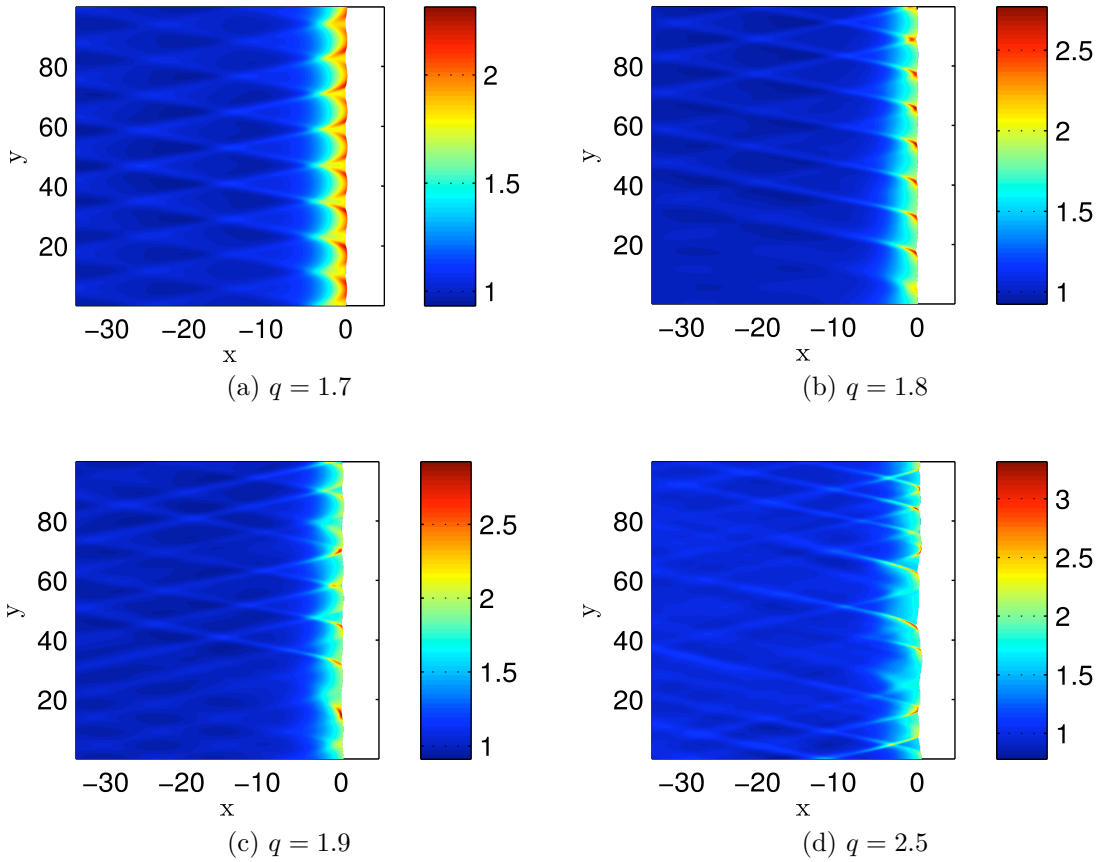

(a) $q = 1.7$ (b) $q = 1.8$

(c) $q = 1.9$ (d) $q = 2.5$

Figure 5.13: Dynamics of the asymptotic model for varying heat release at a fixed width $L = 100$ and activation energy $\theta = 1.65$.

by $u_a/x_{1/2}$.

In Figure 5.14, we show a comparison between the asymptotic solutions and the solutions of the reactive Euler equations. The parameters chosen are the same as in Figure 5.6b, i.e., $\gamma = 1.2$, $Q = 0.4$ and $E = 50$, which in the asymptotic variables are given by $q = 2.4$ and $\theta = 50/36 \approx 1.389$. We start both simulations with the ZND solution and solve for a time interval large enough such that instabilities have already fully developed. Notice that since the asymptotic model uses the slow time variable, τ, we only need to solve it for a relatively short time interval, $\tau \approx 100$. The reactive Euler system, on the other hand, was non-dimensionalized in the conventional way using the regular time variable, t, and thus we must solve the system up to $t \approx \tau/\epsilon = 600$.

We perform all necessary scaling conversions between the variables so that the lengths and amplitudes shown in Fig. 5.14 are consistent. The length of the y domain is fixed in the asymptotic model to be 20, which corresponds to a length 27.83 in the regular dimensionless y, while the x domain is of length 40.

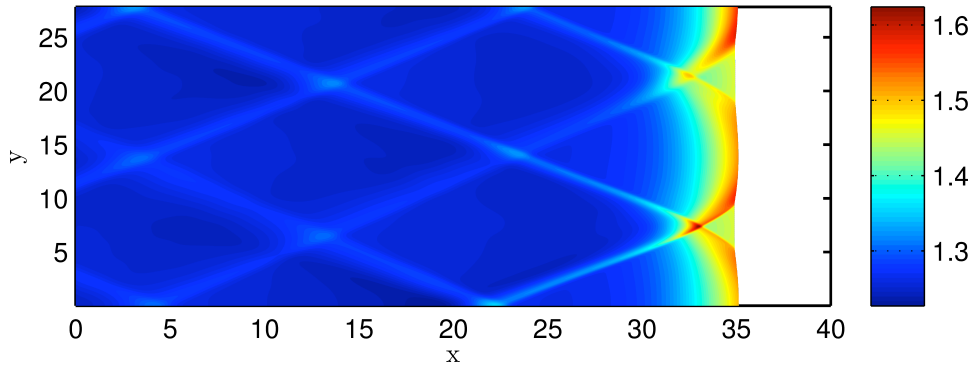

(a) Density field, $\rho = 1 + \epsilon\sqrt{q}u$, as predicted by the asymptotic model.

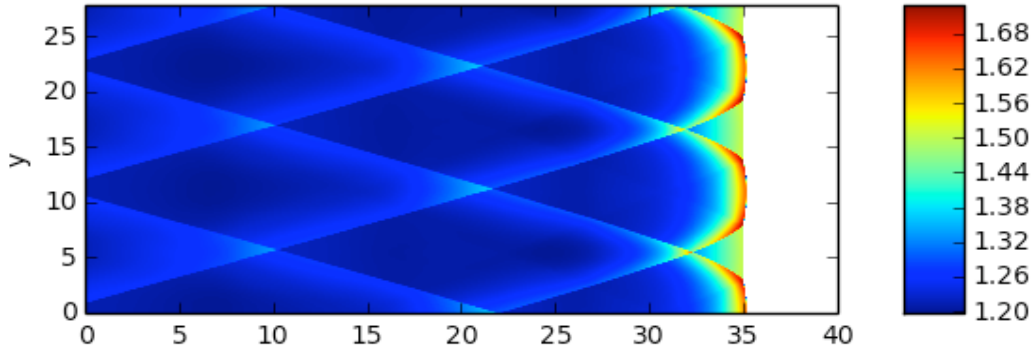

(b) Density field computed from the reactive Euler equations.

Figure 5.14: Comparison between asymptotic and full solutions of the reactive Euler equations for a cellular detonation in a channel.

We see from Figure 5.14 that the asymptotic model captures the salient features of multi-dimensional detonations with good quantitative agreement. The characteristic scales of the detonation cells are seen to be close. A small difference in the transverse propagation velocity of the triple points is apparent, in the asymptotic case the speed being higher. The transverse shocks in the asymptotic solutions far from the lead shock are seen to be smoother than in the full solutions, which is due to a larger

numerical diffusion in the algorithm for the asymptotic model.

Finally, we remark that weakly nonlinear detonations operate in the same fluid dynamic regime as weak shock wave focusing or weak shock reflection at near grazing incidence. As pointed out by von Neumann [96], in this limit the "classical" Mach triple point shock structure is impossible. Yet, both experiments and numerical calculations [97] consistently exhibit triple shock structures in this regime. This apparent contradiction is known as the "von Neumann paradox". Although the structures behind the lead shock in our calculations resemble the triple-points observed in detonations (Figure 5.15), a simple algebraic argument can show that the asymptotic equations do not admit "classical" triple points, where three shocks separated by smooth flows meet [82, 81]. Thus, much like in the problem of weak shock reflection, the observed cells in the weak heat release detonations considered in this work present yet another instance of the "von Neumann paradox". Here, we make no attempt to address this problem and simply note that triple-point-like structures appear in our numerical simulations behind the lead shock; whether they are true discontinuities, sharp waves or some singularities remains an open problem.

5.6 Discussion and conclusions

In this chapter, we developed an asymptotic theory of multi-dimensional detonations within the framework of the compressible Navier-Stokes equations for a perfect gas reacting with a one-step heat-release law. The main outcome is a reduced model that consists, in two spatial dimensions, of a forced Burgers-like equation coupled with a heat release equation and an equation that enforces zero vorticity. After specializing the model to the case without dissipative effects, we have analyzed it in detail and have shown that it captures many of the dynamical features of detonations

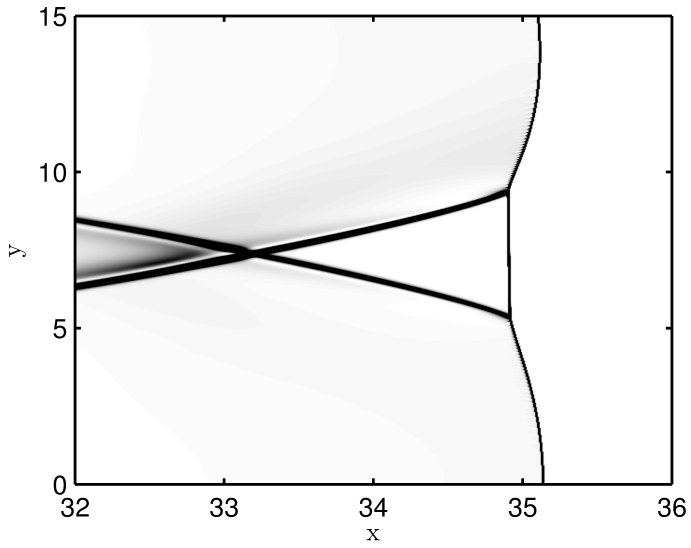

Figure 5.15: Triple-point-like structures in the asymptotic solution of the weakly nonlinear detonation as shown by the magnitude of the density gradient.

in reactive Euler equations. These include: (1) existence of steady-state traveling waves (i.e., ZND solutions), (2) linear instability of the ZND solutions, (3) existence of a period-doubling bifurcation road to chaos in the one-dimensional case, and (4) onset of cellular detonations in the two-dimensional case. Our theory considers weakly nonlinear detonations in the distinguished limit of small heat release, large activation energy and small $\gamma - 1$. In this limit, the dynamics occur on time scales that are long compared with the scale of a characteristic chemical reaction time. Our reduced evolution system builds on the weakly nonlinear theory in [79, 32] by adding the Newtonian approximation to it. In the one-dimensional and non-dissipative special case, our theory contains the model in [47].

As a consequence of the $\gamma - 1 = O(\epsilon)$ assumption, the temperature expansion in our analysis starts with an $O\left(\epsilon^2\right)$ correction to the leading-order term, as opposed to $O\left(\epsilon\right)$ correction in [79, 32]. This is precisely what allows us to escape the fact that in [79, 32] there must be leading-order corrections to temperature, velocity and density that behave exactly the same way. The present scaling highlights an important dif-

ference between a reactive and a non-reactive shock, namely, that the temperature in a reactive shock can increase at some distance from the shock front because of heat release. This increase in the post-shock temperature means that the energy release can possess a maximum inside the reaction zone. As we previously elucidated with a reactive Burgers model [77, 76], the presence of such an internal maximum appears to be a key factor for the mechanism that generates resonances and subsequent amplification of the waves in the reaction zone.

Note that all one-dimensional weakly nonlinear asymptotic models as well as the *ad hoc* models devised to capture detonation dynamics [31, 29, 77, 25] are extensions of the Burgers equation modified by adding a reaction forcing term, with an extra equation for the reaction progress variable. The reason is that the dynamics of any one-dimensional genuinely nonlinear hyperbolic system reduces to that of an inviscid Burgers equation in the weakly nonlinear limit [89].

While the reduced weakly nonlinear asymptotic theory has clear predictive power, as demonstrated in this work, recognizing its limitations is important and helps highlight open problems that require further investigation. For example, at parameter values (especially of the heat release) corresponding to strong cellular and pulsating detonations typical in experiments and numerical simulations, the asymptotic predictions are not sufficiently accurate when compared to the reactive Euler equations. While it is not clear how to extend the present approach directly to strongly nonlinear detonations, the ability of the reduced system obtained in this work to capture essential dynamical characteristics of unsteady and multi-dimensional detonations serves as a strong indication that a theory of comparable simplicity may be possible for strongly nonlinear detonations.

Recent work [98] on the role of dissipation in the compressible reactive Navier-Stokes system in one spatial dimension indicates that dissipation can have non-trivial

effects on the stability of detonation waves. Elucidation of the role played by the transport effects in the asymptotic model is therefore of interest and we believe that the model retaining these effects, as in (5.49-5.51), should be investigated further.

A problem that merits exploration, in our opinion, is that of the evolution of a small-amplitude, localized initial perturbation to a detonation wave, considered in the same weakly nonlinear asymptotic regime as in the present work. All of the underlying assumptions in the theory remain valid for this different initial-value problem, which is relevant to the problem of detonation initiation.

From a mathematical point of view, the reduced system obtained in this work and its connection with the issue of the non-existence of triple-point shock structures for the Zabolotskaya-Khokhlov equation pose some puzzling and challenging problems.

Finally, recall that the qualitative models introduced by Fickett and Majda do not contain instabilities with the rate functions used in prior work with these models (e.g., see [17]). However, using the rate function derived in this paper (and, for that matter, the two-step rate function used in [31]) can be shown to lead to the same complexity of the solutions as occurs in the reactive Euler equations. A modified Fickett's analog can be written as

$$u_t + uu_x = -\frac{1}{2}\lambda_x, \tag{5.103}$$

$$\lambda_t = k\left(1-\lambda\right)\exp\left(\alpha u + \beta\lambda\right), \tag{5.104}$$

with the "activation energy" and "heat release" parameters, α and β, respectively. Clearly, one can treat more general right-hand sides for the rate function in (5.104), such as $\omega = \psi\left(\lambda\right)\phi\left(u\right)$, as long as ψ and ϕ retain the same qualitative properties as their corresponding expressions in (5.104). This modification, even though simple, reflects the physics of the phenomenon responsible for the dynamics of pulsating

detonations by allowing a local maximum in the reaction rate to exist behind the precursor shock in the detonation wave. Mathematical study of the modified analog model is of interest from the point of view of the theory of hyperbolic balance laws and the dynamics of their solutions.

Chapter 6

Some extensions of weakly nonlinear theory

In this chapter, we consider two extensions of the weakly nonlinear detonation model developed in Chapter 5: (1) detonations with algebraic losses, and (2) the effect of heat or species diffusion on detonation waves. In the case of algebraic losses, we shall see that an asymptotic approach yields a system very similar in nature to the toy model studied in Chapter 3, therefore justifying to some extent the *ad hoc* treatment there. When accounting for heat and species diffusion, however, the asymptotic equations change significantly, especially regarding the behavior of the temperature distribution. This opens up the possibility that the new model may contain traveling wave solutions not present in the inviscid counterpart.

6.1 Introduction

As we have seen throughout this thesis, the ZND theory comprises the basis for most of our analytical understanding of detonations, describing them as supersonic combustion waves sustained by chemical reactions that the wave itself triggers. As we have also seen in numerous occasions, some assumptions of the ZND theory (one-

dimensionality and steadiness of the wave) are usually violated in practice; detonations tend to be neither stable nor one-dimensional. This far, our main focus has been on developing a simple, yet non-trivial theory of detonations which predicts the complex behavior observed when the assumptions of the ZND theory fail. To this end, we have been somehow successful, with both the qualitative theory of Part I [76, 69, 83] and the asymptotic study of Chapter 5 [99] reproducing the main dynamical features of inviscid detonations. This chapter aims at rationally incorporating another element, which is absent in the ZND theory: the effect of dissipative processes.

While detonations tend to be very fast, and often dissipative effects can be safely ignored, there are circumstances in which this is not the case. For detonations propagating in porous media, for instance, it has been observed that the speed of propagation can be as low as half the Chapman-Jouguet prediction. For detonations propagating in narrow tubes, the effect of heat/momentum losses to the walls is not negligible. In these cases (and many others), the theory of ideal detonations, using the reactive Euler equations as a modeling basis, must be modified to better reflect reality.

A possible modification is to consider the reactive Navier-Stokes equations instead, together with the appropriate boundary conditions at the obstacles/walls. In complex geometries, however, this approach becomes quite challenging due to the presence of boundary layers which must be resolved. An easier approach, which aims at an approximate description of dissipative effects, is to account for the effective losses caused by dissipation using empirical laws, which enter the governing equations in the form of algebraic terms. Although motivated by first principles, these terms are typically added to the reactive Euler equations in an *ad hoc* fashion. In this chapter, we develop asymptotic theories for both extensions of inviscid detonations: inclusion of algebraic losses and the Navier-Stokes equations in a limit where heat/species

diffusion are important.

In Section 6.2, we consider first the *ad hoc* modifications of the reactive Euler equations. Section 6.2 is, in some sense, the asymptotic justification of the qualitative work performed in Chapter 3, where a toy model for detonation with losses was studied. In particular, we show that a reasonable empirical law for friction forces in turbulent flows, when taken to the asymptotic limit, produces a loss term identical to the one considered in (3.23).

Then, in Section 6.3 we consider the effect of dissipative processes by retaining in the reactive Navier-Stokes equations the terms responsible for viscous/heat/species diffusion. We note here that dissipative detonations tend to be harder to analyze, both from a theoretical and a computational point of view, than their hyperbolic counterpart. It is thus of great interest to have a model, easier than the compressible reactive Navier-Stokes equations, which correctly captures the role played by these different effects. In order to develop an asymptotic theory, we revisit the computations of Chapter 5, but scale the Lewis and Prandtl numbers differently so the desired effects enter the final equations. As we shall see, accounting for heat diffusion increases the complexity of the asymptotic equations. Because of that, further simplification is performed by exploiting the form of the temperature distribution in the limit of small, but not negligible, heat diffusion.

Being the last chapter of this thesis, it differs from the others in that it opens several questions, while only answering a few. In many ways, we present here what we believe to be some promising future directions in detonation theory.

6.2 Detonation with losses: an asymptotic approach

As mentioned in the introduction, very often the only computationally feasible way of accounting for the effect of losses induced by dissipation is through empirical laws. We derive in this subsection an asymptotic model for detonations with algebraic losses. We focus on losses induced by friction and heat dissipation, although other effects can be considered as well.

6.2.1 Governing equations

We take as a starting point the one-dimensional reactive Euler equations in conservation form, i.e.,

$$\begin{aligned}
\rho_t + (\rho U)_X &= 0, && (6.1)\\
(\rho U)_t + \left(p + \rho U^2\right)_X &= 0, && (6.2)\\
\left(\rho\left(e + \frac{U^2}{2}\right)\right)_t + \left(\rho U\left(e + \frac{U^2}{2} + \frac{p}{\rho}\right)\right)_X &= 0, && (6.3)\\
(\rho\Lambda)_t + (\rho U\Lambda)_X &= \rho\tilde{W}, && (6.4)
\end{aligned}$$

where for simplicity we consider

$$\tilde{W} = \tilde{k}(1-\Lambda)\exp(-\tilde{E}/RT), \quad p = \rho RT, \quad e = \frac{pv}{\gamma - 1} - \tilde{Q}\Lambda.$$

The system of equations given by (6.1-6.4) describes an ideal detonation, where "ideal" here stands for the fact that no dissipative effects are considered. The effects of energy loss due to dissipative effect can sometimes be treated, in an empirical way, by adding to the right hand side of (6.1-6.4) algebraic terms representing sinks of momentum or energy. To incorporate these effects, the reactive Euler equations are modified as

follows:

$$\begin{aligned}
\rho_t + (\rho U)_X &= 0, && (6.5)\\
(\rho U)_t + \left(p + \rho U^2\right)_X &= -\tilde{f}, && (6.6)\\
\left(\rho\left(e + \frac{U^2}{2}\right)\right)_t + \left(\rho U\left(e + \frac{U^2}{2} + pv\right)\right)_X &= -\tilde{h}, && (6.7)\\
(\rho\Lambda)_t + (\rho U\Lambda)_X &= \rho\tilde{W}, && (6.8)
\end{aligned}$$

where $\tilde{f}$ and $\tilde{h}$ represent momentum and energy losses, respectively. These could be caused by friction and heat dissipation, for example.

We have started with the equations in conservation form so as to make transparent the meaning of $\tilde{f}$, $\tilde{h}$ as sinks of momentum and energy. In order to simplify some of the steps in the asymptotic expansion, however, it is convenient to recast the governing equations in a form more similar to (5.8-5.12), where the laws of motion are expressed in terms of the Lagrangian derivatives. We therefore rewrite (6.5-6.8) as

$$\rho_t + U\rho_x + \rho U_x = 0, \tag{6.9}$$

$$\rho\left(U_t + UU_X\right) = -p_x - \tilde{f}, \tag{6.10}$$

$$\rho\left(e_t + Ue_x\right) + pU_x = \tilde{Q}\rho\tilde{W} + U\tilde{f} - \tilde{h}, \tag{6.11}$$

$$\Lambda_t + U\Lambda_x = \tilde{W}. \tag{6.12}$$

Letting $D/Dt = \partial_t + U\partial_x$ denote the Lagrangian derivative, and using $e = RT/(\gamma - 1) - \tilde{Q}\lambda$, we rewrite the energy balance as

$$\rho\frac{DT}{Dt} - \frac{\gamma - 1}{R\gamma}\frac{Dp}{Dt} = \frac{\gamma - 1}{R\gamma}\left(\tilde{Q}\rho\tilde{W} + U\tilde{f} - \tilde{h}\right). \tag{6.13}$$

For the discussion that follows, we take

$$\tilde{f} = \tilde{C}_f \rho u|u|; \qquad \tilde{h} = \tilde{C}_h U\left(T - T_a\right).$$

where $\tilde{C}_f$ is the friction coefficient and $\tilde{C}_h$ is the coefficient of heat dissipation, and T_a is the ambient temperature ahead of the detonation wave. Such loss functions have been considered before in [6, 100, 66].

As done in Chapter 5, we follow a localized wave moving into an equilibrium, quiescent state and let ρ_a, p_a, T_a and $u_a = \sqrt{p_a/\rho_a}$ denote, respectively, the density, pressure, temperature and Newtonian sound speed in the fresh mixture ahead of the wave. The independent variables are rescaled as

$$x = \frac{X - D_0 t}{x_0}, \quad \tau = \frac{t}{t_0},$$

where D_0 is a typical wave speed, which is to be determined later. We assume that $\epsilon = x_0/u_a t_0$, and thus the time scale of interest is small compared to the time it takes for acoustic waves to travel the reaction zone. The governing equations in dimensionless form are thus given by

$$\begin{aligned}
L[\rho] + \rho u_x &= 0, \\
\rho L[U] &= -\frac{1}{\epsilon} p_x - f, \\
\rho L[T] - \frac{\gamma - 1}{\gamma} L[p] &= \frac{\gamma - 1}{\gamma}\left(QW + uf - h\right), \\
L[\lambda] &= W,
\end{aligned}$$

where

$$f = C_f \rho u|u|, \qquad C_f = \frac{x_0 \tilde{C}_f}{\epsilon}, \tag{6.14}$$

$$h = C_h U\left(T-1\right), \qquad C_h = \frac{x_0}{\epsilon R \rho_a}\tilde{C}_h, \tag{6.15}$$

$$L[\cdot] = \partial_\tau[\cdot] + \frac{1}{\epsilon}\left(U - D_0\right)\partial_x[\cdot], \tag{6.16}$$

$$W = k(1-\Lambda)\exp\left[E\left(1-\frac{1}{T}\right)\right], \tag{6.17}$$

and

$$Q = \frac{\tilde{Q}}{RT_a}, \quad E = \frac{\tilde{E}}{RT_a}, \quad K = t_0\tilde{k}\exp\left(-E\right). \tag{6.18}$$

Obtaining a weakly nonlinear asymptotic approximation now is straightforward, with the only technical detail required being that f, h have the appropriate size so that: (1) they do not show at the linear level of the expansion and (2) they appear when the solvability condition is called upon.

6.2.2 Asymptotic approximation of detonation with losses

The following asymptotic ordering assumptions are made (see Section 5.3 for discussion of bullets 1-4):

1. $K = k/\epsilon$, $k = O(1)$.
2. $\left(\gamma-1\right)Q/\gamma = \epsilon^2 q$, $q = O\left(1\right)$.
3. $E = \theta/\epsilon^2$, $\theta = O\left(1\right)$.
4. $\frac{\gamma-1}{\gamma} = \epsilon$.
5. $C_f = c_f/\epsilon$, $c_f = O(1)$.
6. $\frac{\gamma-1}{\gamma}C_h = c_h/\epsilon^2$, $c_h = O(1)$.

Assumptions 5 and 6 ensure that both heat and friction losses will show up in the asymptotic approximation. Since we are not considering multi-dimensional effects, the fractional powers of ϵ, which were required in Chapter 5, are not needed, and therefore we can expand the variables in integer power of ϵ, i.e.,

$$\rho = 1 + \rho_1\epsilon + \rho_2\epsilon^2 + o(\epsilon^2), \tag{6.19}$$

$$T = 1 + T_1\epsilon + T_2\epsilon^2 + o(\epsilon^2), \tag{6.20}$$

$$p = 1 + p_1\epsilon + p_2\epsilon^2 + o(\epsilon^2), \tag{6.21}$$

$$U = U_1\epsilon + U_2\epsilon^2 + o(\epsilon^2), \tag{6.22}$$

$$\Lambda = \lambda + o(\epsilon). \tag{6.23}$$

Inserting (6.19-6.23) into governing equations, and collecting powers of ϵ, we obtain

$$\begin{aligned}
(-D_0\rho_{1x} + U_{1x}) \quad &+ \\
\epsilon\left(-D_0\rho_{2x} + U_{2x} + \rho_{1\tau} + U_1\rho_{1x} + \rho_1 U_{1x}\right) \quad &= \quad o(\epsilon^2), \qquad (6.24)\\
(-D_0 U_{1x} + T_{1x} + \rho_{1x}) \quad &+ \\
\epsilon(-D_0 U_{2x} + \rho_{2x} + T_{2x}) \quad &+ \\
\epsilon(-D_0\rho_1 U_{1x} + U_{1\tau} + U_1 U_{1x}) \quad &= \quad -\epsilon c_f u_1|u_1| + o(\epsilon^2), \qquad (6.25)\\
(-D_0 T_{1x}) + \epsilon\left(-D_0 T_{2x} + p_{1x}\right) \quad &= \quad \epsilon\left(q\omega - c_h|u_1|(T_2)\right) + o(\epsilon^2), \qquad (6.26)\\
-D_0\lambda_x \quad &= \quad \omega + o(1), \qquad (6.27)
\end{aligned}$$

where ω is the leading order of the reaction rate. Then, at the leading order, we have

$$\begin{bmatrix} -D_0 & 1 & 0 \\ 1 & -D_0 & 1 \\ 0 & 0 & -1 \end{bmatrix} \begin{bmatrix} \rho \\ U \\ T \end{bmatrix}_{1x} = \begin{bmatrix} 0 \\ 0 \\ 0 \end{bmatrix}. \tag{6.28}$$

Using the same arguments of Section 5.3, we conclude that for nontrivial solutions to exists we need $D_0 = \pm 1$. We also conclude, by integrating each equations in (6.28), that $U_1(x,t) = u(x,t) + \bar{U}(t)$, $\rho_1(x,t) = u(x,t) + \bar{\rho}(t)$, $T_1 = \bar{T}_1(t)$. By assuming that the wave is moving into a constant state, in order for the expansion to remain valid we must have $\bar{\rho} = \bar{U} = \bar{T} \equiv 0$, and therefore $U_1 = \rho_1 = u$, $T_1 = 0$. At the next order, we have in the expansion that

$$\begin{bmatrix} -1 & 1 & 0 \\ 1 & -1 & 1 \\ 0 & 0 & -1 \end{bmatrix} \begin{bmatrix} \rho \\ U \\ T \end{bmatrix}_{2x} = \begin{bmatrix} -u_\tau - 2uu_x \\ -u_\tau - c_f u|u| \\ q\omega - u_x - c_h|u|(T_2) \end{bmatrix}. \tag{6.29}$$

The matrix on the left hand side of (6.29) being singular, we have as a solvability condition that the right hand side must be orthogonal to $\mathbf{l}_0 = [1\,1\,1]$, yielding

$$u_\tau + uu_x = \frac{q}{2}\omega - \frac{1}{2}u_x - \frac{c_f}{2}u|u| - \frac{c_h}{2}|u|T_2, \tag{6.30}$$

which together with

$$\lambda_x = -\omega = -k(1-\lambda)\exp(\theta T_2), \tag{6.31}$$

$$T_{2x} = u_x + q\lambda_x + c_h|u|(T_2), \tag{6.32}$$

form a closed system for u, λ, T_2. We notice here that, unlike the case without heat losses, we no longer have the simple relation $T_2 = u+q\lambda$. Something similar, however, can be obtained by integrating (6.32) to yield

$$T_2 = u + q\lambda - \mathcal{H}_l,$$

where

$$\mathcal{H}_l = c_f \int_x^\infty |u| \, (u + q\lambda) \exp\left(-c_f \left(\int_x^z |u| dy\right)\right) \, dz$$

denotes the effect of the heat loss on the temperature profile. Assuming that we have a shock located at $x = x_s$, and that ahead of the shock we have $u = T_2 = \lambda \equiv 0$, we see that

$$\mathcal{H}_l = \begin{cases} 0 & \text{for } x \geq x_s, \\ c_f \int_x^{x_s} |u| \, (u + q\lambda) \exp\left(-c_f \int_x^z |u| dy\right) dz & \text{for } x < x_s. \end{cases}$$

Redefining $x \to x - \tau/2$ so as to eliminate the linear advective term from (6.30), we get the following system governing the propagation of weakly nonlinear detonations in the presence of heat and momentum losses:

$$u_\tau + uu_x = -\frac{q}{2}\lambda_x - \frac{c_f}{2} u|u| - \frac{c_h}{2}|u|T_2, \tag{6.33}$$

$$\lambda_x = -k \, (1 - \lambda) \exp\left(\theta T_2\right), \tag{6.34}$$

$$T_2 = u + q\lambda - \mathcal{H}_l. \tag{6.35}$$

In the simpler case where we consider only momentum dissipation, the system reduces to

$$u_\tau + uu_x = -\frac{q}{2}\lambda_x - \frac{c_f}{2}u|u|, \tag{6.36}$$

$$\lambda_x = -k(1-\lambda)\exp\left(\theta\left(u+q\lambda\right)\right), \tag{6.37}$$

which can be seen to be closely related to the toy model given by (3.23), which was studied in detail in Chapter 3.

Although we do not study the traveling wave solutions of (6.33-6.35) here, we notice that even in the simpler case when $c_h = 0$, the eigenvalue problem for the ZND waves presents a multiplicity of solutions. In order to find the traveling wave solutions of (6.36-6.37), we must solve

$$\left(u-D\right)u_\eta = -\frac{q}{2}\lambda_x - c_f u|u|,$$

$$\lambda_\eta = -k\left(1-\lambda\right)\exp\left(\theta\left(u+q\lambda\right)\right),$$

where $\eta = x - Dt$. Since $\lambda \to 1$ as $\eta \to -\infty$, for bounded solutions to exist there must be a point where $u = D$ (note, $u - D$ must be negative as $\eta \to -\infty$, otherwise solutions blow up). Thus, the presence of a sonic point is required for bounded solutions. Furthermore, the generalized Chapman-Jouguet condition requires

$$-\frac{q}{2}\lambda_x - c_f u|u| = 0 \qquad \text{when} \qquad u = D.$$

This condition determines a relation $H\left(D, c_f\right) = 0$, which as we have seen in Chapter 3 gives a multiple-valued function $D(c_f)$. It would be interesting to see if the inclusion of heat diffusion would produce set-valued solutions for the eigenvalue problem, as

was recently observed in [66].

6.3 Weakly nonlinear asymptotic model with diffusive effects

In this section, we expand the asymptotic analysis of Chapter 5 in order to retain heat and species diffusion effects. This requires a different assumption on the sizes of Lewis and Prandtl numbers so that their effects become comparable to the size of nonlinearities.

6.3.1 Asymptotic approximation of diffusive detonations

We take the same formulation as in Chapter 6, and assume an ideal polytropic gas, with a single step Arrhenius kinetics. The dimensionless governing equations are then given by (see Section 5.2 for further details):

$$
\begin{aligned}
L[\rho] + \rho\left(\frac{1}{\epsilon}U_x + \frac{1}{\sqrt{\epsilon}}V_y\right) &= 0, && (6.38)\\
\rho L[U] + \frac{1}{\epsilon}p_x &= \frac{1}{3\epsilon\mathrm{Re}}\left(U_{xx} + \sqrt{\epsilon}V_{xy}\right) + \frac{1}{\epsilon\mathrm{Re}}\left(U_{xx} + \epsilon U_{yy}\right), && (6.39)\\
\rho L[V] + \frac{1}{\sqrt{\epsilon}}p_y &= \frac{1}{3\epsilon\mathrm{Re}}\left(\sqrt{\epsilon}U_{xy} + \epsilon V_{yy}\right) + \frac{1}{\epsilon\mathrm{Re}}\left(V_{xx} + \epsilon V_{yy}\right), && (6.40)\\
\rho L[T] - \frac{(\gamma-1)}{\gamma}L[p] &= \frac{\gamma-1}{\gamma}\Bigg(Q\rho W - \frac{2}{3\epsilon\mathrm{Re}}\left(U_x + \sqrt{\epsilon}V_y\right)^2\\
&+ \frac{1}{\epsilon\mathrm{Re}}\left(U_x^2 + \epsilon U_y^2 + V_x^2 + \epsilon V_y^2\right)\Bigg)\\
&+ \frac{\gamma-1}{\gamma}\frac{1}{\epsilon\mathrm{Re}}\left(U_x^2 + \sqrt{\epsilon}U_yV_x + \sqrt{\epsilon}V_xU_y + \epsilon V_y^2\right)\\
&+ \frac{1}{\epsilon\mathrm{RePr}}\left(T_{xx} + \epsilon T_{yy}\right), && (6.41)\\
\rho L[\Lambda] &= \rho W + \frac{1}{\epsilon\mathrm{RePrLe}}\left(\left(\rho\Lambda_x\right)_x + \epsilon\left(\rho\Lambda_y\right)_y\right), && (6.42)
\end{aligned}
$$

where W is defined as

$$W = K(1-\Lambda)\exp\left[E\left(1-\frac{1}{T}\right)\right]. \tag{6.43}$$

In order to make the heat diffusion important, we can see from (6.41) that we must take $\mathrm{Pr} = O(\epsilon)$. Notice that we can still ignore species diffusion in (6.43) if we choose $\mathrm{Le} = O(1/\epsilon)$, but we take $\mathrm{Le} = O(1)$, so that now species diffusion will also enter the final model. Thus, we shall make the following assumptions regarding the size of different dimensionless terms:

1. $K = k/\epsilon$, $k = O(1)$.
2. $(\gamma-1)\,Q/\gamma = \epsilon^2 q$, $q = O\,(1)$.
3. $E = \theta/\epsilon^2$, $\theta = O\,(1)$.
4. $\gamma - 1 = \epsilon$.
5. $\mathrm{Re} = O(1/\epsilon)$.
6. $\mathrm{Pr} = O(1/\epsilon)$.
7. $\mathrm{Le} = O(1)$.

Next, we expand the dependent variables as

$$\rho = 1 + \rho_1\epsilon + \rho_2\epsilon^{3/2} + \rho_3\epsilon^2 + o(\epsilon^2), \tag{6.44}$$

$$T = 1 + T_1\epsilon + T_2\epsilon^{3/2} + T_3\epsilon^2 + o(\epsilon^2), \tag{6.45}$$

$$p = 1 + p_1\epsilon + p_2\epsilon^{3/2} + p_3\epsilon^2 + o(\epsilon^2), \tag{6.46}$$

$$\boldsymbol{u} = \mathbf{u}_1\epsilon + \mathbf{u}_2\epsilon^{3/2} + \mathbf{u}_3\epsilon^2 + o(\epsilon^2), \tag{6.47}$$

$$\Lambda = \lambda + o(\epsilon). \tag{6.48}$$

Inserting these expansions in (6.38-6.41), and collecting powers of ϵ, we obtain

$$\begin{aligned}
(-D_0\rho_{1x} + U_{1x}) + \sqrt{\epsilon}\,(-D_0\rho_{2x} + U_{2x} + V_{1y}) \quad &+ \\
\epsilon\,(\rho_{1\tau} - D_0\rho_{3x} + U_1\rho_{1x} + U_{3x} + \rho_1 U_{1x} + V_{2y}) \quad &= \quad o(\epsilon), \qquad (6.49) \\
(-D_0U_{1x} + T_{1x} + \rho_{1x}) + \sqrt{\epsilon}\,(-D_0U_{2x} + T_{2x} + \rho_{2x}) \quad &+ \\
\epsilon\,(U_{1\tau} - D_0U_{3x} + U_1U_{1x} + T_1\rho_{1x} + T_{3x} + \rho_{3x} - \rho_1\rho_{1x}) \quad &= \quad \frac{4}{3}\frac{1}{\mathrm{Re}}\,(U_1)_{xx} + o(\epsilon), \qquad (6.50) \\
(-D_0V_{1x}) + \sqrt{\epsilon}\,(-D_0V_{2x} + T_{1y} + \rho_{1y}) \quad &+ \\
\epsilon\,(V_{1\tau} - D_0V_{3x} + U_1V_{1x} + T_{2y} + \rho_{2y}) \quad &= \quad \frac{1}{\mathrm{Re}}\,(V_1)_{xx} + o(\epsilon), \qquad (6.51) \\
(-D_0T_{1x}) + \sqrt{\epsilon}\,(-D_0T_{2x}) \quad &+ \\
\epsilon\Big(T_{1\tau} - D_0T_{3x} + U_1T_{1x} + \frac{\gamma_1}{\gamma}D_0\,(\rho_{1x} + T_{1x}) - q\omega\Big) \quad &= \quad \frac{(T_3)_{xx}}{\epsilon\mathrm{RePr}} + o(\epsilon), \qquad (6.52) \\
-D_0\lambda_x - \omega \quad &= \quad \frac{\lambda_{xx}}{\epsilon^2\mathrm{RePrLe}} + o(1). \qquad (6.53)
\end{aligned}$$

First, looking at the $O(1)$ terms, we have

$$\begin{bmatrix} -D_0 & 1 & 0 & 0 \\ 1 & -D_0 & 0 & 1 \\ 0 & 0 & -1 & 0 \\ 0 & 0 & 0 & -1 \end{bmatrix} \begin{bmatrix} \rho \\ U \\ V \\ T \end{bmatrix}_{1x} = \begin{bmatrix} 0 \\ 0 \\ 0 \\ 0 \end{bmatrix}. \qquad (6.54)$$

For nontrivial solutions to exist, we therefore require $D_0 = \pm 1$. Here, we choose $D_0 = 1$ and focus on right going waves. This implies $U_1 = u(x, y, \tau) + \bar{U}(y, \tau),\ \rho_1 = u(x, y, \tau) + \bar{\rho}\,(y, \tau)$. If we consider a wave moving into a constant state, then $\bar{U} = \bar{\rho} \equiv 0$, and $V_1 = T_1 \equiv 0$.

At $O(\epsilon^{1/2})$, we obtain

$$\begin{bmatrix} -1 & 1 & 0 & 0 \\ 1 & -1 & 0 & 1 \\ 0 & 0 & -1 & 0 \\ 0 & 0 & 0 & -1 \end{bmatrix} \begin{bmatrix} \rho \\ U \\ V \\ T \end{bmatrix}_{2x} = \begin{bmatrix} 0 \\ 0 \\ -u_y \\ 0 \end{bmatrix}, \tag{6.55}$$

for which the solvability condition is trivially satisfied. Letting for convenience of notation $V_2 = v$, we get

$$v_x = u_y.$$

Finally, at $O(\epsilon)$, the equations read

$$\begin{bmatrix} -1 & 1 & 0 & 0 \\ 1 & -1 & 0 & 1 \\ 0 & 0 & -1 & 0 \\ 0 & 0 & 0 & -1 \end{bmatrix} \begin{bmatrix} \rho \\ U \\ V \\ T \end{bmatrix}_{3x} = \begin{bmatrix} -u_\tau - 2uu_x - v_y \\ -u_\tau + \frac{4}{3}\frac{1}{\epsilon \mathrm{Re}} u_{xx} \\ -\rho_{2y} \\ q\omega - u_x + \frac{1}{\epsilon^2 \mathrm{RePr}} (T_3)_{xx} \end{bmatrix}. \tag{6.56}$$

for which the solvability condition requires

$$2u_\tau + 2uu_x + v_y = -T_{3x} + \frac{4}{3}\frac{1}{\epsilon \mathrm{Re}} u_{xx}, \tag{6.57}$$

$$T_{3x} = -q\omega + u_x - \frac{1}{\epsilon^2 \mathrm{RePr}} (T_3)_{xx}. \tag{6.58}$$

This far, we have ignored the reaction rate equation, but from (6.53) it can be seen that λ is governed by

$$\lambda_x = -\omega - \frac{1}{\epsilon^2 \mathrm{RePrLe}} \lambda_{xx}.$$

Putting everything together, the final model is given by

$$u_\tau + uu_x + v_y = \frac{-T_{3x}}{2} + \mu u_{xx}, \tag{6.59}$$

$$v_x = u_y, \tag{6.60}$$

$$\lambda_x = -k(1-\lambda)\exp(\theta T_3) - d\lambda_{xx}, \tag{6.61}$$

$$\kappa T_{3xx} + T_{3x} = u_x + q\lambda_x + qd\lambda_{xx}, \tag{6.62}$$

where

$$\mu = \frac{4}{3}\frac{1}{\epsilon \mathrm{Re}}, \quad d = \frac{1}{\epsilon^2 \mathrm{RePrLe}}, \quad \kappa = \frac{1}{\epsilon^2 \mathrm{RePr}}.$$

We can simplify the system by integrating (6.62) once with respect to x, assuming all variables and their derivatives vanish in the limit $x \to \infty$, in order to obtain

$$\kappa T_{3x} + T_3 = (u + q\lambda + qd\lambda_x). \tag{6.63}$$

It is convenient to further integrate equation (6.63) to yield

$$T_3 = e^{\frac{-x}{\kappa}} \int_{-\infty}^{x} \frac{1}{\kappa} e^{\frac{z}{\kappa}} (u + q\lambda + qd\lambda_z)\ dz.$$

Without any further assumptions, we are left with the following system:

$$u_\tau + uu_x + v_y = \frac{-T_{3x}}{2} + \mu u_{xx}, \tag{6.64}$$

$$v_x = u_y, \tag{6.65}$$

$$\lambda_x = -k(1-\lambda)\exp(\theta T_3) - d\lambda_{xx}, \tag{6.66}$$

$$T_3 = e^{\frac{-x}{\kappa}} \int_{-\infty}^{x} \frac{1}{\kappa} e^{\frac{z}{\kappa}} (u + q\lambda + qd\lambda_x)\ dz. \tag{6.67}$$

Equations (6.64-6.67) include the effects of viscosity, heat diffusion, and species diffusion in the parameters μ, κ, and d, respectively.

It is interesting to try to recover the inviscid results from the more general derivation. Formally, we can set $\mu = 0$ and $d = 0$ in (6.64-6.67), but $\kappa = 0$ does not make immediate sense. This is, of course, because we have used the implicit assumption $\kappa > 0$ when integrating equation (6.63). If we assume that κ is small, then the integral formulation of T is amenable to the method of steepest descent. This becomes more transparent after we rewrite (6.67) as:

$$\begin{aligned} T_3 &= \int_{-\infty}^{x} \frac{1}{\kappa} e^{-\frac{1}{\kappa}(x-z)} \left(u + q\lambda + qd\lambda_z\right) \, dz \\ &= \frac{1}{\kappa} \int_{0}^{\infty} e^{-\frac{1}{\kappa}r} \left(u\left(x-r\right) + q\lambda\left(x-r\right) + q\psi\lambda_x\left(x-r\right)\right) \, dr. \end{aligned} \tag{6.68}$$

We then see that, when $\kappa \ll 1$, the main contribution to the integral in (6.68) comes from the neighborhood of $r = x - z = 0$. The asymptotic expansion of (6.68), after applying Watson's lemma, yields

$$T_3 = u + q\lambda + qd\lambda_x - \kappa\left(u_x + q\lambda_x + qd\lambda_{xx}\right) + o\left(\kappa\right).$$

Interestingly, the effect of dissipation on the heat distribution, in the small κ limit, is modeled by including spatial derivatives which modify the inviscid relation, $T = u + q\lambda$. As expected, these effects would only be important in places of high gradients.

The effects of viscosity (μ) and species diffusion (d) have been studied in the past, in the context of the Majda or Rosales-Majda model ([29, 17, 32]). But since these theories lump pressure, velocity and temperature together, heat diffusion is included in the viscous parameter μ. The theory developed here, on the other hand, allows for temperature to behave differently than other primitive variables, which is key for a

correct description of reactive shocks. Because of that, the effect of heat dissipation is no longer lumped into μ, but has a special place in the theory.

We believe it would be interesting, as a starting point, to study the one-dimensional traveling wave solutions when $d = 0$ and in the limit of small κ, in which case the system reduces to

$$u_\tau + uu_x = \frac{-T_{3x}}{2} + \mu u_{xx}, \tag{6.69}$$

$$\lambda_x = -k(1-\lambda)\exp\left(\theta T_3\right), \tag{6.70}$$

$$T_3 = u + q\lambda - \kappa\left(u_x + q\lambda_x\right). \tag{6.71}$$

If $\kappa = 0$, then the theory of viscous detonations developed in [29, 32] applies directly. For $\kappa \neq 0$, however, the possible traveling wave solutions of (6.69-6.71) is a completely open question which requires further exploration. We hope to pursue these investigations in the near future.

6.4 Discussion and conclusions

In this chapter, we developed an asymptotic theory for detonations with dissipative effects retained. Two different cases were considered: empirical losses modeled by the inclusion of algebraic terms in the reactive Euler equations, and the reactive Navier-Stokes equations scaled so that all dissipative effects remain important.

In the case of algebraic losses, we have seen that an asymptotic approach yields equations similar to those considered in Chapter 3. Because friction losses are modeled by the exact same term as employed in Chapter 3, we expect the same interesting dynamics to be present, at least when ignoring heat losses. In particular, the turning point behavior of the D vs c_f curve, with its multiplicity of solutions, and the

lack of traveling wave for large c_f. The effect of heat diffusion appears to be more complex, consistent with recent studies of Semenko *et al* [66]. Whether or not set-valued solutions, like those observed in the reactive Euler equations, are present in the asymptotic model remains an open question.

When considering dissipative effects by retaining the higher order derivative terms in the modeling equations, the asymptotic system obtained was quite different than that of the standard weakly-nonlinear theories. Because the asymptotic equations were still too complex, a further asymptotic approximation was performed in order to obtain a more tractable model. The effect of dissipation is likely to bring some interesting effects which require further exploration. Even the theory for the traveling wave solutions of (6.69-6.71) appears to be nontrivial.

Chapter 7

Concluding Remarks

The main focus of this thesis was on developing qualitative and asymptotic theories capable of capturing the complex features of detonation waves. We started by studying the simplest possible case of a one-dimensional ideal detonation, and showed that all of the rich features (including galloping detonation and chaotic dynamics) can be faithfully represented by a single forced Burgers equation. The qualitative theory of Chapter 2 highlighted the important effects which caused instabilities in detonation waves. In particular, it was elucidated that in order for instabilities to exist, the chemical reactions (represented in Part I by a source in Burgers equation) and the fluid flow had to be coupled in a sensitive manner. Also, the reaction zone should act as a resonator, trapping waves which travel between the shock and the reaction zone, and amplifying them. For our study, having an internal maximum in reaction rate inside the reaction zone proved to be crucial for such resonance mechanism to exist.

The qualitative theory of pulsating detonations was then extended to account for energy losses. Through the simplified model we understood that the essential difficulties related to numerically finding the traveling wave solutions of the reactive Euler equations in the presence of losses could be remedied by an appropriate change of variables. The change of variables exploits the fact that the ODEs which must be

solved when searching for traveling wave solutions come from a system of conservation laws. Motivated by the change of variables, we proposed a new algorithm to solve the eigenvalue problem for the detonation velocity which removes the stiffness associated with the sonic singularity. With the new algorithm, we demonstrated that akin to the reactive Euler equations, the detonation velocity as a function of the loss factor is a multiple-valued function with a turning point. Furthermore, we investigated the effect of losses on the stability of the detonation waves. It was found that losses tend to destabilize detonations, and that the bottom branch of the $D - c_f$ or $D - \kappa$ curves are always unstable, with solutions tending to be near the fixed point associated with the top branch of these curves.

The first analog for two-dimensional detonations was proposed and analyzed in Chapter 4. We showed that even a simple extension of the forced Burgers equation was rich enough to reproduce the multidimensional patterns observed in detonations. The stability of such multi-dimensional waves was analyzed by means of Laplace transform, and the qualitative behavior was found to be exactly analogous to detonations.

The success of the qualitative theory of Part I, and the simplicity of the equations studied, motivated the search for a rational asymptotic theory. Having understood the importance of the right coupling between reaction rate and fluid flow, a new weakly nonlinear theory of detonations was derived and analyzed. We considered the case of a single-step irreversible Arrhenius kinetics, and demonstrated that a rational reduction can be performed in way so as to retain all of the essential features present in detonation waves, including the steady states, the rich linear spectrum, and the complex multi-dimensional dynamics. In Chapter 5, we focused almost exclusively on an inviscid description, showing that the predictions of the proposed asymptotic model are in close agreement with the reactive Euler equations. The asymptotic

theory also allowed us to understand the fundamental drawback of Majda's original analog, and thus the reason why it was incapable of reproducing the unsteady dynamics. A new reaction rate, which highlights the important role played by temperature, was proposed with which both Fickett's and Majda's analogs contain unsteady waves.

In the last chapter of the thesis, we extended the asymptotic reduction of Chapter 5 to account for dissipative effects. It was shown that these effect are likely to make the analysis significantly harder than the inviscid theory. The complete study of dissipative detonations, however, is left for future work. We hope that both the qualitative and asymptotic models proposed in this thesis can serve as a basis for building a mathematical theory of unsteady multi-dimensional detonations.

REFERENCES

[1] B. D. Taylor, A. R. Kasimov, and D. S. Stewart, "Mode selection in weakly unstable two-dimensional detonations," *Combustion Theory and Modelling*, vol. 13, no. 6, pp. 973–992, 2009.

[2] W. Fickett and W. C. Davis, *Detonation: Theory and Experiment*. Courier Dover Publications, 2012.

[3] A. V. Mikhelson, "On the normal ignition velocity of explosive gaseous mixtures," Ph.D. dissertation, Moscow University, 1890.

[4] D. L. Chapman, "On the rate of explosion in gases," *Philosophical Magazine*, vol. 47, pp. 90–104, 1899.

[5] E. Jouguet, "On the propagation of chemical reactions in gases," *Journal de Mathematiques Pures et Appliquees*, vol. 1, pp. 347–425, 1905.

[6] Y. B. Zel'dovich, "On the theory of propagation of detonation in gaseous systems," *Journal of Experimental and Theoretical Physics*, vol. 10, no. 5, pp. 542–569, 1940.

[7] J. von Neumann, "Theory of detonation waves," National Defense Research Committee Div. B, Tech. Rep., 1942.

[8] W. Döring, "Uber den detonationvorgang in gasen," *Annalen der Physik*, vol. 43(6/7), pp. 421–428, 1943.

[9] E. Oran and J. P. Boris, *Numerical simulation of reactive flow*. Cambridge, UK: Cambridge University Press, 2001.

[10] E. Schultz and J. Shepherd, "Validation of the detailed reaction mechanisms for detonation simulation," GALCIT. California Institute of Technology, Tech. Rep., 2000.

[11] C. Campbell and A. C. Finch, "Striated photographic records of explosion waves. Part II. An explanation of the striae," *Journal of Chemical Society*, pp. 2094–2106, 1928.

[12] D. Edwards, T. Jones, and B. Price, "Observations on oblique shock waves in gaseous detonations," *Journal of Fluid Mechanics*, vol. 17, no. 01, p. 21, Mar. 1963.

[13] D. Edwards and J. Morgan, "Instabilities in detonation waves near the limits of propagation," *Journal of Physics D: Applied Physics*, vol. 10, no. 17, pp. 2377–2389, 1977.

[14] J. J. Erpenbeck, "Stability of steady-state equilibrium detonations," *Physics of Fluids*, vol. 5, no. 5, pp. 604–614, 1962.

[15] ——, "Stability of idealized one-reaction detonations," *Physics of Fluids*, vol. 7, no. 5, pp. 684–696, 1964.

[16] H. I. Lee and D. S. Stewart, "Calculation of linear detonation instability: one-dimensional instability of plane detonation," *Journal of Fluid Mechanics*, vol. 216, pp. 103–132, 1990.

[17] J. Humpherys, G. Lyng, and K. Zumbrun, "Stability of viscous detonations for Majda's model," *Physica D: Nonlinear Phenomena*, vol. 259, pp. 63–80, Sep. 2013.

[18] M. Short, "Multidimensional linear stability of a detonation wave at high activation energy," *SIAM Journal on Applied Mathematics*, vol. 57, no. 2, pp. 307–326, 1997.

[19] M. Short and D. S. Stewart, "Low-frequency two-dimensional linear instability of plane detonation," *Journal of Fluid Mechanics*, vol. 340, no. 1, pp. 249–295, 1997.

[20] ——, "Cellular detonation stability. Part 1. A normal-mode linear analysis," *Journal of Fluid Mechanics*, vol. 368, pp. 229–262, Aug. 1998.

[21] W. Fickett and W. W. Wood, "Flow calculations for pulsating one-dimensional detonations," *Physics of Fluids*, vol. 9, no. 5, pp. 903–916, 1966.

[22] A. K. Henrick, T. D. Aslam, and J. M. Powers, "Simulations of pulsating one-dimensional detonations with true fifth order accuracy," *Journal of Computational Physics*, vol. 213, no. 1, pp. 311–329, Mar. 2006.

[23] H. Ng, A. Higgins, C. Kiyanda, M. Radulescu, J. Lee, K. Bates, and N. Nikiforakis, "Nonlinear dynamics and chaos analysis of one-dimensional pulsating detonations," *Combustion Theory and Modelling*, vol. 9, no. 1, pp. 159–170, Feb. 2005.

[24] H. Abderrahmane, F. Paquet, and H. Ng, "Applying nonlinear dynamic theory to one-dimensional pulsating detonations," *Combustion Theory and Modelling*, vol. 15, no. 2, pp. 205–225, 2011.

[25] W. Fickett, "Detonation in miniature," *American Journal of Physics*, vol. 47, no. 12, pp. 1050–1059, 1979.

[26] G. Ledder and J. D. Logan, "Weakly nonlinear asymptotic models and analogs of detonation processes," *International Journal of Engineering Science*, vol. 30, no. 12, pp. 1759–1772, Dec. 1992.

[27] W. Fickett, *Introduction to Detonation Theory*. Univervsity of California Press, 1985.

[28] ——, "Stability of the square-wave detonation in a model system," *Physica D: Nonlinear Phenomena*, pp. 358–370, 1985.

[29] A. Majda, "A qualitative model for dynamic combustion," *SIAM Journal on Applied Mathematics*, vol. 41, no. 1, pp. 70–93, Aug. 1981.

[30] S. Jung and J. Yao, "Stability of ZND detonations for Majda's model," *arXiv preprint arXiv:1205.6991*, 2012.

[31] M. I. Radulescu and J. Tang, "Nonlinear dynamics of self-sustained supersonic reaction waves: Fickett's detonation analogue," *Physical Review Letters*, vol. 107, no. 16, p. 164503, Oct. 2011.

[32] R. R. Rosales and A. Majda, "Weakly nonlinear detonation waves," *SIAM Journal on Applied Mathematics*, vol. 43, no. 5, pp. 1086–1118, Oct. 1983.

[33] T.-P. Liu and L.-A. Ying, "Nonlinear stability of strong detonations for a viscous combustion model," *SIAM Journal on Mathematical Analysis*, vol. 26, no. 3, pp. 519–528, 1995.

[34] T.-P. Liu and S.-H. Yu, "Nonlinear stability of weak detonation waves for a combustion model," *Communications in Mathematical Physics*, vol. 204, no. 3, pp. 551–586, Aug. 1999.

[35] A. R. Kasimov, "Private communication."

[36] M. Short and P. Blythe, "Structure and stability of weak-heat-release detonations for finite Mach numbers," *Proceedings of the Royal Society A: Mathematical, Physical and Engineering Sciences*, vol. 458, no. 2024, pp. 1795–1807, Aug. 2002.

[37] J. B. Bdzil and D. S. Stewart, "The dynamics of detonation in explosive systems," *Annual Review of Fluid Mechanics*, vol. 39, pp. 263–292, 2007.

[38] ——, "Theory of detonation shock dynamics," in *Shock Waves Science and Technology Library, Vol. 6*. Springer, 2012, pp. 373–453.

[39] J. Yao and D. S. Stewart, "On the dynamics of multi-dimensional detonation," *Journal of Fluid Mechanics*, vol. 309, pp. 225–275, 1996.

[40] A. R. Kasimov and D. S. Stewart, "Asymptotic theory of evolution and failure of self-sustained detonations," *Journal of Fluid Mechanics*, vol. 525, pp. 161–192, Feb. 2005.

[41] D. S. Stewart, "The shock dynamics of multidimensional condensed and gas-phase detonations," in *Symposium (International) on Combustion*, vol. 27, no. 2. Elsevier, 1998, pp. 2189–2205.

[42] A. Bourlioux, A. Majda, and V. Roytburd, "Theoretical and numerical structure for unstable one-dimensional detonations," *SIAM Journal of Applied Mathematics*, vol. 51, no. 2, pp. 303–343, Apr. 1991.

[43] A. Bourlioux and A. J. Majda, "Theoretical and numerical structure of unstable detonations," *Philosophical Transactions of Royal Society of London*, vol. A350, no. 1692, pp. 29–68, Jan. 1995.

[44] A. Bourlioux and A. Majda, "Theoretical and numerical structure for unstable two-dimensional detonations," *Combustion and Flame*, vol. 90, no. 3-4, pp. 211–229, Sep. 1992.

[45] P. Clavin and L. He, "Stability and nonlinear dynamics of one-dimensional overdriven detonations in gases," *Journal of Fluid Mechanics*, vol. 306, pp. 353–378, 1996.

[46] P. Clavin and B. Denet, "Diamond patterns in the cellular front of an overdriven detonation," *Physical Review Letters*, vol. 88, no. 4, p. 44502, 2002.

[47] P. Clavin and F. A. Williams, "Dynamics of planar gaseous detonations near Chapman-Jouguet conditions for small heat release," *Combustion Theory and Modelling*, vol. 6, no. 1, pp. 127–139, 2002.

[48] J. Lee, *The Detonation Phenomenon*. Cambridge University Press, 2008.

[49] S. Taki and T. Fujiwara, "Numerical analysis of two-dimensional nonsteady detonations," *AIAA Journal*, vol. 16, no. 1, pp. 73–77, Jan. 1978.

[50] E. S. Oran, J. W. Weber, E. I. Stefaniw, M. H. Lefebvre, and J. D. Anderson, "A numerical study of a two-dimensional H2-O2-Ar detonation using a detailed chemical reaction model," *Combustion and Flame*, vol. 113, no. 1-2, pp. 147–163, Apr. 1998.

[51] F. Zhang, *Shock Waves Science and Technology Library, Vol. 6: Detonation Dynamics*, F. Zhang, Ed. Springer, 2012.

[52] P. Clavin and F. A. Williams, "Analytical studies of the dynamics of gaseous detonations," *Philosophical Transactions of the Royal Society A: Mathematical, Physical and Engineering Sciences*, vol. 370, no. 1960, pp. 597–624, Feb. 2012.

[53] W. Fickett, "Approach to the steady solution for a plane Chapman-Jouguet detonation," *Physics of Fluids A: Fluid Dynamics*, vol. 1, no. 2, p. 371, Feb. 1989.

[54] P. Clavin and L. He, "Acoustic effects in the nonlinear oscillations of planar detonations," *Physical Review E*, vol. 53, no. 5, pp. 4778–4784, 1996.

[55] P. Clavin, L. He, and F. A. Williams, "Multidimensional stability analysis of overdriven gaseous detonations," *Physics of Fluids*, vol. 9, no. 12, pp. 3764–3785, 1997.

[56] R. Zaidel, "The stability of detonation waves in gaseous mixtures," *Dokl. Akad. Nauk SSSR*, vol. 136, no. 5, p. 1142, 1961.

[57] J. J. Erpenbeck, "Structure and stability of the square-wave detonation," *Symposium (International) on Combustion*, pp. 442–453, 1963.

[58] B. Texier and K. Zumbrun, "Transition to longitudinal instability of detonation waves is generically associated with Hopf bifurcation to time-periodic galloping solutions," *Communications in Mathematical Physics*, vol. 302, no. 1, pp. 1–51, Jan. 2011.

[59] M. Short and G. Sharpe, "Pulsating instability of detonations with a two-step chain-branching reaction model: theory and numerics," *Combustion Theory and Modelling*, vol. 7, no. 2, pp. 401–416, 2003.

[60] A. R. Kasimov and D. S. Stewart, "On the dynamics of self-sustained one-dimensional detonations: A numerical study in the shock-attached frame," *Physics of Fluids*, vol. 16, no. 10, pp. 3566–3578, 2004.

[61] F. Takens, "Detecting strange attractors in turbulence," in *Dynamical systems and turbulence*. Springer, 1981, pp. 366–381.

[62] C. Merkwirth and U. Parlitz, "OpenTSTOOL," 2009. [Online]. Available: http://www.physik3.gwdg.de/tstool/

[63] A. M. Fraser and H. L. Swinney, "Independent coordinates for strange attractors from mutual information," *Physical Review A*, vol. 33, no. 2, pp. 1134–1140, 1986.

[64] M. T. Rosenstein, J. J. Collins, C. D. Luca, and C. J. De Luca, "A practical method for calculating largest Lyapunov exponents from small data sets," *Physica D: Nonlinear Phenomena*, vol. 65, no. 1, pp. 117–134, 1993.

[65] P. Grassberger and I. Procaccia, "Measuring the strangeness of strange attractors," *Physica D: Nonlinear Phenomena*, vol. 9, no. 1, pp. 189–208, 1983.

[66] R. Semenko, L. M. Faria, A. Kasimov, and B. Ermolaev, "Set-valued solutions for non-ideal detonation," *arXiv preprint arXiv:1312.2180*, Dec. 2013.

[67] Y. Zel'dovich and A. Kompaneets, *Theory of Detonation*. Academic Press, 1960.

[68] I. Brailovsky, L. Kagan, and G. Sivashinsky, "Combustion waves in hydraulically resisted systems." *Philosophical Transactions. Series A, Mathematical, Physical, and Engineering Sciences*, vol. 370, no. 1960, pp. 625–46, Feb. 2012.

[69] L. M. Faria and A. R. Kasimov, "Qualitative modeling of the dynamics of detonations with losses," *Proceedings of the Combustion Institute*, Aug. 2014. [Online]. Available: http://linkinghub.elsevier.com/retrieve/pii/S1540748914003162

[70] A. J. Higgins, "Steady one-dimensional detonations," in *Shock Waves Science and Technology Library, Vol. 6*. Springer, 2012, pp. 33–105.

[71] M. R. Flynn, A. R. Kasimov, J.-C. Nave, R. R. Rosales, and B. Seibold, "Self-sustained nonlinear waves in traffic flow," *Phys. Rev. E*, vol. 79, no. 056113, 2009.

[72] A. R. Kasimov, "A stationary circular hydraulic jump, the limits of its existence and its gasdynamic analogue," *J. Fluid Mech.*, vol. 601, pp. 189–198, 2008.

[73] R. LeVeque, *Finite Volume Methods for Hyperbolic Problems*. Cambridge University Press, 2002.

[74] D. C. Bull, J. E. Elsworth, and G. Hooper, "Initiation of spherical detonation in hydrocarbon/air mixtures," *Acta Astronautica*, vol. 5, no. 11-12, pp. 997–1008, Nov. 1978.

[75] S. Watt and G. Sharpe, "Linear and nonlinear dynamics of cylindrically and spherically expanding detonation waves," *Journal of Fluid Mechanics*, 2005.

[76] L. M. Faria, A. R. Kasimov, and R. R. Rosales, "Study of a model equation in detonation theory," *SIAM Journal on Applied Mathematics*, vol. 74, no. 2, pp. 547–570, 2014.

[77] A. R. Kasimov, L. M. Faria, and R. R. Rosales, "Model for shock wave chaos," *Physical Review Letters*, vol. 110, no. 10, p. 104104, Mar. 2013.

[78] R. M. May, "Simple mathematical models with very complicated dynamics," *Nature*, vol. 261, no. 5560, pp. 459–467, 1976.

[79] R. R. Rosales, "Diffraction effects in weakly nonlinear detonation waves," in *Nonlinear Hyperbolic Problems*. Springer, 1989, pp. 227–239.

[80] E. Coddington and N. Levinson, *Theory of Ordinary Differential Equations*. Tata McGraw-Hill Education, 1955.

[81] J. K. Hunter and M. Brio, "Weak shock reflection," *Journal of Fluid Mechanics*, vol. 410, pp. 235–261, 2000.

[82] E. G. Tabak and R. R. Rosales, "Focusing of weak shock waves and the von Neumann paradox of oblique shock reflection," *Physics of Fluids (1994-present)*, vol. 6, no. 5, pp. 1874–1892, 1994.

[83] L. M. Faria, A. R. Kasimov, and R. R. Rosales, "A two-dimensional detonation analog," *(in preparation)*.

[84] B. V. Voitsekhovskii, V. V. Mitrofanov, and M. Y. Topchian, *The Structure of Detonation Front in Gases*. Wright Patterson Air Force Base, OH (AD 633-821).: Report FTD-MTD-64-527. Foreign Technology Division, 1966.

[85] M. Short and D. S. Stewart, "The multi-dimensional stability of weak-heat-release detonations," *Journal of Fluid Mechanics*, vol. 382, pp. 109–135, 1999.

[86] D. S. Stewart, T. D. Aslam, and J. Yao, "On the evolution of cellular detonation," in *Proceedings of the Combustion Institute*, vol. 26. Pittsburgh, PA: The Combustion Institute, 1996, pp. 2981–2989.

[87] F. A. Williams, *Combustion Theory*. Westview Press, 1985.

[88] J. K. Hunter, "Asymptotic equations for nonlinear hyperbolic waves," in *Surveys in Applied Mathematics*. Springer, 1995, pp. 167–276.

[89] R. R. Rosales, "An introduction to weakly nonlinear geometrical optics," in *Multidimensional Hyperbolic Problems and Computations*. Springer, 1991, pp. 281–310.

[90] G. B. Whitham, *Linear and Nonlinear Waves*. New York, NY: John Wiley and Sons, 1974.

[91] J. B. Keller, "Rays, waves and asymptotics," *Bulletin of the American mathematical society*, vol. 84, no. 5, pp. 727–750, 1978.

[92] C. C. Lin, E. Reissner, and H. S. Tsien, "On two-dimensional non-steady motion of a slender body in a compressible fluid," *Journal of Mathematics and Physics*, vol. 27, no. 3, p. 220, 1948.

[93] E. A. Zabolotskaya and R. V. Khokhlov, "Quasi-planes waves in the nonlinear acoustics of confined beams," *Sov. Phys. Acoust.*, vol. 15, no. 1, pp. 35–40, 1969.

[94] S. H. Strogatz, *Nonlinear dynamics and chaos: With applications to physics, biology, chemistry, and engineering*. Westview Press, 1994.

[95] D. I. Ketcheson, K. T. Mandli, A. Ahmadia, A. Alghamdi, M. Quezada, M. Parsani, M. G. Knepley, and M. Emmett, "PyClaw: Accessible, extensible, scalable tools for wave propagation problems," *SIAM Journal on Scientific Computing*, vol. 34, no. 4, pp. C210—-C231, 2012.

[96] J. von Neumann, "Oblique reflection of shocks," in *Comm. Off. Tech. Serv. No. PB37079*. Pergamon, New York, 1963, vol. VI, pp. 238–299.

[97] H. M. Glaz, P. Colella, I. I. Glass, and R. L. Deschambault, "A numerical study of oblique shock-wave reflections with experimental comparisons," *Proceedings of the Royal Society of London. A. Mathematical and Physical Sciences*, vol. 398, no. 1814, pp. 117–140, 1985.

[98] B. Barker, J. Humpherys, G. Lyng, and K. Zumbrun, "Viscous hyperstabilization of detonation waves in one space dimension," *arXiv preprint arXiv:1311.6417*, 2013.

[99] L. M. Faria, A. R. Kasimov, and R. R. Rosales, "Theory of weakly nonlinear self sustained detonations," *arXiv preprint arXiv:1407.8466*, 2014.

[100] I. Brailovsky and G. Sivashinsky, "Hydraulic resistance and multiplicity of detonation regimes," *Combustion and flame*, vol. 122, no. 1, pp. 130–138, 2000.

[101] C.-W. Shu, "Essentially non-oscillatory and weighted essentially non-oscillatory schemes for hyperbolic conservation laws," in *Advanced Numerical Approximation of Nonlinear Hyperbolic Equations*, ser. Lecture Notes in Mathematics, A. Quarteroni, Ed. Springer, Berlin, 1998, vol. 1697, pp. 325–432.

[102] S. Gottlieb and C.-W. Shu, "Total variation diminishing Runge-Kutta schemes," *Mathematics of Computation*, vol. 67, no. 221, pp. 73–85, 1998.

APPENDICES

Appendix A

WENO5 with TVD-RK3 algorithm

Here we describe the algorithm used to solve the hyperbolic equations proposed in Chapter 2. For the spatial discretization, we used a 5-point weighted essentially non-oscillatory (WENO) method based on [101]. As usually done in WENO methods, we introduce a small parameter ϵ to guarantee that the denominators do not become 0 when we are computing WENO weights. For the problems investigated here, we experimented with ϵ between 10^{-5} and 10^{-10}, and the solutions seemed to be unaffected by this choice. The chosen ϵ for all computation was $\epsilon = 10^{-6}$.

In order to avoid spurious oscillations we have chosen a total variation dimishing (TVD) time stepping algorithm. The choice made here is a third order TVD Runge-Kutta method as presented in [102]. The value of u_s, which is present in the flux and the source term (see (2.6)), was taken to be the right boundary value of u at the current time step.

On the left of the domain we used a first order extrapolation, where the values

of the leftmost grid cell was copied into the left ghost cells required by the WENO algorithm. Since the equations were solved in a shock attached frame, the right boundary corresponds to the shock, and therefore the right boundary required a more careful treatment. Unlike [22], where the WENO algorithm is modified so that it becomes biased to the left near the shock, avoiding the need to use ghost points, we chose instead to extrapolate the solution to the right of the shock, using the extrapolated values in the ghost points. We noticed that, unlike the left boundary, the order of the extrapolation of the right boundary crucially affected the overall convergence of the algorithm. We used a fifth order extrapolation for the right ghost points.

Convergence tests were performed by comparing the numerical wave speed, given by $D(t) = 2u_s(t)$, to the exact value it should attain when the wave is stable, $D = 2$. We observed fifth order convergence, as seen in Figure A.1a, where the error was measured in the L_∞-norm.

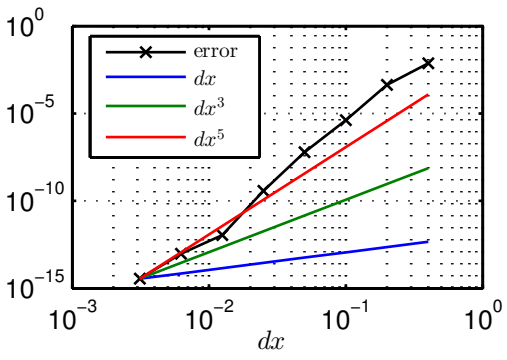

(a) Fifth order convergence with high order extrapolation of right boundary

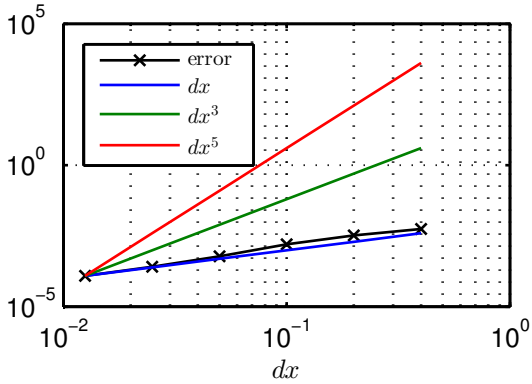

(b) First order convergence with low order extrapolation of right boundary

Figure A.1: Convergence of WENO algorithm

We mention here that when a lower order extrapolation was used on the right boundary, the order of the algorithm degraded to the order of the extrapolation procedure, as can be seen on Figure A.1b. This may be because the shock value critically

affects the whole solution through the source term $f(x, u_s)$, which is nonlocal.

Appendix B

Largest Lyapunov Exponent

The algorithm for the LLE consists of the following steps:

1. Given a time series u_s^n, embed it in an m-dimensional space with delay τ, as outlined in Section 2.4.4.1.

2. For a given point p_i, find the closest point p_{j_i} such that $|i-j_i| > \textit{the mean period}$, where the mean period is estimated by the inverse of the dominant frequency of the power spectrum.

3. Define $d_i^m(n) = \|p_{i+n} - p_{j+n}\|$. Then, $d_i(n)$ represents the divergence between trajectories starting at p_i and p_{j_i}.

4. Choose N points randomly on the attractor and compute an average divergence of trajectories by $d^m(n) = \frac{1}{N}\sum_{l=1}^{N} d_l^m(n)$. The number N is limited either by the amount of available data or by computational restrictions.

5. Plot $\log(d^m(n))$ versus $n\Delta t$.

6. Repeat steps 1-5 for different values of embedding dimension, m, and find a region $t_{min} < t < t_{max}$ such that the plot of $\log(d^m(n))$ vs. $n\Delta t$ is nearly a straight line for the values of m used.

7. Do a least squares fit in the region $t_{\min} < t < t_{\max}$ to extract λ_1^m for each embedding dimension m.

8. If the values of λ_1^m do not vary much for a wide range of embedding dimensions, m, let λ_1 be the average over all embedding dimensions computed.

The algorithm suggested above, which is presented in [64], has some parameters that are not objectively chosen. The value of λ_1 depends, among other things, on the choices of τ, the range of m considered, the choices of $t_{\min}$ and $t_{\max}$, and on N. Of course, it also depends on the quality of the data set and the amount of noise present in it. In [64], a numerical study of this parameter dependence is performed, and it is claimed that the algorithm is rather robust. In our study, we use the range $3 \leq m \leq 20$, fix $\tau = 150$, choose $N = 20,000$, and choose $t_{\min}$ and $t_{\max}$ by looking at the plot of $\log(d)$ vs t. A typical plot is show in Figure B.1a, where $\alpha = 5$, $t_{\min} = 100$, and $t_{\max} = 200$.

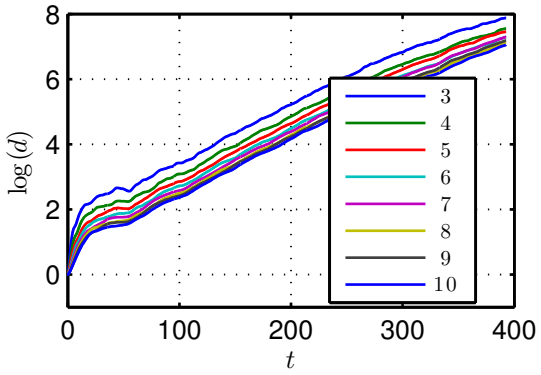

(a) Divergence of trajectories for different embedding dimensions.

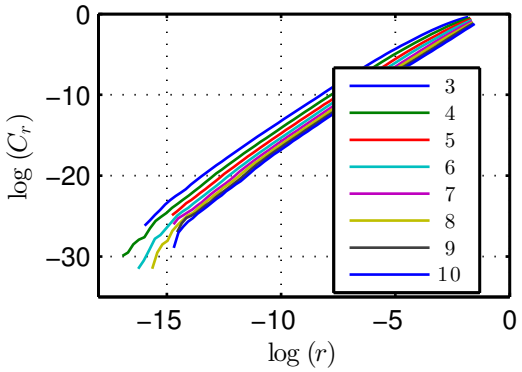

(b) Plots of $\log(C_r)$ vs $\log(r)$ for different embedding dimensions.

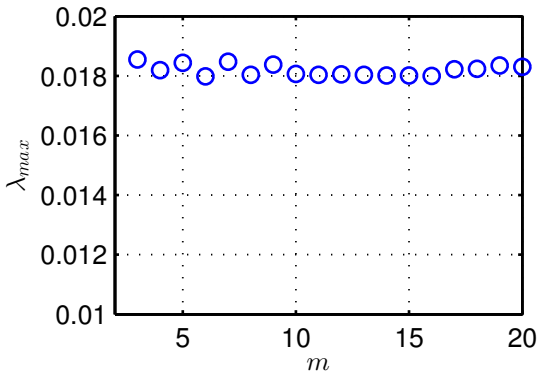

(c) LLE estimated from (a).

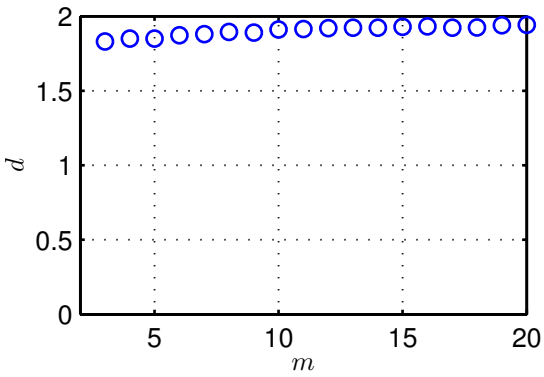

(d) The correlation dimension estimated from (b).

Figure B.1: Dependence of the largest Lyapunov exponent and correlation dimension on the choice of the embedding dimension.

In Table B.1, we present the values of LLE calculated for each given dimension from Figure B.1c.

m	3	4	5	8	10	15	20
LLE	0.0185	0.0182	0.0184	0.0180	0.0181	0.0180	0.0183
D_C	1.8306	1.8507	1.8500	1.8904	1.9147	1.9317	1.9432

Table B.1: The LLE and the correlation dimension for different embedding dimensions.

For other values of α, the same methodology is applied. The values shown in Table 2.3 are obtained by averaging the LLE over multiple dimensions. The error estimates are the maximum differences between the averages and the entries.

Appendix C

Correlation Dimension

The algorithm for computing the correlation dimension follows that of [65]. It consists of the following steps:

1. Given a time series u_s^n, embed it in an m dimensional space with delay τ, as outlined in Section 2.4.4.1.

2. Construct a grid $\bar{r} = (r_1, \cdots, r_L)$ where $r_1 > \min_{i,j}(\|u_s^i - u_s^j\|)$ and $r_L < \max_{i,j}(\|u_s^i - u_s^j\|)$.

3. For each r_i define the correlation sum, at a given dimension m, to be $C^m(r_k) = \frac{1}{N^2}\sum_{i,j=1}^{N}\theta(r_k - \|u_s^i - u_s^j\|)$, where θ is the Heaviside function.

4. Plot $\log(C^m(r_k))$ versus $\log(r_k)$.

5. Repeat steps 1-4 for different values of the embedding dimension m, and find a region $r_{min} < r < r_{max}$ such that the plot of $\log(C^m(r))$ vs. $\log(r)$ is nearly a straight line for the values of m used.

6. Do a least squares fit over the region $r_{\min} < r < r_{\max}$ to extract D_C^m for each embedding dimension m.

7. If the values of D_C^m do not vary much for a wide range of embedding dimensions m, let D_C be the average over all embedding dimensions.

Similar to the LLE calculation, the computed value of D_C depends on many parameters that cannot be objectively chosen. The choices of $\tau,\ m,\ r_{\min},\ r_{\max}$ in particular have an appreciable effect on the value of D_C. In our study, we use the range $3 \leq m \leq 20$, fix $\tau = 150$, choose $N = 5000$, and choose $r_{\min}$ and $r_{\max}$ by looking at the plot of $\log(C^m(r))$ vs $\log(r)$. A typical plot is shown in Figure B.1b, where $\alpha = 5$, $\log(r_{\min}) = -8$, and $\log(r_{\max}) = -4$.

In Table B.1, we show the computed values of the correlation dimension for the data presented in Figure B.1b. Notice that the variability here is much higher than in the computation for the largest Lyapunov exponent.

Appendix D

Dimensionless reactive compressible Navier-Stokes equations

In this appendix we include the details of nondimensionalization of the governing equations presented in Chapter 5. We focus on the two dimensional case, so that (5.8,5.9,5.11,5.12) reduce to

$$\begin{aligned}
\frac{D\rho}{Dt} + \rho\left(U_X + V_Y\right) &= 0, && \text{(D.1)}\\
\rho\frac{\mathrm{D}U}{\mathrm{D}t} + p_X &= \frac{1}{3}\tilde{\mu}\left(U_{XX} + V_{XY}\right) + \tilde{\mu}\left(U_{XX} + U_{YY}\right), && \text{(D.2)}\\
\rho\frac{\mathrm{D}V}{\mathrm{D}t} + p_Y &= \frac{1}{3}\tilde{\mu}\left(U_{XY} + V_{YY}\right) + \tilde{\mu}\left(V_{XX} + V_{YY}\right), && \text{(D.3)}\\
\rho\frac{DT}{Dt} - \frac{\gamma-1}{R\gamma}\frac{Dp}{Dt} &= \frac{\gamma-1}{R\gamma}\Bigg(\tilde{Q}\rho\tilde{W} - \frac{2}{3}\tilde{\mu}\left(\nabla\cdot\mathbf{u}\right)^2 + \tilde{\mu}\left(\nabla\mathbf{u}\right)^2 \\
&+ \tilde{\mu}\left(\nabla\mathbf{u} : \nabla\mathbf{u}^T\right) - \nabla\cdot\left(\tilde{\kappa}\nabla T\right)\Bigg) && \text{(D.4)}\\
\rho\frac{\mathrm{D}\Lambda}{\mathrm{D}t} &= \rho\tilde{W} - \nabla\cdot\left(\tilde{d}\rho\nabla\Lambda\right). && \text{(D.5)}
\end{aligned}$$

where $\mathbf{u} = (U, V)^T$. Rescale density, pressure, temperature and velocities by ρ_a, p_a, T_a and $u_a = \sqrt{p_a/\rho_a}$ respectively. The independent variables rescaled as

$$x = \frac{X - D_0 t}{x_0}, \quad y = \frac{Y}{y_0}, \quad \tau = \frac{t}{t_0}, \tag{D.6}$$

Let $\epsilon = x_0/u_a t_0,\ y_0 = x_0/\sqrt{\epsilon}$. Define

$$\mathrm{Re} = \frac{\rho_a u_a x_0}{\tilde{\mu}}, \quad \mathrm{Pr} = \frac{c_p \tilde{\mu}}{\tilde{\kappa}}, \quad \mathrm{Le} = \frac{\tilde{\kappa}}{\rho_a c_p \tilde{d}}, \tag{D.7}$$

From now on all variables are dimensionless, but the same notation is used. Thus ρ, U, V, T, Λ below denote dimensionless quantities. Furthermore, let

$$Q = \frac{\tilde{Q}}{RT_a}, \quad E = \frac{\tilde{E}}{RT_a}, \quad K = t_0 \tilde{k} \exp(-E).$$

The conservation of mass equation, i.e. (D.1), is written in dimensionless variables as

$$\rho_\tau + \frac{1}{\epsilon}(U - D_0)\rho_x + \frac{1}{\sqrt{\epsilon}} V \rho_y + \rho \left(\frac{1}{\epsilon} U_x + \frac{1}{\sqrt{\epsilon}} V_y \right) = 0.$$

The x momentum equation, i.e. (D.2), becomes

$$\begin{aligned} \rho \left(U_\tau + \frac{1}{\epsilon}(U - D_0) U_x + \frac{1}{\sqrt{\epsilon}} V U_x \right) + \frac{1}{\epsilon} p_x &= \frac{1}{3} \frac{\tilde{\mu}}{\rho_a u_a x_0} \frac{u_a t_0}{x_0} \left(U_{xx} + \sqrt{\epsilon} V_{xy} \right) \\ &+ \frac{\tilde{\mu}}{\rho_a u_a x_0} \frac{u_a t_0}{x_0} (U_{xx} + \epsilon U_{yy}) \\ &= \frac{1}{3} \frac{1}{\epsilon Re} \left(U_{xx} + \sqrt{\epsilon} V_{xy} \right) \\ &+ \frac{1}{\epsilon Re} (U_{xx} + \epsilon U_{yy}). \end{aligned}$$

The y momentum equation, (D.3),

$$\begin{aligned}
\rho\left(V_\tau+\frac{1}{\epsilon}(U-D_0)V_x+\frac{1}{\sqrt{\epsilon}}VV_y\right)+\frac{1}{\sqrt{\epsilon}}p_y &= \frac{1}{3}\frac{\tilde{\mu}}{\rho_a u_a x_0}\frac{u_a t_0}{x_0}\left(\sqrt{\epsilon}U_{xy}+\epsilon V_{yy}\right)\\
&+ \frac{\tilde{\mu}}{\rho_a u_a x_0}\frac{u_a t_0}{x_0}\left(V_{xx}+\epsilon V_{yy}\right)\\
&= \frac{1}{3}\frac{1}{\epsilon Re}\left(\sqrt{\epsilon}U_{xy}+\epsilon V_{yy}\right)\\
&+ \frac{1}{\epsilon Re}\left(V_{xx}+\epsilon V_{yy}\right).
\end{aligned}$$

The energy equation, i.e. (D.4), is given in dimensionless form by

$$\begin{aligned}
\rho\left(T_\tau+\frac{1}{\epsilon}(U-D_0)T_x+\frac{1}{\sqrt{\epsilon}}VT_y\right) &-\\
\frac{(\gamma-1)}{\gamma}\left(p_\tau+\frac{1}{\epsilon}(U-D_0)p_x+\frac{1}{\sqrt{\epsilon}}Vp_y\right) &= \frac{\gamma-1}{R\gamma}\frac{t_0}{\rho_a T_a}\Bigg(\rho_a\tilde{Q}\rho\tilde{W}-\frac{2}{3}\mu\frac{u_a^2}{x_0^2}\left(U_x+\sqrt{\epsilon}V_y\right)^2\\
&+ \mu\frac{u_a^2}{x_0^2}\left(U_x^2+\epsilon U_y^2+V_x^2+\epsilon V_y^2\right)\\
&+ \mu\frac{u_a^2}{x_0^2}\left(U_x^2+\sqrt{\epsilon}U_yV_x+\sqrt{\epsilon}V_xU_y+\epsilon V_y^2\right)\\
&- T_a\frac{d_1}{x_r^2}\left(T_{xx}+\epsilon T_{yy}\right)\Bigg)\\
&= \frac{\gamma-1}{\gamma}\Bigg(Q\rho W-\frac{2}{3}\frac{1}{Re}\left(U_x+\sqrt{\epsilon}V_y\right)^2\\
&+ \frac{1}{\epsilon Re}\left(U_x^2+\epsilon U_y^2+V_x^2+\epsilon V_y^2\right)\\
&+ \frac{1}{\epsilon Re}\left(U_x^2+\sqrt{\epsilon}U_yV_x+\sqrt{\epsilon}V_xU_y+\epsilon V_y^2\right)\Bigg)\\
&- \frac{1}{\epsilon RePr}\left(T_{xx}+\epsilon T_{yy}\right),
\end{aligned}$$

where

$$W=K(1-\Lambda)\exp\left[E\left(1-\frac{1}{T}\right)\right].$$

Finally, the reaction rate, (D.5), becomes

$$\begin{aligned}
\rho\left(\Lambda_\tau + \frac{1}{\epsilon}(U-D_0)\Lambda_x + \frac{1}{\sqrt{\epsilon}}V\Lambda_y\right) &= t_0\rho\tilde{W} - \frac{\tilde{d}t_0}{x_r^2}\left((\rho\Lambda x)_x + \epsilon\left(\rho\Lambda_y\right)_y\right) \\
&= t_0\rho\tilde{W} - \frac{\tilde{d}}{u_a\epsilon x_0}\left((\rho\Lambda_x)_x + \epsilon\left(\rho\Lambda_y\right)_y\right) \\
&= \rho W - \frac{1}{\epsilon RePrLe}\left((\rho\Lambda_x)_x + \epsilon\left(\rho\Lambda_y\right)_y\right).
\end{aligned}$$

Defining

$$L = \partial_\tau + \frac{1}{\epsilon}(U-D_0)\partial_x + \frac{1}{\sqrt{\epsilon}}V\partial_y,$$

we obtain the following dimensionless formulation:

$$\begin{aligned}
L[\rho] + \rho\left(\frac{1}{\epsilon}U_x + \frac{1}{\sqrt{\epsilon}}V_y\right) &= 0, \\
\rho L[U] + \frac{1}{\epsilon}p_x &= \frac{1}{3\epsilon\mathrm{Re}}\left(U_{xx} + \sqrt{\epsilon}V_{xy}\right) + \frac{1}{\epsilon\mathrm{Re}}\left(U_{xx} + \epsilon U_{yy}\right), \\
\rho L[V] + \frac{1}{\sqrt{\epsilon}}p_y &= \frac{1}{3\epsilon\mathrm{Re}}\left(\sqrt{\epsilon}U_{xy} + \epsilon V_{yy}\right) + \frac{1}{\epsilon\mathrm{Re}}\left(V_{xx} + \epsilon V_{yy}\right), \\
\rho L[T] - \frac{(\gamma-1)}{\gamma}L[p] &= \frac{\gamma-1}{\gamma}\Bigg(Q\rho W - \frac{2}{3\epsilon\mathrm{Re}}\left(U_x + \sqrt{\epsilon}V_y\right)^2 \\
&\quad + \frac{1}{\epsilon\mathrm{Re}}\left(U_x^2 + \epsilon U_y^2 + V_x^2 + \epsilon V_y^2\right)\Bigg) \\
&\quad + \frac{\gamma-1}{\gamma}\frac{1}{\epsilon\mathrm{Re}}\left(U_x^2 + \sqrt{\epsilon}U_yV_x + \sqrt{\epsilon}V_xU_y + \epsilon V_y^2\right) \\
&\quad + \frac{1}{\epsilon\mathrm{RePr}}\left(T_{xx} + \epsilon T_{yy}\right), \\
\rho L[\Lambda] &= \rho W + \frac{1}{\epsilon\mathrm{RePrLe}}\left((\rho\Lambda_x)_x + \epsilon\left(\rho\Lambda_y\right)_y\right).
\end{aligned}$$

Appendix E

Details of weakly nonlinear asymptotic expansion

Here we present the algebraic calculations involved expanding the dimensionless equations in the considered asymptotic sequence. We start from

$$
\begin{aligned}
L[\rho] + \rho\left(\frac{1}{\epsilon}U_x + \frac{1}{\sqrt{\epsilon}}V_y\right) &= 0, \\
\rho L[U] + \frac{1}{\epsilon}p_x &= \frac{1}{3\epsilon\mathrm{Re}}\left(U_{xx} + \sqrt{\epsilon}V_{xy}\right) + \frac{1}{\epsilon\mathrm{Re}}\left(U_{xx} + \epsilon U_{yy}\right), \\
\rho L[V] + \frac{1}{\sqrt{\epsilon}}p_y &= \frac{1}{3\epsilon\mathrm{Re}}\left(\sqrt{\epsilon}U_{xy} + \epsilon V_{yy}\right) + \frac{1}{\epsilon\mathrm{Re}}\left(V_{xx} + \epsilon V_{yy}\right), \\
\rho L[T] - \frac{(\gamma-1)}{\gamma}L[p] &= \frac{\gamma-1}{\gamma}\Bigg(Q\rho W - \frac{2}{3\epsilon\mathrm{Re}}\left(U_x + \sqrt{\epsilon}V_y\right)^2 \\
&+ \frac{1}{\epsilon\mathrm{Re}}\left(U_x^2 + \epsilon U_y^2 + V_x^2 + \epsilon V_y^2\right)\Bigg) \\
&+ \frac{\gamma-1}{\gamma}\frac{1}{\epsilon\mathrm{Re}}\left(U_x^2 + \sqrt{\epsilon}U_yV_x + \sqrt{\epsilon}V_xU_y + \epsilon V_y^2\right) \\
&+ \frac{1}{\epsilon\mathrm{RePr}}\left(T_{xx} + \epsilon T_{yy}\right), \\
\rho L[\Lambda] &= \rho W + \frac{1}{\epsilon\mathrm{RePrLe}}\left(\left(\rho\Lambda_x\right)_x + \epsilon\left(\rho\Lambda_y\right)_y\right),
\end{aligned}
$$

where W is defined as

$$W = K(1-\Lambda)\exp\left[E\left(1-\frac{1}{T}\right)\right]. \tag{E.1}$$

and expand the variables in the following asymptotic series:

$$\rho = 1 + \rho_1\epsilon + \rho_2\epsilon^{3/2} + \rho_3\epsilon^2 + o(\epsilon^2), \tag{E.2}$$

$$T = 1 + T_1\epsilon + T_2\epsilon^{3/2} + T_3\epsilon^2 + o(\epsilon^2), \tag{E.3}$$

$$p = 1 + p_1\epsilon + p_2\epsilon^{3/2} + p_3\epsilon^2 + o(\epsilon^2), \tag{E.4}$$

$$\boldsymbol{u} = \mathbf{u}_1\epsilon + \mathbf{u}_2\epsilon^{3/2} + \mathbf{u}_3\epsilon^2 + o(\epsilon^2), \tag{E.5}$$

$$\Lambda = \lambda + o(\epsilon). \tag{E.6}$$

The mass conservation equation

$$\rho_\tau + \frac{1}{\epsilon}(U-D_0)\rho_x + \frac{1}{\sqrt{\epsilon}}V\rho_y + \rho\left(\frac{1}{\epsilon}U_x + \frac{1}{\sqrt{\epsilon}}V_y\right) = 0$$

yields

$$\begin{aligned}(-D_0\rho_{1x} + U_{1x}) + \sqrt{\epsilon}\,(-D_0\rho_{2x} + U_{2x} + V_{1y}) + \\ \epsilon\,(\rho_{1\tau} - D_0\rho_{3x} + U_1\rho_{1x} + U_{3x} + \rho_1 U_{1x} + V_{2y}) \;\;=\;\; O(\epsilon^{3/2}).\end{aligned}$$

The x-momentum equation

$$U_\tau + \frac{1}{\epsilon}(U-D_0)U_x + \frac{1}{\sqrt{\epsilon}}VU_y + \frac{1}{\rho}\left(\frac{1}{\epsilon}p_x\right) = \frac{1}{3}\frac{1}{\epsilon Re}\left(U_{xx} + \sqrt{\epsilon}V_{xy}\right) + \frac{1}{\epsilon Re}\left(U_{xx} + \epsilon U_{yy}\right),$$

gives

$$\begin{aligned}(-D_0U_{1x}+T_{1x}+\rho_{1x})+\sqrt{\epsilon}\,(-D_0U_{2x}+T_{2x}+\rho_{2x}) \quad &+\\ \epsilon\,(U_{1\tau}-D_0U_{3x}+U_1U_{1x}+T_1\rho_{1x}+T_{3x}+\rho_{3x}-\rho_1\rho_{1x}) \quad &= \quad \frac{4}{3}\frac{1}{Re}\,(U_1)_{xx}+o(\epsilon).\end{aligned}$$

The y-momentum equation

$$V_\tau+\frac{1}{\epsilon}(U-D_0)V_x+\frac{1}{\sqrt{\epsilon}}VV_y+\frac{1}{\rho}\left(\frac{1}{\sqrt{\epsilon}}p_y\right)=\frac{1}{3}\frac{1}{\epsilon Re}\left(\sqrt{\epsilon}U_{xy}+\epsilon V_{yy}\right)+\frac{1}{\epsilon Re}\left(V_{xx}+\epsilon V_{yy}\right),$$

gives

$$\begin{aligned}(-D_0V_{1x})+\sqrt{\epsilon}\,(-D_0V_{2x}+T_{1y}+\rho_{1y})+&\\ \epsilon\,(V_{1\tau}-D_0V_{3x}+U_1V_{1x}+T_{2y}+\rho_{2y}) \quad &= \quad \frac{1}{Re}\,(V_1)_{xx}+o(\epsilon).\end{aligned}$$

The energy equation

$$\begin{aligned}\rho\left(T_\tau+\frac{1}{\epsilon}(U-D_0)T_x+\frac{1}{\sqrt{\epsilon}}VT_y\right)-&\\ \epsilon\frac{\gamma_1}{\gamma}\left(p_\tau+\frac{1}{\epsilon}(U-D_0)p_x+\frac{1}{\sqrt{\epsilon}}Vp_y\right)=\frac{\gamma-1}{\gamma}\Bigg(&Q\rho W-\frac{2}{3}\frac{1}{\epsilon Re}\left(U_x+\sqrt{\epsilon}V_y\right)^2\\ &+\frac{1}{\epsilon Re}\left(U_x^2+\epsilon U_y^2+V_x^2+\epsilon V_y^2\right)\Bigg)\\ &+\frac{\gamma-1}{\gamma}\frac{1}{\epsilon Re}\left(U_x^2+\sqrt{\epsilon}U_yV_x+\sqrt{\epsilon}V_xU_y+\epsilon V_y^2\right)\\ &-\frac{1}{\epsilon RePr}\left(T_{xx}+\epsilon T_{yy}\right)\end{aligned}$$

gives

$$\begin{aligned} (-D_0 T_{1x}) + \sqrt{\epsilon}\,(-D_0 T_{2x}) \quad &+ \\ \epsilon\left(T_{1\tau} - D_0 T_{3x} + U_1 T_{1x} + \frac{\gamma_1}{\gamma} D_0\left(\rho_{1x} + T_{1x}\right)\right) \quad &= \quad \epsilon q\omega + o(\epsilon), \end{aligned}$$

where $\omega = k(1-\lambda)\exp(\theta T_3)$ is the leading order expansion of the reaction rate W.

Finally the reaction rate equation

$$\Lambda_\tau + \frac{1}{\epsilon}(U - D_0)\Lambda_x + \frac{1}{\sqrt{\epsilon}} V \Lambda_y = \rho W - \frac{1}{\epsilon RePrLe}\left((\rho\Lambda_x)_x + \epsilon\,(\rho\Lambda_y)_y\right)$$

gives

$$-D_0\Lambda_x \quad = \quad \omega + o(1).$$

Appendix F

von Neumann stability analysis of a simple explicit scheme

In order to motivate the use of a semi-implicit scheme to solve (5.49-5.51), here we perform a von-Neumann stability analysis of a "natural/reasonable" explicit scheme and show that it leads to instabilities. Since such an analysis requires a constant coefficient linear system, we consider here the linearized, UTSD equations

$$u_t + u_x + v_y = 0, \tag{F.1}$$

$$v_x = u_y. \tag{F.2}$$

We discretized these equations using forward finite differences in t and x, and centered finite differences in y. This leads to the scheme

$$U_{i,j}^{n+1} = U_{i,j}^n - \Delta t \left(\frac{U_{i,j}^n - U_{i-1,j}^n}{\Delta x} + \frac{V_{i,j+1}^n - V_{i,j-1}^n}{2\Delta y} \right), \tag{F.3}$$

$$V_{i,j}^n = V_{i+1}^n - \Delta x \left(\frac{U_{i,j+1}^n - U_{i,j-1}^n}{2\Delta y} \right). \tag{F.4}$$

Then we compute the (periodic) discrete eigenfunctions for the scheme using the ansatz

$$U_{p,q}^n = AG^n e^{i(kx_p+ly_q)}, \tag{F.5}$$

$$V_{p,q}^n = BG^n e^{i(kx_p+ly_q)}, \tag{F.6}$$

where k and l are the discrete wave numbers, G is the growth factor, A and B are constants, $x_p = p\Delta x$, $y_q = q\Delta y$, and

$$U_{p,q}^n = U(x_q, y_p, t^n), \tag{F.7}$$

$$V_{p,q}^n = V(x_q, y_p, t^n). \tag{F.8}$$

In the standard fashion of the von Neumann stability analysis, this leads to an eigenvalue problem for the vector with components A and B, with eigenvalue G. Solving this problem yields

$$G = 1 - \frac{\Delta t}{\Delta x}\frac{1-e^{-ik\Delta x}}{\Delta x} - \frac{\Delta t \Delta x}{\Delta y^2}\frac{\sin^2(l\Delta y)}{(1-e^{ik\Delta x})}. \tag{F.9}$$

Note that, in (F.9), the term

$$\frac{\Delta t \Delta x}{\Delta y^2}\frac{\sin^2(l\Delta y)}{(1-e^{ik\Delta x})} \tag{F.10}$$

can be traced back to the explicit treatment of v_y. This term causes instability, since it can become arbitrarily large for $k\Delta x$ small and $\sin^2(l\Delta y)$ away from zero, independently of the size of Δt. Hence, the scheme is unstable. Instabilities like this one are inevitable in explicit finite difference schemes, regardless of the choice. The reason is that the wave speeds in the y-direction are unbounded. No explicit scheme

can hence satisfy the CFL (Courant-Friedrichs-Lewy) condition.

Appendix G

Self-convergence of algorithm for two-dimensional asymptotic system

As discussed in Subsection 5.5.2.1, the asymptotic equations obtained in Chapter 5 have to be solved in a semi-implicit way. Since we use a second order approximation to all terms in the governing equations, we obtain a formally second order algorithm. The convergence rate is tested using a smooth solution. In particular, we run the solver with initial condition

$$u(x, y, 0) = \exp\left(-\left(x^2 + y^2\right)\right),$$

up to a time $t = 0.5$, for varying grid resolution. The solutions are then compared to the finest grid, and the error is measured in L^2 norm. The domain is $[-5, 5] \times [-5, 5]$, and the resolution goes from 100×100 on the coarsest grid to 6400×6400 on the finest. As we can see in Figure G.1, second order self-convergence is obtained.

Note that the actual detonation problem we must solve contains not only shocks, but also a discontinuous source term (which was shut off in the convergence study mentioned above). Thus, what we have really tested is convergence of our algorithm in approximating the UTSD equations for smooth solutions. The other tests performed

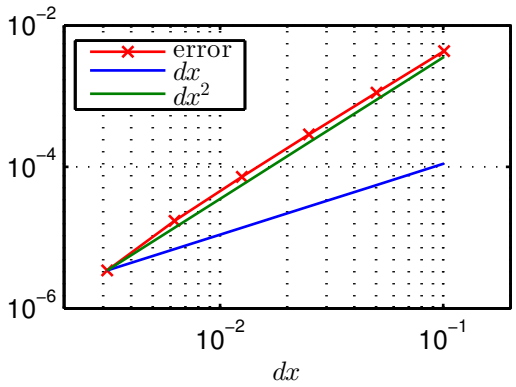

Figure G.1: Self-convergence of 2d algorithm.

in Figure G.1 , namely that the algorithm captures the correct ZND solutions, wave speeds, and stability boundaries, further validated the method used. Without resorting to shock fitting, however, only first order convergence should be expected for the problem of interest due to the presence of shocks and the discontinuous source term.